A FINITE ELEMENT FOR SHELL ANALYSIS AND ITS APPLICATION TO BIOLOGICAL OBJECTS

A Thesis

Presented to the Faculty of the Graduate School

of Cornell University

in Partial Fulfillment of the Requirements for the Degree of

Doctor of Philosophy

by

Jae Young Lee

June 1986

A FINITE ELEMENT FOR SHELL ANALYSIS AND
ITS APPLICATION TO BIOLOGICAL OBJECTS

Jae Young Lee, Ph.D.
Cornell University 1986

A new method of element decomposition is introduced in the formulation of a new shell finite element. The actual element is decomposed into a translational element defined completely by the nodal translations and a difference element representing the difference between the actual element and the translational element. An alternative form of coordinate transformation is also suggested to achieve a simple and systematic formulation. Three different types of elements, designated as types I, II and III, are derived by employing different assumptions on the displacement field of each component element. The type III element, in which the rotation of the translational element and the translation of the difference element are suppressed, gives the most favorable results. The element has properties similar to Ahmad's degenerate shell element, but shows better performance than the latter for all test problems considered in this study.

However, the element suffers from locking phenomena for sensitive problems under thin shell situation. Three complementay devices, i.e., reduced integration, addition of internal degees of freedom, and mixed formulation, are considered in order to remove the phenomena. Combination of reduced integration and internal degrees of freedom cures the locking phenomena effectively. But an element with these combined complementary devices gets into trouble due to spurious zero-energy modes for cases with minimum boundary conditions. Two different zero-energy control methods, i.e., α–control

and e–control schemes, are used to eliminate these spurious modes. Proper zero-energy control indices, which can avoid both the locking phenomena and the spurious zero-energy modes, are obtained through numerical studies.

The element is applied in analyses of two biological problems, eggshell breakage and stomatal opening, which have been frequently studied by many researchers. The stresses and the deformed shapes are graphically represented by a microcomputer based postprocessor developed for this study.

BIOGRAPHICAL SKETCH

The author was born on November 12, 1948, in Seoul, Korea. He graduated from Seoul National University with honor in 1970, and received B.S. degree in Agricultural Engineering. He attended a one–year postgraduate course at International Institute in Hydraulic Engineering in Delft, the Netherlands in 1977. He received M.S. degree at Seoul National University in 1980. He worked at Korea Electric Company and Agricultural Development Corporation in Korea from 1970 to 1980. He joined Jeonbug National University in 1980. He started his Ph.D. program at the Department of Agricultural Engineering, Cornell University in 1982. He has a special interest in finite element method and its application to agricultural engineering. He is living with his wife, Young Ja and a daughter, Kyoung Hee.

ACKNOWLEDGEMENTS

TABLE OF CONTENTS

LIST OF FIGURES

LIST OF TABLES

Chapter 1

INTRODUCTION

A *shell* is defined as a curved surface wall. Shells can be found in many places such as the dome of a building, an arch dam, a pressure vessel, a machine part, the hull of an airplane or a ship, etc. Shells have become many of the structural or architectural parts ever since ancient times, not only due to aesthetic reasons, but also due to the fact that combination of proper geometrical form and usual surface loading leads to efficient behavior–almost pure compression or tension over most of shell. For these reasons, shells tend to be present in 'natural' or biological structures as well. Accordingly, it has long been of great interest for structural theorists, as well as structural designers. Many shell theories and analysis tools have been developed and used. However, exact closed-form solutions by classical shell theories involve formidable complexity and difficulties even for a simple configuration, and therefore have been limited to special geometric shapes like circular cylinders, spheres, conical shells, and so on. After all, analytical methods are not applicable to irregular problems with arbitrary geometry, load conditions, and boundary conditions. There have also been experimental approaches. But experimentally measured data are not available for every general case encountered in common structures. Thus, approximate analysis methods based on simplification and idealization of shell behaviors have been predominantly used in practice by engineers.

Generality of solution can be achieved only by numerical approaches which came into actual use after the advent of computers in the 1950's. Above all things, the appearance of the finite element method began an epoch for both

1

numerical methods and structural analysis. Neither the complexity of the geometry nor that of boundary conditions poses a restriction in the analysis due to this powerful numerical technique.

Many engineering disciplines have been involved in developing or applying the finite element method. Application of the method became diverse and manifold. One of the areas in which the finite element method can play an important role is biological engineering or more specifically biomechanics. Recently, there has been growing interest in applying the finite element technique to the analysis of biological systems. The present study was first motivated by that kind of interest. Many biological systems can be modelled as a shell. This study was intended for the analysis of shell-type biological objects. And there was a need for an analysis tool. Thus, the finite elements for shell analysis became the primary concern of the study.

One can find that a great portion of the development effort in the finite element method have been devoted to shell analysis. This fact reflects not only the importance but also the difficulties involved in the finite element analysis of shells. The development of the finite element method for shell analysis has been stimulated by the need of civil, mechanical, and aerospace structural design, and has been active for the last twenty years. There are many shell elements available today as recounted in Section 1.1. Various shell elements have been applied to biological problems. Some of them are mentioned in Section 1.3. There are a few finite elements or computer programs specialized for certain biological problems. Those elements or programs may be most effective for the given problems. However, they are devoid of generality and not applicable to others. If there is really a reliable and generalized element, it should be able to relieve the burden of developing such special-purpose finite elements.

There has been a constant desire to obtain a shell element good for both thick and thin shells. That is also a desire to achieve more generality and reliability. As another effort to satisfy that desire, a new finite element for shell analysis is formulated in the present study. A new method of element decomposition is also suggested as a basis for the formulation.

The formulation presented in this study is not destined for exclusive application to biomechanics. Accordingly, the focus of the study is more fundamental and general than biological problems.

The finite element analysis consists of three phases: formulation, implementation, and application. All these three phases are integrated in this study. The greatest portion of the study is related to the formulation of a new finite element for shell analysis. Only one chapter is devoted to the application to biological systems. But this study will serve as preparation for more extensive application to biological problems. Thus it will have significance for both finite element method and biological engineering.

1.1. Shell elements

As a result of extensive studies on the finite element analysis of shells during the last two decades, many shell elements have been developed and are being used. Shell elements can be classified largely into the following four types:

1. A *flat element*, obtained by superposition of a plane stress element and a plate bending element.

2. A *curved thin shell element* based on Kirchhoff-Love assumptions and formulated by shell theory.

3. A *three-dimensional solid element* applied to shells.

4. A *degenerate shell element* obtained by collapsing the thickness of a three dimensional solid element.

1.1.1 Flat elements

Shell problems can be modelled efficiently by an assembly of the flat elements. Each flat element has an approximate displacement field for both membrane and bending stresses. A flat triangular shell element was first introduced by Green et al. (1961). Clough and Johnson (1968) divided the plate element into three subelements and assumed nine displacement functions in each subelement in order to develop displacement functions which maintain full compatibility along the three edges. The flat element can handle rigid body displacement and can be made fully compatible. This element is attractive because it is easily formulated and requires simple geometric description. However, it has a critical shortcoming due to the uncoupling of membrane and bending actions. The coupling between in-plane and bending behavior occurs only at nodes joining adjacent elements which are not coplanar. In the case of a slit cylinder subject to torsion, all stresses except the twisting moment should be negligible everywhere, but the flat element cannot achieve the correct answer for this problem. A cylinder under uniform internal pressure is another case for which the flat element fails to give the correct solution because it produces artificial bending moments.

A modified version of the flat element (Knowles et al., 1976) was obtained by combining the constant-strain triangle and the famous BCIZ plate bending element (Bazeley et al., 1965). Moderately good performance can be obtained by this element when either membrane or bending action is predominant. But it becomes extremely poor when there exists a strong coupling between membrane and bending stiffness (Knowles et al., 1976).

Melosh (1965) and Utku (1967) developed a flat triangular element in which the transverse shear deformations are considered. These elements are

effective for a thick shell, but are quite uneconomical for the thin shell situation due to large transverse stiffness. To achieve convergence to Kirchhoff solutions, Wempner (1968) applied discrete Kirchhoff constraints to a shell element similar to Melosh's element.

A number of higher order flat elements have also been developed. Olson and Bearden (1979) obtained an 18 degee-of-freedom flat triangular element by incorporating in-plane rotations at each vertex of the original flat element. The resulting displacement element is compatible but not complete. Although the element produces rapid convergence, the answers deviate from the correct ones in many applications. Argyris *et al.* (1977) derived another 18 d.o.f. facet triangular shell element (TRUMP) based on a physical lumping idea with a mechanical interpretation. The element gives a relatively economical solution with engineering accuracy. The element should be used with caution because the stiffness matrix becomes indefinite if one of the vertex angles exceeds 90°.

1.1.2 Curved thin shell elements based on shell theory

The classical curved thin shell element formulations are based on either shallow or deep shell theories. The displacement field is generally defined by the mid-surface displacements based on the Kirchhoff assumptions. The rotation of the midsurface involves second derivatives of the normal displacement of the surface. Therefore, C^1 continuity of normal displacement is required for convergence. Even relatively small interelement discontinuities of slope may lead to large perturbations in the local stress distributions (Strickland and Loden, 1968). Conner and Brebbia (1967) developed a rectangular thin shell element based on shallow shell assumptions. The element employs

linear variation of displacements and does not include all the required rigid-body modes. Yang (1973) also developed a rectangular shallow shell element with displacement functions expressed as products of one dimensional, first-order Hermitian interpolation formulas. By use of such displacement functions, the six rigid-body modes required for the shell are implicitly included.

Rectangular shell elements are easily formulated and give fast convergence (Connor and Brebbia, 1967). However, the poor geometrical representation of curved surfaces and boundaries is a critical shortcoming of the rectangular elements. The curved triangular thin shell element of Strickland and Loden (1968) is also derived from shallow shell theory. Linear variation of in-plane displacements and cubic variation of normal displacements are assumed. The interelement slope continuity is achieved in a similar way as in the *BCIZ plate bending element* (Bazeley *et al.*, 1965) which enables all the required rigid body modes to be included. However, the performance of the element is only slightly better than the flat triangular element (Clough and Johnson, 1968).

Bonnes *et al.* (1968) employed a cubic variation for all three displacement components. They divided an element into three subtriangles to satisfy the interelement compatibility requirements. This element is similar to the flat triangular family of elements in that the membrane and bending stiffness matrices are determined separately and are then superimposed. But the geometry of the elements is specified by constant curvatures assumed within each element by a quadratic function. The desired coupling of the in-plane and the bending actions is introduced by the presence of the curvature. The performance of the element for the cylindrical roof case shows some improvement over the element of Strickland and Loden (1968). Another 36 d.o.f. shallow shell element by Cowper *et al*. (1970) uses a constrained quintic

polynomial (21 terms) for normal displacements and cubic polynomials (10 terms each) for tangential displacements. They chose the displacement field so as to provide equivalent accuracy for both the tangential and the normal displacement components.

Dawe (1975,1976) contended that it is more efficient to use quintic polynomial for all the three displacement components. A triangular thin shell element of Stolarski *et al.* (1964) is also similar to the flat element. It is formed by combination of a constant *membrane element* and a *discrete Kirchhoff bending element*. However, the strain-displacement relationship is based on the shallow shell assumption, and bending and membrane actions are coupled. They introduced a mode decomposition technique to avoid membrane locking and to achieve the correct relationship between membrane and bending effects.

The equations in most *shallow shell formulations* have been written on a flat base plane onto which the actual surface is projected, and the curvature is assumed to be constant over the element. These assumptions make the shallow shell formulations simpler than the *deep shell formulations* (Cook, 1981). However, as indicated by Morris(1973,1976), the mapping between a curved and a flat surface transforms the polynomial solutions into transcendental form. Another difficulty is the appearance of interelement gaps between adjacent curved elements, although these shrink as the mesh is refined.

The shallow shell formulation can be used to derive deep shell elements. Cowper *et al.* (1971) extended their shallow shell element (1970) to obtain a deep shell element using a suitable transformation between the shallow shell d.o.f. and those for the deep shell.

A more general approach in deep shell formulation is based on *non-shallow* or deep shell theory. There are many shell theories (Baker,1972;

Flügge,1960; Gould,1977) which are distinguished chiefly by their strain-displacement relationships. A different element will be derived depending on which of the theories is applied. The displacement behavior is commonly expressed with reference to curvilinear coordinates in the mid-surface of the shell. The formulation and implementation of deep shell elements is relatively complex, and requires much more effort than simpler elements. Therefore, construction of an individual element stiffness matrix tends to result in high computing cost even though the convergence is fast.

The *SHEBA deep-shell element* of Argyris and Scharpf (1971) is based on the natural strain concept. The strain-displacement relationship and the geometry are described in terms of triangular natural coordinates. Adoption of natural coordinates considerably simplifies the formulation and assures the existence of rigid-body modes. (Argyris and Scharpf,1968) The displacement field for bending action is identical to that of the *TUBA plate bending element* (Argyris *et al.*,1968; Argyris and Buck,1968) which is based on complete polynomial functions for the normal deflection of order higher than quintic. The nodal d.o.f at the vertices of the triangle include the first and the second derivatives as well as the values of displacements. The inclusion of second derivatives is intended to ensure the continuity of stresses and moments at the vertices but may cause an overcompatibility and thus stiffen the element. The overcompatibility is likely to make higher order elements too stiff, and their performance deteriorates. Nevertheless, the element is known to be relatively accurate.

Dupuis and Goel (1970) developed a similar thin shell element based on *Koiter's theory of thin shells.* In order to assure C^1 continuity and thus convergence, they used *basic functions* which are equivalent to the *rational functions* (Bazeley *et al.*,1965) employed in the BCIZ element.

Wu (1981) adopted a similar approach based on the *natural strain concept*. The displacement fields are expressed by complete cubic polynomials and rational functions (Belytschko,1981) which are added in order to satisfy C^1 continuity. *Substitute shape functions* (Razzaque, 1973) are employed to make the element more flexible. Mohr (1980) also applied the natural strain concept to his 27 d.o.f. element which is obtained by coupling a quartic bending element with a linear strain membrane element.

1.1.3 Three-dimensional solid elements

A shell can be considered as a special case of a three-dimensional continuum, and 3-D solid elements with quadratic or cubic shape functions can be used directly in the analysis of curved shells simply by reducing their dimension in the shell thickness direction. (Zienkiewicz, 1977) The *20-node brick element* with quadratic isoparametric shape function has been commonly used in thick shell analysis. Dovey (1974) applied the 3-dimensional approach to thin shell analysis by incorporating geometric constraints on the permissible displacements of individual nodes. A cubic shape function gives improved results with additional computing cost. One can eliminate the mid-surface node points from the quadratic or cubic element by assuming zero normal strain and linear variation of tangential strains in the thickness direction. However, the transverse shear strains are still retained. Numerical evidence has shown that the above assumptions are not sufficient to recapture the behavior of curved thin shells (Gallagher,1976). The element is too stiff to represent the bending behavior of thin shells.

Various schemes have been proposed to overcome these difficulties (Dupuis,1970, Wilson,1971, Dovey,1974). However, the use of 3-D elements

has distinct disadvantages. First, it is economically inefficient because several layers of elements or a large number of degrees of freedom in the thickness direction are required in order to model the bending behavior properly. Second, numerical troubles may arise as the thickness to length ratio becomes large. And third, it is difficult to attach these elements to their neighbors at lines of abrupt curvature changes. The degenerate shell element can be regarded as an extension of the 3-D element devised to surmount these difficulties.

1.1.4. Degenerate shell elements

Ahmad *et al.* (Ahmad,1970) formulated the 8-node degenerate shell element for application to the thick shell. The element is often called an *isoparametric shell element*, although it is in fact superparametric. The element is obtained by collapsing the nodes, in the thickness direction, of a three-dimensional solid element into one node on the middle surface. The mid-surface translations and the rotations of the normal are independently interpolated from nodal variables using the *serendipity shape functions*, a procedure which is analogous to the *Mindlin plate element theory* (Cook,1981). This relieves the Kirchhoff assumption, and incorporates the transverse shear effects. The normal sections are assumed to remain plane but not normal after deformation. The major difficulty in thin shell elements originates from C^1 continuity requirements due to the Kirchhoff assumptions. It is difficult to construct shape functions which satisfy C^1 continuity.

The formulation of the degenerate shell element is relatively simple because the full C^1 continuity requirement is not imposed. *Melosh's flat triangular element* (Melosh,1965) and the element by Key and Beisinger (1970) are similar in this point. The performance of these elements with

transverse shear effect is poor in the thin shell situation, and may not be acceptable for sensitive problems. Zienkiewicz *et al.* (1971) and Pawsey and Clough (1971) applied a reduced or selective integration technique to the degenerate shell element to improve the convergence of the element in thin shell applications. Takemoto and Cook (1973) modified the element by an alternative form of coordinate transformation, use of stiffness coefficients for sandwich construction, and inclusion of *bubble functions*. They showed that the formulation can be simplified by adopting global Cartesian coordinates instead of local coordinates as in the original formulation. Irons and Razzaque (1973) obtained a thin plate bending element by imposing *discrete Kirchhoff constraints* at 2x2 integration points of *Ahmad's element*. It was found later that the element significantly violates interelement compatibility and gives erroneous results for elements of other than triangular shape (Irons ,1976).

Kanoknukulchai (1979) developed a four node bilinear shell element based on the degeneration concept. The element is basically the same as Ahmad's degenerate element except that it uses three rotational d.o.f. instead of two. The solution may not converge as the mesh becomes refined, because the d.o.f. associated with in-plane rotation causes a weakly-restrained torsional mode. As a remedy, torsional stiffness is added by two penalty functions, but there are inherent numerical difficulties in selecting the values of the penalty parameters.

The *SemiLoof element* by Irons (1976) is another form of degenerate shell element with discrete Kirchhoff constraints. The element has eight Loof nodes in addition to the corner and midside nodes. The nodal translations and rotations are interpolated independently as in Ahmad's element but two different shape functions are used. The unconstrained 'virgin element' has 43 d.o.f. The 11 constraints are imposed to make the appropriate shear strains

vanish at the 2x2 Gauss points, the *Loof nodes*, and the center. As a result, the total number of d.o.f. is reduced to 32. The element has high accuracy, but the formulation is very complex and its implementation into a computer program is difficult. The element is too flexible under a point load.

1.2   Motivation for a new element

There have been enormous efforts to find a good element for use with both thin and thick shells. As a result, a great number of elements have been developed, and more continue to be proposed. Only a few of these were mentioned in the previous section. However, none of them has appeared as the best one. An element good for a certain type of problems may be poor for others. Hughes and Cohen (1977,1978) expressed their dissatisfaction with the current shell elements as follows:

> None of the (shell) elements developed so far is suitable for inclusion in finite element codes which are widely disseminated. The reason for this is that the most important attribute of elements in the hands of the average user is reliability.
> One of the first tasks facing a potential practitioner of the finite element method is element selection. At this stage one is confronted with the bewildering array of elements that has resulted from over twenty years of research activity. No one particular element has emerged as the so called 'best ' element.

The most important attributes of an element are accuracy, simplicity and generality. Flat elements are simple and easy to formulate and implement but are not accurate. The solution may not converge to the correct one for certain problems. Thin shell elements based on shell theories are relatively accurate but tend to be extremely complicated and require high computational cost, especially when deep shell theories are involved. These elements are applicable only to thin shells and are therefore devoid of generality. Generality should be stressed in view of practical applications, because even the choice

between thin and thick shell categories is in the hands of average users. There may be some problems which contain both thin and thick shell categories.

There are also cases, such as fracture analysis, for which transverse shear effects are important. The stress intensity factor for mode III fracture is a function of transverse shear stresses. However, any information about the transverse shear stresses can not be retrieved by thin shell elements. Barsoum (1976) indicated that there exist no thin plate or shell elements which contain the required singularity of $r^{-1/2}$.

Some of the thin shell elements are not valid for plate bending analysis. Under these circumstances, acceptance or general use of these thin shell elements is precluded. Furthermore, thin shell elements require significant efforts for data preparation, because accurate geometric representation is essential for these elements. Some of the thin shell elements have the second derivatives of the normal displacements as nodal variables which make the specification of boundary conditions even more difficult. These may be some of the reasons that the degenerate type of shell elements has been used more and more recently even though these elements are not as accurate as the thin shell elements. The loss in accuracy is more than compensated for by reduced computational cost of an efficient element (Gallagher,1975). The most popular among these degenerate shell elements might be Ahmad's element (1970). The element may have more generality than any other types of elements, because it has become applicable not only to thick shells but also to thin shells by the use of the reduced integration technique. Strangely enough, however, most of the previous studies on Ahmad's element have been limited to quadrilateral shapes although the triangular elements are practically more useful. The satisfactory performance of the quadrilateral degenerate shell element is unexpected (Irons, 1976) and it is due to coincidence that the

transverse shear strain vanishes at the reduced integration points (Cook,1981). Unfortunately, this coincidence does not happen for triangular elements. Numerical studies in the present work have revealed that the performance of the element with triangular or significantly distorted quadrilateral shape is much poorer than that of regular quadrilateral shape. Batoz *et al.* (1980) and Belytscheko *et al.* (1984) also observed that the reduced integration is ineffective for triangular elements.

The quadrilateral element with reduced integration gives satisfactory solutions for the so-called sensitive problems (Morris,1973,1976). It was found that the element suffers from the locking phenomenon, as shown in Fig.B.3, for a quarter cylinder subjected to pure bending. This suggests that the element is not as reliable as was reported in previous studies (Fezan,1982; Takemoto,1973; Zienkiewicz 1971). The formulation of the element is too loyal to the degeneration concept. One can easily identify that the bending and the membrane actions are artificially coupled in the process of coordinate transformation and interpolation within a curved element. Inextensional bending is disabled by this undesirable coupling. It causes locking for a curved shell under pure bending action. The number of zero eigenvalues decreases as the curvature increases, which implies a lack of rigid body modes.

As will be shown in subsequent chapters, one can derive an element equivalent to the degenerate shell element through a completely different but simpler and more generalized procedure based on a new concept of element decomposition and a new procedure of coordinate transformation. The element has the correct number of rigid body modes regardless of the shell curvature, and is capable of representing a pure bending state. As described in the fourth chapter, numerical tests prove that the performance of the element is always better than that of the popular Ahmad's degenerate element. It is relatively easy

to modify, or add complementary devices to, the element. To obtain satisfactory performance for triangular shapes, several modifications are made to the element, which include the addition of internal d.o.f. and application of mixed formulation. <u>The eventual objective is to construct an element which is applicable for both thin and thick shells and which can be of triangular as well as of quadrilateral shape.</u>

1.3   Finite element   shell analysis in biomechanics

Hatze (1974) defined *Biomechanics* as a study of the structure and function of biological systems by means of the methods of mechanics. The subject of the study ranges from the microscopical cellular level to the human or animal body. Most of the work in this area has been done by mechanical engineers and medical scientists who have been oriented towards medical applications. On the other hand, agricultural engineers together with biologists have shown more concern for basic knowledge of biological objects which may be related to production, processing or handling of food and agricultural products.

Biomechanics has a long history of development (Fung 1976, King 1984). Classical solid and fluid mechanics have been the major analysis tools. Recently, biomechanics has made rapid progress due to numerical methods and computer simulations. Especially, the finite element method has broadened the methodology of biomechanics to a large extent. There is also a tendency that many classical problems are reviewed by use of this powerful method which enables more realistic and sophisticated modelling. Although biomechanics usually imports the advances in finite element method achieved in other disciplines, there are a number of finite element formulations (Spilker

1982, Beaupre and Hayes 1985) and computer programs (Pao 1982) specialized for biological problems.

There are many biological systems which have a shell-like geometry and mechanical behavior. The following is a brief review of some shell-type biological problems which have been modeled by the finite element method.

The mechanical behavior of individual cells consisting biological tissues is often modeled as a shell. Pitt and Davis (1984) analyzed a parenchyma cell as a thin-walled, fluid filled sphere. They used axisymmetric solid elements for both the inside fluid and the cell wall, and assigned a single layer of elements to the latter.

Zarda *et al.* (1977) formulated a finite element specialized for red blood cell analysis. They modeled the biconcave cell shape as a shell of revolution. Their modeling is considered to be more realistic and accurate than previous analytical ones, because the analytical solutions assumed spherical shapes and could not represent the bending actions properly.

Cooke *et al.* (1976) analyzed stomatal guard cell deformation using 7-node thin shell elements for orthotropic elastic materials of doubly elliptical torus and examined the mechanism for opening and closure of stomatal pores. A follow-up study by Cooke *et al.* (1977) modeled the same problem with consideration of geometric nonlinearity.

The finite element modellings at the cellular level may have a difficulty supplying accurate material properties and loading conditions, and are usually based on approximate estimates rather than experimentally measured values. They are, in fact, intended to relate the mechanical behavior with assumed material properties and loading conditions to obtain only quantitative insight into the behavior. Or those unknown parameters are sometimes estimated from the results of analyses.

This is not the case for a large-scaled cell like an egg. Manceau and Henderson (1970) and Upadhyaya *et al.* (1985) used experimentally measured material properties for their finite element analysis of the egg shell. Both groups fit the mathematically expressed eggshell geometry by shell-of-revolution elements. Gates *et al.* (1984) used doubly curved thin shell elements (ANSYS) for the problem of flat plate loading at the equator of an egg.

Yettram *et al.* (1982) suggested a computer graphical technique reconstructing the three-dimensional geometry of human left ventricle, which is intended for mesh generation of finite shell elements.

Gould *et al.* (1973) and Cataloglu *et al.* (1976) analyzed the human aortic valve using 6-node triangular thin shell elements. Humid *et al.* (1985) compared the finite element analysis of aortic valve by membrane shell elements and three-dimensional solid elements.

Pao *et al.* (1974) applied the finite element method for stress analysis of the left ventricular wall. They followed the pattern of a previous simplified analytical approach (Gould, 1972) and partitioned the ventricular wall into two parts, each of which was modeled independently by several layers of axisymmetric solid elements.

McPherson and Kriewall (1980) investigated the deformation of human fetal head using 4-node thin shell elements (SAP IV).

The above review represents only part of the previous work in finite element shell analysis related to biological systems. Many complicated problems have been solved by the finite element method. However, some of the previous works are far from complete, and some aspects of the finite element modelling are not realistic. Although biomechanics is not a new subject, the application of the finite element method in this area is rather new. Careless use of the method by average users in this area may lead to

erroneous results. This is more likely in the case of shell analysis due to its sophisticated characteristics. Therefore, suggesting a methodology for proper application of finite elements to biological problems is as valuable as developing a good finite element.

There still remain many other biological problems which require the use of the finite element analysis technique. It is a challenging task to do more accurate and sophisticated modelling of biological systems using appropriate shell elements.

1.4 Objectives and overview of the study

The objective of this study, in short, is to develop an efficient and simple finite element for both thin and thick shells and to present the potential application of the element to biological problems. The study consists of four major parts: formulation of a new element for shell analysis, implementation of the element, numerical studies, and application to practical problems. A graphical postprocessing program has been developed for use in the present study. However, the discussion of its implementation is not elaborated in this study. That is a subject to be handled in a separate document.

In Chapter 2, a new method of element decomposition is presented for the formulation of shell elements. Three different possibilities of element decomposition are discussed. The displacement model is constructed for each of the possibilities. Subsequently, the strain-displacement relationships and the element stiffness matrices are derived and expressed in a unified format. Several complementary devices are also suggested to improve the performance of the elements. Spurious zero energy modes and their control are treated at the end of the chapter.

Chapter 3 gives a guideline for efficient implementation of the formulation. Computational procedures are suggested for the evaluation of the transformation matrix, numerical integration, and evaluation of load vectors. Section 3.3 describes a slight modification of a frontal solver. The nodal stress smoothing for the shell element is also discussed in this chapter.

Numerical studies based on benchmark problems are presented in Chapter 4. The numerical tests cover convergence tests, patch tests, element distortion tests, and tests on locking behavior and zero energy modes. The accuracy of the new formulation is also examined through comparisons with analytical solutions. The interrelationship of locking and spurious modes is studied thoroughly using two sensitive cases. Many of the figures related to numerical studies are provided in an appendix to improve the readability of Chapter 4.

In Chapter 5, actual biological problems are analyzed using the shell element developed in this study. Stress analysis of an eggshell is the major portion of the work. Stomata of plant leaves are also analyzed. This chapter is intended not only to present the results of the analysis but also to give criticism of previous work and to suggest a methodology for future work with the same kind of problems.

The last chapter summarizes the discussions in the preceding chapters and draws conclusions to the present study. Further extensions of the study are suggested at the end of this chapter.

Chapter 2

FORMULATION OF A NEW FINITE ELEMENT

A new method of element decomposition is suggested for formulation of finite elements for shell analysis. Three different types of elements are derived based on the three different methods of decomposition. The formulation uses a new method of coordinate transformation which facilitates a systematic and simple approach. The element stiffness matrix is derived in three steps: construction of the displacement field by element decomposition, derivation of the strain-nodal displacement relationship, and evaluation of the element stiffness matrix. Complementary devices to remove locking phenomena are also suggested. Zero energy control schemes are discussed at the end of this chapter.

2.1 Coordinate transformation

Formulation of a shell element usually involves rigorous coordinate transformations. The coordinate systems used in the present formulation are first defined, and a new method of coordinate transformation is introduced in this section. The actual computation of transformation matrices is detailed in Section 3.1.

2.1.1 Definition and notation of coordinates

The three coordinate systems used in the formulation are illustrated in Fig.2.1 and defined in the following.

20

Global coordinates

Cartesian coordinates are used as global coordinates for the complete system comprising all elements. Any values expressed in global coordinates are denoted in upright letters such as x,y or δ.

Local coordinates

The local coordinate is a Cartesian coordinate defined by three orthogonal axes *x, y* and *z* at a point in an element. Some of the values expressed in local coordinate are denoted in italic letters such as *x,y* or δ, if necessary for distinction. The local *z* axis is set in the direction normal to the midsurface. Accordingly, the *x* and *y* axes are tangential to the surface. The directions of the three axes are expressed by unit vectors, $\mathbf{v}_1$, $\mathbf{v}_2$, and $\mathbf{v}_3$, each of which has three directional cosines with respect to the global coordinates. A vector in the *z* direction can be found as a cross product of any two vectors tangent to the midsurface (Ahmad *et al.*, 1970).

Natural coordinates

The natural coordinates are dimensionless coordinates representing a relative location of a point within an element. On a surface parallel to the midsurface, ξ and η are either the two independent area coordinates for a triangular element or the $(-1,+1)$ range intrinsic coordinates for a quadrilateral element. In the thickness direction, ζ is a $(-1,+1)$ range intrinsic coordinate normal to the midsurface. Some of the values expressed with respect to natural coordinates are denoted with underlines, if necessary for distinction. For example, $\underline{\alpha}$ and $\underline{\beta}$ are rotations about the axes normal to the ξ and η directions, respectively.

2.1.2 Alternative form of coordinate transformation

One usually obtains a vector $\boldsymbol{\delta}$ at a point p within an element by interpolation of the nodal vectors $\boldsymbol{\delta}_i$. Then, one applies coordinate transformation to convert it into the other coordinate system, say local coordinates.

$$\boldsymbol{\delta} = \sum_{i=1}^{n} N_i \boldsymbol{\delta}_i \qquad (2.1.1)$$

and

$$\delta = \mathbf{R}\,\boldsymbol{\delta} \qquad (2.1.2)$$

in which δ is a vector expressed in the local coordinates, and $\mathbf{R}$ is a rotation matrix transforming the global coordinates into the local coordnates at a desired point.

As an alternative, one may think of reversing the order of interpolation and transformation. That is, one transforms all the nodal values first

$$\delta_i = \mathbf{R}\,\boldsymbol{\delta}_i, \qquad (2.1.3)$$

and interpolates them later

$$\delta = \sum_{i=1}^{n} N_i \delta_i \qquad (2.1.4)$$

This requires more multiplication by the rotation matrix, because one must transform all the nodal values instead of transforming values at point p only. However, as will be shown later, this procedure is more efficient for evaluating the curvature, if required, as well as the Jacobian matrix and other derivative matrices. By this alternative form of the transformation, one can write directly
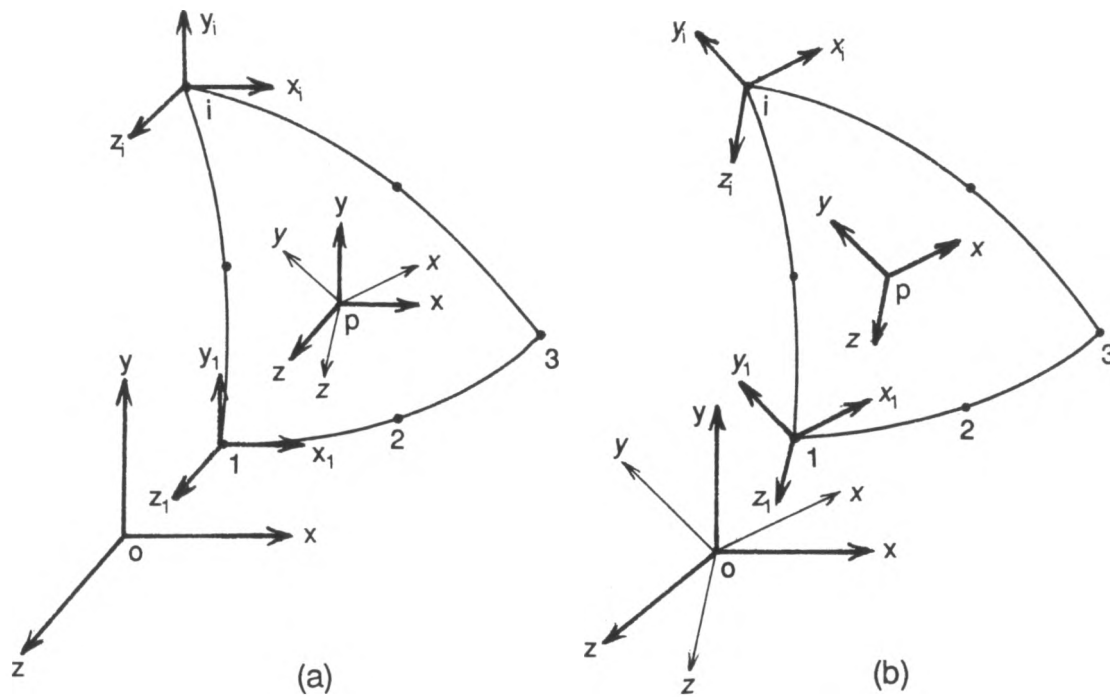
Fig. 2.1   Two alternative procedures of coordinate transformation
(a) transforming the coordinates after interpolation
(b) interpolating the transformed coordinates
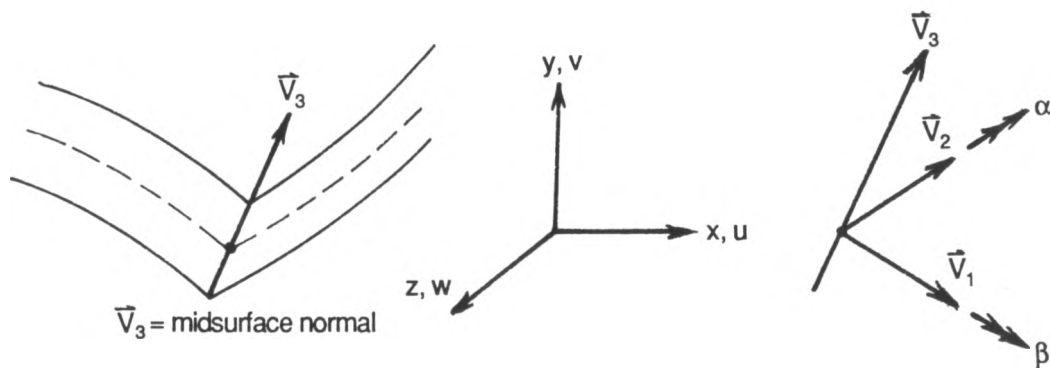
Fig. 2.2   Nodal degrees of freedom in global coordinates

the Jacobian matrix $\mathbf{J}$ which relates the local coordinates and the natural coordinates:

$$\nabla_\xi = \mathbf{J}\,\nabla_x \tag{2.1.5}$$

with

$$\nabla_\xi = \left\{ \begin{array}{c} \dfrac{\partial}{\partial \xi} \\[2mm] \dfrac{\partial}{\partial \eta} \end{array} \right\} \qquad \nabla_x = \left\{ \begin{array}{c} \dfrac{\partial}{\partial x} \\[2mm] \dfrac{\partial}{\partial y} \end{array} \right\} \tag{2.1.5a}$$

and the Jacobian matrix

$$\mathbf{J} = \begin{bmatrix} x_{,\xi} & y_{,\xi} \\ x_{,\eta} & y_{,\eta} \end{bmatrix} \tag{2.1.5b}$$

One can define a new *transformation matrix* $\mathbf{J}_2$ which transforms the first and the second derivatives from local to natural coordinates.

$$\nabla_{\xi\xi} = \mathbf{J}_2\,\nabla_{xx} \tag{2.1.6}$$

with

$$\nabla_{\xi\xi} = \left\{ \begin{array}{c} \dfrac{\partial}{\partial \xi} \\[2mm] \dfrac{\partial}{\partial \eta} \\[2mm] \dfrac{\partial^2}{\partial \xi^2} \\[2mm] \dfrac{\partial^2}{\partial \eta^2} \\[2mm] \dfrac{\partial^2}{\partial \xi \partial \eta} \end{array} \right\} \qquad \nabla_{xx} = \left\{ \begin{array}{c} \dfrac{\partial}{\partial \xi} \\[2mm] \dfrac{\partial}{\partial y} \\[2mm] \dfrac{\partial^2}{\partial x^2} \\[2mm] \dfrac{\partial^2}{\partial y^2} \\[2mm] \dfrac{\partial^2}{\partial \xi \partial y} \end{array} \right\} \tag{2.1.6a}$$

and

$$
\mathbf{J}_2 = \begin{bmatrix}
x_{,\xi} & y_{,\xi} & 0 & 0 & 0 \\
x_{,\eta} & y_{,\eta} & 0 & 0 & 0 \\
x_{,\xi\xi} & y_{,\xi\xi} & (x_{,\xi})^2 & (y_{,\xi})^2 & 2x_{,\xi}y_{,\xi} \\
x_{,\eta\eta} & y_{,\eta\eta} & (x_{,\eta})^2 & (y_{,\eta})^2 & 2x_{,\eta}y_{,\eta} \\
x_{,\xi\eta} & y_{,\xi\eta} & x_{,\xi}x_{,\eta} & y_{,\xi}y_{,\eta} & x_{,\xi}y_{,\eta}+x_{,\xi}y_{,\eta}
\end{bmatrix}
\tag{2.1.6b}
$$

in which the higher order derivatives are also evaluated using interpolation equations. If $\mathbf{J}_2^{-1}$ exists, the inverse relation of Eqn.(2.1.6) can be written as

$$
\nabla_{xx} = \mathbf{J}_2^{-1} \nabla_{\xi\xi}
\tag{2.1.7}
$$

It is convenient to denote $\mathbf{S} = \mathbf{J}_2^{-1}$ and define another 3X5 transformation matrix $\mathbf{S}^*$ for future use:

$$
\mathbf{S}^* = \begin{bmatrix}
S_{31} & S_{32} & \cdots & S_{35} \\
S_{41} & S_{42} & \cdots & S_{45} \\
2S_{51} & 2S_{52} & \cdots & 2S_{55}
\end{bmatrix}
$$

$$
= \begin{bmatrix}
\xi_{,xx} & \eta_{,xx} & (\xi_{,x})^2 & (\eta_{,x})^2 & 2\xi_{,x}\eta_{,x} \\
\xi_{,yy} & \eta_{,yy} & (\xi_{,y})^2 & (\eta_{,y})^2 & 2\xi_{,y}\eta_{,y} \\
2\xi_{,xy} & 2\eta_{,xy} & 2\xi_{,x}\xi_{,y} & 2\eta_{,x}\eta_{,y} & 2(\xi_{,x}\eta_{,y}+\xi_{,x}\eta_{,y})
\end{bmatrix}
\tag{2.1.8}
$$

With these, one can relate the two differential operators using the transformation matrix.

$$
\nabla^*_x = \mathbf{S}^* \nabla_{\xi\xi}
\tag{2.1.9}
$$

with

$$
\nabla^{*}_{x} = \left\{ \begin{array}{c} \dfrac{\partial}{\partial x^2} \\[2mm] \dfrac{\partial^2}{\partial y^2} \\[2mm] \dfrac{2\partial^2}{\partial \xi \partial \eta} \end{array} \right\}
\tag{2.1.9a}
$$

Now, the convenience of the coordinate transformation will be exemplified by the evaluation of surface curvatures, even though the curvature is not involved in the present formulation. To obtain the curvatures at a point p within an element, one first transforms all the coordinates of the nodal points into the local coordinates at that point,

$$
\left\{ \begin{array}{c} x_i \\ y_i \\ z_i \end{array} \right\} = \mathbf{R} \left\{ \begin{array}{c} x_i \\ y_i \\ z_i \end{array} \right\}
\tag{2.1.10}
$$

and interpolates the nodal coordinates:

$$
z = \sum_{i=1}^{n} N_i z_i
$$

$$
\nabla_{\xi\xi}(z) = \nabla_{\xi\xi} \left(\sum_{i=1}^{n} N_i z_i \right) = \sum_{i=1}^{n} \nabla_{\xi\xi}(N_i) z_i
\tag{2.1.11}
$$

in which $\nabla_{\xi\xi}$ is the differential operator defined in Eqn.(2.1.10a). If one denotes $\mathbf{S} = \mathbf{J}_2^{-1}$, then the curvatures of a shallow shell at point p are

$$
k = \begin{Bmatrix} z_{i,xx} \\ z_{i,yy} \\ 2z_{i,xy} \end{Bmatrix} = \begin{bmatrix} S_{31} & S_{32} & \cdots & S_{35} \\ S_{41} & S_{42} & \cdots & S_{45} \\ 2S_{51} & 2S_{52} & \cdots & 2S_{55} \end{bmatrix} \begin{Bmatrix} z_{i,\xi} \\ z_{i,\xi} \\ z_{i,\xi\xi} \\ z_{i,\eta\eta} \\ z_{i,\xi\eta} \end{Bmatrix} \tag{2.1.12}
$$

or

$$
k = \nabla^*_x (z) = S^* \nabla_{\xi\xi}(z) \tag{2.1.12a}
$$

Thus, one can evaluate the curvature without resorting to extra coordinates defined relative to the *base triangle* employed in other references (Strickland *et al.*, 1968; Bonnes *et al.*, 1968)

2.2 New concept of element decomposition

Decomposition of an element is not new and has been used in many other plate and shell elements. For example, the flat element is composed of membrane and bending elements. The BCIZ element (Bazeley *et al.*, 1965) is obtained by superpostition of two displacement fields, i.e., the rigid body displacement field and the remaining ones. Moreover, Stolarsky *et al.* (1984) separated the displacement field into two different modes. However, the concept of decomposition is more generalized in the present study. The actual element is termed the *total element* and is decomposed into a *translational element* and a *difference element* . The nodal displacements are decomposed into the part for the translational element and the remaining part for the difference element. The displacements within each element are determined by independent interpolation of the respective parts of the nodal displacements. The total element is built by superposition of the two component elements. The decomposition is intended not only to simplify and systematize the formulation
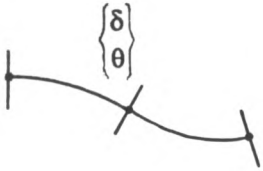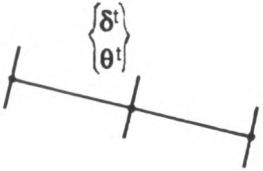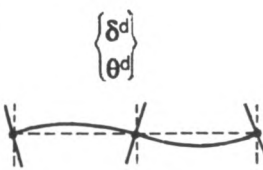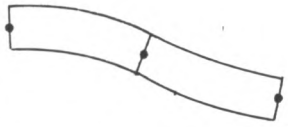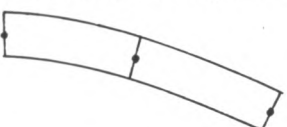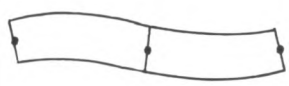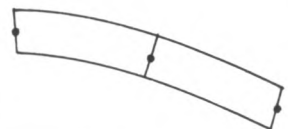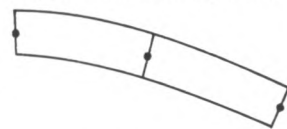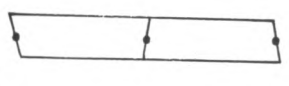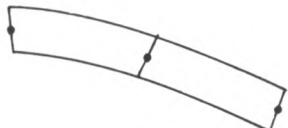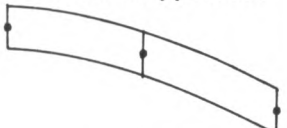
	Total element	Translational element	Diffference element
Displacements of component elements	$\Delta_i = \begin{Bmatrix} u_i \\ v_i \\ w_i \\ \alpha_i \\ \beta_i \end{Bmatrix} = \begin{Bmatrix} \delta_i \\ \theta_i \end{Bmatrix}$ $\Delta = T\Delta^e$	$\delta^t_i = \delta_i$ $\theta^t_i = f(\delta^t_i)$ $\Delta^t = T^t\Delta^e$	$\delta^d_i = 0$ $\theta^d_i = \theta_i - \theta^t_i$ $\Delta^d = T^d\Delta^e$
Type I		Kirchhoff assumptions	Kirchhoff assumptions
Type II		Kirchhoff assumptions	Translation suppressed
Type III		Rotation suppressed	Translation suppressed

Fig. 2.3   Methods of element decomposition

but also to ensure the rigid body displacements. One can arrive at different types of elements depending on the method of decomposing the nodal displacements.

2.2.1 Total element

The total element represents the actual displacement field. The displacement field is defined by five displacement components,

$$\Delta = \lfloor u \quad v \quad w \quad \alpha \quad \beta \rfloor \qquad (2.2.1)$$

in which u, v, and w are translations respectively in the x, y, and z Cartesian directions , and α and β are rotations about two orthogonal axes as illustrated in Fig.2.2. For future convenience, a translation vector and a rotation vector are also defined as

$$\delta = \lfloor u \quad v \quad w \rfloor$$
$$\theta = \lfloor \alpha \quad \beta \rfloor. \qquad (2.2.2)$$

The total element at each node should represent the actual nodal displacements. That is,

$$\Delta(\text{at node i}) = \Delta_i = \lfloor \delta_i \quad \theta_i \rfloor. \qquad (2.2.3)$$

The element nodal d.o.f are denoted by Δ^e.

$$\Delta^e = \lfloor \Delta_1 \cdots \Delta_n \rfloor$$
$$= \lfloor \delta_1 \theta_1 \cdots \delta_n \theta_n \rfloor \qquad (2.2.4)$$
$$= \lfloor u_1 \quad v_1 \quad w_1 \quad \alpha_1 \quad \beta_1 \cdots u_n \quad v_n \quad w_n \quad \alpha_n \quad \beta_n \rfloor$$

2.2.2 Translational element

The translational element is defined completely by nodal translations. The element is denoted with superscript t.

$$\Delta^t = \lfloor \delta^t \; \theta^t \rfloor \tag{2.2.5}$$

The translations represented by the translational element should match the actual nodal translations at each node,

$$\delta^t_i = \delta_i \,,$$

$$\Delta^{te} = \lfloor \delta^t_1 \; \theta^t_1 \; \cdots \; \delta^t_n \; \theta^t_n \rfloor = \lfloor \delta_1 \; \theta^t_1 \cdots \; \delta_n \; \theta^t_n \rfloor . \tag{2.2.6}$$

2.2.3 Difference element

The difference element represents the difference between the total element and the translational element. The element is denoted with superscript d.

$$\Delta^d = \Delta - \Delta^t \tag{2.2.7}$$

The nodal translations of the element are always zero,

$$\delta^d_i = 0, \quad \forall \, i$$

Therefore,

$$\Delta^{de} = \lfloor \delta^d_1 \; \theta^d_1 \; \cdots \; \delta^d_n \; \theta^d_n \rfloor = \lfloor 0 \; \theta^d_1 \; \cdots \; 0 \; \theta^d_n \rfloor \tag{2.2.8}$$

2.2.4 Decomposition of nodal d.o.f.

The nodal d.o.f. can be decomposed in many different ways. One may logically think of   four possibilities depending on whether any or all of the

component elements are subject to the Kirchhoff assumption. The fourth possibility, in which the difference element satisfies the Kirchhoff assumption and the translational element does not, is excluded in the present study because it may not allow rigid body displacement. The other three types of decomposition are designated as type I, type II and type III decompositions. Each type of decomposition is defined below.

Type I decomposition

The displacement fields are decomposed so that both the translational and the difference elements satisfy the Kirchhoff assumption. First the nodal rotations of the translational element are evaluated as a function of surface normal displacement with $\theta^t = \nabla_\xi (w^t)$ which is the statement of the Kirchhoff assumption. And then, the nodal rotations of the difference element are obtained by $\theta^d = \theta - \theta^t$. The translations within the translational element are determined by interpolation of nodal translations, and the normal displacement within the difference element is determined from nodal values of θ^d.

Type II decomposition

In type II decomposition, the translational element satisfies the Kirchhoff assumption but the difference element allows transverse shear deformations. The nodal displacements are decomposed in the same way as the type I decomposition. The translations of the translational element are determined by interpolation of nodal translations. The normal displacement of the difference element is restrained to be zero, and the rotations are evaluated by independent evaluation of the nodal values of α^d and β^d.

Type III decomposition

In type III decomposition, the rotation of the translational element and the translations of the difference element are restrained to zero. The translations of the translational element and the rotations of the difference element are obtained by independent interpolation of corresponding nodal values.

2.3   Decomposition of an element

The concept of element decomposition has been introduced in the preceding section. In this section, the displacement field within an element is constructed on the basis of each decomposition method. An element is, hereinafter, designated as type I, type II or type III element, according to the method of decomposion. Interpolations of the displacement field from the nodal displacements are expressed by the *displacement function matrix* which is given in the same format for all three different types of element decomposition.

2.3.1 Type I decomposition

Translational element

The displacement vector of the translational element is given by Eqn. (2.2.6). The translations are obtained by interpolation of nodal values,

$$\delta^t = \sum_{i=1}^{n} N_i \delta_i \tag{2.3.1}$$

and in local coordinates,

$$\delta^t = \sum_{i=1}^{n} N_i \delta_i = \sum_{i=1}^{n} N_i \mathbf{R} \, \delta_i \tag{2.3.2}$$

in which δ denotes a translation vector in the local coordinates and $\mathbf{R}$ is the rotation matrix evaluated at the point of consideration. One can relate δ^t to the element nodal d.o.f. in the form of

$$\delta^t = \mathbf{L}\,\Delta^e \qquad (2.3.3)$$

with

$$\Delta^e = \lfloor u_1 \;\; v_1 \;\; w_1 \;\; \alpha_1 \;\; \beta_1 \cdots u_n \;\; v_n \;\; w_n \;\; \alpha_n \;\; \beta_n \rfloor \qquad (2.2.4)$$

$$\underset{3\times 5n}{\mathbf{L}} = [\; \underset{3\times 3}{N_1\mathbf{R}} \quad \underset{3\times 2}{\mathbf{0}} \quad N_2\mathbf{R} \quad \mathbf{0} \cdots N_n\mathbf{R} \quad \mathbf{0}\;] \qquad (2.3.3a)$$

or

$$\underset{3\times 5n}{\mathbf{L}} = \begin{bmatrix} \mathbf{L}_1 \\ \mathbf{L}_2 \\ \mathbf{L}_3 \end{bmatrix} = \begin{bmatrix} N_1 R_{11} & N_1 R_{12} & N_1 R_{13} & 0 & 0 \cdots N_n R_{11} & N_n R_{12} & N_n R_{13} & 0 & 0 \\ N_1 R_{21} & N_1 R_{22} & N_1 R_{23} & 0 & 0 \cdots N_n R_{21} & N_n R_{22} & N_n R_{23} & 0 & 0 \\ N_1 R_{31} & N_1 R_{32} & N_1 R_{33} & 0 & 0 \cdots N_n R_{31} & N_n R_{32} & N_n R_{33} & 0 & 0 \end{bmatrix}$$

$$(2.3.3b)$$

For simplicity, Eqn.(2.3.3c) can be rewritten as

$$\underset{1\times 5n}{\mathbf{L}_k} = [\; \underset{1\times 3}{\mathbf{H}_{k1}} \quad \underset{1\times 2}{\mathbf{0}} \quad \mathbf{H}_{k2} \quad \mathbf{0} \cdots \mathbf{H}_{k3} \quad \mathbf{0}\;] \quad \text{for } k=1,2,3 \qquad (2.3.4)$$

with

$$\mathbf{H}_{k1} = N_1 \mathbf{R}_k \qquad (2.3.4a)$$

$$\mathbf{R}_k = \lfloor R_{k1} \;\; R_{k2} \;\; R_{k3} \rfloor \qquad (2.3.4b)$$

Let $\underline{\mathbf{L}}_k'$ be the first derivative of $\mathbf{L}_k$ with respect to the natural coordinates. Differentiation of Eqn.(2.3.4) with respect to the natural coordinate ξ and η yields $\underline{\mathbf{L}}_k'$.

$$\underset{2\times 5n}{\underline{\mathbf{L}}_k'} = \nabla_\xi(\mathbf{L}_k) = [\; \underset{2\times 3}{\underline{\mathbf{H}}_{k1}'} \quad \underset{2\times 2}{\mathbf{0}} \quad \underline{\mathbf{H}}_{k2}' \quad \mathbf{0} \cdots \underline{\mathbf{H}}_{kn}' \quad \mathbf{0}\;] \qquad (2.3.5)$$

$$\underline{\mathbf{H}}_{ki}' = \nabla_\xi(\mathbf{H}_{ki}) = \nabla_\xi(N_i)\mathbf{R}_k + N_i\nabla_\xi(\mathbf{R}_k) \qquad (2.3.5a)$$

Once $\underline{L}_k{}'$ is evaluated, the derivatives with respect to the local coordinates are obtained simply by use of the Jacobian inverse.

$$L_k{}' = J^{-1}\underline{L}_k{}' = \begin{bmatrix} H'_{k1} & 0 & H'_{k2} & 0 & \cdots & H'_{kn} & 0 \end{bmatrix} \qquad (2.3.6)$$
$$\underset{2\times5n}{} \qquad \underset{2\times3}{} \quad \underset{2\times2}{}$$

$$H'_{ki} = J^{-1}\underline{H}'_{ki} \qquad (2.3.6a)$$

When R is evaluated by interpolation of nodal values using $\sum\limits_{i=1}^{n} N_i R_{(i)}$

$$\nabla_\xi(R_k) = \nabla_\xi\left(\sum_{i=1}^{n} N_i R_{k(i)}\right) = \sum_{i=1}^{n} \nabla_\xi(N_i) R_{k(i)} \qquad (2.3.7)$$

where $R_{(i)}$ is a rotation matrix evaluated at node i. Assuming that the curvature of an element is not large, one may set $\nabla_\xi(R_k) = 0$.

If one denotes with underlines the rotations expressed in natural coordinates such as

$$\underline{\theta} = \nabla_\xi(w)$$
$$\underline{\theta}^t = \nabla_\xi(w^t), \text{ etc.} \qquad (2.3.8)$$

then,

$$\underline{\theta}^t = J\theta^t \qquad \text{or} \qquad \theta^t = J^{-1}\underline{\theta}^t \qquad (2.3.9)$$

Since the translational element, in type I decomposition, is subject to the Kirchhoff assumption, the rotation can be expressed in terms of the surface normal translation.

$$\underline{\theta}^t = \begin{Bmatrix} \underline{\alpha}^t \\ \underline{\beta}^t \end{Bmatrix} = \begin{Bmatrix} w^t{}_{,\xi} \\ w^t{}_{,\eta} \end{Bmatrix} = \nabla_\xi(w^t) \qquad (2.3.10)$$

From eq.(2.3.3) and (2.3.10)

$$\underline{\theta}^t = \nabla_\xi(L_3\Delta^e) = \underline{L}_3{}' \Delta^e \qquad (2.3.11)$$

$$\theta^t = \mathbf{J}^{-1}\underline{\theta}^t = \mathbf{J}^{-1}\underline{\mathbf{L}}_3{}' \Delta^e = \mathbf{L}_3{}' \Delta^e$$

Now, the displacements of the translational element can be written in terms of the element nodal d.o.f. of the total element.

$$\Delta^t = \begin{Bmatrix} u^t \\ v^t \\ w^t \\ \alpha^t \\ \beta^t \end{Bmatrix} = \begin{Bmatrix} \delta^t \\ \theta^t \end{Bmatrix} = \begin{bmatrix} \mathbf{L} \\ \mathbf{L'}_3 \end{bmatrix} \Delta^e = \mathbf{T}^t \Delta^e \qquad (2.3.12)$$

in which

$$\mathbf{T}^t = \begin{bmatrix} \mathbf{L} \\ {\scriptstyle 3x5n} \\ \mathbf{L}_3{}' \\ {\scriptstyle 2x5n} \end{bmatrix} \qquad \text{or} \qquad \begin{bmatrix} \mathbf{T}^t{}_1 \\ \mathbf{T}^t{}_2 \\ \mathbf{T}^t{}_3 \end{bmatrix} = \mathbf{L} \qquad (2.3.12a)$$

$$\begin{bmatrix} \mathbf{T}^t{}_4 \\ \mathbf{T}^t{}_5 \end{bmatrix} = \mathbf{L}_3{}'$$

For future use, the k$\underline{\text{th}}$ row of $\mathbf{T}^t$ is denoted by $\mathbf{T}^t{}_k$. The matrix $\mathbf{T}$ is designated as the displacement function matrix. The matrix $\mathbf{T}^t$ represents the portion of the displacement function matrix contributed by the translational element.

Difference element

Although the total element is constructed by superposition of the translational and the difference elements and is not determined yet, the nodal contribution of the difference element is obtained using the relation

$$\Delta^d = \Delta - \Delta^t \qquad (2.3.13)$$

or in local coordinates,

$$\Delta^d = \Delta - \Delta^t \qquad (2.3.14)$$

Here, one must distinguish beween two different notations. Δ_i denotes the displacements of node i expressed in the local coordinates of a point in consideration within the element, while $\Delta_{(i)}$ is the displacements expressed in the local coordinates of node i. Naturally, $\Delta_{j(i)}$ implies the displacement of node j expressed in the local coordinates of node i. For simplicity, however, the displacement at node i expressed in the local coordinate of node i will be denoted by $\Delta_{(i)}$ instead of $\Delta_{i(i)}$.

$$\Delta^d_{(i)} = \Delta_{(i)} - \Delta^t_{(i)} \tag{2.3.15}$$

$$\left\{ \begin{array}{c} \delta^d_{(i)} \\ \theta^d_{(i)} \end{array} \right\} = \left\{ \begin{array}{c} \delta_{(i)} \\ \theta_{(i)} \end{array} \right\} - \left\{ \begin{array}{c} \delta^t_{(i)} \\ \theta^t_{(i)} \end{array} \right\} \tag{2.3.15a}$$

The nodal translation consists only of the contribution of the translational element; therefore,

$$\delta^t_{(i)} = \delta_{(i)} \quad \text{and} \quad \delta^d_{(i)} = 0 \tag{2.3.16}$$

The rotation of the translational element at node i can be evaluated by applying Eqn.(2.3.6) and (2.3.11) at the node,

$$\theta^t_{(i)} = L'_{3(i)} \Delta^e = [\ \underset{2\times3}{H'_{31(i)}} \quad \underset{2\times2}{0} \quad H'_{32(i)} \quad 0 \quad \cdot \quad \cdot \quad \cdot \quad H'_{3n(i)} \quad 0\ ] \Delta^e \tag{2.3.17}$$

One can express the relation between $\theta_{(i)}$ and the element nodal d.o.f. as follows;

$$\theta_{(i)} = [\ \underset{\underset{1}{2\times3}}{0} \quad \underset{2\times2}{0} \quad \underset{\underset{2}{2\times3}}{0} \quad 2\times2} \cdot \cdot \cdot 0 \quad \underset{\underset{i}{2\times3} \ 2\times2}{I} \cdot \cdot \cdot 0 \quad \underset{\underset{n}{2\times3} \ 2\times2}{0}\ ] \Delta^e \tag{2.3.18}$$

in which I is a (2x2) unit matrix. Substituting Eqn.(2.3.17) and (2.3.18) into $\theta^d_{(i)} = \theta_{(i)} - \theta^t_{(i)}$, one obtains

$$\theta^d_{(i)} = [\ \underset{2\times3}{-H'_{31(i)}} \quad \underset{2\times2}{0} \quad \cdot \quad \cdot \quad \cdot \quad \underset{2\times3}{-H'_{3i(i)}} \quad \underset{2\times2}{I} \quad \cdot \quad \cdot \quad \cdot \quad -H'_{3n(i)} \quad 0\ ] \Delta^e \tag{2.3.19}$$

The rotation expressed in natural coordinates at node i is obtained using the Jacobian matrix.

$$\underline{\theta}^d_{(i)} = \mathbf{J}_{(i)} \theta^d_{(i)} \tag{2.3.20}$$

$$= [\,-\underline{\mathbf{H}}'_{31(i)} \quad \mathbf{0} \; \cdot \; \cdot \; \cdot \; -\underline{\mathbf{H}}'_{3i(i)} \quad \mathbf{J}_{(i)} \; \cdot \; \cdot \; \cdot \; -\underline{\mathbf{H}}'_{3n(i)} \quad \mathbf{0} \;] \, \Delta^e$$

since $\underline{\mathbf{H}}'_{3k(i)} = \mathbf{J}_{(i)} \mathbf{H}'_{3k(i)}$ is the inverse relation of Eqn.(2.3.6a), where $\mathbf{J}_{(i)}$ is the Jacobian matrix evaluated at node i. Now, the nodal rotations of the difference element with respect to natural coordinates can be expressed in terms of the element nodal d.o.f.

$$
\begin{Bmatrix}
\underline{\theta}^d_{(1)} \\
\underline{\theta}^d_{(2)} \\
\cdot \\
\cdot \\
\cdot \\
\underline{\theta}^d_{(n)}
\end{Bmatrix}
=
\begin{bmatrix}
-\underline{\mathbf{H}}'_{31(1)} & \mathbf{J}_{(1)} & -\underline{\mathbf{H}}'_{32(1)} & \mathbf{0} & \cdot\;\cdot\;\cdot\;\cdot & -\underline{\mathbf{H}}'_{3n(1)} & \mathbf{0} \\
-\underline{\mathbf{H}}'_{31(2)} & \mathbf{0} & -\underline{\mathbf{H}}'_{32(2)} & \mathbf{J}_{(2)} & \cdot\;\cdot\;\cdot\;\cdot & -\underline{\mathbf{H}}'_{3n(2)} & \mathbf{0} \\
\cdot & \cdot & \cdot & \cdot & \cdot\;\cdot\;\cdot\;\cdot\;\cdot & \cdot & \cdot \\
\cdot & \cdot & \cdot & \cdot & \cdot\;\cdot\;\cdot\;\cdot\;\cdot & \cdot & \cdot \\
\cdot & \cdot & \cdot & \cdot & \cdot\;\cdot\;\cdot\;\cdot\;\cdot & \cdot & \cdot \\
-\underline{\mathbf{H}}'_{31(n)} & \mathbf{0} & -\underline{\mathbf{H}}'_{32(n)} & \mathbf{0} & \cdot\;\cdot\;\cdot\;\cdot & -\underline{\mathbf{H}}'_{3n(n)} & \mathbf{J}_{(n)}
\end{bmatrix}
\begin{Bmatrix}
\delta_1 \\
\theta_1 \\
\cdot \\
\cdot \\
\delta_n \\
\theta_n
\end{Bmatrix}
\tag{2.3.21}
$$

or

$$\underline{\theta}^{de} = \mathbf{Q}\,\Delta^e \tag{2.3.21a}$$

in which

$$
\underline{\theta}^{de} =
\begin{Bmatrix}
\underline{\theta}^d_{(1)} \\
\underline{\theta}^d_{(2)} \\
\cdot \\
\cdot \\
\cdot \\
\underline{\theta}^d_{(n)}
\end{Bmatrix}
\tag{2.3.21b}
$$

$$
\mathbf{Q}_{2n \times 5n} = \begin{bmatrix}
-\underline{\mathbf{H}}'_{31(1)} & \mathbf{J}_{(1)} & -\underline{\mathbf{H}}'_{32(1)} & 0 & \cdots & -\underline{\mathbf{H}}'_{3n(1)} & 0 \\
-\underline{\mathbf{H}}'_{31(2)} & 0 & -\underline{\mathbf{H}}'_{32(2)} & \mathbf{J}_{(2)} & \cdots & -\underline{\mathbf{H}}'_{3n(2)} & 0 \\
\cdot & \cdot & \cdot & \cdot & \cdots & \cdot & \cdot \\
\cdot & \cdot & \cdot & \cdot & \cdots & \cdot & \cdot \\
\cdot & \cdot & \cdot & \cdot & \cdots & \cdot & \cdot \\
-\underline{\mathbf{H}}'_{31(n)} & 0 & -\underline{\mathbf{H}}'_{23(n)} & 0 & \cdots & -\underline{\mathbf{H}}'_{3n(n)} & \mathbf{J}_{(n)}
\end{bmatrix}
\tag{2.3.21c}
$$

In the foregoing, the relation between the nodal rotation of the difference element and the element nodal d.o.f. has been derived. The next goal is to evaluate the displacements of the difference element at a point of consideration within an element. We can assume that $u^t = u$ and $v^t = v$. This assumption is legitimate as well as natural because there is no rotation around the axis in the surface normal direction. It is equivalent to the assumption of

$$
u^d = v^d = 0
\tag{2.3.22}
$$

As already given in Eqn.(2.3.10) for the translational element, there exists a functional relation between the normal displacement and the rotations of each element subject to the Kirchhoff assumption.

$$
\underline{\theta}^d = \left\{ \begin{matrix} \alpha^d \\ \beta^d \end{matrix} \right\} = \left\{ \begin{matrix} w^d{}_{,\xi} \\ w^t{}_{,\eta} \end{matrix} \right\} = \nabla_\xi (w^d)
\tag{2.3.23}
$$

Now, the difference element will be constructed such that $\underline{\theta}^d$ at each node satisfies the nodal value given in Eqn.(2.3.21). This can be achieved by use of generalized coordinates in a similar way as was done in the derivation of the displacement interpolation function from generalized coordinates. One first defines w^d in terms of generalized coordinates.

$$w^d = a_1 + a_2\xi + a_3\eta + \cdots + a_{3n}\xi^p\eta^q \tag{2.3.24}$$

or

$$w^d = \mathbf{p}^T \mathbf{a} \tag{2.3.24a}$$
$$\underset{1\times 3n}{}\ \underset{3n\times 1}{}$$

with

$$\mathbf{p}^T = \lfloor 1 \quad \xi \quad \eta \quad \cdots \quad \xi^p\eta^q \rfloor \tag{2.3.24b}$$

$$\mathbf{a}^T = \lfloor a_1 a_3 \quad \cdots \quad a_{3n} \rfloor \tag{2.3.24c}$$

in which **p** is a vector of polynomial terms selected from Pascal's triangle and **a** is a vector of generalized coordinates.

$$
\begin{Bmatrix}
0 \\
\alpha^r_{(1)} \\
\beta^r_{(1)} \\
\cdot \\
\cdot \\
\cdot \\
0 \\
\alpha^r_{(n)} \\
\beta^r_{(n)}
\end{Bmatrix}
=
\begin{bmatrix}
1 & \xi_1 & \eta_1 & \xi_1^2 & \eta_1^2 & \cdots & \xi_1^p\eta_1^q \\
0 & 1 & 0 & 2\xi_1 & 0 & \cdots & q\xi_1^{p-1}\eta_1^q \\
0 & 0 & 1 & 0 & 2\eta_1 & \cdots & q\xi_1^p\eta_1^{q-1} \\
\cdot & \cdot & \cdot & \cdot & \cdot & \cdots & \cdot \\
\cdot & \cdot & \cdot & \cdot & \cdot & \cdots & \cdot \\
\cdot & \cdot & \cdot & \cdot & \cdot & \cdots & \cdot \\
1 & \xi_n & \eta_n & \xi_n^2 & \eta_n^2 & \cdots & \xi_n^p\eta_n^q \\
0 & 1 & 0 & 2\xi_n & 0 & \cdots & q\xi_n^{p-1}\eta_n^q \\
0 & 0 & 1 & 0 & 2\eta_n & \cdots & q\xi_n^p\eta_n^{q-1}
\end{bmatrix}
\begin{Bmatrix}
a_1 \\
a_2 \\
a_3 \\
\cdot \\
\cdot \\
\cdot \\
\cdot \\
\cdot \\
a_{3n}
\end{Bmatrix}
\tag{2.3.25}
$$

Denote

$$
\theta^{de}_{\underset{2n\times 1}{}} =
\begin{Bmatrix}
\alpha^d_{(1)} \\
\beta^d_{(2)} \\
\cdot \\
\cdot \\
\cdot \\
\alpha^d_{(n)} \\
\beta^d_{(n)}
\end{Bmatrix}
\qquad
\Theta^{de}_{\underset{3n\times 1}{}} =
\begin{Bmatrix}
0 \\
\alpha^d_{(1)} \\
\beta^d_{(2)} \\
\cdot \\
\cdot \\
0 \\
\alpha^d_{(n)} \\
\beta^d_{(n)}
\end{Bmatrix}
\qquad
\mathbf{a}_{\underset{3n\times 1}{}} =
\begin{Bmatrix}
a_1 \\
a_2 \\
\cdot \\
\cdot \\
\cdot \\
a_{3n}
\end{Bmatrix}
\tag{2.3.25a}
$$

$$
\mathbf{A} = \begin{bmatrix}
1 & \xi_1 & \eta_1 & \xi_1^2 & \eta_1^2 & \cdots\cdots & \xi_1^p\eta_1^q \\
0 & 1 & 0 & 2\xi_1 & 0 & \cdots\cdots & q\xi_1^{p-1}\eta_1^q \\
0 & 0 & 1 & 0 & 2\eta_1 & \cdots\cdots & q\xi_1^p\eta_1^{q-1} \\
\cdot & \cdot & \cdot & \cdot & \cdot & \cdots\cdots & \cdot \\
\cdot & \cdot & \cdot & \cdot & \cdot & \cdots\cdots & \cdot \\
\cdot & \cdot & \cdot & \cdot & \cdot & \cdots\cdots & \cdot \\
1 & \xi_n & \eta_n & \xi_n^2 & \eta_n^2 & \cdots\cdots & \xi_n^p\eta_n^q \\
0 & 1 & 0 & 2\xi_n & 0 & \cdots\cdots & q\xi_n^{p-1}\eta_n^q \\
0 & 0 & 1 & 0 & 2\eta_n & \cdots\cdots & q\xi_n^p\eta_n^{q-1}
\end{bmatrix}
\qquad (2.3.25b)
$$

$\mathbf{A}$ is $3n \times 3n$

Then,

$$
\underline{\Theta}^{de} = \mathbf{A} \ \mathbf{a} \qquad\qquad (2.3.26)
$$

$\underline{\Theta}^{de}$ is $3n \times 1$, $\mathbf{A}$ is $3n \times 3n$, $\mathbf{a}$ is $3n \times 1$

Therefore,

$$
\mathbf{a} = \mathbf{A}^{-1} \underline{\Theta}^{de} = \mathbf{G} \ \underline{\theta}^{de} \qquad\qquad (2.3.27)
$$

in which $\mathbf{G}$ is a $(3n \times 2n)$ matrix obtained from $\mathbf{A}^{-1}$ by removing the columns corresponding to zero entries in vector $\underline{\Theta}^{de}$. Substituting Eqn. (2.3.27) in (2.3.24a), one obtains

$$
w^d = \mathbf{p}^T \mathbf{G} \ \underline{\theta}^{de} = \mathbf{p}^T \mathbf{G} \mathbf{Q} \Delta^e \qquad\qquad (2.3.28)
$$

and since only $\mathbf{p}$ in the above equation is a function of coordinates,

$$
\underline{\theta}^d = \nabla_\xi (w^d) = \nabla_\xi (\mathbf{p}^T) \mathbf{G} \mathbf{Q} \Delta^e = \underline{\mathbf{p}}' \mathbf{G} \mathbf{Q} \Delta^e \qquad\qquad (2.3.29)
$$

$$
\theta^d = \mathbf{J}^{-1}\underline{\theta}^d = \mathbf{J}^{-1}\underline{\mathbf{p}}' \mathbf{G} \mathbf{Q} \Delta^e = \mathbf{p}' \mathbf{G} \mathbf{Q} \Delta^e
$$

with

$$
\underline{\mathbf{p}}' = \nabla_\xi(\mathbf{p}) = \begin{bmatrix}
0 & 1 & 0 & 2\xi & 0 & \cdots\cdots & q\xi^{p-1}\eta^q \\
0 & 0 & 1 & 0 & 2\eta & \cdots\cdots & q\xi^p\eta^{q-1}
\end{bmatrix} \qquad (2.3.29a)
$$

$$
\mathbf{p}' = \mathbf{J}^{-1}\underline{\mathbf{p}}'
$$

The following is the displacement function matrix of the difference element, which summarizes Eqn.(2.3.22), (2.3.28) and (2.3.29).

$$\begin{bmatrix} T^d_1 \\ T^d_2 \\ T^d_3 \end{bmatrix} = \begin{bmatrix} 0 \\ 0 \\ \mathbf{p}^T \mathbf{G} \mathbf{Q} \end{bmatrix} \qquad (2.3.30)$$

$$\begin{bmatrix} T^d_4 \\ \\ T^d_5 \end{bmatrix} = \mathbf{L'}_3 + \mathbf{p'} \mathbf{G} \mathbf{Q}$$

Total element

The displacements of the translational and the difference element have been related to the nodal displacement by the displacement function matrices of each element.

$$\Delta^t = \mathbf{T}^t \Delta^e \qquad\qquad \Delta^d = \mathbf{T}^d \Delta^e \qquad (2.3.31)$$

Superposition of the displacement fields in both elements yields that of the total element.

$$\Delta = \mathbf{T} \Delta^e = (\mathbf{T}^d + \mathbf{T}^t) \Delta^e \qquad (2.3.32)$$

Accordingly, the displacement function matrix for the total element is obtained by addition of Eqn.(2.3.12a) and (2.3.30).

$$\begin{bmatrix} T_1 \\ T_2 \\ T_3 \end{bmatrix} = \begin{bmatrix} L_1 \\ L_2 \\ L_3 + \mathbf{p}^T \mathbf{G} \mathbf{Q} \end{bmatrix} \qquad (2.3.33)$$

$$\begin{bmatrix} T_4 \\ \\ T_5 \end{bmatrix} = \mathbf{L'}_3 + \mathbf{p'} \mathbf{G} \mathbf{Q}$$

in which $\mathbf{T}_k$ is the kth row of $\mathbf{T}$.

2.3.2 Type II decomposition

Translational element

The displacement field of the translational element in type II decomposition is identical to that of type I decomposition. Therefore, the displacement function matrix derived in the previous section is applicable for the type II decomposition as well.

$$\begin{bmatrix} T^t_1 \\ T^t_2 \\ T^t_3 \end{bmatrix} = L$$

$$\begin{bmatrix} T^t_4 \\ T^t_5 \end{bmatrix} = L_3{}'$$

(2.3.12a)

Difference element

In type II decomposition, all the translations of the difference element are suppressed, i.e.

$$\delta^d = 0 ,$$

(2.3.34)

and the rotations of the element are obtained by independent interpolation of nodal rotations, $\underline{\theta}^d_i$.

$$\underline{\theta}^d = \sum_{i=1}^n N_i \underline{\theta}^d_i = N \underline{\theta}^{de}$$

(2.3.35)

with

$$\underset{2 \times 2n}{N} = \begin{bmatrix} N_1 & 0 & N_2 & 0 & \cdots & N_n & 0 \\ 0 & N_1 & 0 & N_2 & \cdots & 0 & N_n \end{bmatrix}$$

(2.3.35a)

It should be noted that an interpolation has been applied to $\underline{\theta}^d$ instead of θ^d. Direct interpolation of θ^d may damage the geometric isotropy, because one

obtains different sets of θ^d depending on the establishment of the local coordinate which is not uniquely defined at each node. Substitution of Eqn.(2.3.21a) into (2.3.35) gives the rotations of the difference element expressed as a function of the nodal displacements.

$$\underline{\theta}^d = N \, Q \, \Delta^e \tag{2.3.36}$$

which can also be converted into the local coordinates.

$$\theta^d = J^{-1}\underline{\theta}^d = J^{-1}N \, Q \, \Delta^e \tag{2.3.37}$$

Thus, the displacement function matrix of the difference element is obtained from Eqn.(2.3.34) and (2.3.37).

$$\begin{bmatrix} T^d_1 \\ T^d_2 \\ T^d_3 \end{bmatrix} = 0$$

$$\begin{bmatrix} T^d_4 \\ T^d_5 \end{bmatrix} = J^{-1}N \, Q \tag{2.3.38}$$

Total element

The addition of Eqn.(2.3.12a) and (2.3.38) yields the displacement function matrix of the total element with type II decomposition.

$$\begin{bmatrix} T_1 \\ T_2 \\ T_3 \end{bmatrix} = L$$

$$\begin{bmatrix} T_4 \\ T_5 \end{bmatrix} = L_3' + J^{-1}N \, Q \tag{2.3.39}$$

2.3.3 Type III decomposition

Translational element

The rotations of the translational element in type III decomposition are suppressed to zero, while the translations of the element are retained as in the type I and II decompositions. Therefore, one can write the displacement function matrix of the translational element directly by use of the previous formulations.

$$
\begin{bmatrix} \mathbf{T}^t{}_1 \\ \mathbf{T}^t{}_2 \\ \mathbf{T}^t{}_3 \end{bmatrix} = \mathbf{L}
$$

$$
\begin{bmatrix} \mathbf{T}^t{}_4 \\ \mathbf{T}^t{}_5 \end{bmatrix} = \mathbf{0}
$$

$$(2.3.40)$$

Difference element

In type III decomposition, all the translations of the difference element are suppressed, i.e.

$$\delta^d = \mathbf{0} \, ,$$

$$(2.3.41)$$

and the rotations of the element are equivalent to that of the total element. The rotation vector expressed in natural coordinate can be written as a function of the element nodal d.o.f.

$$\underline{\theta}^d{}_{(i)} = \mathbf{J}_{(i)} \, \boldsymbol{\theta}_{(i)}$$

$$\underline{\theta}^{de} = \mathbf{Q}_o \, \Delta^e$$

$$(2.3.42)$$

with

$$\underset{2n\times5n}{\mathbf{Q}_o} = \begin{bmatrix} \mathbf{0} & \mathbf{J}_{(1)} & \mathbf{0} & \mathbf{0} & \cdot & \cdot & \cdot & \cdot & \mathbf{0} & \mathbf{0} \\ \mathbf{0} & \mathbf{0} & \mathbf{0} & \mathbf{J}_{(2)} & \cdot & \cdot & \cdot & \cdot & \mathbf{0} & \mathbf{0} \\ & 2\times3 & 2\times3 & 2\times3 & 2\times3 & & & & & \\ \cdot & \cdot & \cdot & \cdot & \cdot & \cdot & \cdot & \cdot & \cdot & \cdot \\ \mathbf{0} & \mathbf{0} & \mathbf{0} & \mathbf{0} & \cdot & \cdot & \cdot & \cdot & \mathbf{0} & \mathbf{J}_{(n)} \end{bmatrix}$$

(2.3.42a)

in which $\mathbf{J}_{(i)}$ denotes the Jacobian matrix evaluated at node i. The rotations at the desired point are obtained by independent interpolation of nodal rotations.

$$\underline{\theta}^d = \sum_{i=1}^{n} N_i \underline{\theta}^d_i = \mathbf{N}\underline{\theta}^{de}$$

(2.3.43)

The reason why one should interpolate $\underline{\theta}^d_i$ instead of θ^d_i is explained after Eqn. (2.3.35) in the previous section. In Ahmad's degenerate shell element (Ahmad *et al.*,1970), the nodal rotations are first converted into translations in global coordinates and then these translations are interpolated to a desired point. This type of interpolation, physically loyal to the degeneration concept, prevents rigid body rotation of a curved element. That is the reason why the degenerate shell element performs poorly for the case shown in Fig.4.3. It is obvious that the interpolation of $\underline{\theta}^d$ allows rigid body rotations, as does isoparametric interpolation of translational d.o.f. (Cook,1981) Substituting Eqn.(2.3.42) in (2.3.43), one obtains

$$\underline{\theta}^d = \mathbf{N}\,\mathbf{Q}_o\,\Delta^e$$

(2.3.44)

The rotations expressed in Cartesian coordinates are obtained again by use of the Jacobian inverse.

$$\theta^d = \mathbf{J}^{-1}\underline{\theta}^d = \mathbf{J}^{-1}\mathbf{N}\,\mathbf{Q}_o\,\Delta^e$$

(2.3.45)

From Eqn. (2.3.41) and (2.3.45), the displacement function matrix for the difference element can be written as

$$
\begin{bmatrix} T^d_1 \\ T^d_2 \\ T^d_3 \end{bmatrix} = 0
$$

$$
\begin{bmatrix} T^d_4 \\ \\ T^d_5 \end{bmatrix} = J^{-1} N Q_o
$$

(2.3.48)

Total element

In type III decomposition, the total element has only the contribution of translational element for translation and only the contribution of difference element for rotation.

$$
\begin{bmatrix} T_1 \\ T_2 \\ T_3 \end{bmatrix} = \begin{bmatrix} T^t_1 \\ T^t_2 \\ T^t_3 \end{bmatrix} = L
$$

$$
\begin{bmatrix} T_4 \\ \\ T_5 \end{bmatrix} = \begin{bmatrix} T^d_4 \\ \\ T^d_5 \end{bmatrix} = J^{-1} N Q_o
$$

(2.3.47)

The above displacement function matrix reveals uncoupling of the translations and rotations in the type III decompostion. However, they are coupled by imposition of transverse shear constraints as shown subsequently in Eqn.(2.4.8).

2.4 Strain-displacement relationship

The displacement field within an element has been related to the nodal displacements by displacement function matrix. Differentiation of the matrix yields the strain-nodal displacement relationship which is directly involved in

the stiffness matrix evaluation. The *strain-displacement matrices* relating the strain field to the nodal displacements are derived for each type of element decomposition in the following.

2.4.1 General form of strain-nodal displacement relationship

In a situation where the transverse shear strains are zero or constant through the thickness, the displacement field can be represented in terms of the midsurface translations and rotations.

$$
\begin{Bmatrix} u' \\ v' \\ w' \end{Bmatrix} = \begin{Bmatrix} u \\ v \\ w \end{Bmatrix} - \frac{1}{2} t \zeta \begin{bmatrix} 1 & 0 \\ 0 & 1 \\ 0 & 0 \end{bmatrix} \begin{Bmatrix} \alpha \\ \beta \end{Bmatrix} \tag{2.4.1}
$$

where $\lfloor u' \; v' \; w' \rfloor$ represents the translations of a point on the surface a distance of $\frac{1}{2}(t\zeta)$ from the midsurface, whereas $\lfloor u \; v \; w \rfloor$ are the translations on the midsurface. The displacements also can be related to the element nodal d.o.f. by use of the displacement function matrix derived in the previous sections.

$$
\begin{Bmatrix} u' \\ v' \\ w' \end{Bmatrix} = \left[\begin{bmatrix} T_1 \\ T_2 \\ T_3 \end{bmatrix} - \frac{1}{2} t \zeta \begin{bmatrix} T_4 \\ T_5 \\ 0 \end{bmatrix} \right] \Delta^e \tag{2.4.2}
$$

The strains are defined in local coordinates. All six strains can be included for a shell element in which the transverse shear effects are included. However, the strain ε_z need not be included in the formulation, because the normal stress σ_z in the thickness direction is negligible according to the Love assumption, and all the other stresses are decoupled from the thickness direction strain ε_z in order to relieve the excessive stiffness. Therefore, one retains only five strain components expressed in local coordinates.

$$\varepsilon = \begin{Bmatrix} \varepsilon_x \\ \varepsilon_y \\ \gamma_{xy} \\ \gamma_{yz} \\ \gamma_{xz} \end{Bmatrix} \tag{2.4.3}$$

For the convenience of the formulation, the *in-plane* strains $\lfloor \varepsilon_x \ \varepsilon_y \ \gamma_{xy} \rfloor$ and the transverse shear strains $\lfloor \gamma_{yz} \ \gamma_{xz} \rfloor$ are considered separately. Here, 'in-plane' implies the directions parallel to the mid-surface. One applies to the in-plane strains the strain-displacement relationship of two-dimensional plane elasticity.

$$\begin{Bmatrix} \varepsilon_x \\ \varepsilon_y \\ \gamma_{xy} \end{Bmatrix} = \begin{Bmatrix} u'_{,x} \\ v'_{,y} \\ u'_{,x} + v'_{,y} \end{Bmatrix} = \begin{Bmatrix} u_{,x} \\ v_{,y} \\ u_{,x} + v_{,y} \end{Bmatrix} - \frac{1}{2} t \zeta \begin{Bmatrix} \alpha_{,x} \\ \beta_{,y} \\ \alpha_{,y} + \beta_{,x} \end{Bmatrix} \tag{2.4.4}$$

The in-plane strains can be divided into membrane strains ε^m and bending strains ε^b.

$$\varepsilon^m = \begin{Bmatrix} \varepsilon_x^m \\ \varepsilon_y^m \\ \gamma_{xy}^m \end{Bmatrix} = \begin{Bmatrix} u_{,x} \\ v_{,y} \\ u_{,x} + v_{,y} \end{Bmatrix} \qquad \varepsilon^b = \begin{Bmatrix} \varepsilon_x^b \\ \varepsilon_y^b \\ \gamma_{xy}^b \end{Bmatrix} = -\frac{1}{2} t \zeta \begin{Bmatrix} \alpha_{,x} \\ \beta_{,y} \\ \alpha_{,y} + \beta_{,x} \end{Bmatrix} \tag{2.4.5}$$

The strains can be related to the element nodal d.o.f. in the form of

$$\varepsilon^m = \mathbf{B}^m \Delta^e$$
$$\varepsilon^b = -\frac{1}{2} t \zeta \mathbf{B}^b \Delta^e \tag{2.4.6}$$

in which the matrices $\mathbf{B}^m$ and $\mathbf{B}^b$ are to be determined. Substitution of Eqn.(2.4.2) into (2.4.4) yields

$$\mathbf{B}^m_{3 \times 5n} = \begin{bmatrix} \mathbf{T}_{1,x} \\ \mathbf{T}_{2,y} \\ \mathbf{T}_{1,y} + \mathbf{T}_{2,x} \end{bmatrix} \qquad \mathbf{B}^b_{3 \times 5n} = \begin{bmatrix} \mathbf{T}_{4,x} \\ \mathbf{T}_{5,y} \\ \mathbf{T}_{4,y} + \mathbf{T}_{5,x} \end{bmatrix} \tag{2.4.7}$$

The transverse shear strains are

$$\varepsilon^s = \begin{Bmatrix} \gamma_{xz} \\ \gamma_{yz} \end{Bmatrix} = \begin{Bmatrix} w'_{,x} + u'_{,z} \\ w'_{,y} + v'_{,z} \end{Bmatrix} = \begin{Bmatrix} w_{,x} \\ w_{,y} \end{Bmatrix} - \begin{Bmatrix} \alpha \\ \beta \end{Bmatrix} \tag{2.4.8}$$

since $z = \frac{1}{2}(t\,\zeta)$ and $\alpha_{,z} = \beta_{,z} = 0$, neglecting higher order terms. The transverse shear strains can also be related to the element nodal d.o.f.

$$\varepsilon^s = \mathbf{B}^s\,\Delta^e \tag{2.4.9}$$

with

$$\mathbf{B}^s = \begin{bmatrix} \mathbf{T}_{3,x} \\ \mathbf{T}_{3,y} \end{bmatrix} - \begin{bmatrix} \mathbf{T}_4 \\ \mathbf{T}_5 \end{bmatrix} \tag{2.4.10}$$

Thus, one can establish a general form of the strain-nodal displacement relationshipas follows.

$$\varepsilon = \begin{Bmatrix} \varepsilon^m + \varepsilon^b \\ \varepsilon^s \end{Bmatrix} = \begin{bmatrix} \mathbf{B}^m - \frac{1}{2}\,t\,\zeta\,\mathbf{B}^b \\ \mathbf{B}^s \end{bmatrix} \Delta^e \tag{2.4.11}$$

or

$$\varepsilon = \mathbf{B}\,\Delta^e \tag{2.4.11a}$$

with

$$\mathbf{B} = \begin{bmatrix} \mathbf{B}^m - \frac{1}{2}\,t\,\zeta\,\mathbf{B}^b \\ \mathbf{B}^s \end{bmatrix} \tag{2.4.11b}$$

The matrices $\mathbf{B}$, $\mathbf{B}^m$, $\mathbf{B}^b$ and $\mathbf{B}^s$ are designated as strain-displacement matrices and more specifically membrane strain-displacement matrix, etc. In the following sections, the strain-displacement matrices are derived for each type of element decomposition.

2.4.2 Strain-nodal displacement relationship for type I decomposition

Substituting Eqn.(2.3.33) in (2.4.7), one obtains the membrane strain-displacement matrix for type I decomposition.

$$
\underset{3 \times 5n}{\mathbf{B}^m} = \begin{bmatrix} \mathbf{T}_{1,x} \\ \mathbf{T}_{2,y} \\ \mathbf{T}_{1,y} + \mathbf{T}_{2,x} \end{bmatrix} = \begin{bmatrix} 1 & 0 & 0 & 0 \\ 0 & 0 & 0 & 1 \\ 0 & 1 & 1 & 0 \end{bmatrix} \begin{bmatrix} \mathbf{L'}_1 \\ \\ \mathbf{L'}_2 \end{bmatrix} \tag{2.4.12}
$$

$$
4 \times 5n
$$

The bending strain-displacement matrix can also be derived from Eqn.(2.3.33) and (2.4.7) [*]

$$
\mathbf{B}^b = \begin{bmatrix} \mathbf{T}_{4,x} \\ \mathbf{T}_{5,y} \\ \mathbf{T}_{4,y} + \mathbf{T}_{5,x} \end{bmatrix} = \mathbf{\nabla}^*_x \, (\mathbf{L}_3 + \mathbf{p}\,\mathbf{G}\,\mathbf{Q}) = \mathbf{S}^*(\underline{\mathbf{L}}_3" + \underline{\mathbf{p}}"\,\mathbf{G}\,\mathbf{Q}) \tag{2.4.13}
$$

because

$$
\begin{bmatrix} \mathbf{T}_{4,x} \\ \mathbf{T}_{5,y} \\ \mathbf{T}_{4,y} + \mathbf{T}_{5,x} \end{bmatrix} = \begin{bmatrix} \partial/\partial x & 0 \\ 0 & \partial/\partial y \\ \partial/\partial y & \partial/\partial x \end{bmatrix} \begin{bmatrix} \mathbf{T}_4 \\ \mathbf{T}_5 \end{bmatrix} = \begin{bmatrix} \partial/\partial x & 0 \\ 0 & \partial/\partial y \\ \partial/\partial y & \partial/\partial x \end{bmatrix} \left\{ \begin{matrix} \partial/\partial x \\ \partial/\partial y \end{matrix} \right\} (\mathbf{L}_3 + \mathbf{p}\,\mathbf{G}\,\mathbf{Q}) \tag{2.4.13a}
$$

---

[*]The same strain-displacement matrix can be derived based on the Kirchhoff assumption adopted in the type I decomposition,

$$\alpha_{,x} = w_{,xx} \qquad \beta_{,y} = w_{,yy} \qquad \alpha_{,x} = \beta_{,y} = w_{,xy}$$

Therefore, the bending strains can be written purely in terms of the normal displacement.

$$
\varepsilon^b = -\frac{1}{2}\, t\, \zeta \left\{ \begin{matrix} w_{,xx} \\ w_{,yy} \\ 2w_{,xy} \end{matrix} \right\} = -\frac{1}{2}\, t\, \zeta\, \mathbf{\nabla}^*_x (w)
$$

$$
\begin{aligned}
\mathbf{\nabla}^*_x (w) &= \mathbf{S}^*\, \mathbf{\nabla}_{\xi\xi}(w) \\
&= \mathbf{S}^*\, \mathbf{\nabla}_{\xi\xi}(\mathbf{L}_3 + \mathbf{p}^T\mathbf{G}\,\mathbf{Q})\, \Delta^e \\
&= \mathbf{S}^*\, (\underline{\mathbf{L}}_3" + \underline{\mathbf{p}}^*\mathbf{G}\,\mathbf{Q})\, \Delta^e
\end{aligned}
$$

Therefore, $\quad \mathbf{B}^b = \mathbf{S}^* (\underline{\mathbf{L}}_3" + \underline{\mathbf{p}}"\,\mathbf{G}\,\mathbf{Q})$

in which **G** and **Q** are constant within an element. The first and second derivatives of L_3 and **p** are obtained by differentiating respectively Eqn.(2.3.4) and (2.3.24b) with respect to the natural coordinates ξ and η.

$$\underset{5\times 5n}{\mathbf{L_3}''} = \nabla_{\xi\xi}(\mathbf{L_3}) = [\ \underset{5\times 3}{\underline{\mathbf{H}}''_1}\ \ \underset{5\times 2}{\mathbf{0}}\ \ \mathbf{H}''_2\ \ \mathbf{0}\ \cdot\ \cdot\ \cdot\ \mathbf{H}''_n\ \ \mathbf{0}\ ] \tag{2.4.14}$$

$$\underset{5\times 3n}{\mathbf{p}''} = \nabla_{\xi\xi}(\mathbf{p^T}) = \begin{bmatrix} 0 & 1 & 0 & 2\xi & 0 & \eta & \cdots & p\xi^{p-1}\eta^q \\ 0 & 0 & 1 & 0 & 2\eta & \xi & \cdots & q\xi^p\eta^{q-1} \\ 0 & 0 & 0 & 2 & 0 & 0 & \cdots & p(p-1)\xi^{p-2}\eta^q \\ 0 & 0 & 0 & 0 & 2 & 0 & \cdots & q(q-1)\xi^p\eta^{q-2} \\ 0 & 0 & 0 & 0 & 0 & 1 & \cdots & pq\xi^{p-1}\eta^{q-1} \end{bmatrix} \tag{2.4.15}$$

The transformation matrix $\mathbf{S}^*$ is defined in Eqn.(2.1.8). Assuming that the curvature is not large within an element, one can write

$$\underline{\mathbf{H}}''_i = \nabla_{\xi\xi}(\mathbf{H}_i) = \nabla_{\xi\xi}(N_i)\mathbf{R_3} \tag{2.4.16}$$

Because the transverse shear strains are neglected in type I decomposition, the transverse shear strain-displacement matrix is null.

$$\mathbf{B^s} = \mathbf{0} \tag{2.4.17}$$

2.4.3 Strain-nodal displacement relationship for type II decomposition

Since the translation element of type II decomposition is identical to that of type I decomposition, the membrane strains are obtained from the same relation,

$$\underset{3\times 5n}{\mathbf{B^m}} = \begin{bmatrix} 1 & 0 & 0 & 0 \\ 0 & 0 & 0 & 1 \\ 0 & 1 & 1 & 0 \end{bmatrix} \underset{4\times 5n}{\begin{bmatrix} \mathbf{L'_1} \\ \\ \mathbf{L'_2} \end{bmatrix}} \tag{2.4.12}$$

The bending strain-displacement matrix with type II decomposition is derived from Eqn.(2.3.39) and (2.4.3).

$$\mathbf{B}^b = \begin{bmatrix} \mathbf{T}_{4,x} \\ \mathbf{T}_{5,y} \\ \mathbf{T}_{4,y} + \mathbf{T}_{5,x} \end{bmatrix} = \begin{bmatrix} \partial/\partial x & 0 \\ 0 & \partial/\partial y \\ \partial/\partial y & \partial/\partial x \end{bmatrix} (\mathbf{L}_3' + \mathbf{J}^{-1}\mathbf{N}\,\mathbf{Q}) \tag{2.4.18}$$

After a rigorous manipulation, presented in Appendix A, of the left hand side, the matrix $\mathbf{B}^b$ can be written as

$$\mathbf{B}^b = \mathbf{S}^*(\underline{\mathbf{L}}_3'' + \mathbf{N}^*\,\mathbf{Q}) \tag{2.4.19}$$

where $\mathbf{S}^*$ is defined in Eqn.(2.1.8), and

$$\mathbf{N}^* = \begin{bmatrix} N_1 & 0 & N_2 & 0 & \cdots\cdots & N_n & 0 \\ 0 & N_1 & 0 & N_2 & \cdots\cdots & 0 & N_n \\ N_{1,\xi} & 0 & N_{2,\xi} & 0 & \cdots\cdots & N_{n,\xi} & 0 \\ 0 & N_{1,\eta} & 0 & N_{2,\eta} & \cdots\cdots & 0 & N_{n,\eta} \\ \frac{1}{2}N_{1,\eta} & \frac{1}{2}N_{1,\xi} & \frac{1}{2}N_{2,\eta} & \frac{1}{2}N_{2,\xi} & \cdots\cdots & \frac{1}{2}N_{n,\eta} & \frac{1}{2}N_{n,\xi} \end{bmatrix} \tag{A.1.12}$$

The transverse shear strain-displacement matrix is obtained by substituting Eqn.(2.3.39) into (2.4.10).

$$\mathbf{B}^s = \mathbf{L}_3' - (\mathbf{L}_3' + \mathbf{J}^{-1}\mathbf{N}\,\mathbf{Q}) = -\mathbf{J}^{-1}\mathbf{N}\,\mathbf{Q} \tag{2.4.20}$$

since

$$\begin{bmatrix} \mathbf{T}_{3,x} \\ \mathbf{T}_{3,y} \end{bmatrix} = \mathbf{L}_3' \tag{2.4.21}$$

The right hand side of Eqn.(2.4.20) is equivalent to $(-\boldsymbol{\theta}^d)$. This implies that the transverse shear strain in type II decomposition is equivalent to the rotation of the difference element. According to Eqn.(2.4.20), the transverse shear strains have been obtained by direct interpolation of their nodal values.

2.4.4 Strain-nodal displacement relationship for type III decomposition

The membrane strains have the same relationship with the nodal displacements as in type I and II decompositions.

$$
\mathbf{B}^m_{\substack{\\3x5n}} = \begin{bmatrix} 1 & 0 & 0 & 0 \\ 0 & 0 & 0 & 1 \\ 0 & 1 & 1 & 0 \end{bmatrix} \begin{bmatrix} \mathbf{L'}_1 \\ \\ \mathbf{L'}_2 \end{bmatrix}
$$
$$
{\scriptstyle 4x5n}
$$

(2.4.12)

The bending strain-displacement matrix of type III decomposition is obtained from Eqn.(2.3.47) and (2.4.7).

$$
\mathbf{B}^b = \begin{bmatrix} \mathbf{T}_{4,x} \\ \mathbf{T}_{5,y} \\ \mathbf{T}_{4,y} + \mathbf{T}_{5,x} \end{bmatrix} = \begin{bmatrix} \partial/\partial x & 0 \\ 0 & \partial/\partial y \\ \partial/\partial y & \partial/\partial x \end{bmatrix} (\mathbf{J}^{-1}\mathbf{N}\,\mathbf{Q}_o)
$$

(2.4.22)

By the same analogy to Eqn.(2.4.18), the matrix $\mathbf{B}^b$ can be written as

$$
\mathbf{B}^b = \mathbf{S}^*\mathbf{N}^*\,\mathbf{Q}_o
$$

(2.4.23)

The matrix $\mathbf{B}^s$ for the transverse shear strain can also be obtained from Eqn.(2.3.47) and (2.4.10).

$$
\mathbf{B}^s = \mathbf{L}_3' - \mathbf{J}^{-1}\mathbf{N}\mathbf{Q}_o = \mathbf{J}^{-1}(\underline{\mathbf{L}}_3' - \mathbf{N}\mathbf{Q}_o)
$$

(2.4.24)

Thus, all the strain-displacement matrices necessary for stiffness matrix evaluation are obtained.

2.5 Element stiffness matrix

Once the strain-displacement relations are established, the stiffness matrix can be evaluated directly using the following standard equation of displacement finite element formulation:

$$k^e = \int_V B^T E \, B \, dV \qquad (2.5.1)$$

in which k^e is the element stiffness matrix, and E is the stress-strain matrix. Derivation of the equation can be found in many references (Desai and Abel, 1972; Zienkiewicz, 1977) and will not be repeated here. As the stresses and strains are expressed in local coordinates, one has a 5x5 stress-strain matrix which can be represented as

$$\underset{5 \times 5}{E} = \begin{bmatrix} \underset{2 \times 2}{E^p} & \underset{2 \times 3}{E^{ps}} \\ \underset{2 \times 2}{E^{sp}} & \underset{3 \times 3}{E^s} \end{bmatrix} \qquad (2.5.2)$$

in which $E^{sp} = (E^{ps})^T$ and E, E^p, and E^s are symmetric. For isotropic or stratified anisotropic materials, $E^{ps}=0$. If the material is isotropic,

$$E^p = \frac{E}{(1-v^2)} \begin{bmatrix} 1 & v & 0 \\ v & 1 & 0 \\ 0 & 0 & (1-v)/2 \end{bmatrix}$$

$$\qquad (2.5.3)$$

$$E^s = \frac{E}{2k(1+v)} \begin{bmatrix} 1 & 0 \\ 0 & 1 \end{bmatrix}$$

in which E is the Young's modulus, and v is the Poisson's ratio. The constant k is a factor to compensate the strain energy for transverse shear displacement approximation. Substituting Eqn.(2.4.11b) and (2.5.2) into (2.5.1), one obtains

$$k^e = \int_V \begin{bmatrix} B^m - \tfrac{1}{2}t\,\zeta\,B^b \\ B^s \end{bmatrix}^T \begin{bmatrix} E^p & E^{ps} \\ E^{sp} & E^s \end{bmatrix} \begin{bmatrix} B^m - \tfrac{1}{2}t\,\zeta\,B^b \\ B^s \end{bmatrix} dV \qquad (2.5.4)$$

Changing to integration in terms of natural coordinates, one may write

$$k^e = \int_{-1}^{1} \int_A \begin{bmatrix} B^m - \tfrac{1}{2}t\,\zeta\,B^b \\ B^s \end{bmatrix}^T \begin{bmatrix} E^p & E^{ps} \\ E^{sp} & E^s \end{bmatrix} \begin{bmatrix} B^m - \tfrac{1}{2}t\,\zeta\,B^b \\ B^s \end{bmatrix} |J^*| d\xi \, d\eta \, d\zeta \qquad (2.5.4)$$

in which $\mathbf{J}^*$ is a Jacobian matrix which transforms the local coordinate into the natural coordinate, and $|\mathbf{J}^*|$ is its determinant in three dimensions. Evaluation of $|\mathbf{J}^*|$ is detailed in Section 3.1.1. The integration in the thickness direction can be performed explicitly. And integration of $\zeta d\zeta$ yields zero. Therefore, the equation can be expanded as follows

$$\mathbf{k}^e = t \int_A (\mathbf{B}^{mT}\mathbf{E}^p\,\mathbf{B}^m + \tfrac{1}{12}\,t^2\,\mathbf{B}^{bT}\,\mathbf{E}^p\,\mathbf{B}^b + \mathbf{B}^{sT}\,\mathbf{E}^s\mathbf{B}^s + \mathbf{B}^{mT}\mathbf{E}^{ps}\,\mathbf{B}^s + \mathbf{B}^{sT}\mathbf{E}^{sp}\mathbf{B}^m)|\mathbf{J}|\,dA$$

(2.5.5)

The stiffness matrix can therefore be divided into four parts.

$$\mathbf{k}^e = \mathbf{k}^m + \mathbf{k}^b + \mathbf{k}^s + \mathbf{k}^{ps}$$

(2.5.6)

with

$$\mathbf{k}^m = \int_A \mathbf{B}^{mT}\mathbf{E}^p\,\mathbf{B}^m|\mathbf{J}|\,t\,dA$$

$$\mathbf{k}^b = \frac{1}{12} \int_A \mathbf{B}^{bT}\mathbf{E}^p\,\mathbf{B}^b\,|\mathbf{J}|\,t^3\,dA$$

$$\mathbf{k}^s = \int_A \mathbf{B}^{sT}\mathbf{E}^s\,\mathbf{B}^s\,|\mathbf{J}|\,t\,dA \qquad (2.5.6a)$$

$$\mathbf{k}^{ps} = \int_A (\,\mathbf{B}^{mT}\mathbf{E}^{ps}\,\mathbf{B}^s + \mathbf{B}^{sT}\mathbf{E}^{sp}\,\mathbf{B}^m)|\mathbf{J}|\,t\,dA$$

The matrices $\mathbf{k}^m$, $\mathbf{k}^b$ and $\mathbf{k}^s$ correspond respectively to the commonly-called membrane, bending and transverse shear stiffness matrix. The matrix $\mathbf{k}^{ps}$ represents the cross-effect of membrane and transverse shear strain, and vanishes when $\mathbf{E}^{ps} = (\mathbf{E}^{sp})^T = \mathbf{0}$. Thus, the stiffness matrix equation can be simplified further for isotropic or stratified anisotropic materials.

$$\mathbf{k}^e = \mathbf{k}^m + \mathbf{k}^b + \mathbf{k}^s$$

(2.5.7)

The formulations based on the three types of element decompostion are summarized in Table 2.1.

Table 2.1 Summary of the formulation

Classification		Type I	Type II	Type III
Element decomposition	Transl. element	Kirchhoff	Kirchhoff	rotation suppressed
	Differ. element	Kirchhoff	translation suppressed	translation suppressed
Displacement functions	$\begin{bmatrix} T_1 \\ T_2 \\ T_3 \end{bmatrix}$	$\begin{bmatrix} L_1 \\ L_2 \\ L_3 + p^T GQ \end{bmatrix}$	$\begin{bmatrix} L_1 \\ L_2 \\ L_3 \end{bmatrix}$	$\begin{bmatrix} L_1 \\ L_2 \\ L_3 \end{bmatrix}$
	$\begin{bmatrix} T_4 \\ T_5 \end{bmatrix}$	$L'_3 + p'GQ$	$L'_3 + J^{-1}NQ$	$J^{-1}NQ_o$
Strain-displacement matrix	B^m	$\begin{bmatrix} 1 & 0 & 0 & 0 \\ 0 & 0 & 0 & 1 \\ 0 & 1 & 1 & 0 \end{bmatrix}\begin{bmatrix} L'_1 \\ L'_2 \end{bmatrix}$	same as type I	same as type I
	B^b	$S^*(\underline{L}_3'' + \underline{p}''GQ)$	$S^*(\underline{L}_3'' + N^*Q)$	$S^*N^*Q_o$
	B^s	0	$-J^{-1}NQ$	$J^{-1}(\underline{L}_3' - NQ_o)$
Similar elements		BCIZ plate bend.[1] and Strickland's 3-node shell[2]		Ahmad's degenerate shell[3]

[1]Bazeley *et al.* (1965),   [2]Strickland and Loden (1968), [3]Ahmad *et al.* (1970)

2.6 Complementary devices for improvement of the formulation

The greatest difficulty in thin shell formulation originates from the Kirchhoff assumption which mandates C^1 interelement continuity (Wempner *et al.,* 1968; Key *et al.* 1970; Gallagher, 1970). The difficulty has been overcome simply by including the transverse shear effect in the element of the present study as well as in the degenerate family of elements. The included transverse shear energy is of order t, while the bending energy is of order t^3, where t represents the thickness of the shell. Consequently, the elements have the tendency to become too stiff in thin shell and plate situations. The convergence is unacceptably slow for some cases. It has been commonly understood that this undesirable behavior, called *shear locking* , is chiefly due to excessive shear strain. As will be discussed in the following chapter, the numerical tests on the new element developed in the present study also show the significance of the locking behavior for thin shells and plates.

Many approaches have been proposed to alleviate shear and membrane locking phenomena (Zienkiewicz, 1977). Some of such approaches for displacement formulation are reduced integration (Zienkiewicz *et al.,* 1971; Pawsey *et al.,* 1971), the discrete Kirchhoff constraint approach (Bathe *et al.,* 1974; Irons, 1980), the addition of internal d.o.f. (Cook, 1972; Takemoto *et al.,* 1973; Hughes *et al.,* 1978), penalty methods (Zienkiewicz, 1977), energy balancing (Fried, 1974), mode decomposition (Stolarski *et al.,* 1984; Stolarski *et al.,* 1985), and derivative smoothing by substitute shape functions(Razzaque, 1973). Other alternative formulations such as hybrid formulation (Pian *et al.,* 1969; Pian, 1971, 1983; Morley, 1984), the mixed formulation (Hermann, 1965; Chatterjee, 1972; 1984a, Lee *et al.,* 1978, 1982, 1984, 1985; Karamanlidis *et al.,* 1984), and the assumed stress or strain formulation (Pian, 1964; MacNeal,

1982) have also been suggested. In the present study, the first three approaches for displacement formulation and the mixed formulation are investigated in association with the new element. However, application of the discrete Kirchhoff constraint approach was not successful.

2.6.1 Reduced Integration

Doherty *et al.* (1969) pointed out that the element performance can be improved greatly by evaluating the shear strain energy in the element by a lower-order integration procedure than is used for the normal strain energy. This lower-order integration neglects the extraneous shear strain imposed by the assumed displacement functions, and thus tends to relax the overstiffness of the element. The idea of reducing the order of the integration in evaluating the stiffness matrix called, *reduced integration*, was applied to the degenerate shell element concurrently and independently by Zienkiewicz *et al.* (1971) and Pawsey and Clough (1971). The latter used a 2X2 integration scheme for transverse shear strain components and a 3X3 for the others, and demonstrated the resulting improvement for thin, as well as thick, shell applications. On the other hand, the former discovered that reduced integration of all stress components gives better improvement than the *selective reduced integration* of the transverse shear strains. It was found that the lower-order integration reduces substantially computational cost at the same time (Zienkiewicz *et al.*, 1976).

The application of reduced integration was successful but was not well understood at the beginning. The validity of reduced integration is mathematically proved by Zienkiewicz *et al.* (1976). The reduced integration relaxes a certain constraint by the introduction of a matrix singularity and thus

a : ξ = 0.3333   η = 0.3333
b : ξ = 0.4701   η = 0.0597
c : ξ = 0.7974   η = 0.1013

a : ξ = 0.3333   η = 0.3333
b : ξ = 0.6   η = 0.2

a : ξ = 0.5   η = 0

a : ξ = 0.6667   η = 0.1667

a : ξ = 0   η = 0
b : ξ = ±0.7746   η = 0
c : ξ = ±0.7746   η = ±0.7746

a : ξ = ±0.5774   η = ±0.5774
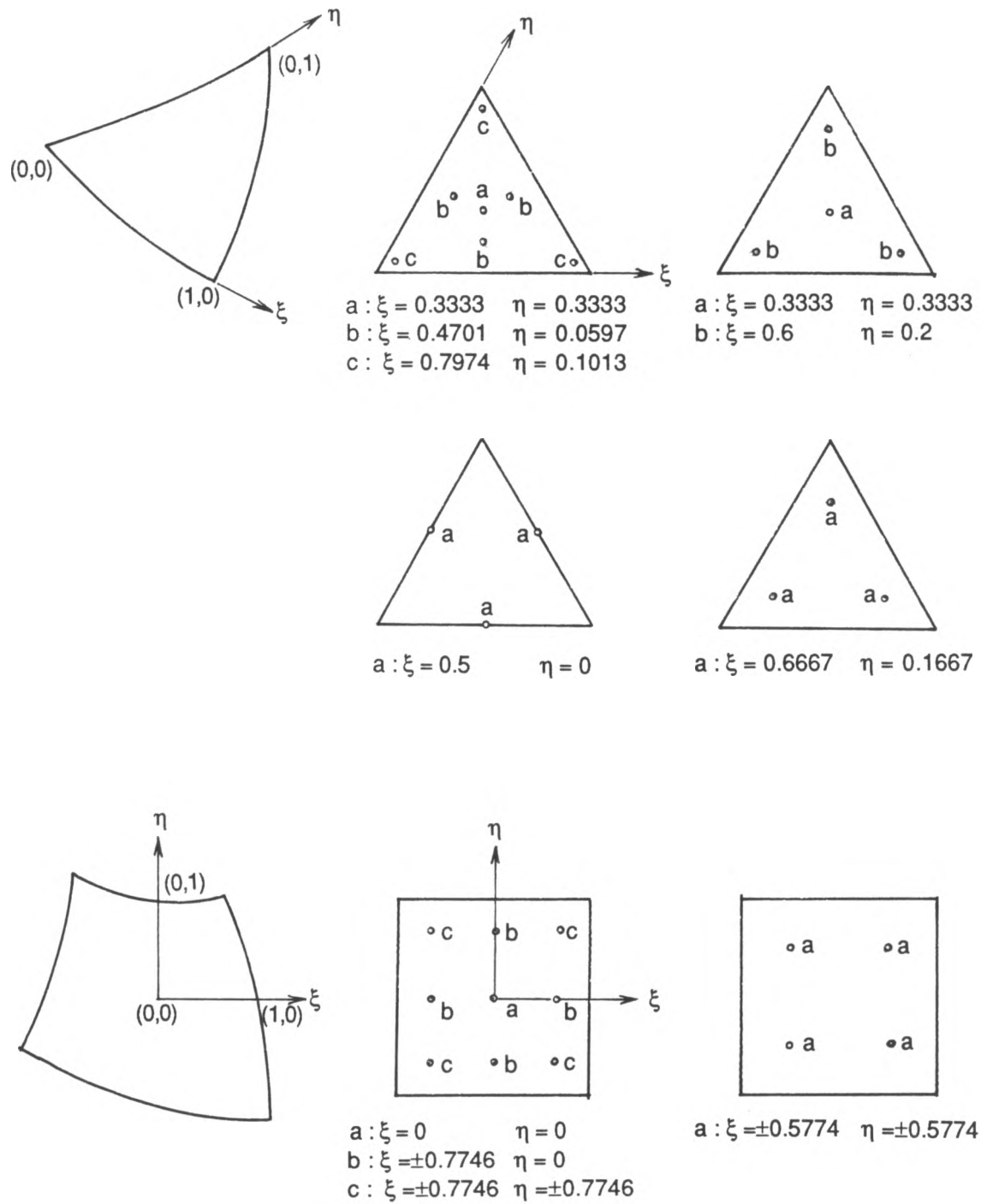
Fig. 2.4   Integration schemes for triangular and quadrilateral elements

relieves locking phenomena (Pugh *et al.*, 1978). Other aspects of reduced integration are fully discussed in other references(Zienkiewicz *et al.*, 1976; Pugh *et al.*, 1976; Hughes *et al.*, 1977). Stolarski and Belytschko (1982,1983,1984) observed that overintegration of the membrane strains also retards the convergence. This phenomenon is called *membrane locking*. The membrane locking results from the effects of the curvature on the bending stiffness, whenever membrane displacements are represented by polynomials of lower order (Stolarski *et al.*, 1982). It was also found that there exists an interdependence between membrane and shear locking. This is the reason why *uniform reduced ntegration* generally gives faster convergence than selective reduced integration. It has been recognized that uniform reduced integration also has a greater advantage over selective reduced integration in computational economy. The selective integration requires a more complex computational procedure than the uniform reduced integration. Lack of geometric isotropy is another disadvantage of selective integration. Pawsey (1972) argued that spurious zero-energy modes may appear in isoparametric elements when the uniform reduced integration is used. However, this does not appear to be a hindrance in practical problem solving. It has been confirmed that the element does not show this singularity of an assembly if two or more elements are used (Hughes *et al.*, 1978; Zienkiewicz, 1972). Boundary conditions make the assembled stiffness matrix positive definite such that the zero-energy modes are not globally present.

It should be noted that application of reduced integration has so far been limited to the quadrilateral element. The reasons why one obtains such a dramatic improvement for quadrilateral elements by the reduced integration are well explained in beam analogy (Cook, 1981). One may simply apply the same idea to a triangular element. Unfortunately, however, one cannot extend the

beam analogy to a triangular element. Thus, the reduced order integration does not work for triangular or severely distorted quadrilateral elements so dramatically as for regular quadrilateral elements. Collapsed quadrilateral elements have often been used in lieu of the triangular ones. According to the numerical tests in this study, however, the collapsed quadrilateral elements perform no better than the triangular elements with reduced integration. For triangular elements, a three-point integration, as opposed to six- or seven-point rules, may be regarded as a reduced scheme. A four-point integration for triangular elements results in non-positive definite stiffness matix and thus should be precluded. Various integration schemes shown in Fig. 2.4 have been investigated in association with the elements formulated in the present study. The numerical results are illustrated in Fig. 3.3.

2.6.2. Addition of internal degrees-of-freedom

Tsach (1981) observed that an element does not lock when the interpolated shear strain function contains more variables than the number of equations obtained when equating the shear strains to zero. Therefore, one can avoid locking either by increasing the number of variables or by reducing the number of equations. Reduced integration is equivalent to reducing the number of equations. One may increase the number of variables simply by adding internal d.o.f. Cook (1972) advocated the use of single, lateral displacement internal d.o.f. in eight-noded plate elements and also suggested a scheme for avoiding possible zero-energy modes. Takemoto and Cook (1973) studied analogous treatment of the degenerate shell element. They added three translational d.o.f. in the middle of the quadrilateral element. The element suffers from spurious zero-energy deformation mode. As a remedy, the authors

suggested multiplying each on-diagonal stiffness coefficient associated with an internal d.o.f. by 1.003 prior to condensation of the internal freedoms. As a result, the performance of the element was improved for some cases, but was little affected, in general, by the internal d.o.f.

Hughes and Cohen (1978) added two rotational, instead of translational, d.o.f. at the center of the serendipity Mindlin plate element, and named it the *heterosis element*. They also considered the *Lagrange element* which has all three d.o.f., i.e. one translational and two rotational, as internal freedoms. A few numerical examples showed that the Lagrange and heterosis elements are consistently superior to the serendipity element. The elements with internal d.o.f. are better than the serendipity element also for distorted configuration as demonstrated by numerical study in Chapter 4. Both elements demonstrated almost equivalent convergence properties, with the former being somewhat more accurate. They observed that the Lagrange element may suffer from rank deficiency in certain singular situations and produce significant oscillations in displacements. The addition of internal d.o.f. is usually accompanied by rank deficiency. To avoid rank deficiency, selective reduced integration was applied to the heterosis element and Lagrange element.

The assemblage of elements with internal d.o.f. is well explained elsewhere (Gallagher, 1975; Cook, 1981). The element stiffness equation is first assembled with all the external and the internal d.o.f. If the external d.o.f. are denoted by Δ_r and the internal d.o.f. by Δ_e, the stiffness equation can be partitioned into the part associated with Δ_r and the other part with Δ_e.

$$\begin{bmatrix} k_{rr} & k_{re} \\ k_{er} & k_{ee} \end{bmatrix} \begin{Bmatrix} \Delta_r \\ \Delta_e \end{Bmatrix} = \begin{Bmatrix} f_r \\ f_e \end{Bmatrix} \tag{2.6.1}$$

The internal d.o.f are eliminated before assembly of element stiffness matrix

$$k^e = k_{rr} - k_{re} \, k_{ee}^{-1} \, k_{er} \qquad (2.6.2a)$$

$$f^e = f_r - k_{re} \, k_{ee}^{-1} \, f_e \qquad (2.6.2b)$$

and recovered later for stress computation. One can assign either absolute or relative values[*] to the internal d.o.f., and will obtain identical results whichever option chosen (Gallagher, 1975). However, assigning relative values makes the formulation simpler because the shape function of the internal node can be constructed by a hierarchical formulation.

Denote the shape functions with and without an internal nodes respectively by N_i (i = 1 , . ., n) and N_i^* (i = 1, . . . , n+1) where n is the number of external nodes for an element. In an hierarchical formulation,

$$N_i^* = N_i \qquad (2.6.3)$$

for i = 1, . . . , n and a bubble function is used for N_{n+1}^* . As an example, for a 6-node triangular element,

$$N_7^* = 27 \, \xi\eta \, (\, 1 - \xi - \eta \,) \qquad (2.6.4)$$

More than one internal node can be added. These nodes can be located not only at the center but also at any point within an element. Consider an internal node k at $\xi = \xi_k$ and $\eta = \eta_k$ within a triangular element. The shape function of the node, N_k^* should have zero value at the boundary of the element. Therefore, the shape function can be written in the form of

$$N_k^* = h \, \xi\eta \, (\, 1 - \xi - \eta \,) \, (\, 1 - a\xi - b\eta \,) \qquad (2.6.5)$$

in which a, b, and h are coefficients to be determined from the conditions,

$$N_{k,\xi}^* = N_{k,\eta}^* = 0 \quad \text{and} \quad N_k^* = 1 \quad \text{for } \xi = \xi_k \text{ and } \eta = \eta_k. \qquad (2.6.6)$$

---

[*]Internal d.o.f. assigned with relative values are commonly called *bubble* modes.

It is not necessary to force the shape function to vanish at other internal nodes, because the internal d.o.f. represent only relative values in an hierarchical formulation. When the internal node is located at the center of a triangle, i.e. $\xi_k=\eta_k= 1/3$, Eqn.(2.6.5) reduces to (2.6.4). For the case of a 6-node triangular element with three internal nodes at $(\xi_7=\eta_7=1/6)$, $(\xi_8=2/3, \eta_8=1/6)$ and $(\xi_9=1/6, \eta_9=2/3)$, the following shape functions are derived:

$$
\begin{aligned}
N^*_7 &= 135\,\xi\eta\,(\,1-\xi-\eta\,)\,(\,1-\tfrac{9}{5}\xi-\tfrac{9}{5}\eta\,) \\
N^*_8 &= -108\,\xi\eta\,(\,1-\xi-\eta\,)\,(\,1-\tfrac{9}{4}\xi\,) \\
N^*_9 &= -108\,\xi\eta\,(\,1-\xi-\eta\,)\,(\,1-\tfrac{9}{4}\eta\,)
\end{aligned}
\tag{2.6.7}
$$

In this study, the addition of internal d.o.f. was intended chiefly for triangular elements, because the new element of quadrilateral shape with reduced integration already shows satisfactory performance. But, the identical logic is applied to both triangular and quadrilateral shape, since the shape of the element is not distinguished in the present formulation. At the implementation stage, the addition of internal d.o.f. is achieved simultaneously for both shapes. Only different shape functions associated with the internal node(s) should be provided for each element shape.

One can think of several different ways of selecting the internal d.o.f. The following four possibilities of assigning internal d.o.f. have been considered in the present study:

1) three translations at the center

2) two rotations at the center

3) three translations and two rotations at the center

4) two surface tangential translations and two rotations at the center

There are many other possibilities of adding internal nodes and d.o.f. Because the internal d.o.f. get relative values rather than absolute ones, they

can be specified either in global coordinates or in local coordinates, whichever d.o.f. are chosen.

2.6.3 Mixed formulation based on Hellinger-Reissner principle

Another simple approach to cure the locking effect may be to use the *Hellinger-Reissner principle* which was first introduced by Hellinger and later refined by Reissner (Zienkiewicz *et al.*, 1984). In this principle, the stationary point of a functional is sought by taking variations of the displacements and stresses at the same time. The application of this principle leads to a *mixed formulation*. Herrmann applied the principle to plate bending (1967) and incompressible problems (1965). Lee and Pian (1978) demonstrated the improvement of plate and shell elements by the mixed formulation. Lee and Wong (1982), and Lee and Zhang (1985) developed Mindlin type plate bending element based on the modified Hellinger-Reissner principle. The equivalence between the mixed model and displacement models with reduced integration was observed by Lee and Pian (1978), Malkus and Hughes (1978), and Batoz *et al.* (1980). Shimodaira (1985) investigated the conditions under which the mixed model and the displacement model with reduced or selective integration become identical, and found that both models are not identical for a 6-node triangular element. The advantage of the mixed formulation is that it is more flexible than reduced integration and simpler than the selective reduced integration (Lee *et al.*, 1985).

The functional of the Hellinger-Reissner principle is written as

$$\Pi_R = \int_v (\varepsilon^T E \bar{\varepsilon} - \frac{1}{2} \varepsilon^T E \varepsilon) \, dv - W \tag{2.6.8}$$

with

$$\varepsilon^T = \lfloor \varepsilon_x \cdots \gamma_{xz} \rfloor \tag{2.6.8a}$$

$$\bar{\varepsilon}^T = \lfloor u_{,x} \cdots w_{,x} + u_{,z} \rfloor \tag{2.6.8b}$$

in which ε is the strain vector and $\bar{\varepsilon}$ is the displacement derivative vector. $\mathbf{E}$ and W denote the constitutive matrix and the external load potential respectively. Applying the principle to the shell element formulated in the present study with $\mathbf{E}^{ps} = 0$, one obtains

$$\Pi_R = \int_v (\varepsilon^{pT} \mathbf{E}^p \, \bar{\varepsilon}^p - \frac{1}{2} \varepsilon^{pT} \mathbf{E}^p \, \varepsilon^p + \varepsilon^{s\,T} \mathbf{E}^s \bar{\varepsilon}^s - \frac{1}{2} \varepsilon^{sT} \mathbf{E}^s \varepsilon^s) \, dv - W \tag{2.6.9}$$

in which

$$\varepsilon^p = \varepsilon^m + \varepsilon^b = \begin{Bmatrix} \varepsilon^m_x \\ \varepsilon^m_y \\ \gamma^m_{xy} \end{Bmatrix} + \begin{Bmatrix} \varepsilon^b_x \\ \varepsilon^b_y \\ \gamma^b_{xy} \end{Bmatrix} \tag{2.6.9a}$$

$$\bar{\varepsilon}^p = \bar{\varepsilon}^m + \bar{\varepsilon}^b = \begin{Bmatrix} u_x \\ v_y \\ u_y + v_x \end{Bmatrix} - \frac{1}{2} t \zeta \begin{Bmatrix} \alpha_{,x} \\ \beta_{,y} \\ \alpha_{,y} + \beta_{,x} \end{Bmatrix} \tag{2.6.9b}$$

$$\varepsilon^s = \begin{Bmatrix} \gamma_{yz} \\ \gamma_{zx} \end{Bmatrix} \tag{2.6.9c}$$

$$\bar{\varepsilon}^s = \begin{Bmatrix} \overline{\gamma_{yz}} \\ \overline{\gamma_{zx}} \end{Bmatrix} = \begin{Bmatrix} w_{,x} \\ w_{,y} \end{Bmatrix} - \begin{Bmatrix} \alpha \\ \beta \end{Bmatrix} \tag{2.6.9d}$$

As derived in the previous sections,

$$\bar{\varepsilon}^p = (\mathbf{B}^m - \frac{1}{2} t \, \zeta \mathbf{B}^b) \, \Delta^e \tag{2.6.10}$$

$$\bar{\varepsilon}^s = \mathbf{B}^s \Delta^e \tag{2.6.10a}$$

One assumes the strain distributions in polynomial form:

$$\varepsilon^p = \mathbf{P}_1 \, \mathbf{a} \tag{2.6.11}$$

$$\varepsilon^s = \mathbf{P}_2 \, \mathbf{b} \tag{2.6.11a}$$

with

$$P_1 = \begin{bmatrix} g_1 & 0 & 0 & \zeta g_1 & 0 & 0 \\ 0 & g_1 & 0 & 0 & \zeta g_1 & 0 \\ 0 & 0 & g_1 & 0 & 0 & \zeta g_1 \end{bmatrix} = [\,f \;\; \zeta f\,] \tag{2.6.11b}$$

$$P_2 = \begin{bmatrix} g_2 & 0 & 0 \\ 0 & g_2 & 0 \\ 0 & 0 & g_2 \end{bmatrix} \tag{2.6.11c}$$

$$f = \begin{bmatrix} g_1 & 0 & 0 \\ 0 & g_1 & 0 \\ 0 & 0 & g_1 \end{bmatrix} \tag{2.6.11d}$$

$$g_1 = \lfloor\, 1 \quad \xi \quad \eta \quad \xi\eta \quad \cdots \,\rfloor \tag{2.6.11e}$$
$$\text{1x m}$$

$$g_2 = \lfloor\, 1 \quad \xi \quad \eta \quad \xi\eta \quad \cdots \,\rfloor \tag{2.6.11f}$$
$$\text{1x n}$$

and a and b are unknown parameter vectors. Each formulation will be designated as an $m\,g_1/n\,g_2$ scheme by the number of terms m and n, respectively in g_1 and g_2. For example, for the $4g_1/3g_2$ scheme,

$$g_1 = \lfloor\, 1 \quad \xi \quad \eta \quad \zeta\eta \,\rfloor \tag{2.6.12}$$
$$g_2 = \lfloor\, 1 \quad \xi \quad \eta \,\rfloor$$

Substituting Eqn.(2.6.10) and (2.6.11) into (2.6.9), one obtains

$$\Pi_R = (\, a^T G_1\, \Delta^e - \tfrac{1}{2}\, a^T H_1\, a + b^T G_2\, \Delta^e - \tfrac{1}{2}\, b^T H_2\, b\,) - W \tag{2.6.13}$$

with

$$G_1 = \int_v P_1{}^T E^p(B^m - \tfrac{1}{2} t\, \zeta B^b)\, dv = \begin{bmatrix} \int_v f^T E^p B^m\, dv \\ \tfrac{1}{2} t \int_v f^T E^p B^b\, \zeta^2\, dv \end{bmatrix} \tag{2.6.13a}$$

$$H_1 = \int_v P_1{}^T E^p P_1\, dv = \begin{bmatrix} \int_v f^T E^p f\, dv & 0 \\ 0 & \tfrac{1}{2}\int_v f^T E^p f\, \zeta^2\, dv \end{bmatrix} \tag{2.6.13b}$$

$$G_2 = \int_v P_2{}^T E^s B^s \, dv \tag{2.6.13c}$$

$$H_2 = \int_v P_2{}^T E^s P_2 \, dv \tag{2.6.13d}$$

Taking the variation of Π_R with respect to **a** and **b**, one obtains

$$a = H_1{}^{-1} G_1 \Delta^e \tag{2.6.14}$$

$$b = H_2{}^{-1} G_2 \Delta^e$$

Substitution of Eqn.(2.6.14) into (2.6.13) leads to

$$\Pi_R = \tfrac{1}{2} \Delta^{eT} k^e \Delta^e - W \tag{2.6.15}$$

with

$$k^e = G_1{}^T H_1{}^{-1} G_1 + G_2{}^T H_2{}^{-1} G_2 \tag{2.6.15a}$$

An alternative form of the mixed formulation can be achieved based on the *modified Hellinger-Reissner principle* by which the energy functional for the shell can be expressed as

$$\Pi_R = \int_v (\ \tfrac{1}{2} \varepsilon^{pT} E^p \varepsilon^p + \varepsilon^{sT} E^s \bar{\varepsilon}^s - \tfrac{1}{2} \varepsilon^{sT} E^s \varepsilon^s \ ) \, dv - W \tag{2.6.16}$$

In the same way as above, one can derive the element stiffness matrix.

$$k^e = k_o + G_2{}^T H_2{}^{-1} G_2 \tag{2.6.17}$$

with

$$k_o = \int_v B^T E \, B \, dv \tag{2.6.17a}$$

The matrix k_o is equivalent to the element stiffness matrix derived in the previous sections.

2.6.4 Application of more than one complementary device

In the previous sections, three different complementary devices have been discussed separately. However, any single remedy may not be effective enough to provide satisfactory improvement for certain types of problems. Two or more devices can be applied together to an element to achieve a universal improvement. For example, one may combine the reduced integration and the internal d.o.f., or include the internal d.o.f. in the mixed formulation. The computed results with a single device as well as with combination of several devices are compared and discussed in the next chapter.

2.6.5 Control of zero-energy modes

The locking phenomenon can be removed completely or partially by the complementary devices described in the previous sections. One negative feature of these devices is the *spurious zero-energy modes* or rank deficiencies of the stiffness matrix which may arise. However, it should first be noted that rank deficiency is not always harmful. The presence of spurious zero-energy modes at individual element level does not adversely affect the accuracy of the element as long as these modes are suppressed by assembly of elements (Hughes *et al.*, 1978). In general, the assembled stiffness matrix is positive definite after application of boundary conditions, and therefore, the zero-energy modes are not globally present (Hughes *et al.*, 1978a). This is true for the reduced integration as observed by Zienkiewicz (1972) and Hughes *et al.* (1978a). However, as other complementary devices are combined with the reduced integration scheme, one obtains more zero-energy modes, and the whole system may become unstable or oscillatory results may be obtained due to the zero-energy modes for certain boundary conditions. The element,
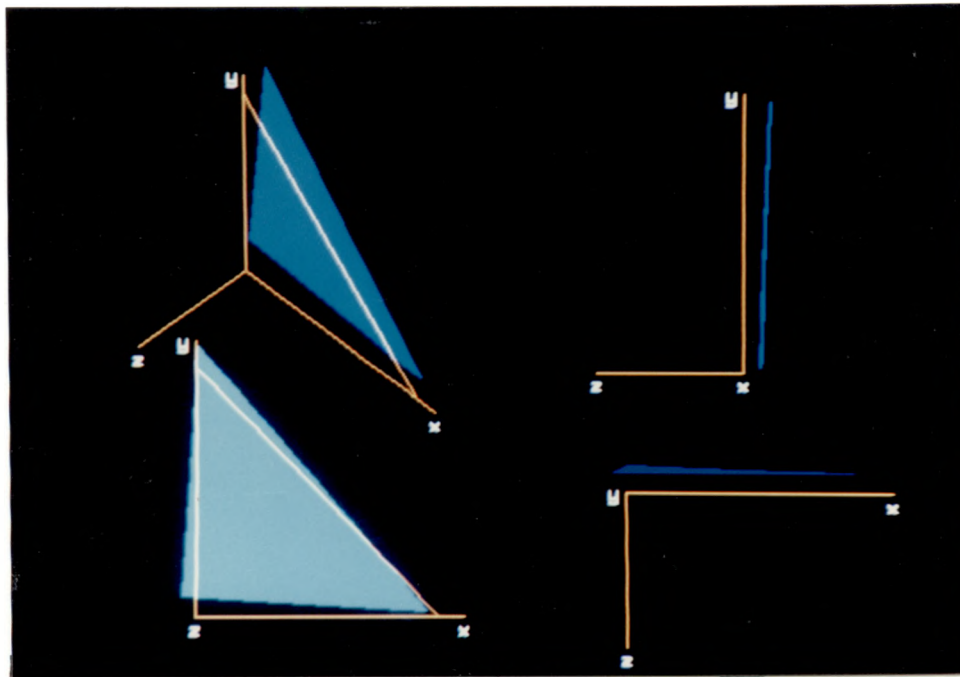
(a)
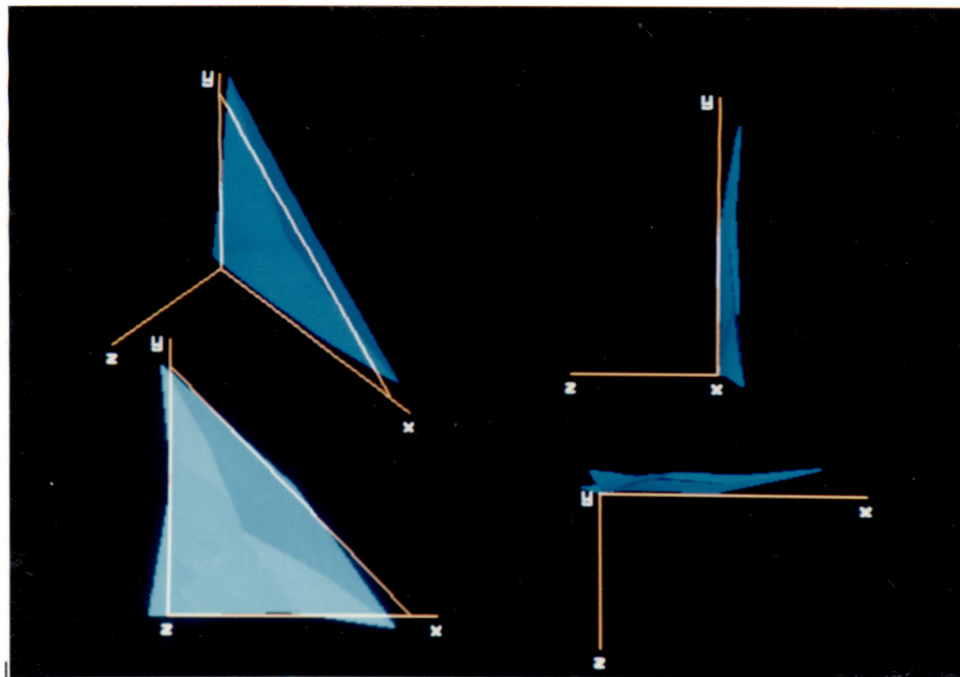
(b)

Fig. 2.5   Graphically represented Eigenvectors associated with zero
            Eigenvalues of the element stiffness matrix (type III element with
            internal d.o.f.)
            (a) Rigid body mode
            (b) Spurious zero-energy mode
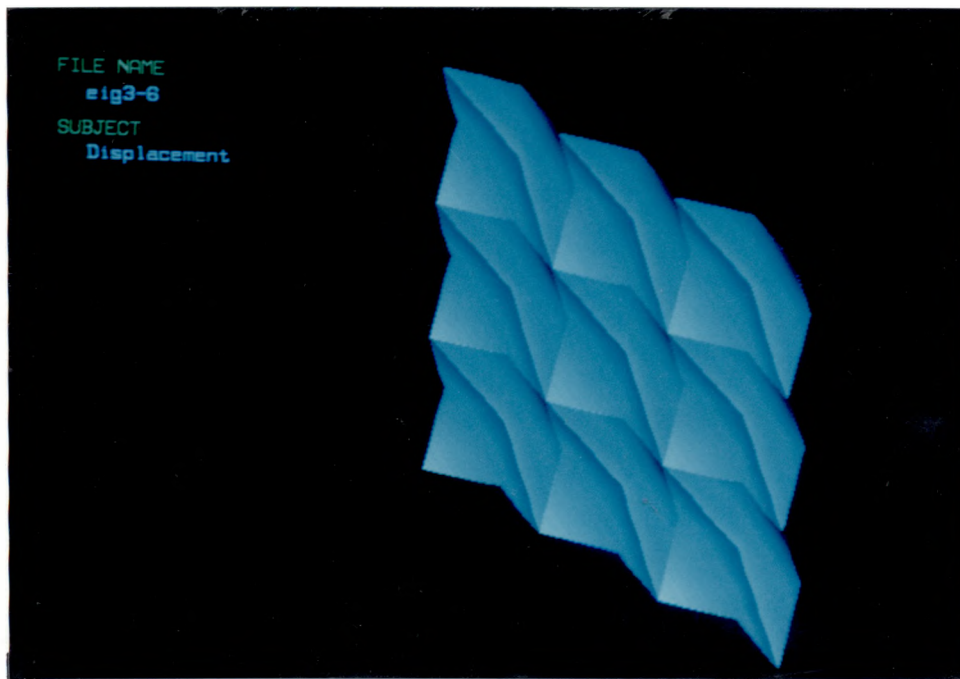
Fig. 2.6   Spurious zero-energy mode in an assembled configuration

complemented by both reduced integration and internal d.o.f., fails for a rectangular plate which is simply supported at four corners.

The zero-energy modes can be detected by an eigenvalue test. The zero eigenvalues of the stiffness matrix represent either the rigid body modes or the spurious zero-energy modes. The eigenvectors correspond to normalized displacements. Therefore, the eigenvectors associated with each zero eigenvalue describe geometrically the form of the rigid body mode or the spurious mode. Thus, one can distinguish the spurious modes from the rigid body modes by graphically visualizing the eigenvectors as shown in Fig. 2.5. The zero-energy modes in assembed configuration can also be displayed as in Fig. 2.6.

Selective reduced integration can be regarded as one of the measures to avoid the spurious modes. The disadvantages of selective reduced integration have already been mentioned. As an alternative for selective reduced integration, Kavanagh and Key (1972) attempted to combine portions of the reduced and unreduced stiffness matrices. The resulting stiffness is formed from the sum

$$\mathbf{K} = \alpha \mathbf{K}_{full} + (1 - \alpha) \, \mathbf{K}_{red} \qquad (2.6.18)$$

where $\mathbf{K}_{full}$ and $\mathbf{K}_{red}$ represent the unreduced and the reduced stiffness matrix respectively, and α has a value between zero and one. The scheme is intended to remove zero-energy modes while maintaining geometric isotropy. The method is designated as the *α-control scheme* in this study. Cook (1972) indicated that the method gives extremely poor results. However, Belytschko *et al.* (1981) suspected that the poor results might be due to use of an improper α value.

The graphically displayed spurious mode in Fig. 2.5. shows an indentation of the element at the center. This spurious mode at the element level can be related with that of the assembled configuration in Fig. 2.6. One can imagine that the spurious modes may be suppressed by preventing the indentation of the element. This can be linked to the idea of Cook (1972) and Takemoto and Cook (1973). They suggested adding a soft spring to the internal d.o.f. to remove the spurious modes in Lagrangian type elements. This can be achieved by multiplying k_c by (1+e), where k_c is the diagonal term of the uncondensed element stiffness matrix $\mathbf{k_e}$ associated with the internal d.o.f. and e is a small number. In this study, the method is designated as the *e-control scheme* and the values e and α are called *zero-energy control indices* .

Belytschko *et al.* (1981) extended the idea of Kavanagh and Key (1972) and proposed a *stabilization matrix* , which is used as a small perturbation to eliminate zero-energy modes. Dovey (1974) applied to a quadrilateral element a five-point integration scheme which was obtained from combination of 2x2 rule and one-point rule. Flanagan and Belytschko (1981) developed *stabilization operators* to suppress the spurious modes. Belytschko and Liu (1984) suggested the *consistent spurious control method* for 9-node Lagrange element based on the degenerate shell theory.

The α–control scheme and the e-control scheme, which were originally devised for quadrilateral elements, have been tested for triangular elements in the present study. Also suggested is an alternative integration scheme in which the stiffness matrix is integrated by linear combination of two different 3-point rules with appropriate proportions. Various proportions of the combination are investigated. As shown by numerical tests in Chapter 4, the scheme is more efficient than the one which is obtained by combination of the full and the reduced integration schemes.

Chapter 3

IMPLEMENTATION

In Chapter 2, the element stiffness matrix has been formulated based on three types of element decomposition. Although most aspects of its implementation are rather routine, not only the computational efficiency but also the accuracy are influenced by how properly it is implemented. Many operations involved in the formulation of the stiffness matrix are articulated for notational simplification. One can economize those operations by taking advantage of their characteristics. It is also desirable to generalize the implementation as much as possible. This chapter deals with practical aspects related to evaluation of the element stiffness matrix and other subsequent computations.

3.1 Computation of element stiffness matrix

The formulation of the element stiffness matrix differs for various types of element decomposition. However, as shown in Table 2.1, the three types of formulation are in the same format, and therefore there are only minor differences between their computational procedures. The flow diagram in Fig.3.3 exemplifies the steps of computing the stiffness matrix for a type III element with three internal d.o.f., u, v and w. One can use the same element stiffness matrix routine for both triangular and quadrilateral elements if the type of decomposition is identical. The number of external nodes for an element is specified by a variable N rather than a certain constant value so that one can easily change the shape and the order of the element by incorporating corresponding shape functions. Various combinations of internal d.o.f. can be

74

achieved simply by switching on or off the loop over the internal node. Only when the tangential displacements, i.e., *u* and *v,* are specified as internal d.o.f. are additional manipulations required to convert the displacement into global coordinates before interpolation. The element stiffness matrix is constructed through four major steps, i.e., evaluation of transformation matrices, computation and storage of strain-displacement matrices, numerical integration, and condensation of internal d.o.f. The general flow diagram for the overall shell analysis is presented in Fig.3.1.

3.1.1 Evaluation of transformation matrices

Rotation matrix

A vector in the *z* direction can be defined as a cross product of any two vectors tangent to the midsurface (Ahmad *et al.*, 1970).

$$\mathbf{V}_3 = \left\{ \begin{array}{c} V_{13} \\ V_{23} \\ V_{33} \end{array} \right\} = \left\{ \begin{array}{c} x_{,\xi} \\ y_{,\xi} \\ z_{,\xi} \end{array} \right\} \times \left\{ \begin{array}{c} x_{,\eta} \\ y_{,\eta} \\ z_{,\eta} \end{array} \right\} \tag{3.1.1}$$

When the nodal coordinates are given as input data, the first derivatives of the global coordinates with respect to the natural coordinates can be evaluated using the interpolation equation.

$$x_{,\xi} = \sum_{i=1}^{n} N_{i,\xi} x_i \quad \text{etc.} \tag{3.1.2}$$

in which N_i is the interpolation function associated with node i, and x_i is the nodal coordinate. In the case where the geometry of the midsurface is defined by a mathematical expression $\phi(x, y, z) = $ constant, a normal vector can be obtained from

$$V_3 = \left\{ \begin{array}{c} \phi_{,x} \\ \phi_{,y} \\ \phi_{,z} \end{array} \right\} \tag{3.1.3}$$

Thus, the unit vector in the direction of z,

$$\mathbf{v}_3 = \mathbf{V}_3 / V_3 \tag{3.1.4}$$

in which $V_3 = \sqrt{(V_{13}^2 + V_{23}^2 + V_{33}^2)}$ is the Euclidean norm of $\mathbf{V}_3$. Two other orthogonal unit vectors are obtained from

$$\mathbf{v}_1 = \mathbf{j} \times \mathbf{v}_3 \quad \text{and} \quad \mathbf{v}_2 = \mathbf{v}_3 \times \mathbf{v}_1 \tag{3.1.5a}$$

or in case the direction of the y axis and that of $\mathbf{v}_3$ coincide,

$$\mathbf{v}_2 = \mathbf{v}_3 \times \mathbf{i} \quad \text{and} \quad \mathbf{v}_1 = \mathbf{v}_2 \times \mathbf{v}_3 \tag{3.1.5a}$$

in which $\mathbf{i}$ and $\mathbf{j}$ are unit vectors, respectively, in the x and the y directions. Thus, the rotation matrix transforming the global coordinates into the local coordinates is given by

$$\mathbf{R} = [\mathbf{v}_1 \ \mathbf{v}_2 \ \mathbf{v}_3] \tag{3.1.6}$$

The rotation matrices are required at all the nodes and integration points. For computational economy, one may compute the rotation matrices only at nodal points and interpolate them to each integration point. In the case where the derivatives of the global coordinates are evaluated by Eqn. (3.1.2), there is a discontinuity of the computed normal direction at an element boundary. The rotation matrix can be evaluated more accurately by averaging the nodal values of adjacent elements. However, the improvement of the accuracy becomes negligible as mesh is refined, and there may exist actual discontinuity of

surface slope at sharp edges. Therefore, it is more practical and efficient to use the rotation matrices evaluated independently for each element.

Jacobian matrix

Since the formulation is based on local coordinates and the integration in the thickness direction is explicit, the Jacobian matrix in three dimensions can be written in the form

$$\mathbf{J}^* = \begin{bmatrix} J_{11} & J_{12} & 0 \\ J_{21} & J_{22} & 0 \\ 0 & 0 & \frac{1}{2}t \end{bmatrix} = \begin{bmatrix} \mathbf{J} & & 0 \\ 2\times 2 & & 0 \\ 0 & 0 & \frac{1}{2}t \end{bmatrix} \tag{3.1.7}$$

in which

$$\mathbf{J} = \begin{bmatrix} J_{11} & J_{12} \\ J_{21} & J_{22} \end{bmatrix} \tag{3.1.7a}$$

is a Jacobian matrix of two dimensions. The inverse and the determinant of the Jacobian matrix are obtained from

$$\mathbf{J}^{*-1} = \begin{bmatrix} \mathbf{J}^{-1} & & 0 \\ 2\times 2 & & 0 \\ 0 & 0 & \frac{1}{2}t \end{bmatrix} \tag{3.1.8}$$

and

$$|\mathbf{J}^*| = \frac{1}{2}t \, |\mathbf{J}| \tag{3.1.8a}$$

in which $\mathbf{J}^{-1}$ and $|\mathbf{J}|$ denote, respectively, the inverse and the determinant of $\mathbf{J}$. Therefore, one manipulates only a 2x2 Jacobian matrix instead of a 3x3. The Jacobian matrices are required at nodal points and integration points. The determinant and the inverse of the Jacobian matrix should be computed at each integration point

Transformation matrix $\mathbf{J}_2$

The transformation matrix $\mathbf{J}_2$ defined in Eqn. (2.1.6b) can be partitioned as follows:

$$\mathbf{J}_2 = \begin{bmatrix} \mathbf{J} & \mathbf{0} \\ \text{2x2} & \text{2x3} \\ \mathbf{B} & \mathbf{C} \\ \text{3x2} & \text{3x3} \end{bmatrix} \tag{3.1.9}$$

with

$$\mathbf{B} = \begin{bmatrix} x_{,\xi\xi} & y_{,\xi\xi} \\ x_{,\eta\eta} & y_{,\eta\eta} \\ x_{,\xi\eta} & y_{,\xi\eta} \end{bmatrix} \tag{3.1.9a}$$

$$\mathbf{C} = \begin{bmatrix} (x_{,\xi})^2 & (y_{,\xi})^2 & 2x_{,\xi}y_{,\xi} \\ (x_{,\eta})^2 & (y_{,\eta})^2 & 2x_{,\eta}y_{,\eta} \\ x_{,\xi}x_{,\eta} & y_{,\xi}y_{,\eta} & x_{,\xi}y_{,\eta}+x_{,\xi}y_{,\eta} \end{bmatrix}$$

The inverse of $\mathbf{J}_2$ can be obtained from

$$\mathbf{J}_2^{-1} = \begin{bmatrix} \mathbf{J}^{-1} & \mathbf{0} \\ -\mathbf{C}^{-1}\mathbf{B}\mathbf{J}^{-1} & \mathbf{C}^{-1} \end{bmatrix} \tag{3.1.10}$$

The inverse of $\mathbf{J}_2$ is required at each integration point.

3.1.2 Computation of the strain-displacement matrices

The strain-displacement matrices are evaluated at each integration point. For type I decompositon, the matrix **G** need be computed no more than once through the whole analysis. The shape function matrix **N** and its derivative matrix **N*** are computed for the first element and updated only when either the shape or the integration scheme of the element is changed from that of the preceding element. In Chapter 2, the strain-displacement equations are written

in a way to simplify and systemize the expressions as much as possible. Thus, most of the matrices are not fully populated, and especially $\mathbf{Q_o}$ is quite sparsely populated. Full expansion of the equations will make the implementation too massive even though it may be conducive to computational economy. However, one can achieve computational efficiency, to some degree, by rewriting the equations in more practical forms. For example, Eqn. (2.4.23) can be converted into the following form:

$$\mathbf{B}^b = \mathbf{S}^*\mathbf{N}^*\mathbf{Q_o} = \mathbf{S}^* \sum_{i=1}^{n} \mathbf{N}^*_i \ \mathbf{J}_{(i)} \tag{3.1.11}$$

with

$$\mathbf{N}^*_i = \begin{bmatrix} N_1 & 0 \\ 0 & N1 \\ N_{1,\xi} & 0 \\ 0 & N_{1,\eta} \\ \tfrac{1}{2}N_{1,\eta} & \tfrac{1}{2}N_{1,\xi} \end{bmatrix} \tag{3.1.11a}$$

3.1.3 Numerical integration

The integration of the stiffness matrix is performed explicitly in the thickness direction and numerically in the tangential direction as already discussed in Section 2.5. Thus, Eqn. (2.5.5a) is replaced by Eqn.(3.1.11) which is expressed in the form of numerical integration.

$$\mathbf{k}^m = \sum_{k=1}^{q} \mathbf{B}^m_k{}^T \mathbf{E}^p_k \ \mathbf{B}^m_k |\mathbf{J}|_k \ t_k \ W_k \tag{3.1.12a}$$

$$\mathbf{k}^b = \frac{1}{12} \sum_{k=1}^{q} \mathbf{B}^b_k{}^T \mathbf{E}^p_k \ \mathbf{B}^b_k \ |\mathbf{J}|_k \ t_k{}^3 \ W_k \tag{3.1.12b}$$

$$\mathbf{k}^s = \sum_{k=1}^{q} \mathbf{B}^s_k{}^T \mathbf{E}^s_k \, \mathbf{B}^s_k \, |\mathbf{J}|_k \, t_k \, W_k \qquad\qquad (3.1.12c)$$

$$\mathbf{k}^{ps} = \sum_{k=1}^{q} (\mathbf{B}^m_k{}^T \mathbf{E}^{ps}_k \, \mathbf{B}^s_k + \mathbf{B}^s_k{}^T \mathbf{E}^{sp}_k \, \mathbf{B}^m_k) |\mathbf{J}|_k \, t_k \, W_k \qquad\qquad (3.1.12d)$$

in which q is the number of integration points, the subscript k is used to denote the values evaluated at integration point k, and W is the integration weight factor. The constitutive matrix **E** and the thickness t at an integration point are obtained by interpolation of given nodal values. In the previous chapter, each strain-displacement matrix has been associated with the entire element d.o.f. for notational convenience. Some of the d.o.f. are not active in the matrix. Only the active part of the matrix is involved in the operation of the numerical integration. Therefore, it is necessary to avoid manipulating or storing the inactive part in order to achieve computational efficiency. The active d.o.f. are indicated in Table 3.1.

For the purpose of generalization, information about a few different integration schemes is stored as a set of internal data which include the number of integration points, their natural coordinates, integration weights, stress extrapolation coefficients, etc. Full or reduced order integration can be achieved simply by specifying the desired set of data. Selective reduced integration is also relatively easy for isotropic materials because one can apply separate integration schemes for $\mathbf{k}^m + \mathbf{k}^b$ and $\mathbf{k}^s$ in Eqn.(2.5.6) without involving any computational complexity. But, as for anisotropic material, the selective integration will involve more complexity due to the coupling of normal strain and transverse shear strain represented by $\mathbf{k}^{ps}$ in Eqn.(2.5.5a). Detailed handling of selective integration can be found in other literature (Pawsey and Clough, 1971;

Hughes *et al.*, 1978). The type I element requires at least three-point integration for membrane strains and nine-point integration for bending strains.

Table 3.1   Active degrees of freedom in strain-displacement matrices

Type of decomp.	Strain-displac. matrix	Associated strain components	Active nodal d.o.f.
Type I	B^m	ε_x, ε_y, γ_{xy}	u, v, w
	B^b	ε_x, ε_y, γ_{xy}	u, v, w, α, β
	B^s	—	—
Type II	B^m	ε_x, ε_y, γ_{xy}	u, v, w
	B^b	ε_x, ε_y, γ_{xy}	u, v, w, α, β
	B^s	γ_{yz}, γ_{xz}	u, v, w, α, β
Type III	B^m	ε_x, ε_y, γ_{xy}	u, v, w
	B^b	ε_x, ε_y, γ_{xy}	α, β
	B^s	γ_{yz}, γ_{xz}	u, v, w, α, β

3.1.4 Condensation of internal d.o.f.

Implementation of this complementary device is applied simultaneously to both triangular and quadrilateral elements, because any specific shape is not assumed in the element formulation. However, separate shape functions associated with each shape should be provided. Various combinations of internal d.o.f. can be achieved simply by switching on or off the loop over the internal node. Only when the tangential displacements, i.e., *u* and *v,* are

specified as internal d.o.f. are additional manipulations required to convert the displacement into global coordinates before interpolation. The element stiffness equation comprising all the external and internal d.o.f. is first constructed. Then the internal d.o.f. are condensed out from the stiffness matrix and from the load vector before assembly of the global system equation. The matrices in Eqn.(3.1.13) are stored for future use in stress computation.

$$\mathbf{k}_s = \mathbf{k}_{re} \, \mathbf{k}_{ee}^{-1} \qquad \qquad (3.1.13a)$$

$$\mathbf{f}_s = \mathbf{k}_{ee}^{-1} \, \mathbf{f}_e \qquad \qquad (3.1.13b)$$

An alternative method of condensation, which uses Gauss elimination directly, is given in the literature (Desai and Abel,1972, pp146-147)

3.1.5 Incorporation of zero energy control devices

The α-control scheme can be handled by the numerical integration in which the control index α is given by the integration weight. Because α has a small value, the integration point associated with α can be excluded from computation of nodal loads and stresses. The e-control scheme can be achieved simply by multiplying the diagonal terms of $\mathbf{k}_{ee}$ before condensation of the internal d.o.f.

3.2 Computation of element nodal loads

A few different types of external forces are expected from input data. Work equivalent nodal loads are computed from the given external forces and assembled into the global load vector as described in the following.

3.2.1 Concentrated forces

The concentrated forces are directly assembled into the global load vector. When the direction of a concentrated force is specified in local coordinates, it should be converted into global coordinates using the relation,

$$\mathbf{f}^c_i = \mathbf{R}_i^T \mathbf{f}^c_i \tag{3.2.1}$$

in which $\mathbf{f}^c_i$ and $\mathbf{f}^c_i$ denote concentrated loads applied at node i which are expressed, respectively, in local and global coordinates.

3.2.2. Distributed surface loads

A distributed load can be specified either by its nodal values or as a uniform load over each element. When the nodal values are given as input data, the values at an arbitrary point within an element are obtained by interpolation. A distribution of a load over an element is denoted by $\mathbf{w}$ and the value at node i by $\mathbf{w}_i$. Thus,

$$\mathbf{w} = \sum_{i=1}^{n} \mathbf{N}_i \mathbf{w}_i = \tilde{\mathbf{N}}^T \mathbf{w}^e \tag{3.2.2}$$

with

$$\tilde{\mathbf{N}}^T = \lfloor N_1 \; N_2 \; N_3 \cdot \;\cdot\; \cdot \; N_n \rfloor \tag{3.2.2a}$$

$$\mathbf{w}^{eT} = \lfloor w_1 \; w_2 \; w_3 \cdot \;\cdot\; \cdot \; w_n \rfloor \tag{3.2.2b}$$

Here, $\tilde{\mathbf{N}}$ should be distinguished from $\mathbf{N}$ in Eqn. (2.3.35a). The work equivalent nodal load is obtained from

$$\mathbf{f}^{de} = \int_A \tilde{\mathbf{N}} \, \mathbf{w} \, dA = \int_A \tilde{\mathbf{N}} \, \tilde{\mathbf{N}}^T \mathbf{w}^e dA = \left(\int_A \tilde{\mathbf{N}} \, \tilde{\mathbf{N}}^T dA \right) \mathbf{w}^e \tag{3.2.3}$$

Applying the numerical integration,

$$\mathbf{f}^{de} = (\sum_{k=1}^{q} \tilde{\mathbf{N}}_k \tilde{\mathbf{N}}_k^T |\mathbf{J}|_k W_k) \, \mathbf{w}^e \tag{3.2.4}$$

in which the subscript k is the index for integration point k. When a uniform load over an element **w** is given, the work equivalent load is obtained from

$$\mathbf{f}^{de} = (\sum_{k=1}^{q} \tilde{\mathbf{N}}_k |\mathbf{J}|_k W_k) \, \mathbf{w} \tag{3.2.5}$$

If a distributed surface load is expressed in local coordinates, it should first be converted into global coordinates before computing the work equivalent load.

3.2.3. Line loads

It is assumed that line loads are applied only along element boundaries. The integration points are set along the boundary.

$$\mathbf{f}^{le} = L (\sum_{k=1}^{r} \mathbf{Y}_k \mathbf{Y}_k^T W^l_k) \, \mathbf{T}^e \tag{3.2.6}$$

where L, r, and W^l are the length of the boundary, number of integration points, and integration weight for one-dimensional integration, respectively, and **Y** is the corresponding interpolation function. The vector $\mathbf{T}^e$ has the nodal values of the line load.

$$\mathbf{f}^{le} = \begin{Bmatrix} 0 \\ \cdot \\ 0 \\ f^l_j \\ \cdot \\ f^l_m \\ 0 \\ \cdot \\ 0 \end{Bmatrix} \qquad \mathbf{T}^e = \begin{Bmatrix} 0 \\ \cdot \\ \cdot \\ T_j \\ \cdot \\ T_m \\ 0 \\ \cdot \\ 0 \end{Bmatrix} \tag{3.2.7}$$

in which the j, · · ·, m are the indices for the nodes along the boundary. Strictly speaking, L should be replaced by a Jacobian determinant when the nodes are not equally spaced along the boundary.

3.2.4. Body forces

The element body force vector is obtained from

$$\mathbf{f}^{be} = \int_{V} \tilde{\mathbf{N}}^{T}\mathbf{X} \, dv = \sum_{k=1}^{q} \tilde{\mathbf{N}}_{k}^{T}|\mathbf{J}|_{k}W_{k} \, t_{k}\mathbf{X}_{k} \tag{3.2.8}$$

in which $\mathbf{X}$ is an inertia force. Assuming that the mass density is uniform within an element, one obtains

$$\mathbf{f}^{be} = (\sum_{k=1}^{q} \tilde{\mathbf{N}}_{k}^{T}|\mathbf{J}|_{k}W_{k} \, t_{k}) \, \mathbf{X} \tag{3.2.9}$$

3.2.5 Global load vector

The global force vector comprises all the external forces, that is,

$$\mathbf{f}_{i} = \mathbf{f}^{c}_{i} + \sum_{e} (\mathbf{f}^{d,e}_{i} + \mathbf{f}^{l,e}_{i} + \mathbf{f}^{b,e}_{i}) \tag{3.2.10}$$

The summation is performed for all the elements meeting at node i.

3.3. Assembly and solution of system equations

The overall effectiveness of the finite element analysis procedure depends especially on how the assembly and solution of the system equations are accomplished. The three most commonly used methods are *band-matrix algorithm*, *skyline storage scheme*, and *frontal solution technique* (Irons, 1970). Although the skyline storage scheme is more efficient than the band-matrix

algorithm, the use of the scheme is still restricted by the available computer memory. The frontal solution technique reduces, to a large degree, the required memory space, but takes more computing time. Many finite element analysis systems (Brebbia, 1985) employ either the skyline storage scheme or the frontal solution method. It is reasonable to include both facilities in one program, as illustrated in Fig. 3.1, providing the opportunity for the users to decide, based on the problem size and the available computer memory, which solution routine to use. If the skyline scheme is chosen and the total skyline length exceeds the dynamically dimensionable space, the solution routine should be switched to the frontal method.

Standardized codes of solution routines are available (Bathe *et al.*, 1976; Hinton *et al.*, 1977; Bathe,1982). Fig. 3.2(a) is the general flow diagram of the frontal solution routine given elsewhere (Hinton and Owen, 1977). The unassembled element stiffness matrices are first recorded in a secondary storage device and recovered at the stage of assembly. Fig.3.2(b) shows an alternative scheme adopted in the present study, in which the element stiffness matrices are directly assembled into the system of equations. The scheme reduces the time consuming I/O operations and the secondary storage usage by bypassing the storage of the element stiffness matrices. It does not harm the reanalysis capability. The scheme in Fig.3.2(a) is more efficient only when some of the element stiffness matrices are updated and the rest of them are retained in the process of reanalysis.

3.4. Computation of stresses

Once the nodal displacements are obtained by solving the system equations, the strains within an element can be computed from the strain-nodal

displacement relationship. The stresses are computed subsequently, using the constitutive relation at the point of consideration. The stresses are usually the final and probably the most useful product of the finite element analysis. Therefore, it is important to use a proper method for stress evaluation.

3.4.1. Stresses at integration points

The computed strains and stresses are most accurate at integration points. Therefore, they are first evaluated at each integration point using the relations

$$\varepsilon_k = B_k \Delta^e \tag{3.4.1}$$

and

$$\sigma_k = E_k \, \varepsilon_k \tag{3.4.2}$$

in which the subscript k denotes the values at integration point k. The strain-displacement matrix B_k is computed at the stage of stiffness matrix evaluation. The matrix, which consists of $B^m{}_k$, $B^b{}_k$ and $B^s{}_k$, takes a huge data space, and therefore should be stored in a secondary storage device and recovered later for stress computation. The computed stresses vary linearly in the thickness direction and are completely defined by the values at the top and the bottom surface. The strains at both surfaces are obtained using the following equations.

$$\varepsilon_k{}^{(top)} = \begin{bmatrix} B^m{}_k - \frac{1}{2} t_k B^b{}_k \\ B^s{}_k \end{bmatrix} \Delta^e \tag{3.4.3a}$$

$$\varepsilon_k{}^{(bot)} = \begin{bmatrix} B^m{}_k + \frac{1}{2} t_k B^b{}_k \\ B^s{}_k \end{bmatrix} \Delta^e \tag{3.4.3b}$$

in which $\varepsilon_k^{(top)}$ and $\varepsilon_k^{(bot)}$ denote the stresses respectively, at the top and the bottom layers. The stresses at an integration point are obtained by Eqn.(3.4.2).

3.4.2 Nodal stresses

There are many techniques to obtain smoothed nodal stresses from the values at integration points. Among these, the local least squares smoothing might be the simplest, but the most suitable method for shell analysis in view of the accuracy and the complexity of shell ellements. According to this method, the stresses are first evaluated at each integration point and extrapolated to the nodes. The nodal stresses are obtained by averaging the contribution of each element which meets at the node. The extrapolation is based on the least squares regression of the values at integration points. The surface of the extrapolation can be expressed as a function of the natural coordinates

$$\sigma_o = a_1 + a_2\xi + a_3\eta + \cdots \cdot \qquad (3.4.4)$$

The coefficients, a_i, are determined such that the deviation of the extrapolation surface from the actual stress surface is minimized in the least squares sense. Thus,

$$E = \int_A \{ \sigma - (a_1 + a_2\xi + a_3\eta + \cdots \cdot)\}^2 \, dA \qquad (3.4.5)$$

is to be minimized, where σ denotes the actual stress. Here, the unknown coefficients a_i can be obtained from the conditions,

$$\frac{\partial E}{\partial a_1} = \frac{\partial E}{\partial a_2} = \cdots \cdot = 0 \qquad (3.4.6)$$

From Eqns. (3.4.5) and (3.4.6), one obtains

$$\int_A \left\{ \begin{array}{c} 1 \\ \xi \\ \eta \\ \vdots \end{array} \right\} \sigma\, dA = \int_A \left[\begin{array}{cccc} 1 & \xi & \eta & \cdots \\ \xi & \xi^2 & \xi\eta & \cdots \\ \eta & \xi\eta & \xi^2 & \cdots \\ \vdots & \vdots & \vdots & \vdots \\ \vdots & \vdots & \vdots & \vdots \end{array} \right] \left\{ \begin{array}{c} a_1 \\ a_2 \\ a_3 \\ \vdots \end{array} \right\} dA \qquad (3.4.7)$$

Assuming that the stress evaluated at an integration point represents the actual stress, and applying numerical integration to the left hand side and explicit integration to the right hand side, one derives the following relation for a 6-node triangular element with 3-point (inside) integration.

$$\left\{ \begin{array}{c} \sigma_1 \\ \sigma_2 \\ \sigma_3 \\ \sigma_4 \\ \sigma_5 \\ \sigma_6 \end{array} \right\} = \frac{1}{3A} \left[\begin{array}{ccc} 5 & -1 & -1 \\ -1 & 5 & -1 \\ -1 & -1 & 5 \\ 2 & 2 & -1 \\ -1 & 2 & 2 \\ 2 & -1 & 2 \end{array} \right] \left\{ \begin{array}{c} |J|_a\,\sigma_a \\ |J|_b\,\sigma_b \\ |J|_c\,\sigma_c \end{array} \right\} \qquad (3.4.8)$$

in which σ_i denotes the stress at node i, and the subscripts a, b and c are used to indicate the values evaluated at the integration points a, b and c respectively. For an 8-node quadrilateral element, the nodal stresses are given by

$$\left\{ \begin{array}{c} \sigma_1 \\ \sigma_2 \\ \sigma_3 \\ \sigma_4 \\ \sigma_5 \\ \sigma_6 \\ \sigma_7 \\ \sigma_8 \end{array} \right\} = \frac{1}{4A} \left[\begin{array}{cccc} 4-2\sqrt{3} & -2 & -2 & 4+2\sqrt{3} \\ -2 & 4+2\sqrt{3} & 4-2\sqrt{3} & -2 \\ 4+2\sqrt{3} & -2 & -2 & 4-2\sqrt{3} \\ -2 & 4-2\sqrt{3} & 4+2\sqrt{3} & -2 \\ 1-\sqrt{3} & 1+\sqrt{3} & 1-\sqrt{3} & 1+\sqrt{3} \\ 1+\sqrt{3} & 1+\sqrt{3} & 1-\sqrt{3} & 1-\sqrt{3} \\ 1+\sqrt{3} & 1-\sqrt{3} & 1+\sqrt{3} & 1-\sqrt{3} \\ 1-\sqrt{3} & 1-\sqrt{3} & 1+\sqrt{3} & 1+\sqrt{3} \end{array} \right] \left\{ \begin{array}{c} |J|_a\,\sigma_a \\ |J|_b\,\sigma_b \\ |J|_c\,\sigma_c \\ |J|_d\,\sigma_d \end{array} \right\} \qquad (3.4.9)$$

The surface area of the element is also obtained by numerical integration.

$$A = \sum_{k=1}^{q} W_k \, |\mathbf{J}|_k \qquad\qquad (3.4.10)$$

The above equations become identical to those appearing in other literature (Hinton and Campbell ,1974; Hinton *et al.*,1975) when $|\mathbf{J}|$ is constant everywhere within the element.

The principal stresses and the principal directions are determined as the eigenvalues and the corresponding eigenvectors of the stress tensor.
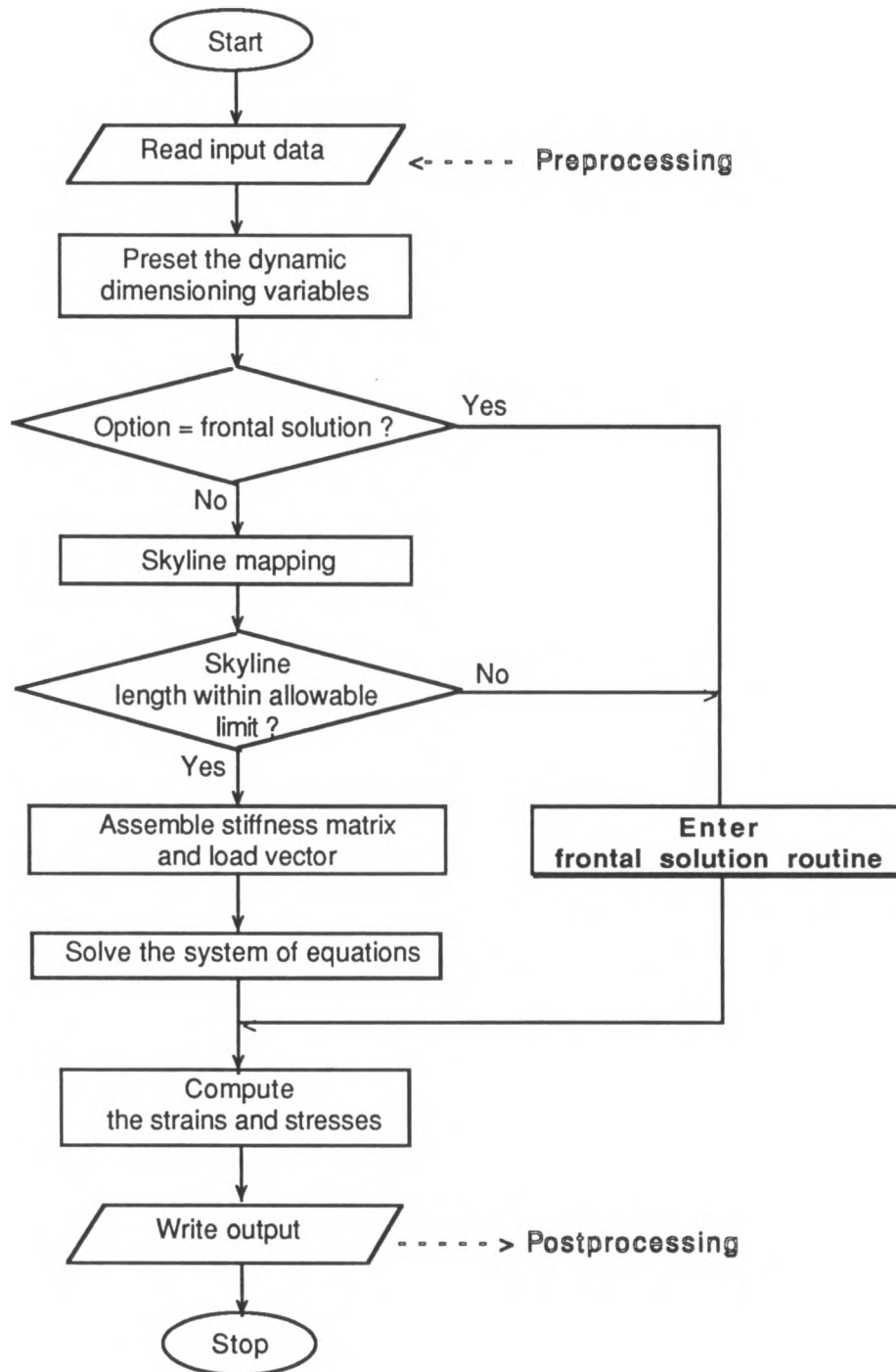
Fig. 3.1   General flow diagram
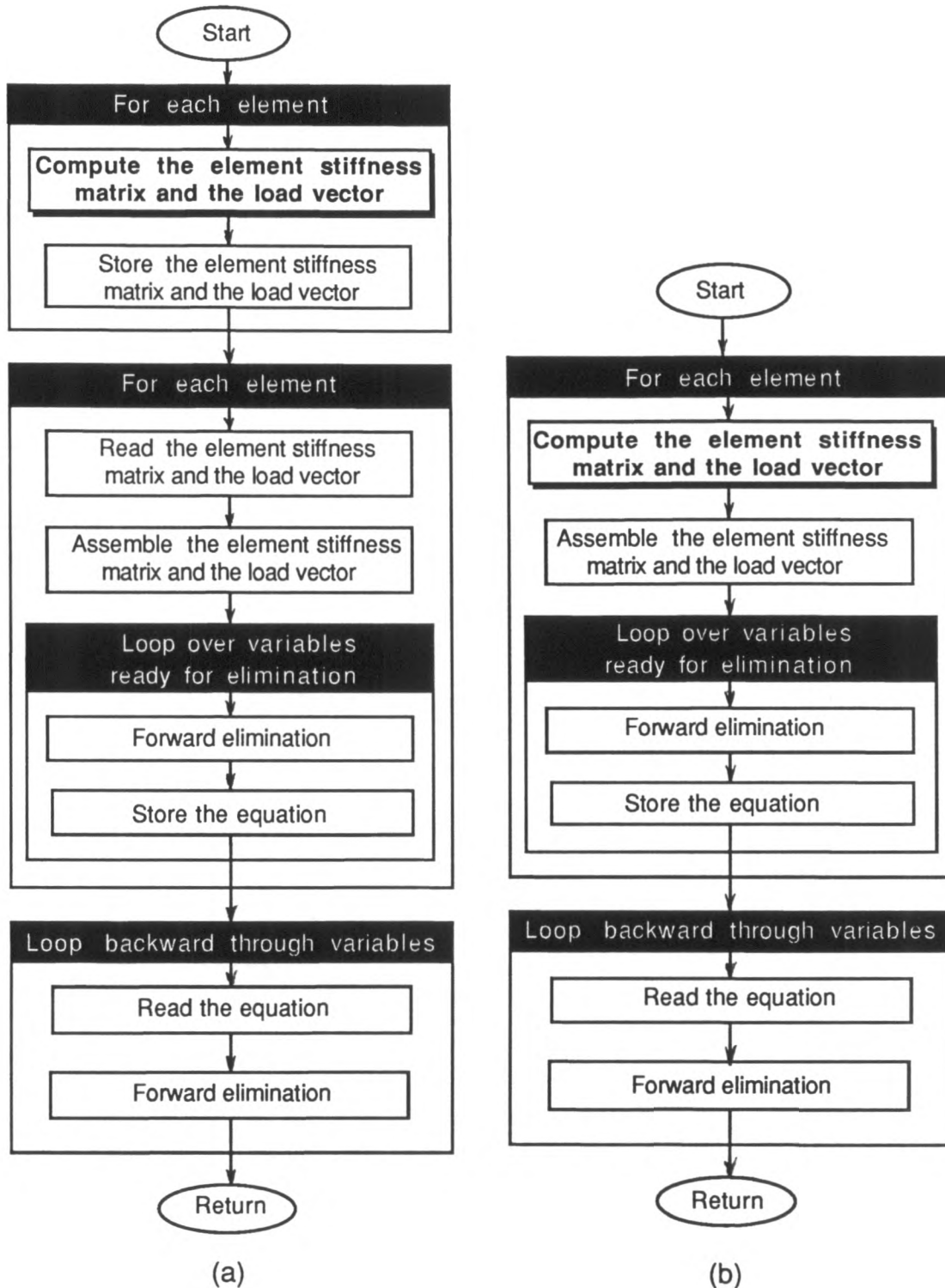
Fig. 3.2   Process of solving system equations
(a) Hinton and Owen (1977)
(b) Present study
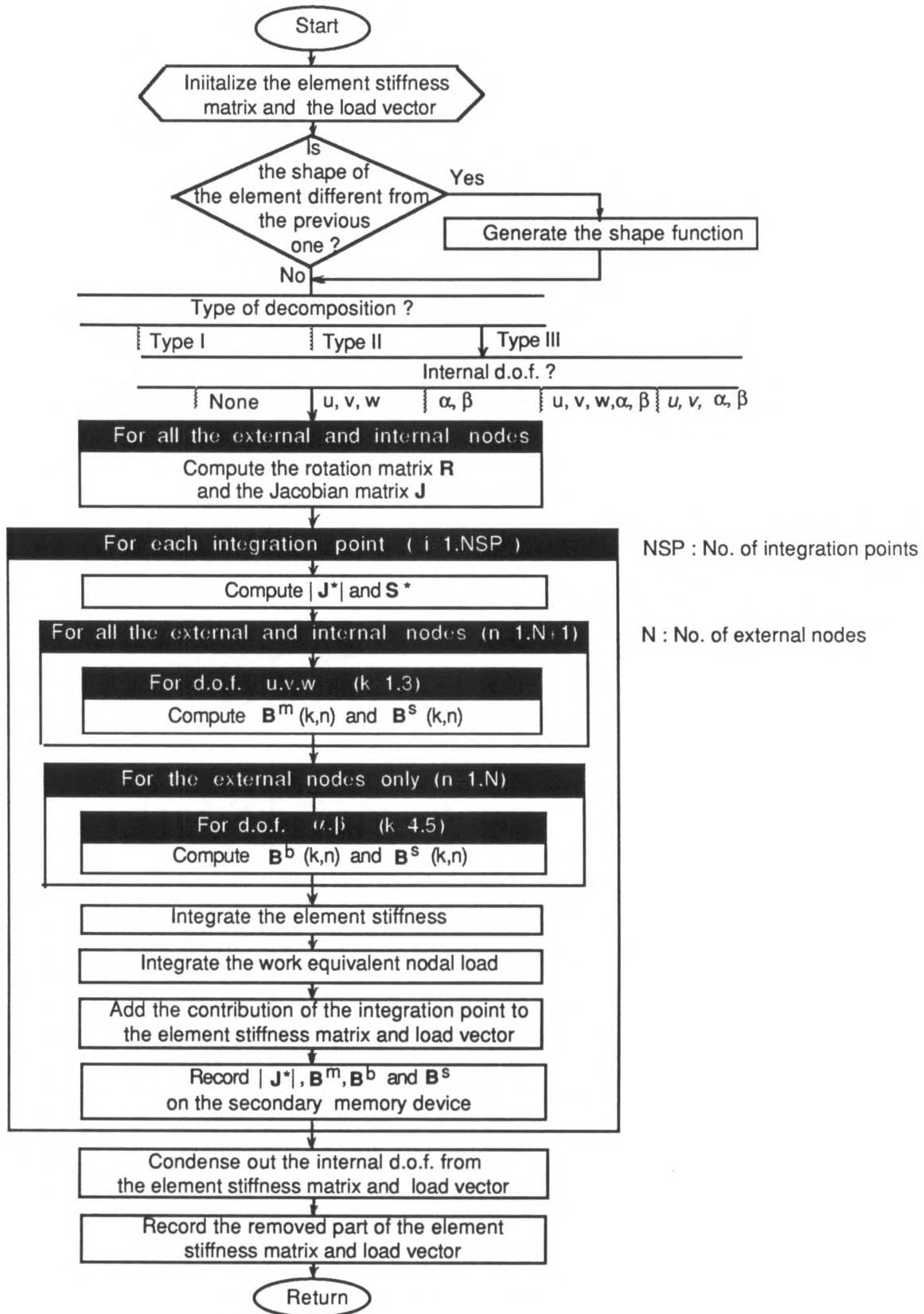
Fig. 3.3 Flow diagram for computation of element stiffness matrix

Chapter 4

NUMERICAL STUDY

This chapter investigates the validity of the newly formulated element and its complementary devices discussed in Chapter 2. The element is also compared with the popular degenerate shell element to distinguish in detail the new formulation from the old one. The effects and limitations of various complementary devices are numerically demonstrated. Attention is also given to finding the possibility of removing the troublesome locking behavior without inducing spurious modes. Finally, the overall evaluation suggests how to achieve the best performance of the element. The following test problems are used in this numerical study:

(1) Cylindrical shell roof under dead weight

(2) Pinched cylinder (thicker case)

(3) Pinched cylinder (thinner case)

(4) Fixed-free quarter cylinder subject to uniform line moment at the free end

(5) Four-corner-supported square plate under uniform load

(6) Clamped circular plate under uniform load

(7) Cantilever plate with uniform line load at the free end

(8) Sphere under uniform internal pressure

(9) Pinched sphere

(10) Truncated half sphere with point loads in two orthogonal directions

Problems (1) through (4) are used for convergence tests and element distortion tests. The interrelation of locking and spurious zero-energy modes are studied based on problems (3) and (5). The patch tests are (4), (7) and (8). The

computed stresses are compared with the analytical solutions for (1), (7), (8), (9) and (10). Figures corresponding to each test are indicated in Table 4.1. The element notations in the figures are given following the rules in Table 4.2.

4.1. Description of test problems

The analytical solutions of the test problems as well as their configurations are given in this section.

Cylindrical shell roof

The cylindrical shell roof in Fig.4.1 has been most widely used as a test case for shell elements. The shell roof is subjected to dead load only and supported by rigid diaphragms at both ends. Only one quarter of the roof is modeled due to its symmetry. Approximate analytical solutions based on the shallow and the deep shell theories give a vertical deflection of 3.703 and 3.598 inches, respectively, at the center of the free edge (Scordelis and Lo, 1964).

Pinched cylinder (thicker and thinner cases)

The cylinder in Fig.4.2 is another popular test case for shell elements. Both ends of the cylinder are free. The numerical tests include cases with two different thicknesses, $t = 0.094$ in. (thicker) and $t = 0.01548$ in. (thinner) The thinner one is sensitive for locking phenomena. A point load is applied at the center of the cylinder (point C) with $P = 100$ lb for the thicker case and $P = 0.10$ lb for the thinner case. One octant of the cylinder (the shaded region in the figure) is modeled. The vertical deflection at point C obtained by analytical solution (Ashwell *et al.* 1972) are 0.1139 in. and 0.02439 in., respectively, for the thicker and the thinner cases.

Table 4.1.   Figure numbers for numerical tests

Test type Prob.#	Convergence test	Comparison w/ analytical sol.	Effect of zero energy control	Element distortion test
(1)	B.1,B.6,B.7,B.11	4.9,4.10	B.15,B.18,B.25	B.30
(2)	B.2,B.8,B.12	–	–	B.31
(3)	B.3,B.9,B.13	–	–	B.32
(4)	B.4,B.10,B.14	–	B.16,B19,B.21,B.23,B.26,B28	B.33
(5)	B.5	–	B.17,B.20,B.22,B.24,B.17,B.29	–
(6)	–	4.11	–	–
(7)	–	–	–	(Table 4.5)
(9)	–	4.12,4.13,4.14	–	–
(10)	(Table 4.3)	–	–	–

Table 4.2 Rules for element notations in figures

Format	shape & type–complementary device-complementary device (integration scheme)

Shape		Type		Complementary Device		Integration Scheme	
T	Triangular	I	Type I	A	IDOF(A)	3	3 point integration
Q	Quadrilatral	II	Type II	B	IDOF(B)	3S	Midside 3 point integr.
		III	Type III	C	IDOF(C)	7	7 point integration
		D	Degenerate	D	IDOF(D)	2x2	2x2 integration
				M	Mixed formulation	3x3	3x3 integration
				MM	Modified mixed form.	3/3	3 point+3 point α control
						3/7	3 point+7 point α control

Examples : QD(2x2)   Degenerate shell element with 2x2 integration
            TIII–A(3S)   Type III element with IDOF(A) and midside 3 point integration
            TIII–A–M(7) Type III element by mixed formulation with IDOF(A) and 7 point integration
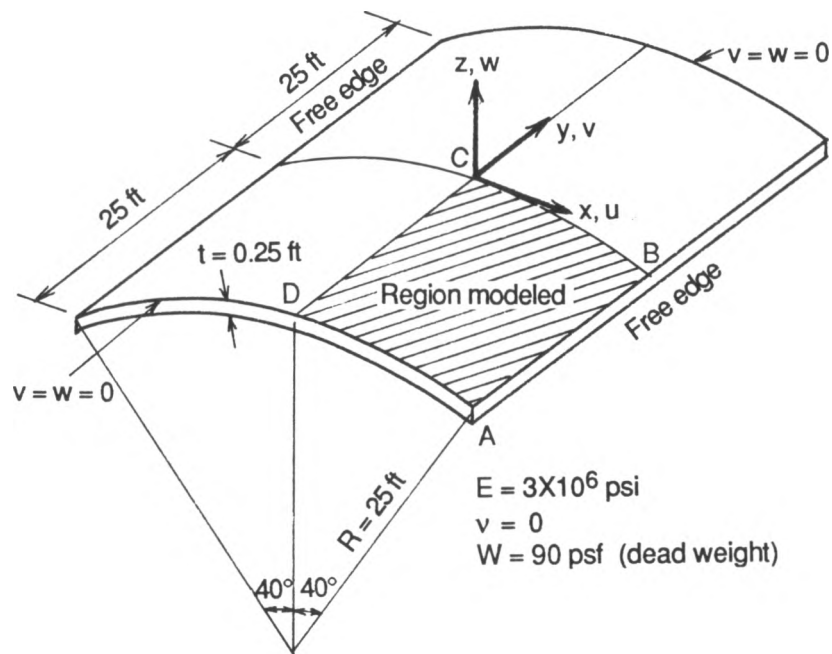
Fig. 4.1   Cylindrical shell roof
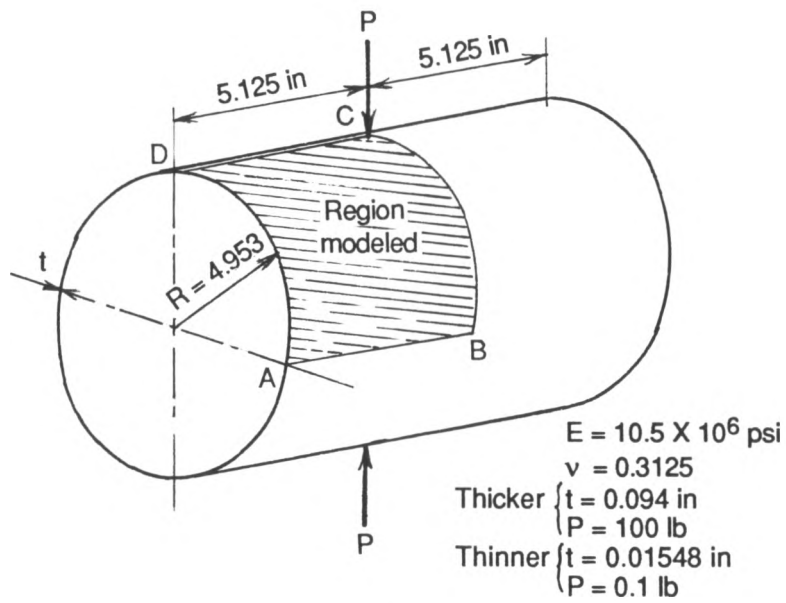
Fig. 4.2   Pinched cylinder

Fixed-free quarter-cylinder

The fixed-free quarter-cylinder with infinite width in Fig.4.3 was considered by Wu (1981) as a case in which the bending action is dominant.

This is a patch test case for pure bending and provides a good test for membrane locking as well. One edge of the cylinder is fixed and the other edge is free. A uniform line moment M is applied along the free edge. Only one strip of the cylinder is modeled. The rotation in the axial direction is suppressed to simulate the infinite width. The exact solution for the horizontal displacement at point B is obtained by

$$u_B = 12\,M\,r^2\,(1 - v^2)/(E\,t^3)\tag{4.1.1}$$

in which r, t, E, and v represent respectively the radius, the thickness of the cylinder, the modulus of elasticity, and the Poisson's ratio. The above equation gives u_B = 10.92 for the dimensions and material properties shown in the figure.

Four-corner-supported square plate

A simply-supported square plate is considered as an extreme case to test the spurious zero-energy modes. The plate is supported at the four corner points. A uniformly distributed load is applied in the transverse direction. Only one quarter of the plate is modeled due to symmetry. The analytical solution (Timoshenko *et al*., 1959) gives the normalized vertical deflection at the center of the plate

$$\frac{w\,a^4}{E\,t^3} = 2.8\tag{4.1.2}$$

for the configuration shown in Fig. 4.4.
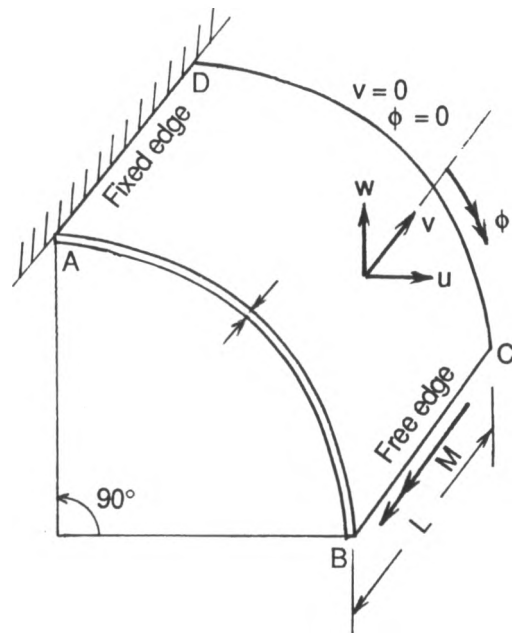
Fig. 4.3   Fixed-free quarter cylinder
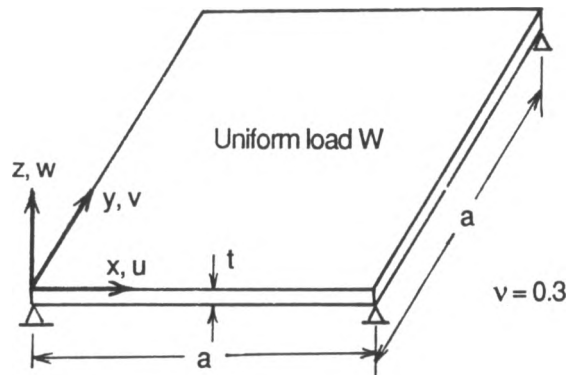
Fig. 4.4   Four-corner-supported square plate

Clamped circular plate under uniform load

A circular plate with a clamped boundary is tested to assess the accuracy of the element. Distorted meshes are used for both triangular and quadrilateral elements. Owing to the symmetry, only a quarter of the plate is modeled. The deflection, along the radial line, under uniform load is given as follows (Timoshenko and Woinowsky-Krieger, 1959) :

$$w = \frac{q}{64D} [(r^2 - x^2)^2 + 4t^2(r^2 - x^2) / (1 - v)] \tag{4.1.3}$$

in which q, r, x and t are defined inFig.4.11.

Cantilever plate with uniform line load at the free end

An infinitely long square plate in Fig.4.5, with one end fixed and the other end free, is subject to a uniform line load, tension or moment, at the free end. It is a patch test case in which all the elements in a distorted mesh should have uniform tensile stress or uniform bending moment and zero values for other stress components.

Sphere under uniform internal pressure

This case tests the capability of representing constant membrane stresses of a doubly curved shell. This is also a patch test with geometric approximation. The normal deflection as well as the normal stresses should be uniform over the whole sphere. The exact solutions are

$$w = q\, r^2 (1 - v) / (2\,E\,t) \tag{4.1.4}$$

and

$$\sigma_x = \sigma_y = q\, r / 2 \tag{4.1.4a}$$

Only one octant of the sphere is modeled due to symmetry and for the convenience of applying boundary conditions (Fig. 4.6). Two cases with different thickness to radius ratio, i.e., t/r=0.01, and 0.1 are tested.
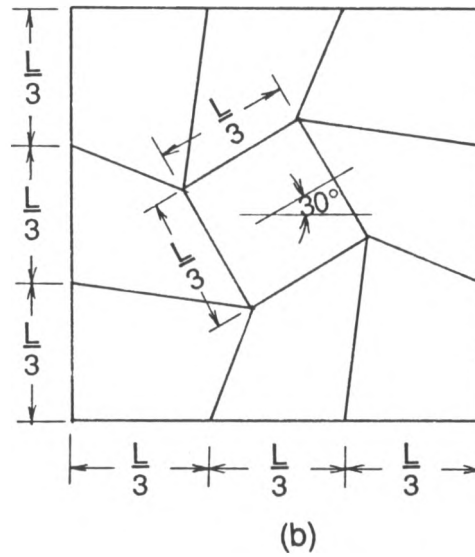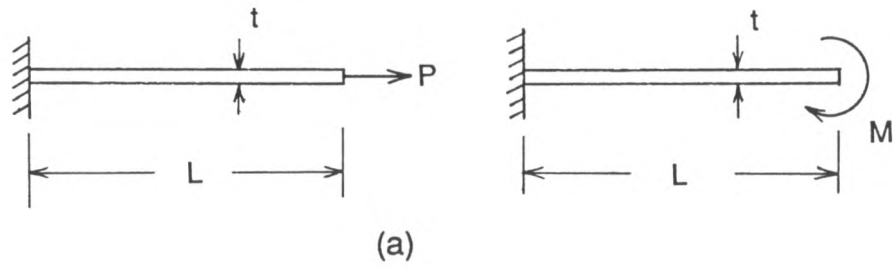
Fig. 4.5   Cantilever plate
(a) Configuration   (b) Distorted mesh

Pinched sphere

A pinched sphere is a doubly curved shell with positive Gaussian curvature. The sphere is subjected to point loads at the crowns as shown in Fig.4.6. It is a case with a stress singularity at the pole. Bending action is dominant around the pole, and membrane action is dominant away from the pole. Only one octant of the sphere is analysed. The analytical solution by Koiter (1963) gives the nondimensionalized vertical displacement at the crown,

$$\frac{E\,t\,w}{p} = 21.2 \qquad\qquad (4.1.5)$$

for the configuration in Fig.4.6.

Truncated half sphere

A half sphere is truncated for 18^0 from the pole (Fig. 4.7). It is a sensitive case with strong coupling of membrane and bending actions. Only a quarter of the half sphere is modelled using the symmetry. The solution for normal displacement at point A and B is given as 0.094 in the reference (MacNeal and Harder, 1984).

Distorted meshes

Problems (1), (2), (3), (4), and (7) are also tested with distorted meshes as shown in Figs. 4.5 and 4.8. Distortion of finite element meshes usually deteriorates the accuracy of the computation. Meshes of real objects are complex and seldom regular. Therefore, it is necessary to evaluate the performance of a finite element with realistic meshes. The distortion has been made by rotating the cenral element of 3X3 mesh as shown in Fig.4.8. The degree of distortion is indicated by the rotation angle.
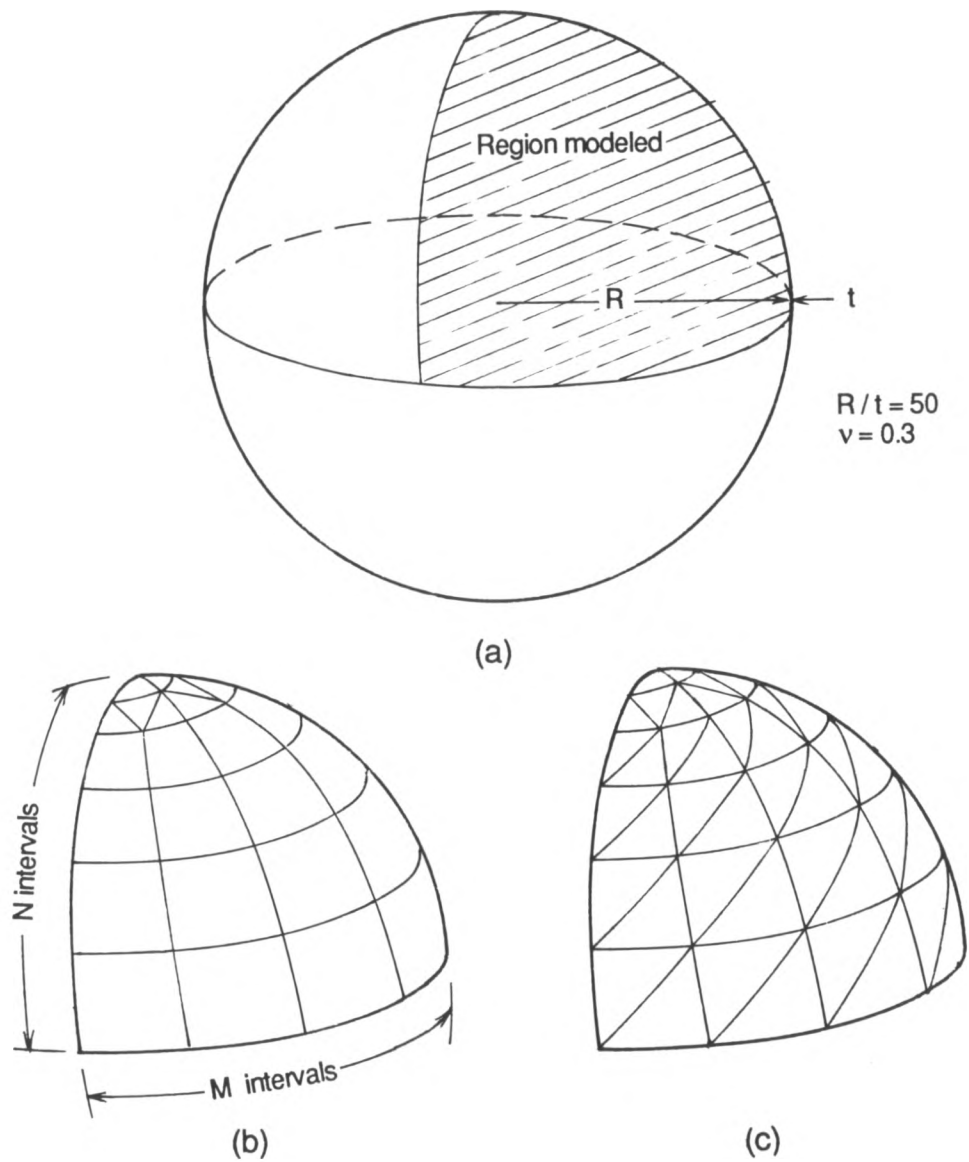
Fig. 4.6   Membrane and pinched sphere
(a) Configuration
(b) MXN mesh with triangular elements around the pole and
    quadrilateral elements elsewhere
(c) MXN mesh with triangular elements
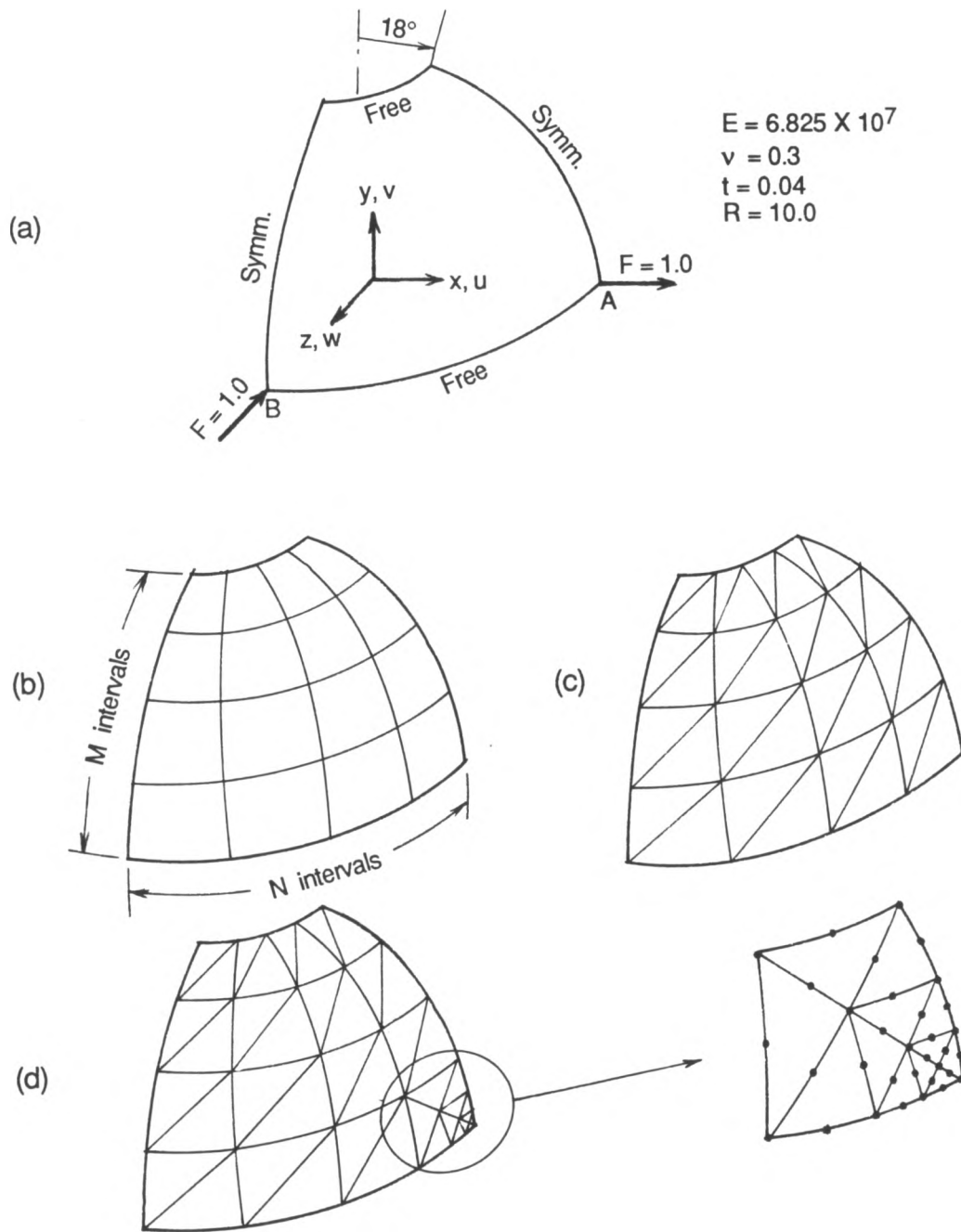
Fig. 4.7   Truncated half sphere
  (a) Configuration
  (b) MXN mesh with quadrilateral elements
  (c) MXN mesh with triangular elements
  (d) Non-uniform mesh with local refinement

(a)

(b)

Fig. 4.8   Finite element mesh for element distortion tests
(a) Configuration   (b) Distorted mesh

4.2   Review of the degenerate shell element

The degenerate shell element has been studied numerically by many researchers (Ahmad *et al.*, 1970; Fezans and Verchery, 1982; Pawsey and Clough, 1971; Takemoto and Cook, 1973; Zienkiewicz *et al.*, 1971). The previous investigators concluded that the element with reduced integration performs satisfactorily for both thick and thin shells. However, all of them are concerned only with the quadrilateral element, and no numerical tests of triangular element are reported in the literature. The present study revealed that the triangular element behaves differently from the quadrilateral element. Reduced integration is not as helpful as for the triangular element. The element suffers from severe locking phenomenon in so-called sensitive problems. Another noteworthy case is a curved shell under pure bending, which has not been studied so far for the degenerate shell element. Even the quadrilateral element suffers from locking phenomena in this case. The convergence tests of the degenerate shell element are presented in Fig. B.1 through B.5 and discussed below.

Cylindrical shell roof

The convergence of quadrilateral elements with 3x3 full integration is relatively slow but drastically improved by 2x2 reduced integration as shown in Fig. B.6. The solution converges to the analytical solution based on shallow shell theory. Two different 3-point rules together with the 7-point rule are compared for triangular element. The inside 3-point rule gives the fastest convergence. However, the convergence of triangular elements is not as satisfactory as that of the quadrilateral element with reduced integration.

Pinched cylinder (thick)

The convergence for the pinched thick cylinder is in the same order as in the cylindrical shell roof case. But the quadrilateral element with reduced integration converges to a value approximately 7 % smaller than the analytical solution by Ashwell and Sabir (1972).

Pinched cylinder (thin)

The quadrilateral element with reduced integration gives satisfactory results also for this case. But the solution converges to a value approximately 5% smaller than the analytical one (Ashwell and Sabir, 1972). The triangular element behaves very poorly regardless of integration order, and its convergence is unacceptably slow for this case.

Fixed-free quarter cylinder

Both the triangular and the quadrilateral element with reduced order integration converge to a value approximately 20% smaller than the exact solution. The convergence cannot be improved further by mesh refinement beyond 100 nodes. Substantial membrane shear stress remains even with refined mesh. Thus, the element suffers from membrane shear locking. The failure for this case implies that the element cannot properly represent the pure bending state of a cylindrically curved shell.

4.3   Convergence of the new elements

The convergence behavior of the new element with each type of decomposition is compared with the degenerate shell element in Fig.B.1 through Fig.B.5. The element behaves better than the degenerate shell element for all cases tested in this study. The type I element converges to

somewhat larger values than the analytical solutions in general. The elements with type II or III decomposition show a convergence to the exact solutions for both thick and thin shells. Although the rate of convergence is almost equivalent to that of the degenerate shell element, the deviation of the converged solution from the analytical one is much smaller, and almost not noticeable. The superiority is more noticeable for bending-dominant cases. A significant difference from the degenerate shell element is that the new element does not lock for the curved shell under pure bending action. However, the element still suffers from locking for thin shell cases, which should be cured by complementary devices discussed in Section 2.6. The element with type III decomposition seems to give the most favorable convergence behavior (Figs. B.1~B.5).

Cylindrical shell roof

The convergence of the element with type II or type III decomposition is slightly faster than, but almost equivalent with, that of the degenerate shell element. The element with type I decomposition gives a more flexible solution which converges to the deep shell solution. The computed vertical displacement on midsection is compared in Fig.4.9. It demonstrates the convergence of the element to the exact solution.

Pinched cylinder (thick)

The type I element gives a solution about 5% larger than the exact one, while the type II and III elements show convergence to the exact solution. All three types of element of triangular shape produce much slower convergence, although they are slightly better than the degenerate shell element of the same shape.

Pinched cylinder (thin)

The type II and the type III elements of quadrilateral shape show quite satisfactory convergence characteristics for this case. All the three types of element of triangular shape produce much slower convergence, although they are slightly better than the degenerate shell element of the same shape.

Fixed-free quarter cylinder

This is a test case which proves the superiority of the new element over the degenerate element. The capability of the element for constant strain state under pure bending is also numerically proved. Membrane stresses vanish completely by mesh refinement with type II or type III elements, while this cannot be achieved by the degenerate shell element. The type II and the type III element converge to the exact solution without any locking phenomenon even if the thickness of the cylinder is reduced to a thin shell category.

4.4 Accuracy of the new elements

The convergence tests revealed that the type I element is not desirable, because the solution does not converge to the correct ones. The type II element yields an almost identical solution to that of the type I element. For these reasons, only the accuracy of the type III element was examined by comparing the computed displacements and stresses with analytical solutions.

The type III element shows relatively good agreement with the analytical solutions for the following test cases.

Cylindrical shell roof

In Fig. 4.9 and Fig. 4.10, the computed normal displacements, tangential displacements, membrane stresses and bending moments are compared with analytical solutions (ASCE Manual No.31,1952; Scordelis and Lo, 1964;
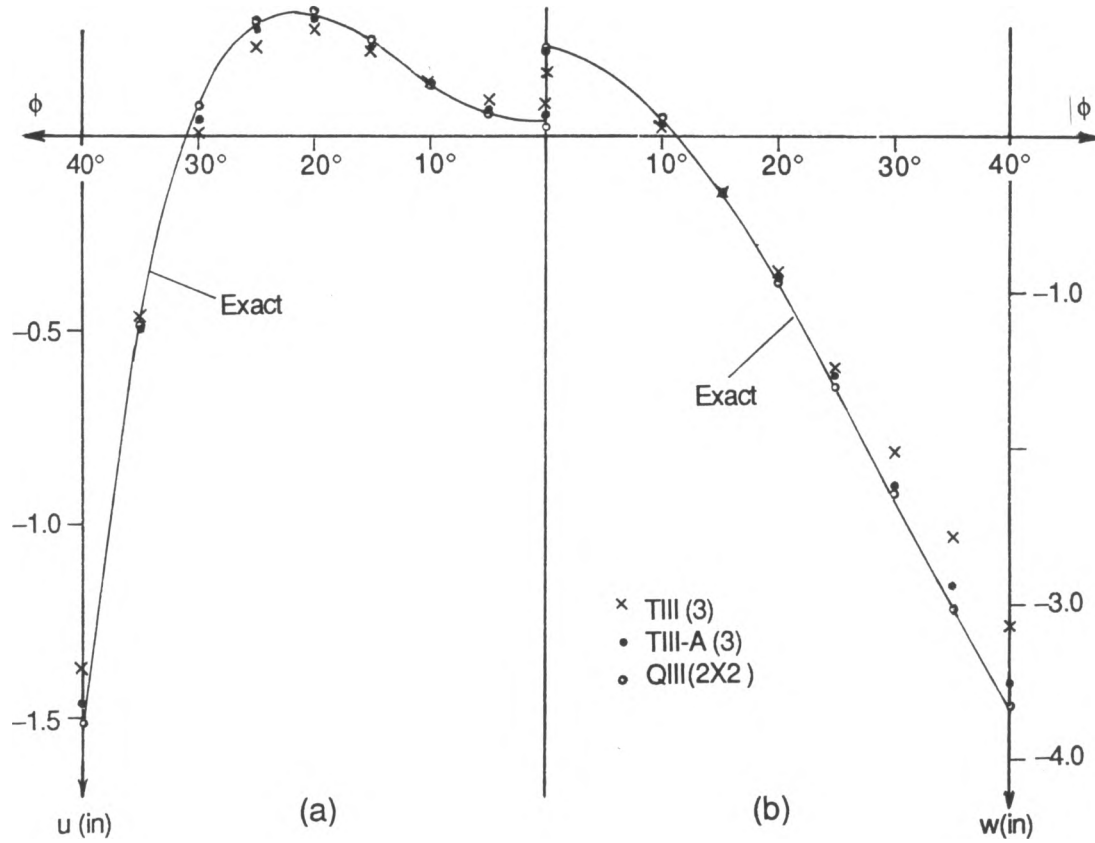
Fig. 4.9   Displacements of the cylindrical shell roof
            (a) Longitudinal displacements at the support
            (b) Vertical displacements on the midsection
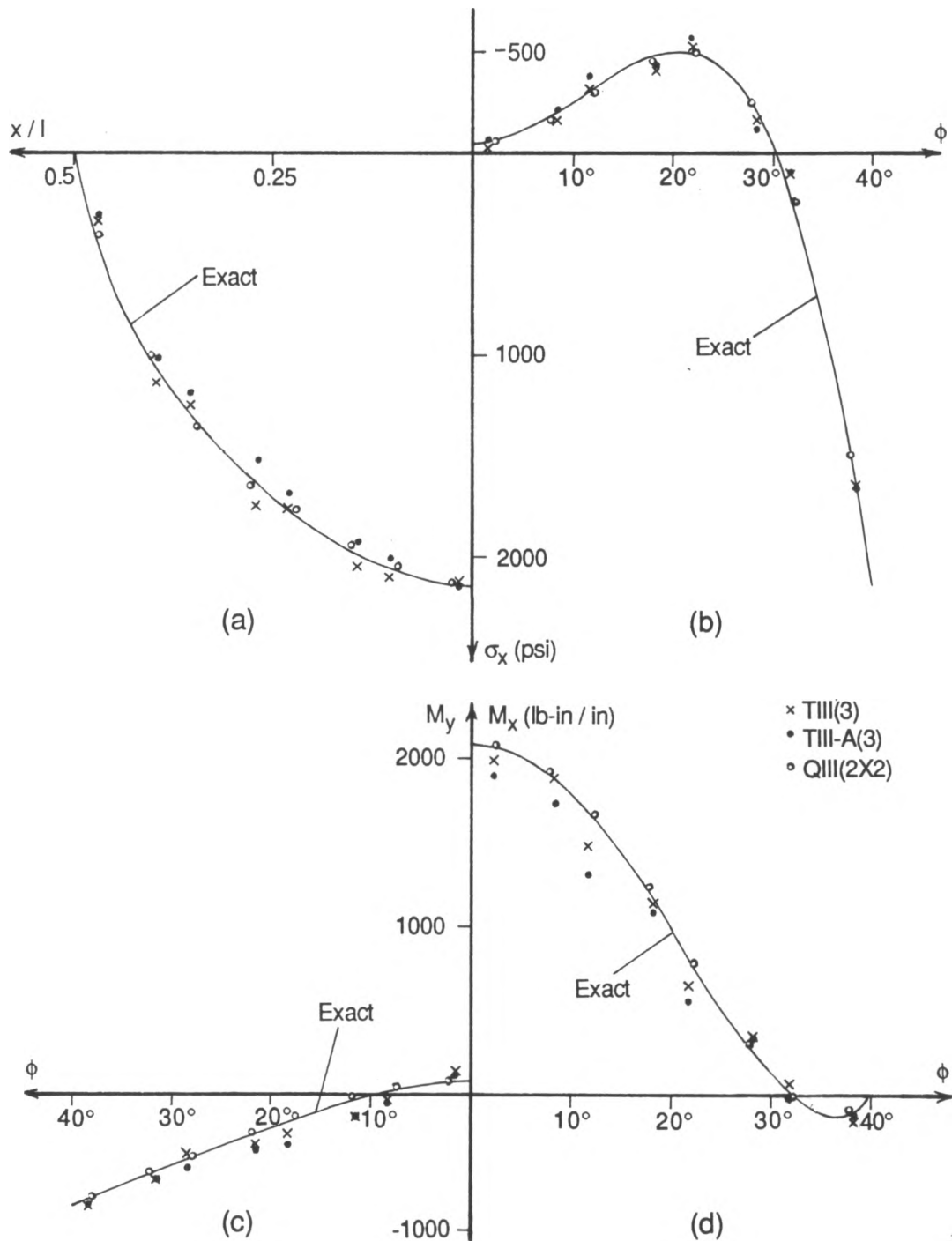
Fig. 4.10 Stresses of the cylindrical shell roof

    (a) Membrane stress σ_x at the midsection ($x=0$)

    (b) Membrane stress σ_y at the free edge ($\phi=40°$)

    (c) Bending moment M_y at the midsection

    (d) Bending moment M_x at the midsection

Zienkiewicz *et al.* 1971). With 4x4 mesh, the quadrilateral element shows good accuracy, but the triangular element shows some discrepancy from the analytical solution. It should be noted that results of the triangular element do not represent the converged solution. The displacement pattern implies that the triangular element will also produce a good accuracy as the mesh is further refined.

Clamped circular plate

In Fig. 4.11, the deflections along a diameter of the circle are compared with the exact solutions for t/r=0.1 and t/r=0.02. The type III element of quadrilateral shape gives relatively good accuracy even with the distorted coarse mesh, while the triangular element shows some descrepancy from the exact solution for t/r=0.02. A more refined mesh of triangular elements would be necessary for this case to obtain satisfactory results.

Pinched sphere

Figs. 4.12, 4.13 and 4.14 show the comparisons of the computed results with the exact solutions for normal deflections, membrane stresses and bending moments along a meridional line. The computed deflections agree well with the membrane solution for a meridional angle greater than 5°. The converged solution of the deflection at the pole is larger than the membrane solution and Koiter's analytical solution with modification for bending. But the solution agrees with the Koiter's solution when the load is distributed over the area of 1° subtended angle. A refined mesh around the pole is needed to obtain a converged solution for this region. Mesh refinement gives almost no effects for the region beyond the 5° subtended angle. A similar pattern of solution is observed for membrane stresses and bending moments.
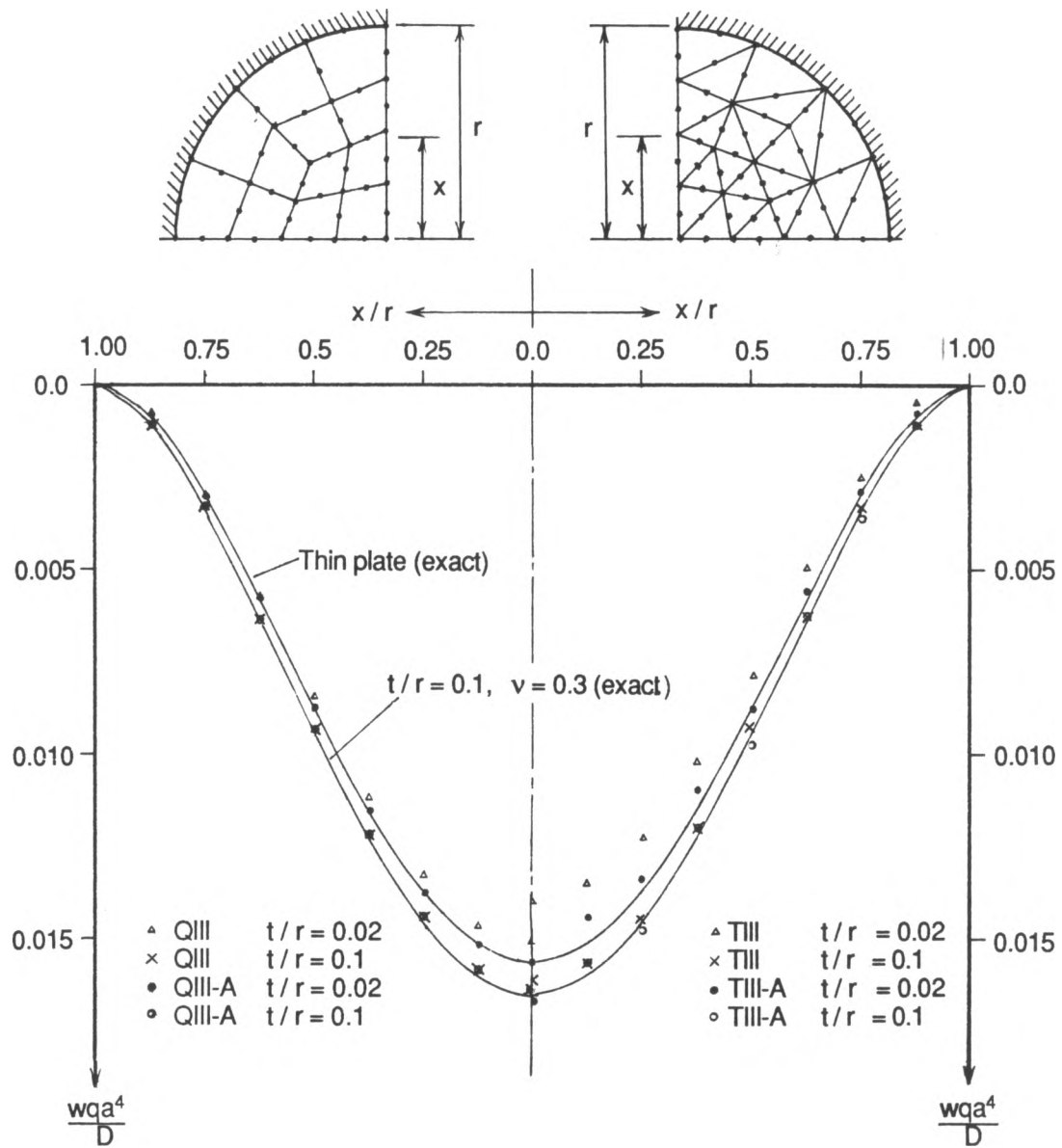
Fig. 4.11 Deflection of a circular plate with clamped boundary and under uniform load
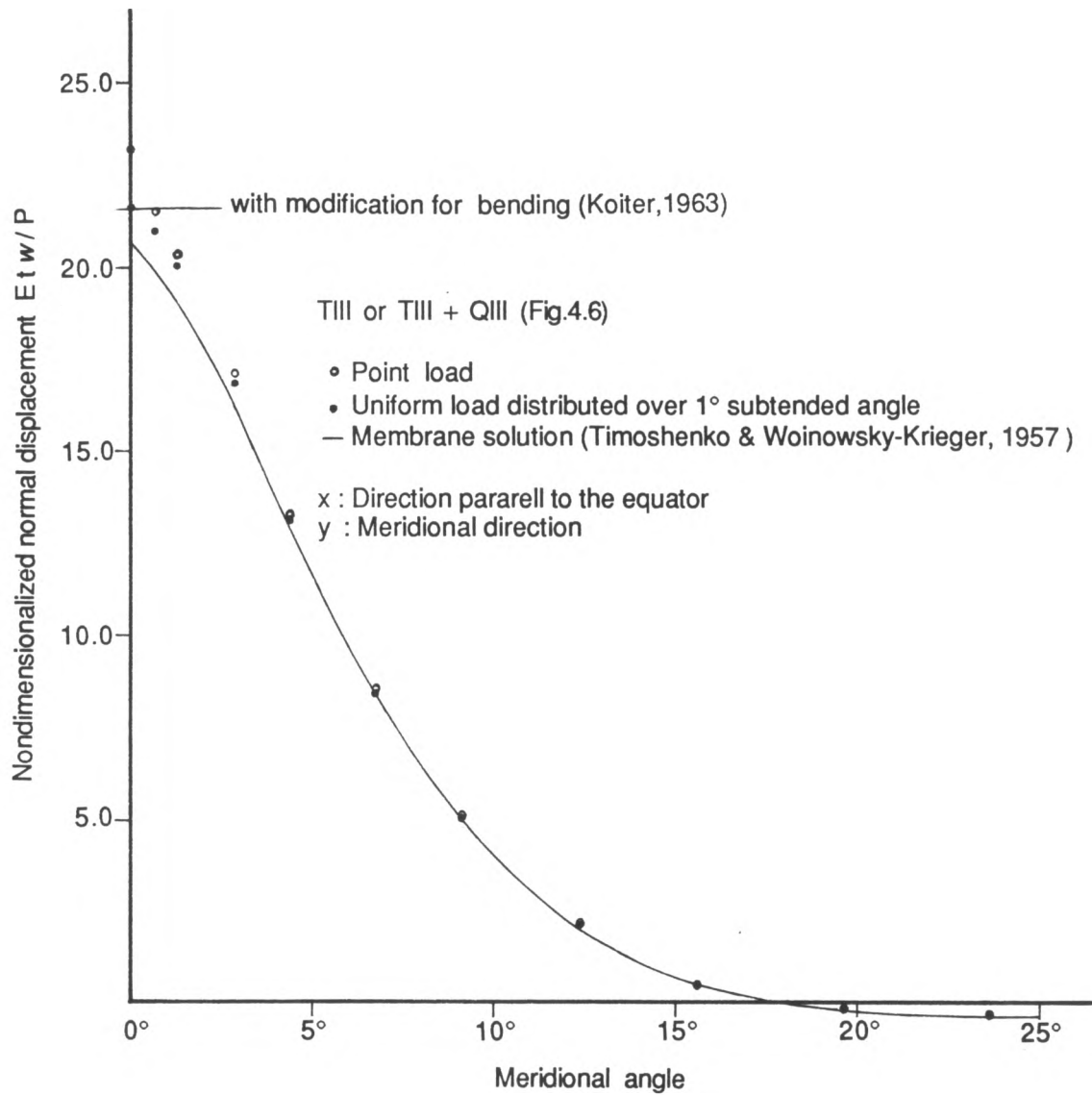
Fig. 4.12 Nondimensionalized normal displacement along the meridian of the pinched sphere
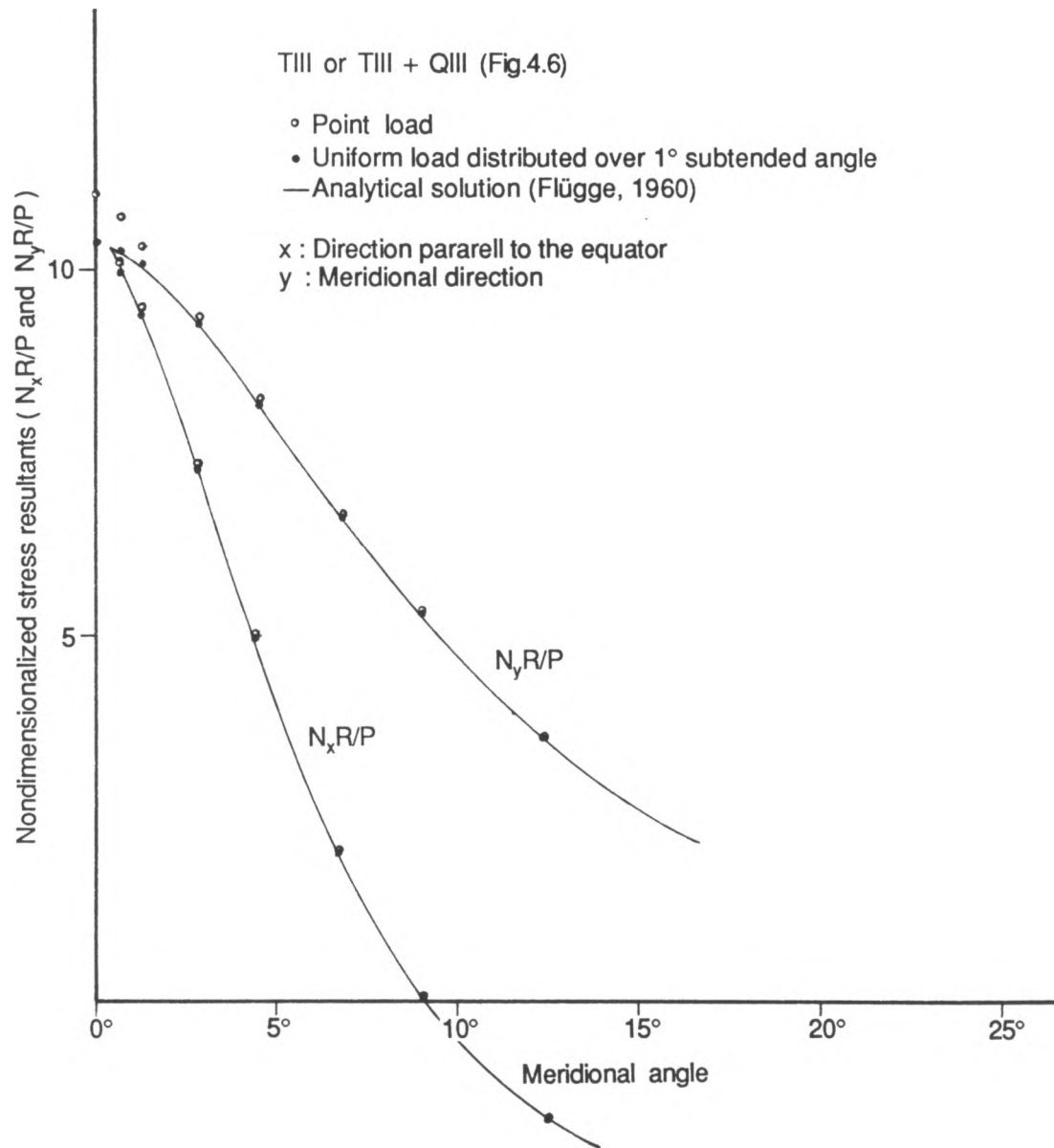
Fig. 4.13 Nondimensionalized stress resultants along the meridian of the pinched sphere
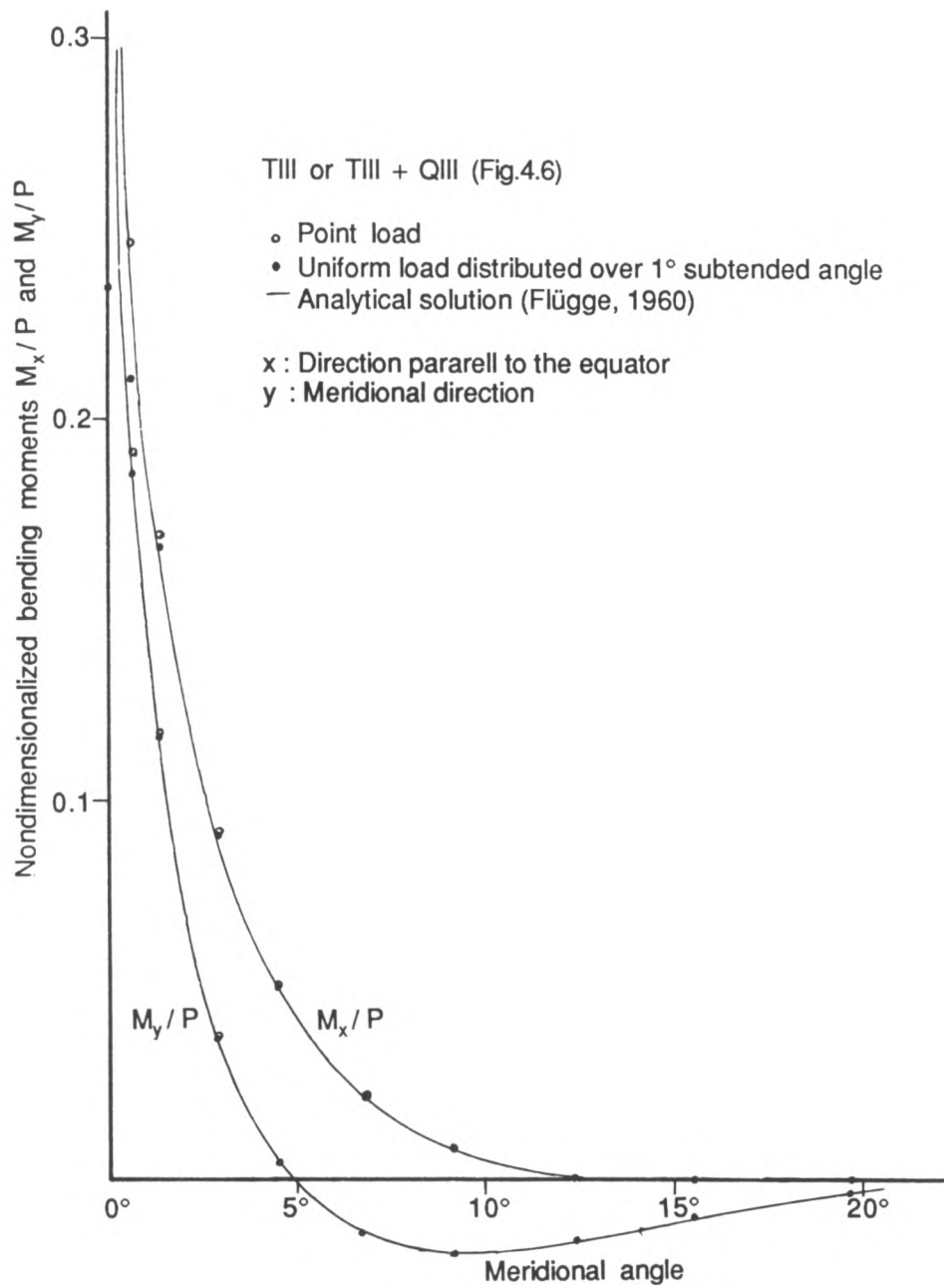
Fig. 4.14 Nondimensionalized bending moment along the meridian of the pinched sphere

Sphere under uniform pressure

The elements of all three types give the correct solution even with relatively coarse mesh refinement. Both quadrilateral and triangular elements produce equivalent accuracy. The type III element shows dependence of its accuracy on the thickness to radius ratio for coarse mesh (4 intervals in meridional and equatorial directions). For t/r=0.01, the maximum error is about 6% in normal displacements and 2% in stresses. But, in the case of t/r=0.1, the maximum error is less than 1% in normal displacements and stresses. With more refined mesh (8 intervals in both directions), the maximum errors in displacements and stresses are in the order of 0.01 % for both t/r=0.1 and 0.01.

Truncated sphere

This is an extremely thin shell case, and the convergence behavior for this case is somewhat similar to that of thin pinched cylinder. The normalized radial displacements at A and B with respect to the exact solutions are presented in Table 4.3.

Table 4.3 Computed deflections[*] at points A and B of the truncated half sphere

Mesh	QIII(2x2) $u_A=w_B$	QD(2x2) $u_A=w_B$	TIII (3) u_A	TIII (3) w_B	TIII-A (3) u_A	TIII-A (3) w_B	TD (3) u_A	TD (3) w_B
4x4	0.796	0.754	0.047	0.045	0.483	0.441	0.048	0.046
8x8	0.990	0.917	0.367	0.366	0.835	0.821	0.357	0.355
12x12	0.996	0.921	0.746	0.749	0.943	0.941	0.701	0.707
15x15	0.997	0.921	0.897	0.899	0.979	0.979	0.838	0.840
985nodes[**]			0.910	−			0.847	−

[*] The results are normalized with respect to $u_A=w_B=0.94$

[**] Nonuniform mesh (12x12 mesh + local mesh refinement around load point). See Fig. 4.8. The displacement u_A is computed from single load using superposition

The non-uniform mesh refinement with the finest grid around the load point does not provide a significant improvement of the accuracy, apparently because the bending action is large throughout the sphere.

4.5 Remedies for locking phenomena

The complementary devices for locking phenomena have been treated in Chapter 2 and their implementation has been discussed in Chapter 3. Their effectiveness is investigated through numerical tests in this section.

4.5.1 Reduced integration

Full and reduced order integration have already been compared in the previous sections. As far as quadrilateral shape elements are concerned, the effectiveness of the reduced integration is conspicuous in most cases for both the degenerate shell element and the new element. As for triangular elements, the convergence is improved by the reduced integration, but the improvement is not complete, and the locking phenomena cannot be removed. The inside 3-point integration gives faster convergence than the midside 3-point rule. selective reduced integration has also been tested, but proved to be not as effective as uniform reduced integration. Eigenvalue tests show that the selective reduced integration destroys the geometric isotropy of the element. The results of the selective integration imply that the membrane locking is as significant as the transverse shear locking.

4.5.2 Addition of internal d.o.f.

Five different possibilities of adding the internal d.o.f. have been considered as described in the previous chapter, but only type III element has been tested numerically in association with these internal d.o.f. The inside 3-point integration rule is applied for all cases. The following notations are used to indicate the various internal degrees of freedom.

IDOF(A) : three translational d.o.f. at the center

IDOF(B) : two rotational d.o.f. at the center

IDOF(C) : all five d.o.f. at the center

IDOF(D) : two translational d.o.f. in the tangential directions and two rotational d.o.f. at the center

In general, IDOF(A) and IDOF(D) show the most favorable convergence behavior for all cases tested in the present study. But IDOF(A) gives fluctuation of the computed normal displacements for the uniform pressure case when coarse meshes are used. The same difficulty arises also for IDOF(C). IDOF(B) fails to remove the locking phenomenon in a sensitive thin shell case. The solution with IDOF(C) generally converges to a value slightly larger than the analytical solution. The convergence of the type III element with different internal d.o.f. is compared in Fig. B.7 through Fig. B.10.

Cylindrical shell roof

The convergence of a type III triangular element is improved conspicuously by the IDOF(A) (Fig. B.7). The solution converges to the analytical solution based on shallow shell assumptions. IDOF(B) gives slower convergence than IDOF(A) while the one with IDOF(C) or IDOF(D) gives faster convergence. However, IDOF(C) and IDOF(D) do not give monotonic

convergence and the solutions with these internal d.o.f. approach a value a bit larger than the analytical solution (Fig. B.7).

Pinched cylinder (thick)

IDOF(A) and IDOF(D), show almost equivalent convergence behavior which approaches the analytical solution. The performance of IDOF(B) is quite poor for this case (Fig. B.8).

Pinched cylinder (thin)

IDOF(A), IDOF(C) and IDOF(D) improve the rate of convergence significantly and remove the locking behavior to such a degree that the element might be acceptable. The improvement by IDOF(B) is not sufficient. IDOF(C) converges to approximately 3% higher value than the analytical solution (Fig. B.9).

Fixed-free quarter cylinder

IDOF(A), IDOF(B), IDOF(C), and IDOF(D) show equivalent rates of convergence for this test case (Fig. B.10).

Sphere under uniform pressure

The converged solutions with IDOF(A) and IDOF(C) show local fluctuation of the surface normal displacement when coarse meshes are used. This is similar to what is usually observed for Lagrange elements of quadrilateral shape. This fluctuation disappears as the mesh is refined. IDOF(B) and IDOF(D) give the correct solution even with a coarse mesh.

Four corner supported square plate

IDOF(A) and IDOF(C) fail for this test case. IDOF(B) and IDOF(D) do not fail but converge to a bit larger value than the exact solution.

4.5.3 Mixed formulation

The mixed formulation was applied only to the type III element. Various combinations of m and n in the mixed formulation were tested, where m and n represent the number of polynomial terms in g_1 and g_2 of Eqn. (2.6.10). The stiffness matrix of a triangular element becomes negative definite unless the $3g_1/3g_2$ scheme is used. The quadrilateral element with the $3g_1/3g_2$ scheme shows favorable convergence for all the test problems except the pinched cylinder and the four corner supported square plate case, for which the element fails due to rank deficiency. The quadrilateral element also fails for other than the $4g_1/3g_2$ or the $4g_1/4g_2$ schemes. However, geometric isotropy is violated when the $4g_1/3g_2$ scheme is used. In short, only the triangular element with the $3g_1/3g_2$ scheme and the quadrilateral element with the $4g_1/4g_2$ scheme are acceptable. Therefore, only those schemes are numerically tested in more detail. The convergence tests show there are no significant differences between the full order and the reduced order integrations for mixed formulation. The computed results are approximately equivalent to that of the displacement formulation with reduced integration. The mixed formulation itself is not effective enough to remove the locking phenomenon of thin shell cases. Thus, the addition of internal d.o.f. will be necessary also for the mixed formulation to avoid the locking phenomena. The advantage of the mixed formulation with full order integration is that it stabilizes the local fluctuation which arises in the displacement formulation when internal d.o.f. are added.

The alternative form of mixed formulation based on the modified Hellinger-Reissner principle was also numerically investigated. There are no noticeable differences in convergence between the original mixed formulation and the modified formulation when reduced integration is applied. But the

Table 4.4 Performance of the Mixed Formulation

Method of formulation	Shape	m	n	Inter. d.o.f.	Integr. schm.	Rate of convergence or property of element stiffness matrix
Mixed Formulation	Triangle	3	3		3-point	Equivalent to D.W.R.(displacement formulation with reduced intgr.)
		3	3		7-point	Equivalent to D.W.R.
		3	3	u,v,w	3-point	Equivalent to D.W.R.
		3	3	u,v,w	7-point	Equivalent to D.W.R., <u>no oscillation for uniform pressure case</u>
		4	3		3-point	Non-positive definite stiffness matrix, geometric isotropy violated
		4	3		7-point	Convergence slower than D.W.R., geometric isotropy violated
		4	4		3-point	Non-positive definite stiffness matrix.
		4	4		7-point	Convergence slower than $4g_1/3g_2$ with 7-point integration.
	Quadril.	3	3		2x2	Rank deficiency for pinched cylinder (thick and thin)
		3	3		3x3	Non-positiveness for cyl. shell roof, rank deficiency for pinched cyl.
		4	3		2x2	Equivalent to D.W.R., geometric isotropy violated
		4	3		3x3	Equivalent to D.W.R., geometric isotropy violated
		4	4		2x2	Equivalent to D.W.R.
		4	4		3x3	Equivalent to D.W.R.
Modified Mixed Formulation	Triangle	-	3		3-point	Equivalent to D.W.R.
		-	3		7-point	Slightly slower than D.W.R.
		-	4		3-point	Non-positive definite stiffness matrix
		-	4		7-point	Slower than $3g_2$ with 7-point integration
	Quadril.	-	3		2x2	Rank deficiency
		-	3		3x3	Rank deficiency for cyl. shell roof
		-	4		2x2	Equivalent to D.W.R.
		-	4		3x3	Significantly slower than D.W.R.

modified formulation gives slower convergence when full order integration is used. The performances of the mixed formulation and the modified mixed formulation are presented in Fig. B.11 through Fig. B.14 and summarized in Table 4.4.

4.6   Control of zero-energy modes

The zero-energy modes and their control were considered for Type III triangular element with internal d.o.f. Two schemes of controlling the zero-energy modes, i.e., e–control and α–control, were tested and compared. A larger value of zero-energy control index (e or α) is more effective for controlling the zero-energy modes, but more likely to induce locking phenomena. Thus, the main point of the numerical tests is to find the range of the index which can control the spurious zero-energy modes without inducing the locking phenomena. The pinched cylinder (thin), which is sensitive for locking, and the four corner supported plate, which is sensitive for zero-energy modes, are the two extreme cases from which one can derive a conclusion probably valid for a wider variety of problems. The test results of zero-energy control are given in Fig. B.15 through Fig. B.29 and are summarized in Table 4.5.

4.6.1 e–control

The control index e ranging from 10^{-12} to 0.1 was examined for both the pinched cylinder and the four corner supported plate case (Fig. B.25 through Fig. B.29). The zero-energy mode is not controlled when the index e is zero. As the index becomes larger, the effect of the internal d.o.f. diminishes and the solution approaches the one without any internal d.o.f. Because 64 bit double

precision is used in the computation, an index less than 10^{-12} will be overwhelmed by computational error.

Pinched cylinder (thin)

Type III elements with various internal d.o.f. are almost unaffected by control with e value of less than 10^{-6}. As the index increases, the convergence becomes slower. The element with IDOF(A) is slightly less sensitive to the value of the control index than those with IDOF(C) or IDOF(D). The element with IDOF(A) suffers from significant locking behavior again when the index is larger than 10^{-3}.

Four corner supported plate

The element with IDOF(A) appears correct for an e value greater than 10^{-10}. However, the computed displacement oscillates across the plate when the index is less than 10^{-4}. The oscillation becomes severe as the index decreases. The amplitude of the oscillation has a tendency to decrease as the mesh is refined. The element shows locking behavior again when the index is larger than 10^{-3}. The element with IDOF(B) and IDOF(D) gives convergence to the analytical solution when the index is greater than 0.1. The converged solution approaches approximately 6 % larger value than the analytical solution as the index decreases below 10^{-4}. When the control index is reduced below 10^{-8}, the solution stabilizes and is not affected by the control index. The element with IDOF(C) is most sensitive to the control index. The element behaves similarly to those with IDOF(B) and IDOF(D) for control index greater than 10^{-8}, but shows oscillation of displacements, as in the case of IDOF(A), for e value less than 10^{-3}.

Table 4.5 Effects of Zero-energy Control

Control Scheme	Internal D.O.F.	Pinched-cylinder	Four-corner-supported plate
e-control	IDOF(A)	Locking if $e>10^{-3}$	Correct center displ. for $e<10^{-10}$ Oscillation for $e>10^{-4}$
	IDOF(B)	Locking for all e values	Convergence to 7 % larger value
	IDOF(C)	Locking if $e>10^{-2}$	Oscillation for $e>10^{-3}$
	IDOF(D)	Locking if $e>10^{-3}$	Convergence to 7 % larger value
α-control 3/3 point integration	IDOF(A)	Locking if $e>10^{-4}$	Correct center displ. for $e<10^{-12}$ Oscillation for $e>10^{-5}$
	IDOF(B)	Locking for all e values	Convergence to 7 % larger value
	IDOF(C)	Locking if $e>10^{-2}$	Oscillation for $e>10^{-4}$
	IDOF(D)	Locking if $e>10^{-3}$	Convergence to 7 % larger value
α-control 3/7 point integration	IDOF(A)	Locking if $e>10^{-6}$	Correct center displ. for $e<10^{-12}$ Oscillation for $e>10^{-6}$
	IDOF(B)	Locking for all e values	Convergence to 7 % larger value
	IDOF(C)	Locking if $e>10^{-2}$	Oscillation for $e>10^{-4}$
	IDOF(D)	Locking if $e>10^{-3}$	Convergence to 7 % larger value

4.6.2 α–control

This control scheme can be achieved by various combinations of integration rules, namely, combination of two 3-point rules (inside 3-point and midside 3-point), 1-point and 3-point rule, or 3-point and 7-point rule. However, 1-point /3-point rule fails, with any value of α, for the four corner supported plate case, and therefore was excluded from detailed numerical study. The control index α ranging from 10^{-12} to 0.5 was examined. The zero-energy mode is not controlled when the index α is zero, and the integration scheme becomes equivalent to 6- or 10-point rule as α approaches 0.5. The scheme gives, in general, similar convergence patterns as the e-control scheme (Fig. B.15 through B.24).

4.7. Other tests to prove the validity of the elements

The convergence and the accuracy of the elements have been investigated in the previous sections. However, most of the computations are performed using uniform rectangular grids. Therefore, it is necessary to examine how the elements behave when they are distorted. Patch tests and element distortion tests are used to prove the validity of the elements with arbitrary shape.

4.7.1 Patch tests

A cantilever plate with uniform tensile load and the one with uniform moment at the free edge are examined for patch tests. The 3x3 distorted mesh shown in Fig.4.5 is used for the test. The central element is kept in rectangular shape and the surrounding elements are distorted by rotating the central element 30°. The type I element fails for the case of edge moment. The type II

and III elements of triangular shape pass the tests. However, the quadrilateral elements show errors (order of 0.1 %) in bending stresses when the meshes are not rectangular. But the error decreases as the mesh is refined. Thus the quadrilateral elements seem to pass the patch test in the limit of mesh refinement.

Table 4.6   Summary of the patch test results

Element	Constant tension	Constant bending
TI	Pass	Fail
TII, TIII	Pass	Pass
TIII-A~D	Pass	Pass
QII, QIII	Pass	Pass if rectangular. Otherwise pass only infinitesimally
QIII-A~D	Pass	Pass if rectangular. Otherwise pass only infinitesimally[*]

[*]   Addition of internal d.o.f. reduces the error in constant bending stresses of distorted elements.

4.7.2 Element distortion tests

Distortion of elements usually degrades the accuracy or retards the rate of convergence. Furthermore, distortion may incapacitate the complementary measures for locking. It is worthwhile to examine how element distortion affects the convergence behavior. Thus, four test cases have been examined for various degrees of element distortion. The type III elements of quadrilateral shape with and without internal d.o.f are compared with the degenerate shell element in Fig. B.30 through Fig. B.33. The effects of element distortion seem more serious for thinner shells. They can still be considered to be within acceptable range, provided that higher degree of distortion is avoided in practical mesh design. It should also be noted that the 3x3 mesh does not give

converged solution even for a rectangular mesh and therefore the results of the element distortion tests reported here may not necessarily represent the behavior for a more refined mesh. Addition of internal d.o.f. generally makes the element less sensitive to distortion. For the pinched cylinder case, quadrilateral elements with internal d.o.f. (u,v, and w) and reduced integration fail due to spurious zero-energy modes. However, these spurious modes disappear as the elements are distorted. The interrelation of the locking penomena and the spurious modes can also be seen in this context.

The clamped circular plate is another case in which element distorsion has been implicitly included (Fig.4.11). Even though the quadrilateral element does not pass the patch test, it gives relatively good performance for this case.

4.8 Overall evaluation

The type I element fails the patch test and gives convergence to somewhat larger values than the exact solutions. This may be due to the fact that the element does not satisfy the C^1 interelement continuity because the rotations in natural coordinate directions are interpolated by incomplete quintic polynomials. Interpolation satisfying the C^1 continuity is a subject for further study.

The convergence behaviors of the type II and III elements are similar. However, the type III element is preferred because its formulation is simpler. The element shows better performance than the degenerate shell element for all the test cases. Especially the element of quadrilateral shape gives satisfactory convergence for both thick and thin shells. The convergence of the triangular element is slow for thin shells. This can be improved by complementary devices together with zero-energy control schemes. Type III

elements give good agreement with analytical solution as demonstrated for the cylindrical shell roof case (Figs.4.9 and 4.10) and the pinched sphere case (Figs.4.12, 4.13 and 4.14). As shown in the case of the pinched sphere and truncated half sphere, the element requires fine mesh refinement to represent properly bending actions of thin shells.

It is recommended that quadrilateral elements be used for thin shells with significant bending action and use triangular elements be used only for places such as sharp corners or crack tips where the quadrilateral element does not fit. Triangular elements should be used with fine grids or with complementary devices for locking and zero-energy control. A high degree of element distortion should be avoided if possible.

It has been discovered that quadratic or higher order isoparametric elements under special restrictions on their geometry can represent the $r^{-1/2}$ stress singularity at a crack tip (Barsoum,1974,1976,1976a). Specifically, triangular quadratic elements with two adjacent side nodes located at the quarter points provides this singularity at the included corner nodes. It has also been proved that the degenerate element with reduced integration has the required singularity. The type III element should possess the same capability, because the element is also based on the isoparametric interpolation. However, it has not yet shown that the element with internal nodes or the the one based on the mixed formulation can represent the same singularity; this demonstration is beyond the scope of this study. Therefore, it is recommended that, at a crack tip, triangular elements without any complementary devices other than reduced integration be used. Special care should be taken in mesh generation to make the sides of elements straight and to place the side nodes exactly at quarter points as shown in Fig.5.25.

Chapter 5

APPLICATION

In preceding chapters, finite elements for shell analysis have been formulated and their accuracy has been examined by numerical studies with various test problems. The role of the finite element technique in biomechanics has been described in Chapter 1 through a brief review of the previous works in this area. This chapter deals with the application of the finite element to practical problems related to biological objects. Two examples are presented here. One is stress and fracture analysis of an eggshell, and the other is modelling of a stomatal opening in plants. The type III elements are used for both cases.

5.1 Analysis of stresses in eggshell

Eggshell breakage during handling and processing is a continuing problem for the poultry industry. About five to twelve percent of the fresh market eggs is lost or downgraded simply because the shell is fractured (Anderson and Carter, 1976, Orr *et al.*, 1977, Washburn, 1982). This results in a substantial financial loss. A better understanding of the eggshell breakage will influence the design of egg processing equipment and research into strengthening eggshells. On the other han, the eggshell is considered as an ideally designed structure and has an analogy to man-made shell structures. Therefore, the investigation of eggshell stresses may give feedback to the structural analysis and design processes.

Primitive stress analyses of eggshells were initiated chiefly for evaluation of physical properties or failure stresses. Although a comprehensive

131

understanding of the shell's reaction to external forces requires a knowledge of the stress distribution throughout the shell, it was extremely difficult for the early researchers to do an accurate analysis of an eggshell due to its complex geometry. To remove the complexity, Voisey and Hunt (1967) assumed a spherical shape of the egg for the stress analysis of the shell. Their result shows the wide discrepancy between the experimentally measured and the theoretically computed values for failure forces. Tung et al. (1969) also assumed a spherical shell and employed Reissner's solution to estimate the elastic properties and the failure strength of eggshells from experimantally measured deformations and crushing forces. In spite of its simplicity, the assumption of spherical shape is not encouraging as shown by Voisey's results, because the actual stress distribution of a shell is generally sensitive to its geometry. In the light of this fact, the results obtained by Sluka et al. (1965) are considered to be more reliable. They devised a hydrostatic pressure tester which raised the internal pressure in an egg until the shell failed in tension. They evaluated the failure tensile stress by applying the simple membrane theory to an eggshell subject to hydrostatic pressure from inside. McRae and Duff (1969) did a similar analysis for the case of hydrostatic compression and determined the ultimate compressive stresses of the eggshell. Voisey and Hunt (1967) applied brittle coating techniques to the eggshell in order to determined the surface stress distribution under quasi-static loading. The stress patterns under various loading conditions were produced. The overall tendency of the stress distribution and the principal directions could be deduced. However, it was diffucult to determine quantitatively the magnitude of each stress componenet from the experiment. Furthermore, direct observation of the stress pattern on the inner shell surface was not possible due to various reasons, while the authors conjectured that the first fracture of an eggshell due to quasi-

static loading is more likely to occur at the inner surface under the point of loading.

Manceau and Henderson (1970) first applied the finite element method to stress analysis of eggshell. They represented the eggshell geometry by a number of axisymmertric shell elements subject to non-axisymmetric loading conditions, and obtained the stress distribution under two loading conditions, i.e., thermal loading and loading on the equator between two flat plates.

Upadhayaya et al. (1984a) studied the thermo-elastic behavior of avian eggs idealized as a fluid filled spherical shell and investigated the effect of eggshell size, thickness and air cell size on the thermally induced stress in the eggshell. The results were compared in another study by Upadhayaya et al. (1984b), which used the finite element method for a stress analysis of avian eggs with various shapes. The latter analyzed the stresses due to temperature change and internal pressure when subjected to flat plate loading using a generalized finite element analysis program.

Eggshell strengths are usually determined by measuring a certain type of external force at failure and relating this with the analytically obtained stresses. The investigation of eggshell strength has been bedevilled by two things: its high variability, and complication involved in the stress analysis. The difficulty in stress analysis has been overcome by the finite element method, and accurate values can now be predicted. However, many researchers (Brooks and Hale, 1955; Orr et al., 1955; Washburn,1982) reported there were large variations in the observed strength and the elastic modulus of eggshells. Thus, the accuracy achieved in computation may be overshadowed by the variability in experimental data which can be attributed chiefly to the measurement error (Rehkugler 1963).

There are many experimental techniques to predict the eggshell strength. They can be classified largely into four groups, 1) flat plate loading tests, 2) uniform pressure tests, 3) deformation tests (Brooks and Hale 1955, Schoorl and Boersma 1982), and 4) puncture tests. Among these techniques, only the deformation test is nondestructive. The nondestructive test is based on the correlation between the elastic modulus and the egg shell strength (Hunt and Voisey, 1966).

The objective of the present analysis is to evaluate the reliability of each measurement technique, based on the results obtained by finite element analysis.

The global stress distribution under the following three loading conditions is studied in the present work.

1) Uniform internal pressure.

2) Point loads at the pole.

3) Point loads at the equator.

The stress distribution around a crack tip is also considered for the first loading condition.

The geometric data and the material properties of the eggshell are input in two different ways: one with computed actual values and the other with normalized values. The analyses with actual values are to show the overall stress distribution and the displacement pattern under each loading condition. The normalized values are used to examine the effect of eggshell geometry and loading conditions on the stress distribution and thus to evaluate the appropriateness of the various widely used measurement techniques for eggshell strength.

5.1.1 The physical characteristics of eggshell

This section decribes the physical properties of eggshells which are necessary in analyzing the eggshell stresses.

Egg shell geometry

A correct expression of the eggshell shape is important in predicting the shell stresses accurately.   There are many methods describing egg shape. Tyler (1961) defined the ratio of the major axis to minor axis as the shape index. Many researchers (Hunt and Voisey,1966; Rehkugler,1964) have used this shape index to define the egg shape. The egg shape index measured by Beyavin and Boorman (1981) ranges from 1.36 to 1.88. For purpose of stress analysis, the principal curvature has also been frequently used as an egg shape characteristic. A mathematical expression defining egg shell geometry is more useful in generating the input data for finite element analysis. Smart (1967) defined the eggshell geometry by the following mathematical expression.

$$\frac{x^2}{a^2} + \frac{y^2}{(b + x\tan\theta)^2} = 1 \tag{5.1.1}$$

in which a and b are a half of the height, and the radius of oval at equator, respectively, and θ is the skew angle as indicated in Fig.5.1.a. This equation is equivalent to Eqn. (5.1.2) with x, y, and z in Fig.5.1.b.

$$\frac{x^2}{a^2} + \frac{y^2 + z^2}{(b + x\tan\theta)^2} = 1 \tag{5.1.2}$$

The thickness of the shell is also an important factor affecting the eggshell stresses and strength. Therefore, accurate evaluation of shell thickness is essential.   Romanoff and Romanoff (1949) obtained a linear relationship between the volume of an egg and the thickness of the shell
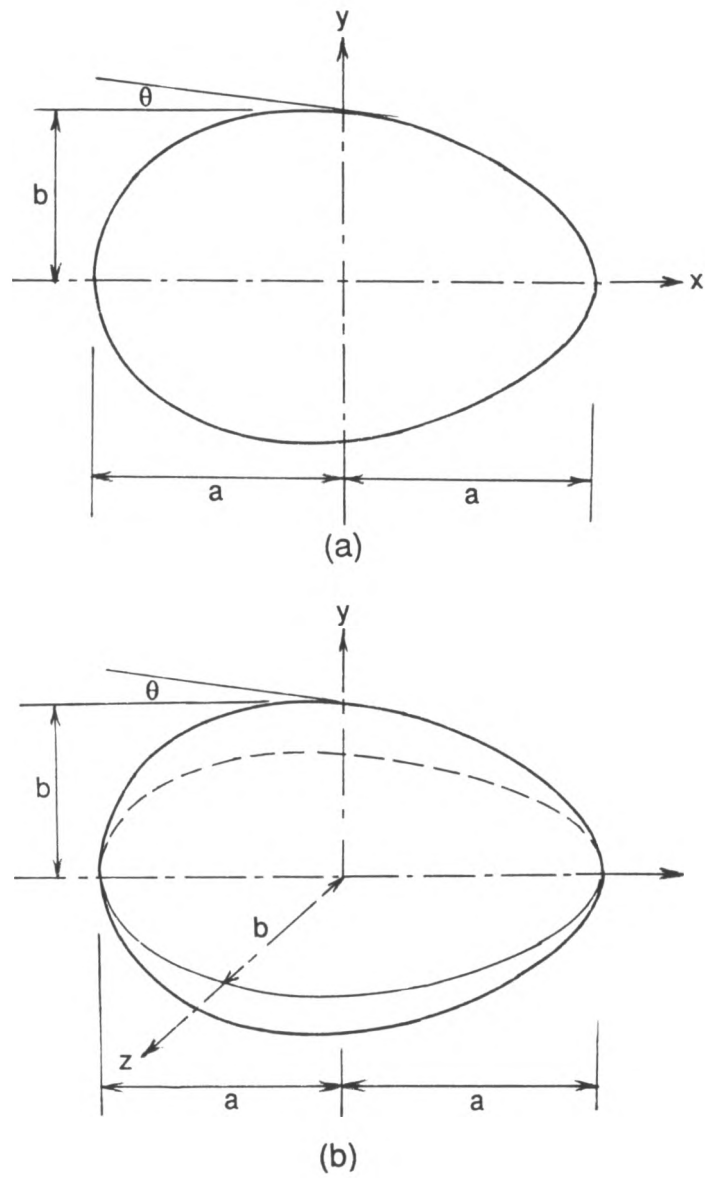
Fig. 5.1   Parameters defining eggshell geometry
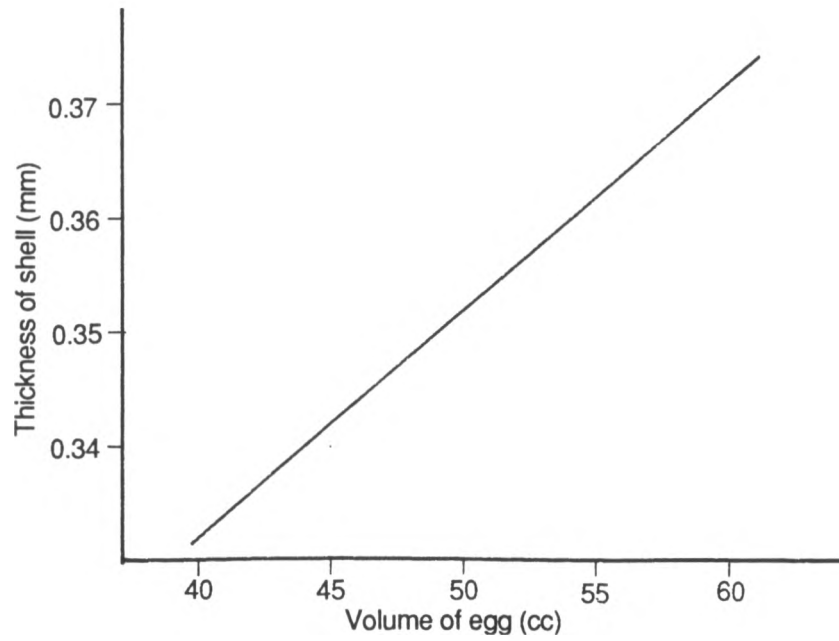
Fig. 5.2   Relationship between the volume of a hen's egg and the thickness of the shell (After Romanoff and Romanoff, 1949)
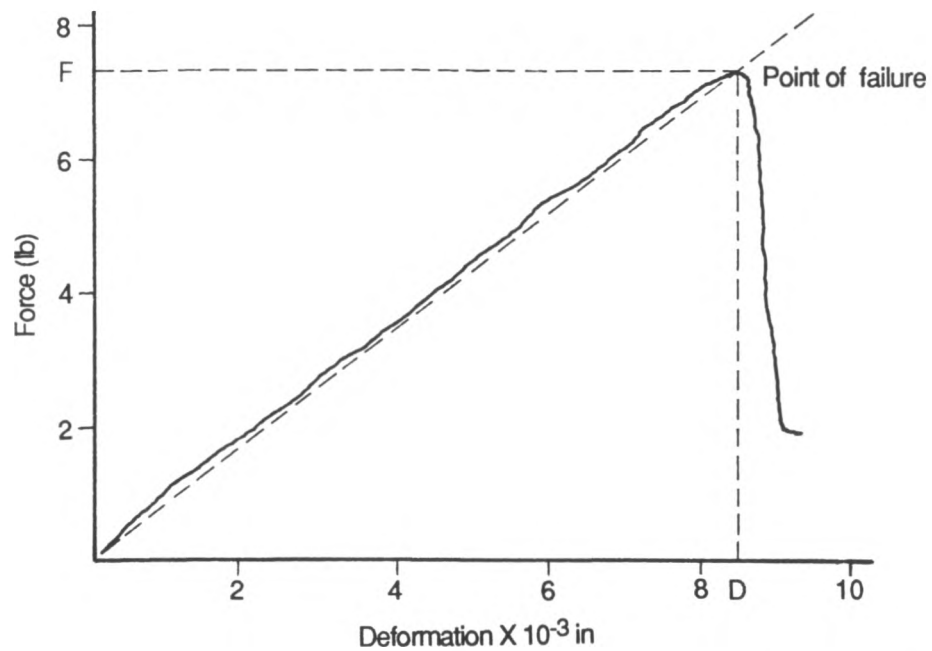

Fig. 5.3   Typical force-deformation record for an eggshell compressed at 0.07 in/min (After Voisey and Hunt, 1967)

(Fig.5.2). Brooks and Hale (1955) found that both the shell thickness t and its squared value t^2 have equivalent correlation with the egg weight. They obtained a mean eggshell thickness of 0.329 mm.

Material properties

The stress-strain relationship of an eggshell is approximately linear and isotropic (Brooks and Hale,1955, Tung *et al.* 1969). The force-deformation behavior of an egg under quasi-static flat plate loading is elastic up to the point of failure as shown in Fig.5.1 (Voisey and Hunt, 1967). To analyze the stresses, material properties should be known beforehand, while they cannot be determined directly by the experimental measurements without stress analysis due to the complex geometry of the eggshell. Rehkugler (1963) tried to separate the geometric effects and measure the modulus of elasticity directly using a ring portion of shell and obtained a value ranging from 4.906×10^6 to 8.460×10^6 psi (3.38×10^4 to 5.83×10^4 MPa). As acknowledged by the author, this considerable variation may be due mainly to the measurement error rather than to inherent variation in the shell property. Tung *et al.* (1961) obtained average values of 4.571×10^4 and 4.694×10^4 MPa, respectively, by point loading and distributed loading over a small area and using Reissner's solution for spherical shell. Manceau and Henderson (1970) obtained the modulus of elasticity and the Poisson's ratio as 6.80×10^6 psi (4.69×10^4 MPa) and 0.307 respectively, using a ring of eggshell specimen. Voisey and Hunt (1967) defined the eggshell stiffness by the force-deformation ratio under flat plate loading, and obtained the stiffness values of 885 and 1450 in/lb for loading at the equator and at the pole respectively.

Hammerle and Mohsenin (1967) obtained the average ultimate tensile strength of 1.9×10^3 psi (13 Mpa) by uniform pressure loading tests. The

compressive ultimate strength ranges from 2.3×10^4 to 2.8×10^4 psi (158 to 193 MPa, McRae and Duff, 1969).

5.1.2 Global stress distribution in the eggshell

The stress distribution in an eggshell has been analyzed here for one geometric configuration and three different loading conditions: uniform pressure, flat plate loading at the equator and at the pole. It is legitimate to assume that the eggshell is hollow, because the shell, not the contents, carries most of the load (McRae and Duff, 1969; Hammerle and Mohsenin, 1967). The following data are used in the analysis:

$a = 28$ mm, $b = 21$ mm, $\theta = 15^0$,

Thickness = 0.3 mm,   Poisson's ratio = 0.3,

$P = 0.1$ N (for flat plate loadings), $p = 10$ KPa (for uniform pressure)

Stresses due to uniform pressure

Internal pressure (Sluka *et al.*, 1965; Hammerie and Mohsenin, 1967) or external compression (McRae and Duff, 1969) are used to measure the eggshell strength. In actual situation, the eggshell may be subjected to internal pressure due to expansion of internal material. Eggshell breakages frequently occur due to pressure type of external loading. Therefore, uniform pressure is a common loading case of eggshell. The membrane action is dominant throughout the egg. Therefore, computational accuracy is achieved even with relatively coarse meshes as shown in Fig.5.4. The bending stress at the point of the maximum principal stress contributes less than 1 % of the total stress. The shear stresses are also negligibly small. The membrane stresses are minimum at the sharp pole and reach the maximum around the equator. These results
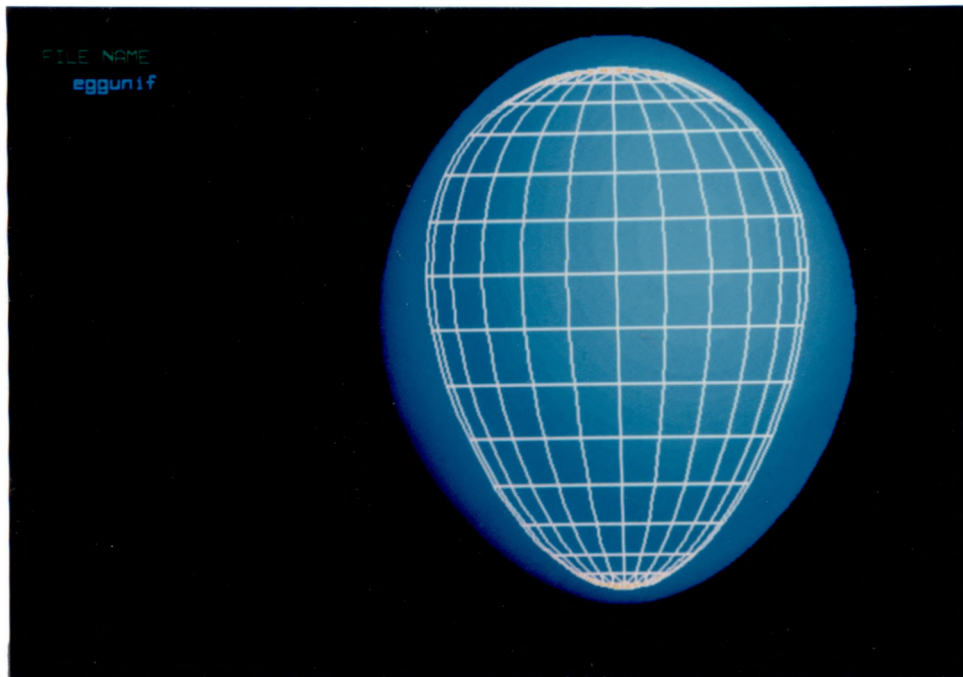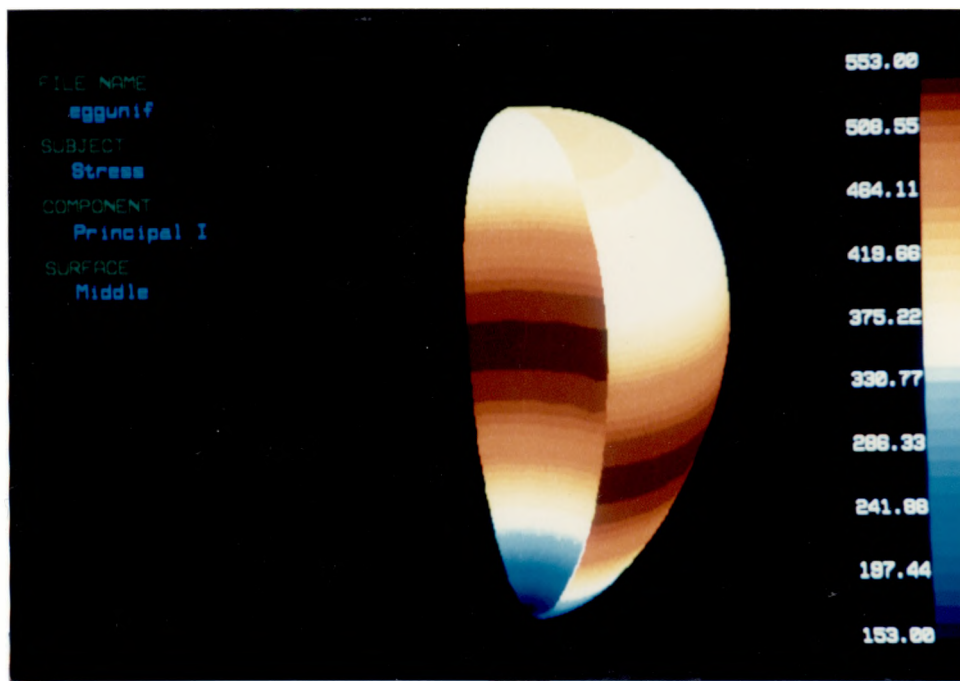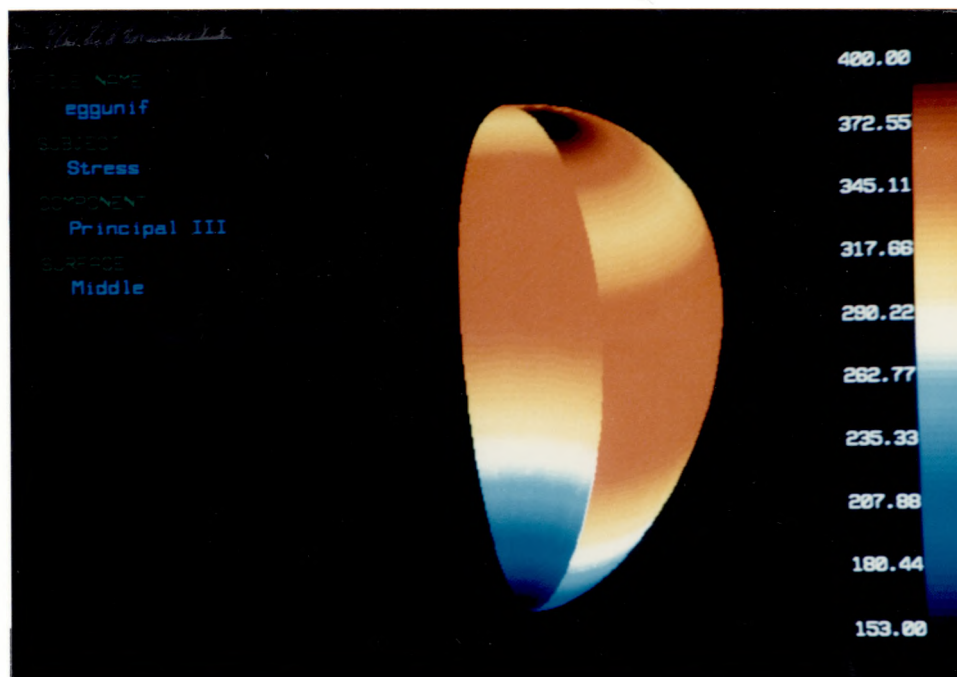
Fig. 5.4   Exaggerated view of the eggshell deformation under uniform internal pressure-overlaid with the undeformed mesh

(a)

(b)

Fig. 5.5   Principal stresses in the middle surface under uniform internal pressure

(a) σ_I (b) σ_{III}

seem to agree with the analytical membrane solution for the uniform pressure case.

$$\sigma_1 = p \, r_2(2r_1 - r_2)/(2 \, t \, r_1) \qquad \qquad (5.1.3a)$$

$$\sigma_2 = pr_2 \, /(2t) \qquad \qquad (5.1.3b)$$

in which σ_1 and σ_2 are the major and the minor principal stresses, and r_1 and r_2 are the major and minor radii of the principal curvatures. The major principal stress reaches maximum at around the waist of the egg as shown in Fig.5.4. The major principal direction is in circumferential direction. That is supposed to result in a meridional crack which is usually observed in eggshell fracture. The computed maximum major principal stress is 553 Kpa. Comparing with a hypothetical ultimate tensile strength 13 MPa (Hammerle and Mohsenin,1967), 0.24 Mpa of uniform internal pressure is required to break the eggshell.

Stresses due to point loads at the poles

This case analogous to an eggshell compressed by two flat plates at the poles. Upadhayaya *et al.* (1984b) reported that the point load applied to the eggshell gave numerical difficulty producing very large stresses, and that the load distribution area affects significantly the magnitude of the stresses. Theoretically, there is a stress singularity under the point load; however, the rotational shell finite element used does not have the capability to represent a stress singularity. It is suspected that the numerical difficulty might be due to the singularity of the rotational shell finite element itself at the pole rather than the theoretical stress singularity. Such a numerical difficulty is not expected for the finite element formulated in the present study.

The theoretical stress singularity can never be achieved in the computation, although higher and higher stresses are obtained at the point of

the load as the mesh is refined. To obtain a bounded convergence, it is necessary to assume that the point load is distributed over a finite contact area. It is a formidable task, and may not be practical, to evaluate the accurate contact area and the contact pressure distribution, because it is extremely difficult to model accurately the uncertain asperity and irregularity of the shell surface around the contact region. Furthermore, the contact area of a hollow shell will always be underestimated if the normal strains in the thickness direction are neglected. Therefore, it is most reasonable to use the contact area which has been observed by experiments. Experimentally measured contact areas at crushing force were reported in the range of 0.2~0.6 mm^2, which is equivalent to contact diameter of 0.5~1.0 mm (Brook *et al.*, 1955).

Upadhayaya *et al.* (1984b) replaced the point load by a pressure over a 1 or 2 degree subtended angle at the pole. Their numerical results showed that the stress distribution close to the load point depends much on the contact area. Upadhayaya *et al.* predicted that the shell would fail at the blunt end, based on the finite element analysis results. This is true if the contact areas at both ends are the same. However, the contact area at the sharp pole is likely to be smaller than that of the blunt end. Therefore, there is no ground to give such a prediction based on the finite element analysis results, unless the contact areas at both ends are evaluated accurately.

In the present analysis, the point loads of 0.1 N are distributed over 1° subtended angle at each end. The contact areas of the sharp and the blunt poles are 0.123 mm^2 and 0.322 mm^2, respectively. Consequently, the stresses are approximately equal at both ends. The membrane shear stresses are negligible at the point under the load, and the normal stresses are the same in the two orthogonal directions. The bending moment reaches the maximum at the pole, and vanishes rapidly away from the pole. The minor principal stress
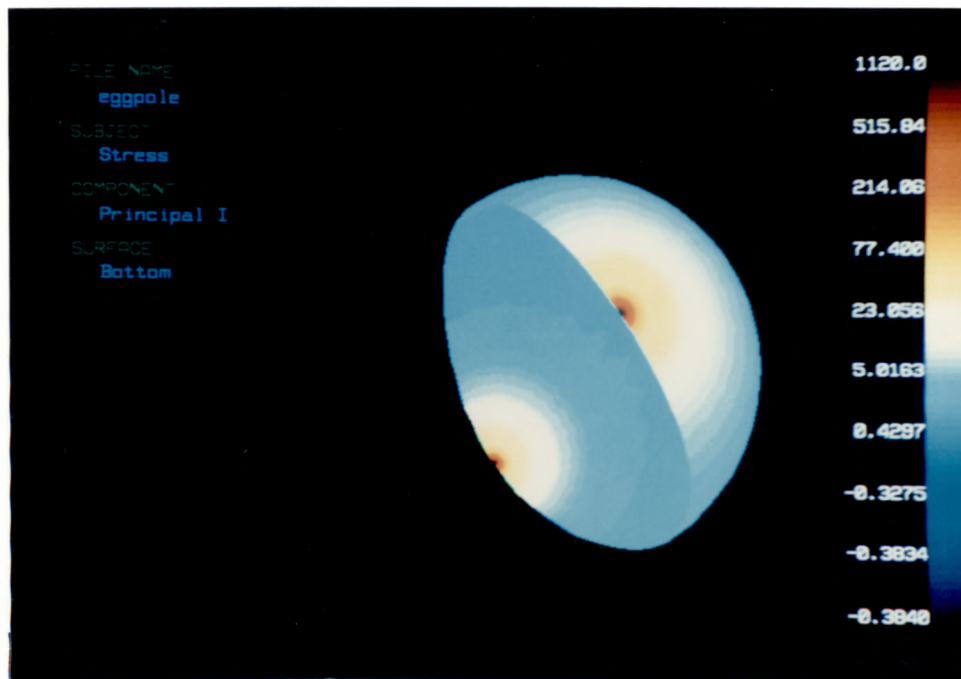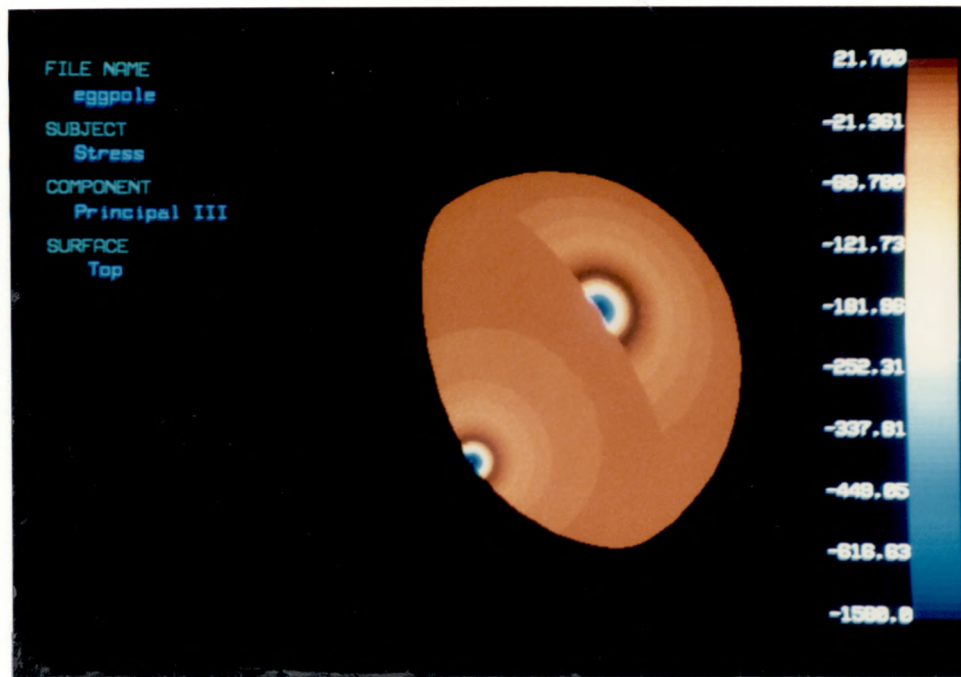
(a)
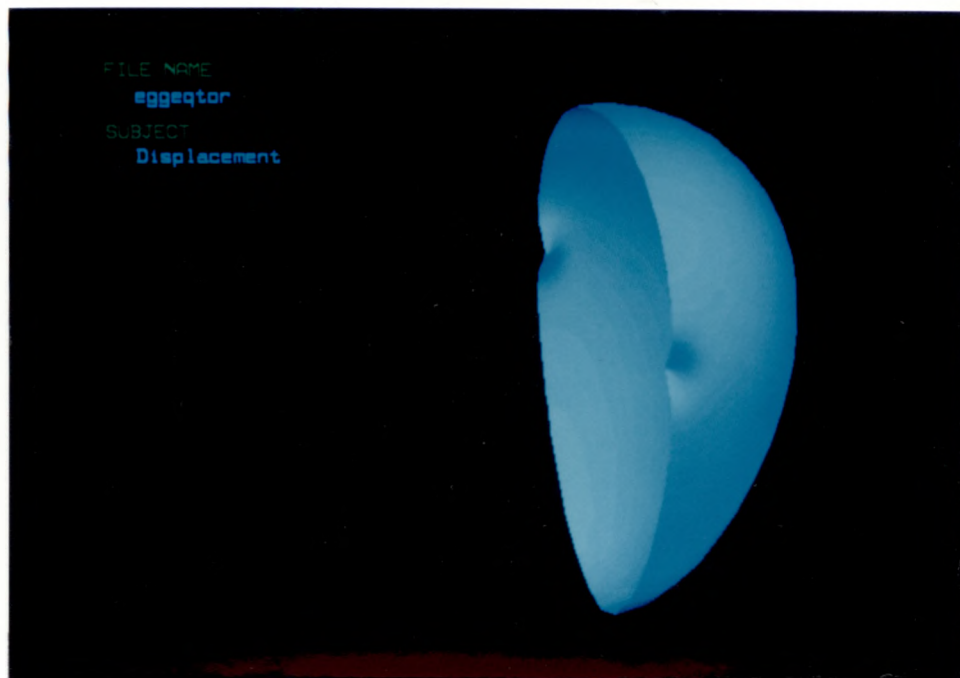
(b)

Fig. 5.6   Exaggerated view of the eggshell deformation
(a) under flat plate loading at the pole
(b) under flat plate loading at the equator

(a)

(b)

Fig. 5.7   Principal stresses of an eggshell under flat plate loading at the pole
(a) σ_I in the inner surface   (b) σ_{III} in the outer surface

(compression) due to membrane action contributes only less than 15 % of the total stress. The bending action is dominant at the poles. The major principal stress (tensile) in the inner surface, which is considered to cause the stress failure, is in latitudinal direction along the meridian of the eggshell. Fig.5.6a is the exaggerated view of the deformed eggshell under point load at the poles. The principal stresses are also shown in Fig.5.7.

Stresses due to point loads at the equator

The flat plate loading can also be applied at the equator. Manceau and Henderson (1970) assumed the forces are applied over an elliptical area. They divided the eggshell with 50 rotational elements, applied the force over 8 elements, and described the force distribution by a finite Fourier series at each nodal circle. Gates *et al.* (1984) also analyzed the same case using doubly curved thin shell elements. In the present analysis, the loads are also distributed over 1° subtended angle, giving a contact area of 0.248 mm^2. The bending action is dominant in the vicinity of the loaded area, but decreases rapidly away from the area. The stresses are approximately the same in all directions at the point of loading. The major principal stress in the inner surface is in the longitudinal direction for this case. The deformed shape and the principal stresses are graphically represented in Fig.5.6b and Fig.5.8.

5.1.3 Effects of egg shape and load conditions on the stress distribution

Stresses and deformations are computed for various egg shapes corresponding to equal volume and for several different loading conditions. The objective of the analysis is to examine the effects of egg shape and loading conditions on the stress distribution and consequently to evaluate the appropriateness of the currently used measurement techniques for eggshell
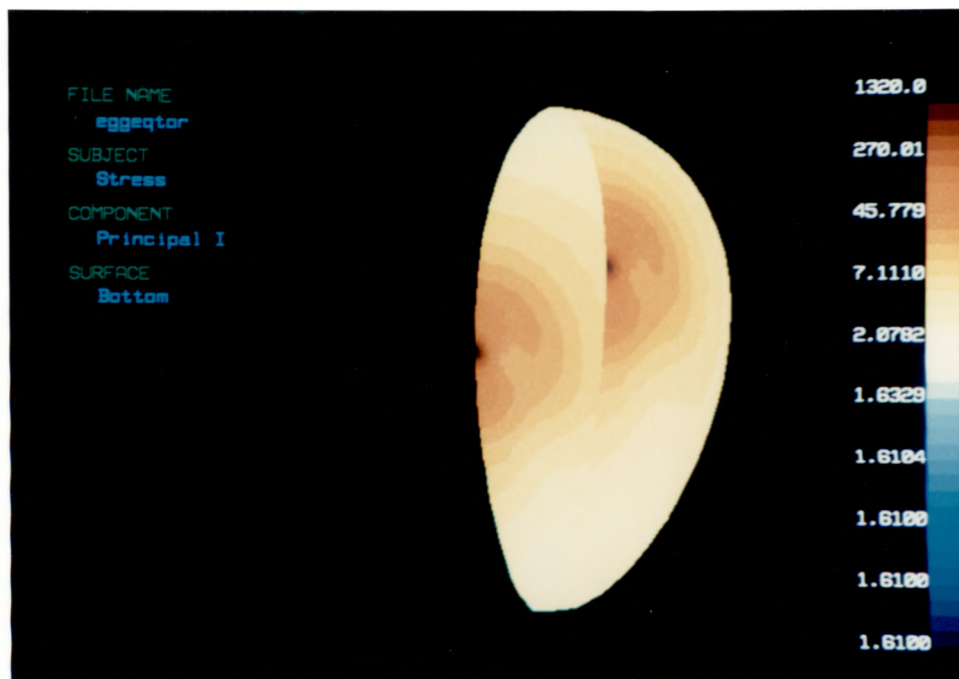
(a)
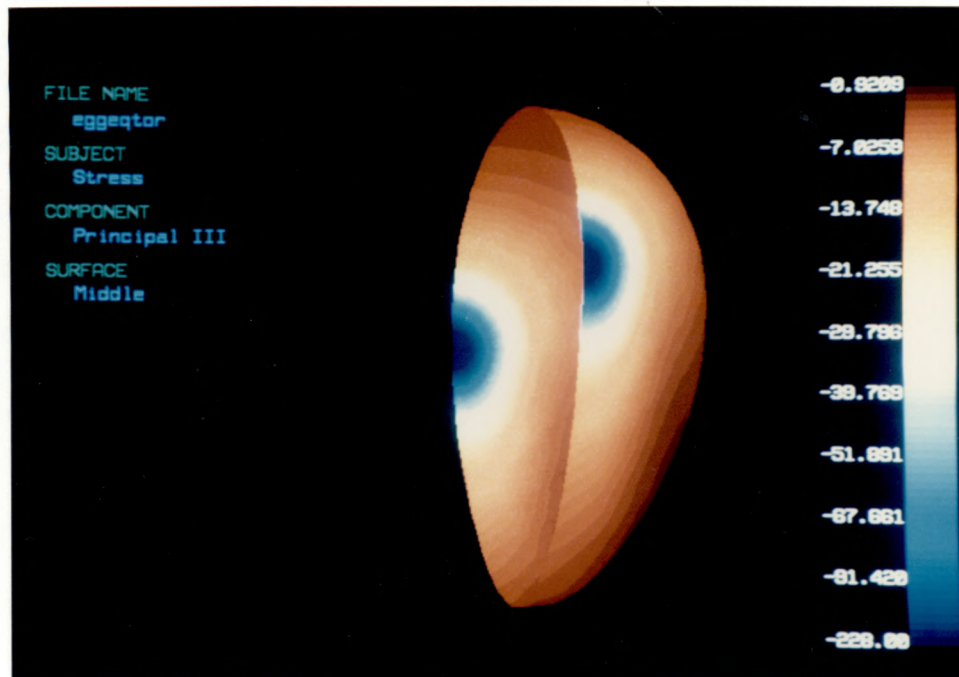
(b)

Fig. 5.8   Principal stresses of an eggshell under flat plate loading at the
equator
(a) σ_I in the inner surface   (b) σ_{III} in the outer surface

strength. Relative results rather than absolute ones are desired for the purpose of comparisons and therefore, normalized dimensionless values are used in the computation. The following eggshell geometry, properties and loading conditions are used in the analysis.

Egg shape: Six different ratios of a and b in Eqn. (5.1.1) were combined with 4 different skew angles 0°, 5°, 10°, and 15°. Thus, 24 different egg shapes were analyzed. The values of a and b are determined to yield a volume equivalent to that of a sphere with radius 1. The size and the shape indices for various egg shapes are given in Table 5.1.

Eggshell thickness: The maximum bending stress is approximately proportional to t^3 and the membrane stress is proportional to t. If one assumes that the variation of the thickness is not large and the thickness is small compared with the curvature, the effect of the thickness to maximum stresses and deformation are rather predictable. The linear relationship between the volume of the egg and the shell thickness has also been observed (Romanoff and Romanoff, 1949, see Fig5.2). This relationship gives one thickness for the normalized volume. Therefore, the effect of eggshell thickness on the stress distribution was excluded from the investigation, and only one thickness of the egg shell was used in the analysis. As a typical dimension (Romanoff and Romanoff, 1949), the thickness is assumed to be one eightieth of the radius of the sphere.

Load conditions: Seven different loading cases were examined, i.e., a uniform pressure case, three cases of flat plat loading at the poles and three others at the equator, respectively, with subtended load angles 1°, 2° and 3°.

Material properties: The material is assumed to be homogeneous and isotropic with the modulus of elasticity 1.0 and the poisson's ratio 0.3.

Table 5.1   Dimensions of ovals with equal volume

Skew angle	$\theta = 0^0$			$\theta = 5^0$				$\theta = 10^0$				$\theta = 15^0$			
a/b	a	b=b'	index*	a	b	b'	index*	a	b	b'	index*	a	b	b'	index*
1.0	1.000	1.000	1.00	0.999	0.999	1.003	.996	0.998	0.998	1.013	.985	0.995	0.995	1.028	.968
1.2	1.129	0.941	1.20	1.128	0.940	0.945	1.19	1.126	0.938	0.958	1.18	1.122	0.935	0.978	1.15
1.4	1.256	0.894	1.40	1.250	0.893	0.900	1.39	1.246	0.890	0.916	1.36	1.240	0.886	0.940	1.32
1.6	1.368	0.855	1.60	1.366	0.854	0.862	1.58	1.361	0.851	0.882	1.54	1.352	0.845	0.910	1.49
1.8	1.480	0.822	1.80	1.477	0.821	0.831	1.78	1.470	0.817	0.854	1.72	1.458	0.810	0.887	1.64
2.0	1.587	0.794	2.00	1.584	0.792	0.804	1.97	1.575	0.787	0.830	1.90	1.558	0.779	0.867	1.80

* shape index

Uniform pressure case

As already observed in the previous section, the bending moment is negligible over the whole eggshell under uniform pressure. The bending effect increases as the skew angle becomes larger, but is still negligible even for 15° skew angle which is already beyond the usual range of egg shapes. Therefore, only the membrane stress has a significant effect for the eggshell breakage.   In Fig. 5.9, the normal stresses in the midsurface are plotted along the meridian of the eggshell for two different egg shapes.   Fig. 5.10 shows the maximum principal membrane stresses for various egg shape ranging from sphere to skewed ovals. The values are normalized with respect to that of a sphere. The results show that the spherical shape gives the minimum value of the maximum membrane stress. For a given a/b ratio, the more skewed egg shell gives larger membrane stress.The maximum stress increases as the skew angle increases. This value also increases as the a/b ratio increases for skew angle 0°, 5°, and 10°, but decreases for 15°. This seems to reflect the fact that the maximum principal stress is proportional to the maximum value of $(2r_1 - r_2) / (2\, t\, r_1)$ in which r_1 and r_2 are, respectively, the radii of the major and the minor principal curvatures at a given point (Flügge,1962).

Most frequently, the ratio a/b is in the range of 1.2 to 1.6, and the skew angle is in the range of 5° to 10° (Stewart,1936; Romanoff,1949). For this range of egg shape, the maximum stress is approximately 1.3 to 1.4 times that of a sphere with equal volume. Therefore, an analysis based on assumption of spherical egg shape (Upadhaya *et al.*, 1985) underestimates, by around 30 to 40 %, the stresses due to uniform pressure.
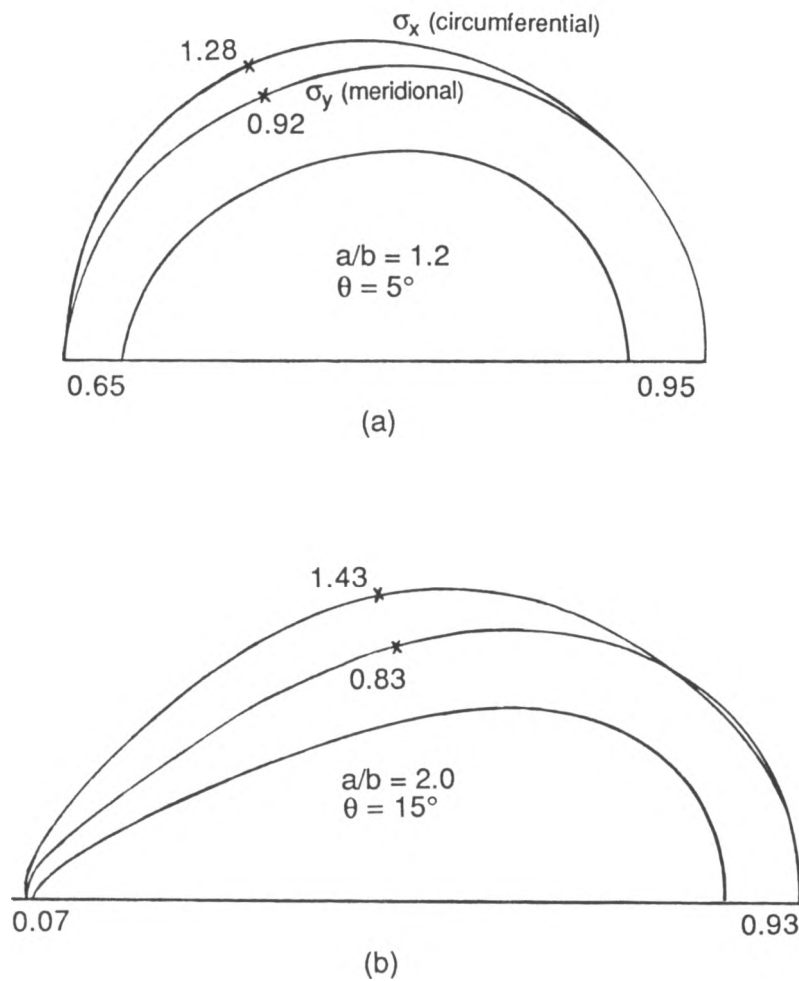
Fig. 5.9 Normal stresses in the middle surface along the meridian of an eggshell under uniform internal presssure (Values are normalized w.r.t. that of a sphere with equivalent volume.)
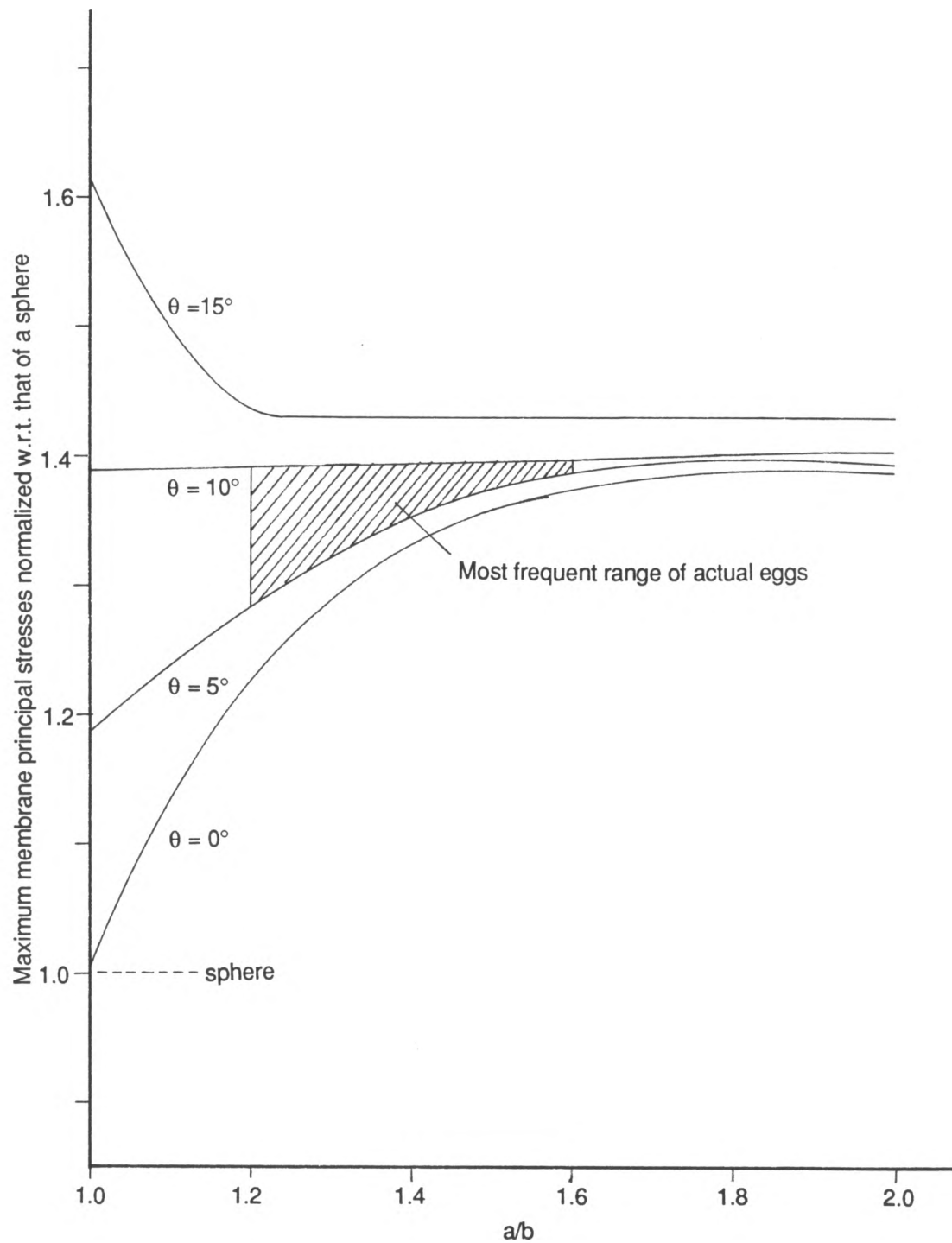(a) $\theta = 5°$, a/b = 1.2   (a) $\theta = 15°$, a/b = 2.0

Fig. 5.10 Maximum principal stresses of ovals with equal volumes and under uniform pressure

Flat plate loading at the equator

In Fig.5.11, the maximum bending moments and the maximum membrane stresses are plotted along the meridian of the eggshell for two different loaded areas. The principal stresses in the inner and outer surfaces are also presented in Fig.5.11c. The effect of egg shape and the load angle on maximum principal bending moments and membrane stresses are shown in Fig.5.12 and 5.13. The stresses are dominated by the bending moment at the pole, but diminish rapidly toward the equator as shown in Fig.5.11. The values corresponding to dimensionless load area 0.1 and 0.2 are obtained by interpolation of those for the three load angles, and presented in Fig.5.14 and 5.15. The egg shape does not affect the maximum membrane stress and especially the bending stress as much as does the load area. By doubling the load area from 0.1 to 0.2, the maximum membrane stress is reduced approximately 5 % and the maximum bending stress approximately 30 %. Because in this case the stresses are dominated by the bending moment, the total stresses are largely dependent on the load area.

The maximum deflection has significant dependence on both the egg shape and the load area as illustrated in Fig.5.16.

Flat plate loading at the pole

Similar graphs as in the preceding case are presented in Figs.5.17 through 5.22. The variations of maximum membrane stress and the bending moment with respect to the egg shape and load area are similar to the preceding case. However, the dependence on the load area is more conspicuous. In contrast to loading at the equator, the deformations depend more on the egg shape than the load angle. It appears that the deformation is approximately proportional to the width at the equator.
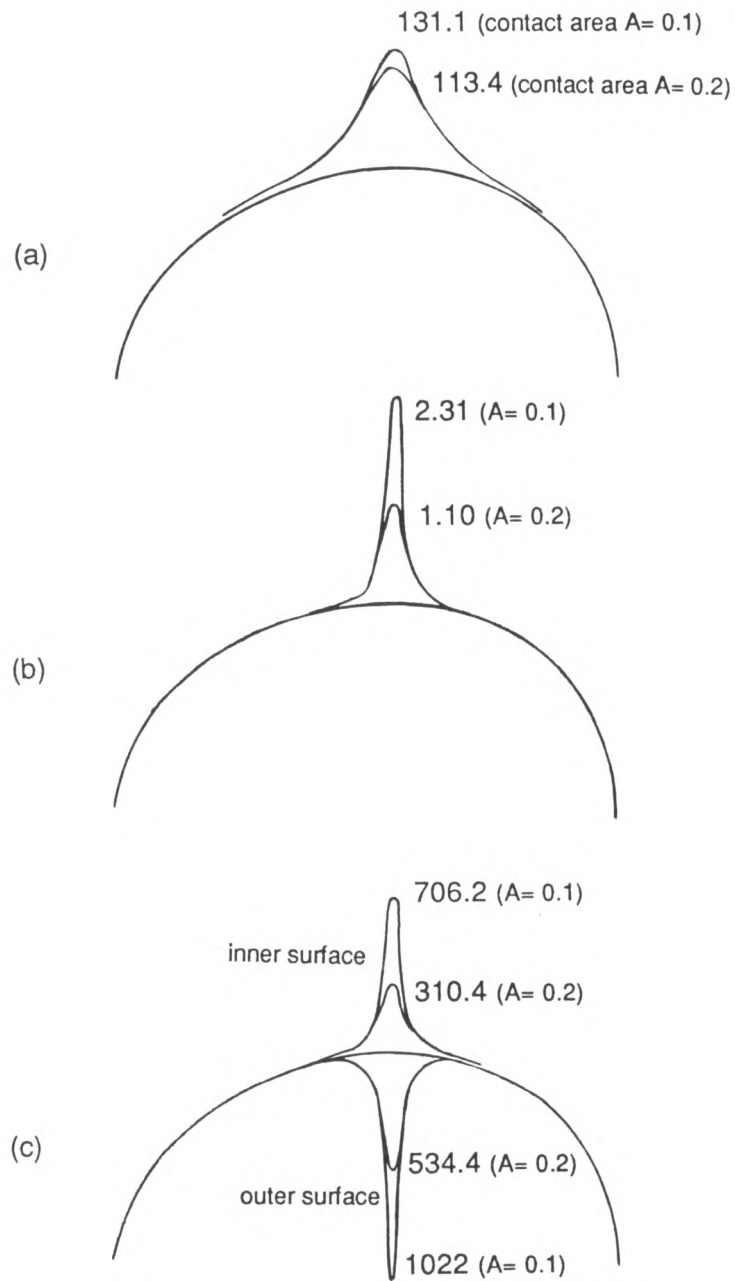
131.1 (contact area A= 0.1)

113.4 (contact area A= 0.2)

(a)

2.31 (A= 0.1)

1.10 (A= 0.2)

(b)

706.2 (A= 0.1)

inner surface

310.4 (A= 0.2)

(c)

534.4 (A= 0.2)

outer surface

1022 (A= 0.1)

Fig. 5.11 Stresses of an eggshell under flat plate loading at the equator
($\theta = 5°$, a/b = 1.2)
(a) Maximum membrane stress
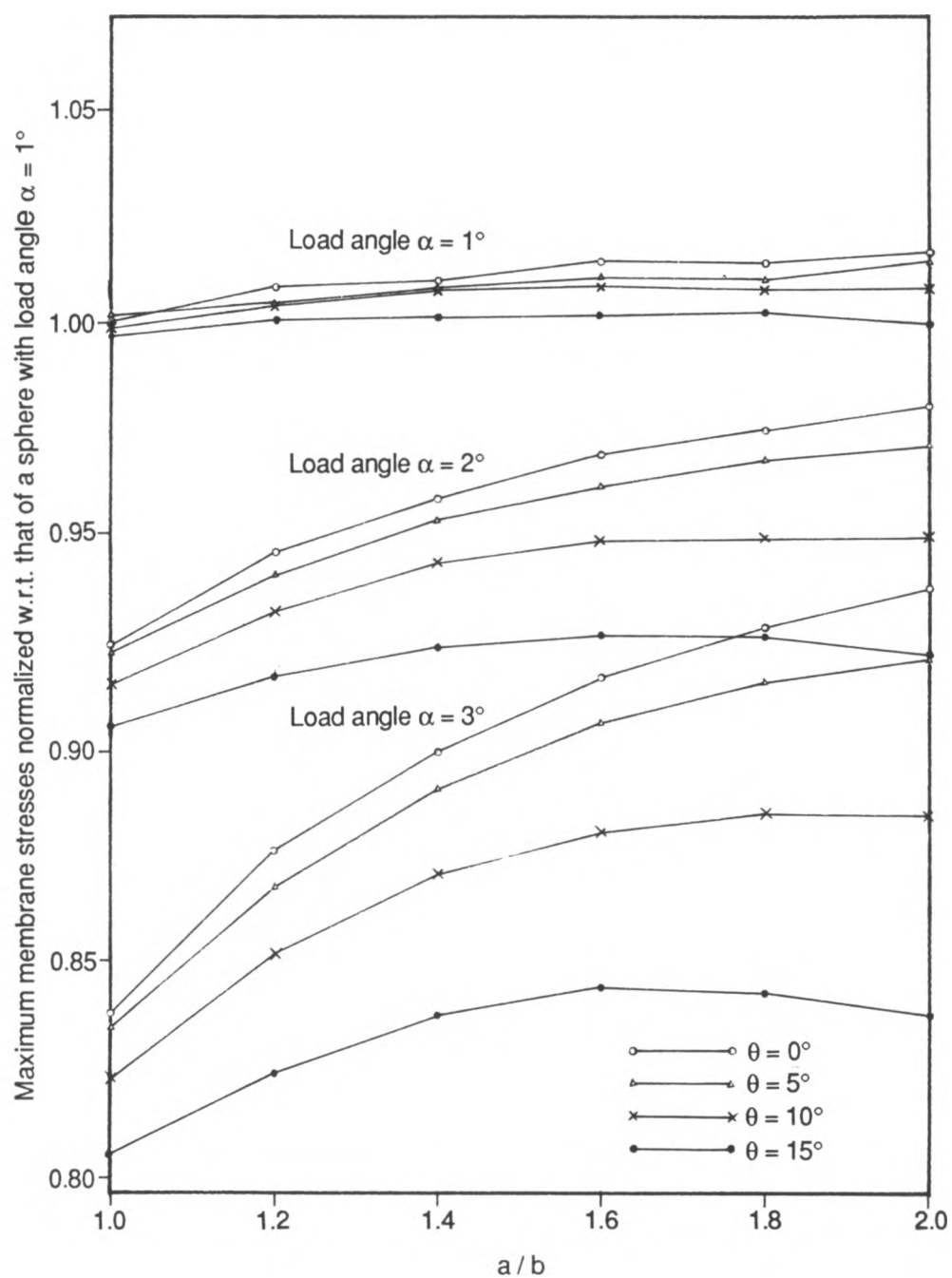(b) maximum bending moment
(c) Coupled principal stresses

Fig. 5.12 Maximum membrane stresses of ovals with equal v(
flat plate loading at the equator (plotted w.r.t. load a⌐
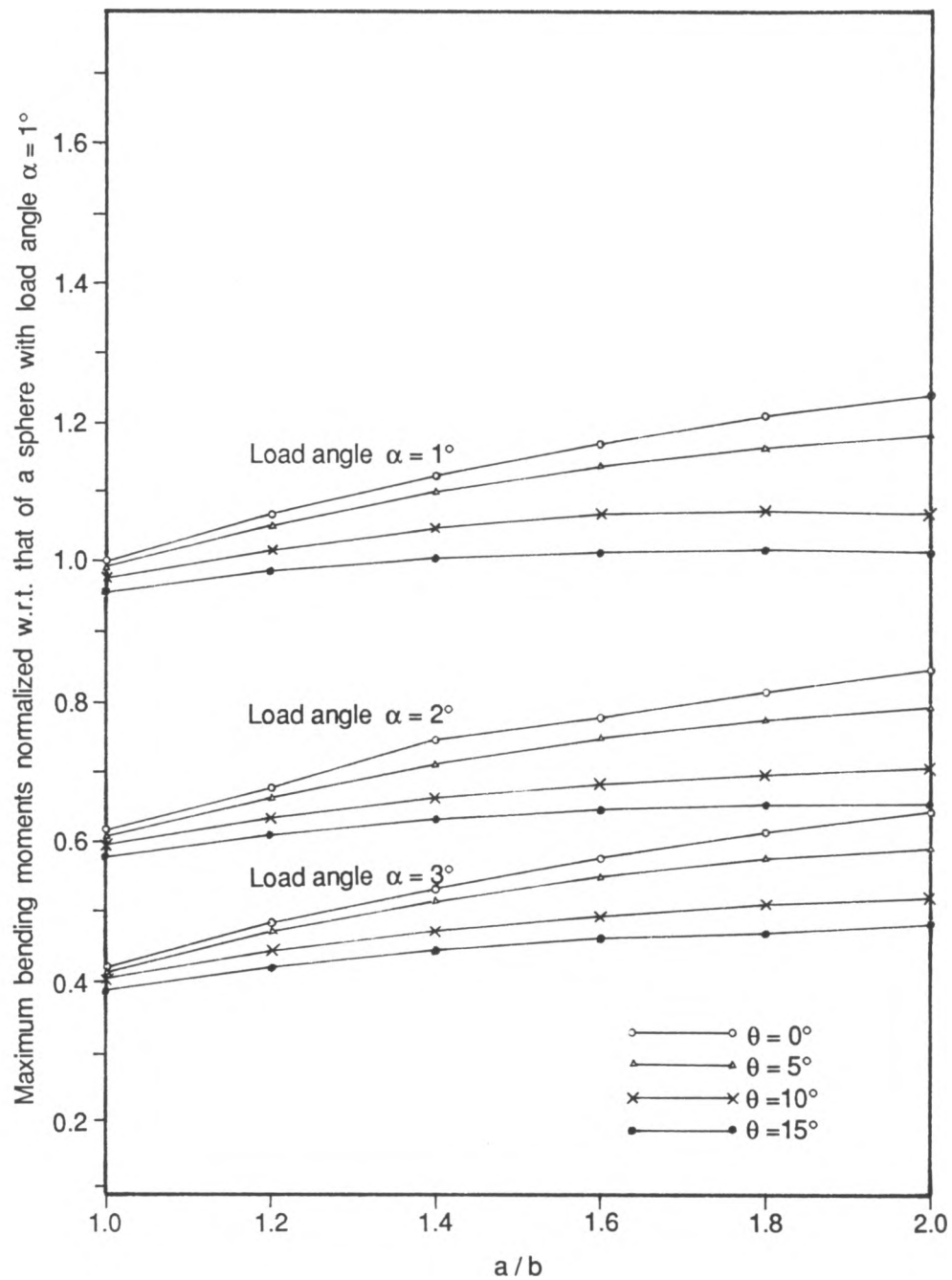
Fig. 5.13 Maximum bending moments of ovals with equal volumes a
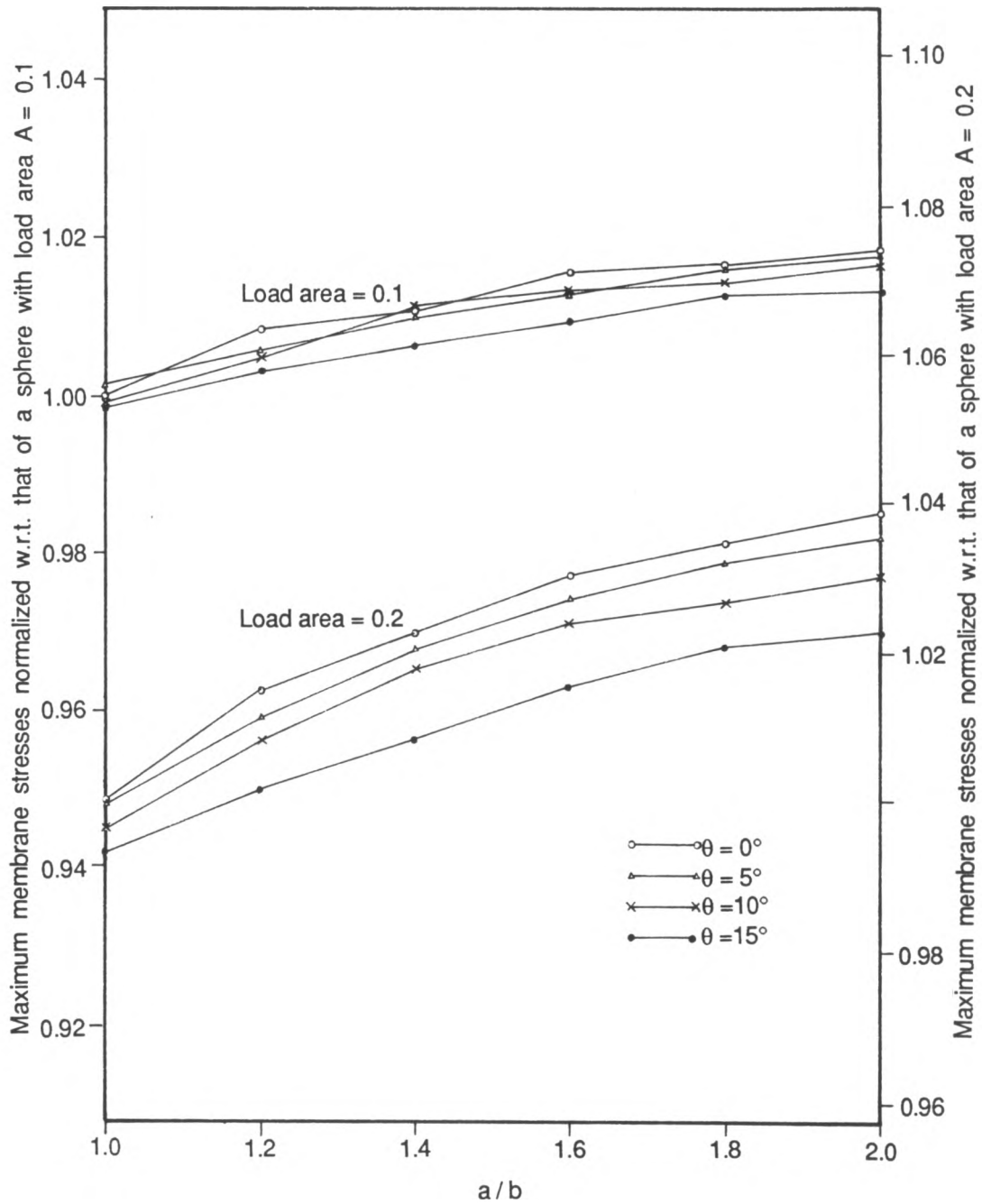flat plate loading at the equator (plotted w.r.t. load angle)

Fig. 5.14 Maximum membrane stresses of ovals with equal volumes and under flat plate loading at the equator (plotted w.r.t. load area)
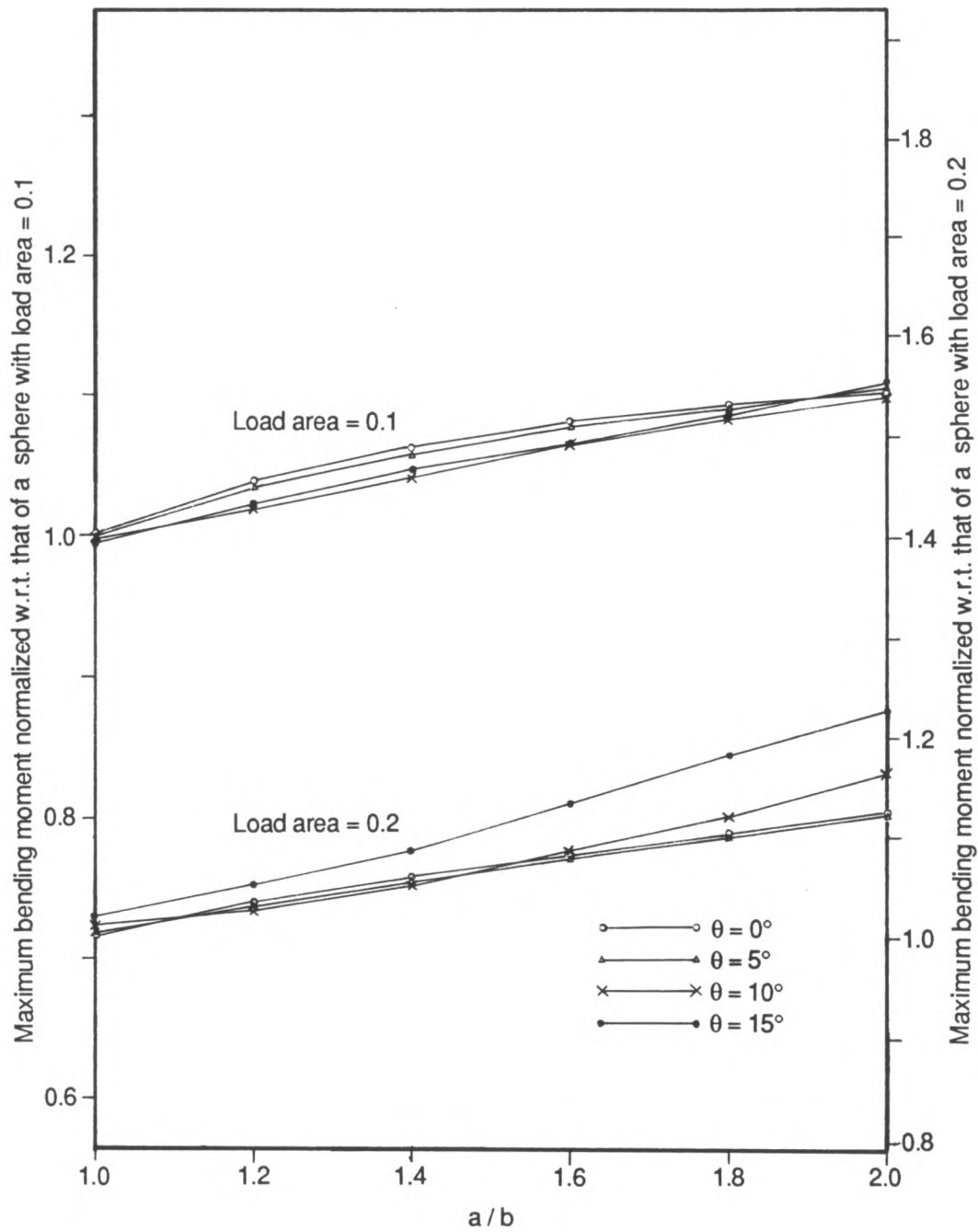
Fig. 5.15 Maximum bending moments of ovals with equal volumes and under flat plate loading at the equator (plotted w.r.t. load area)
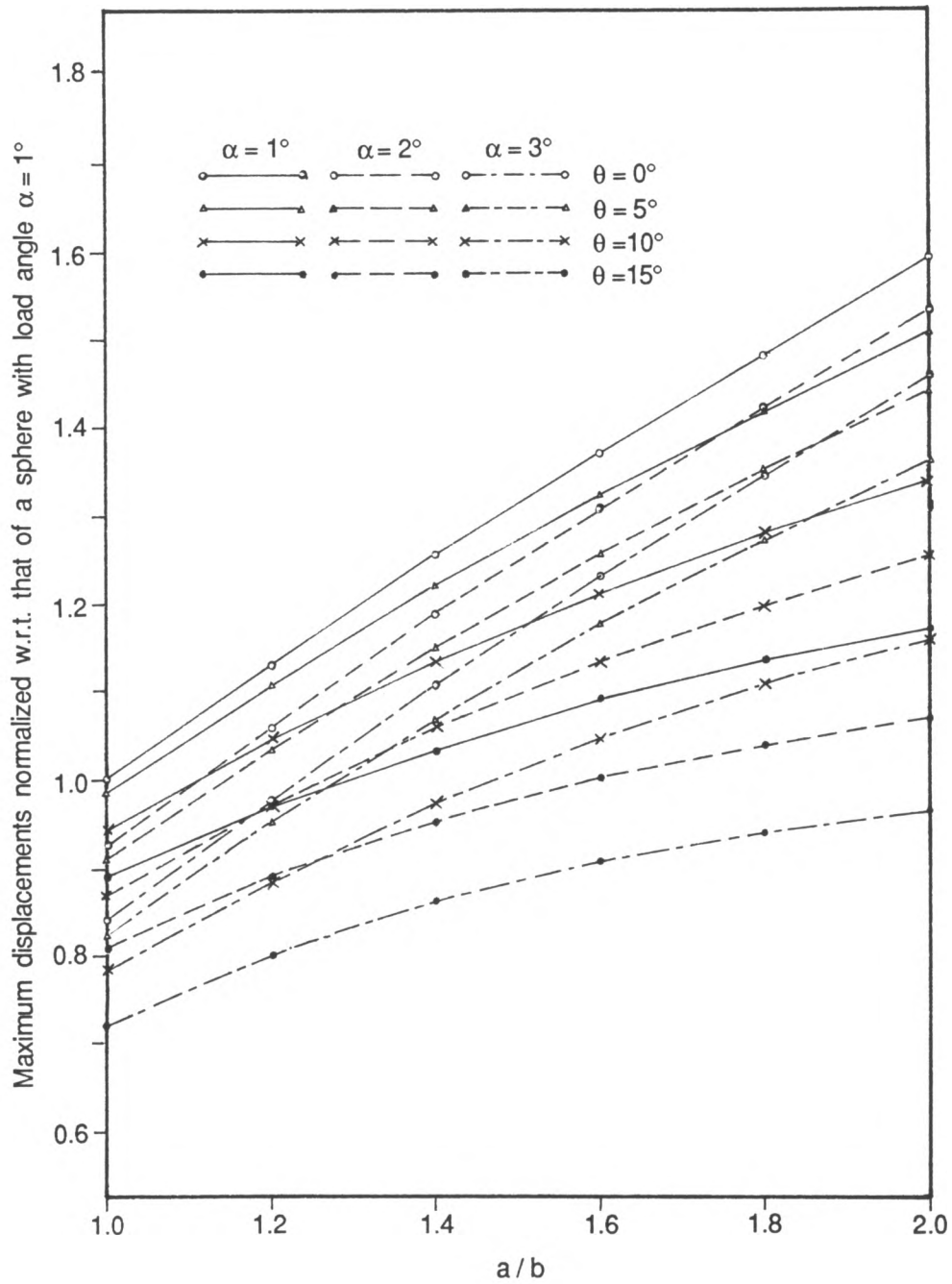
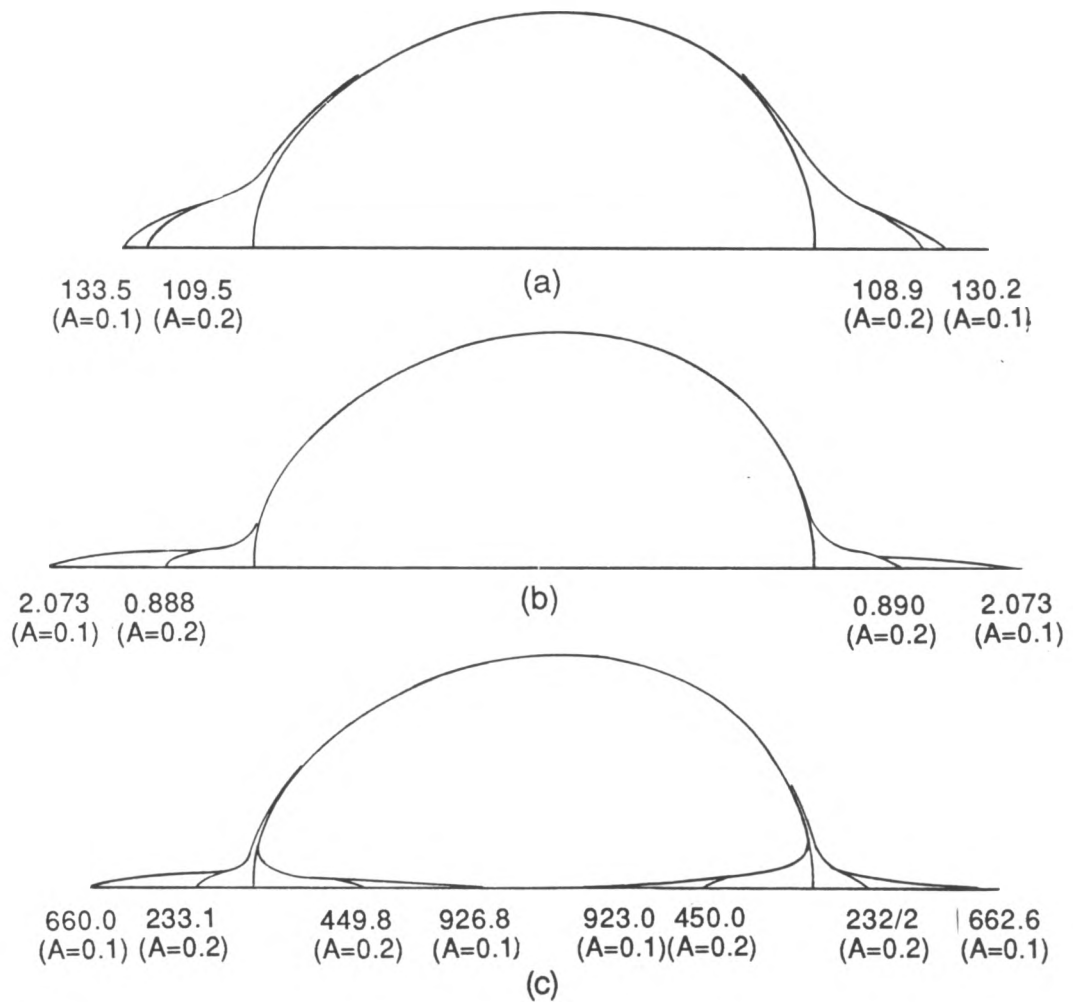Fig. 5.16 Maximum displacements of ovals with equal volumes and under flat plate loading at the equator

133.5   109.5   (a)   108.9   130.2
(A=0.1) (A=0.2)   (A=0.2) (A=0.1)

2.073   0.888   (b)   0.890   2.073
(A=0.1) (A=0.2)   (A=0.2) (A=0.1)

660.0   233.1   449.8   926.8   923.0 450.0   232/2 | 662.6
(A=0.1) (A=0.2)   (A=0.2) (A=0.1)   (A=0.1)(A=0.2)   (A=0.2) (A=0.1)
                                    (c)

Fig. 5.17 Stresses of an eggshell under flat plate loading at the pole
          (θ = 5°, a/b = 1.2)
          (a) Maximum membrane stress
          (b) maximum bending moment
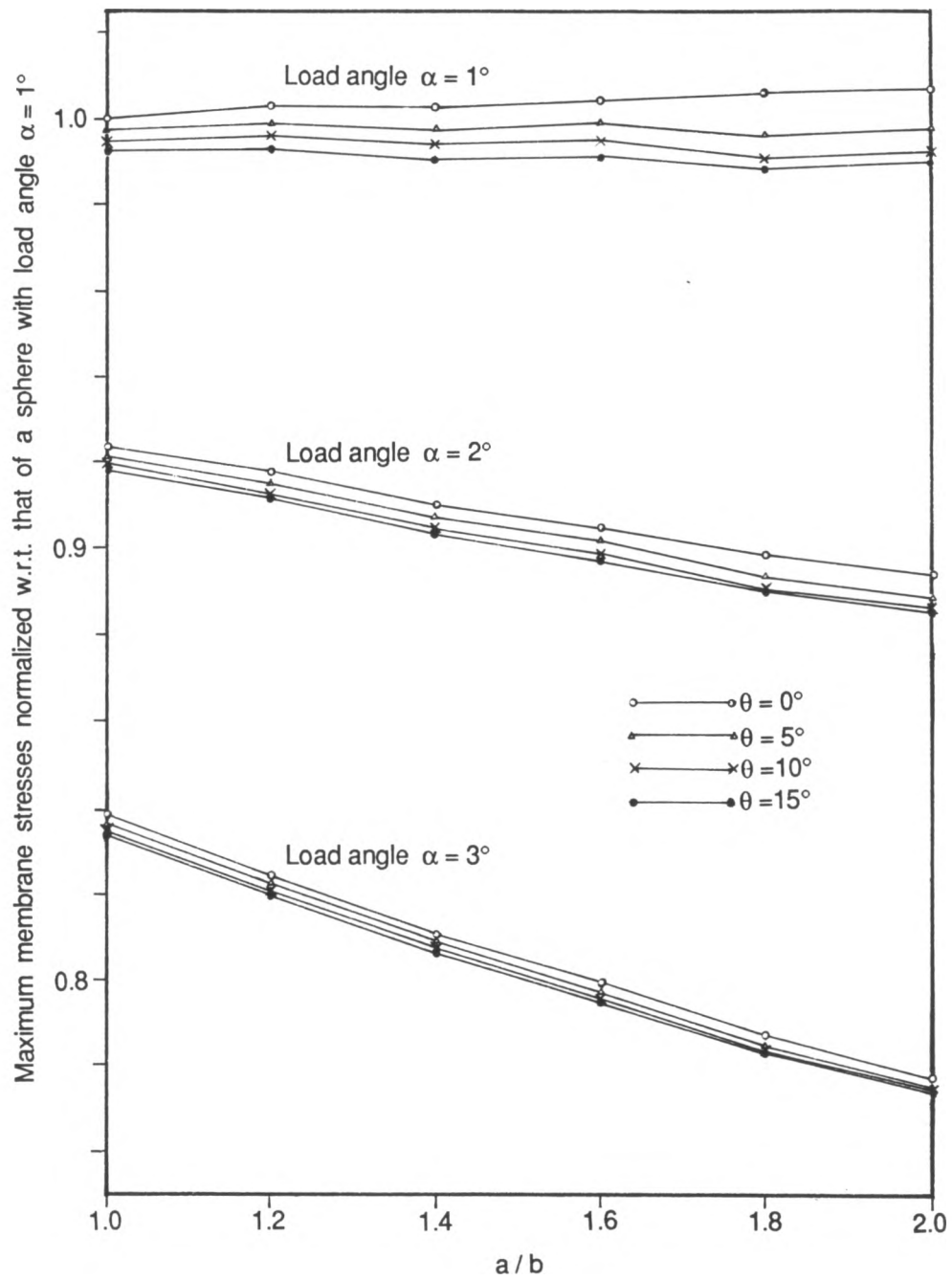   (c) Coupled principal stresses

Fig. 5.18 Maximum membrane stresses of ovals with equal volumes and under flat plate loading at the pole (plotted w.r.t. load angle)
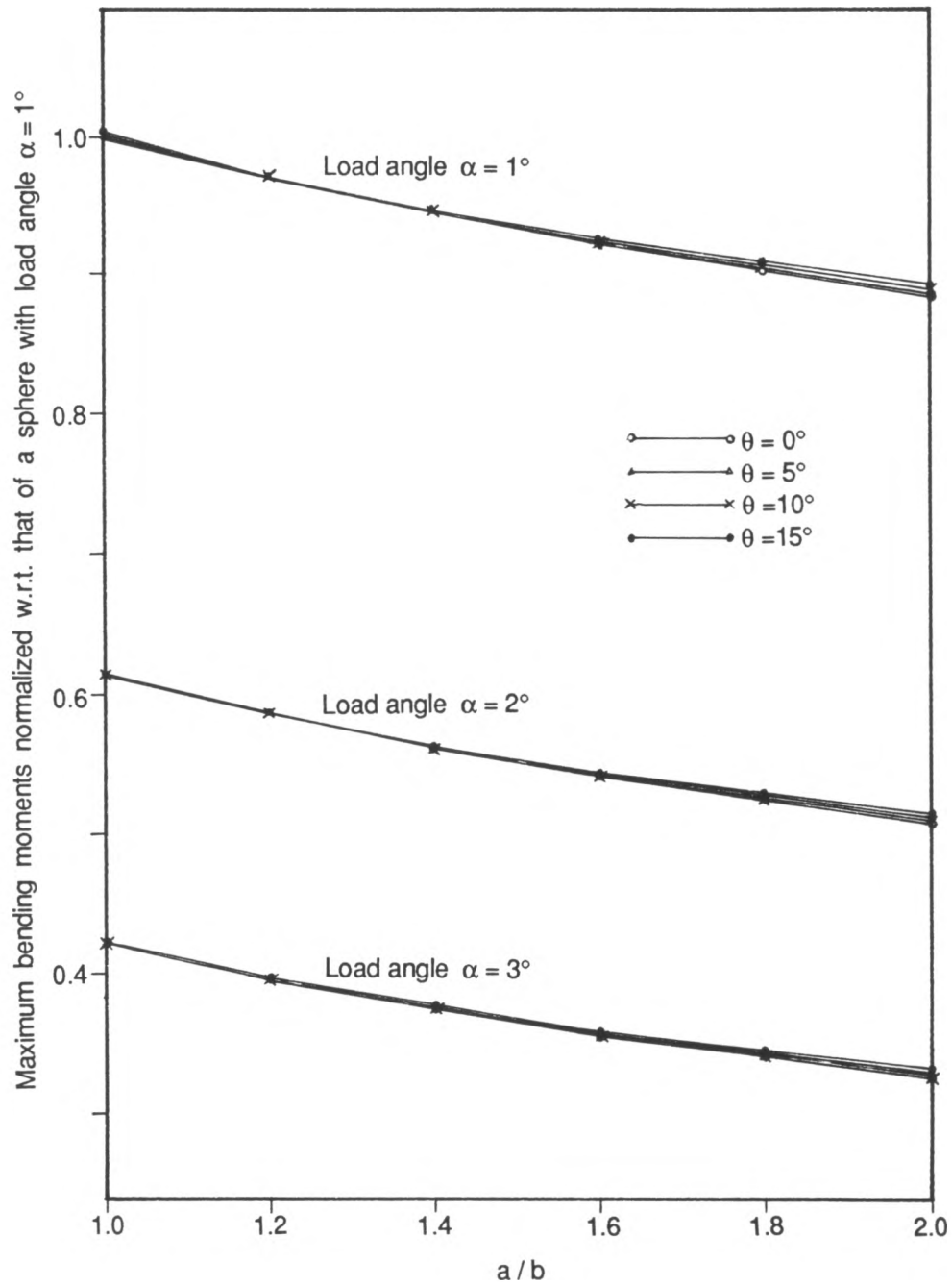
Fig. 5.19 Maximum bending moments of ovals with equal volumes and under flat plate loading at the pole (plotted w.r.t. load angle)
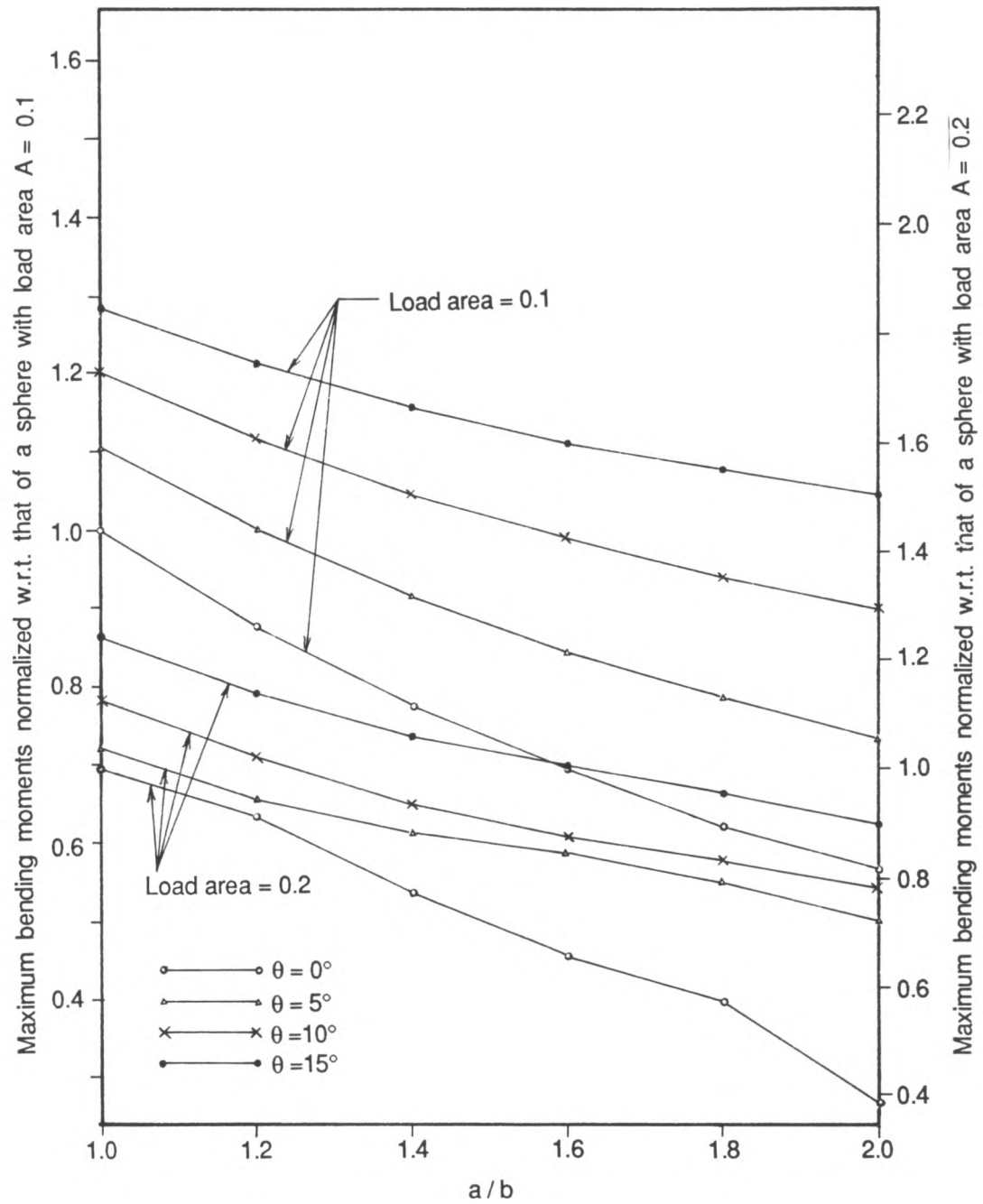
Fig. 5.20 Maximum bending moments of ovals with equal volumes and under flat plate loading at the pole (plotted w.r.t. load area)
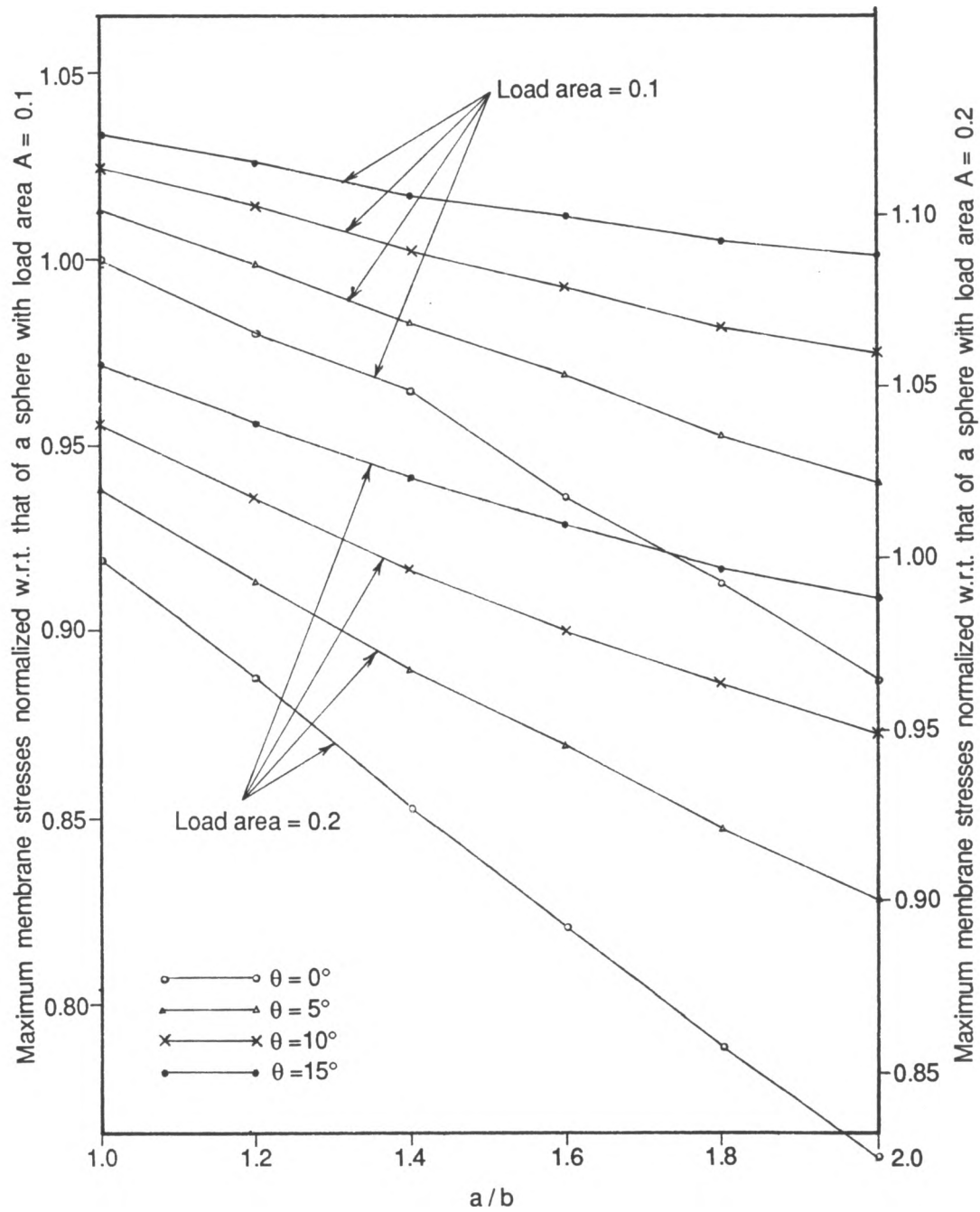
Fig. 5.21 Maximum membrane stresses of ovals with equal volumes and under flat plate loading at the pole (plotted w.r.t. load area)
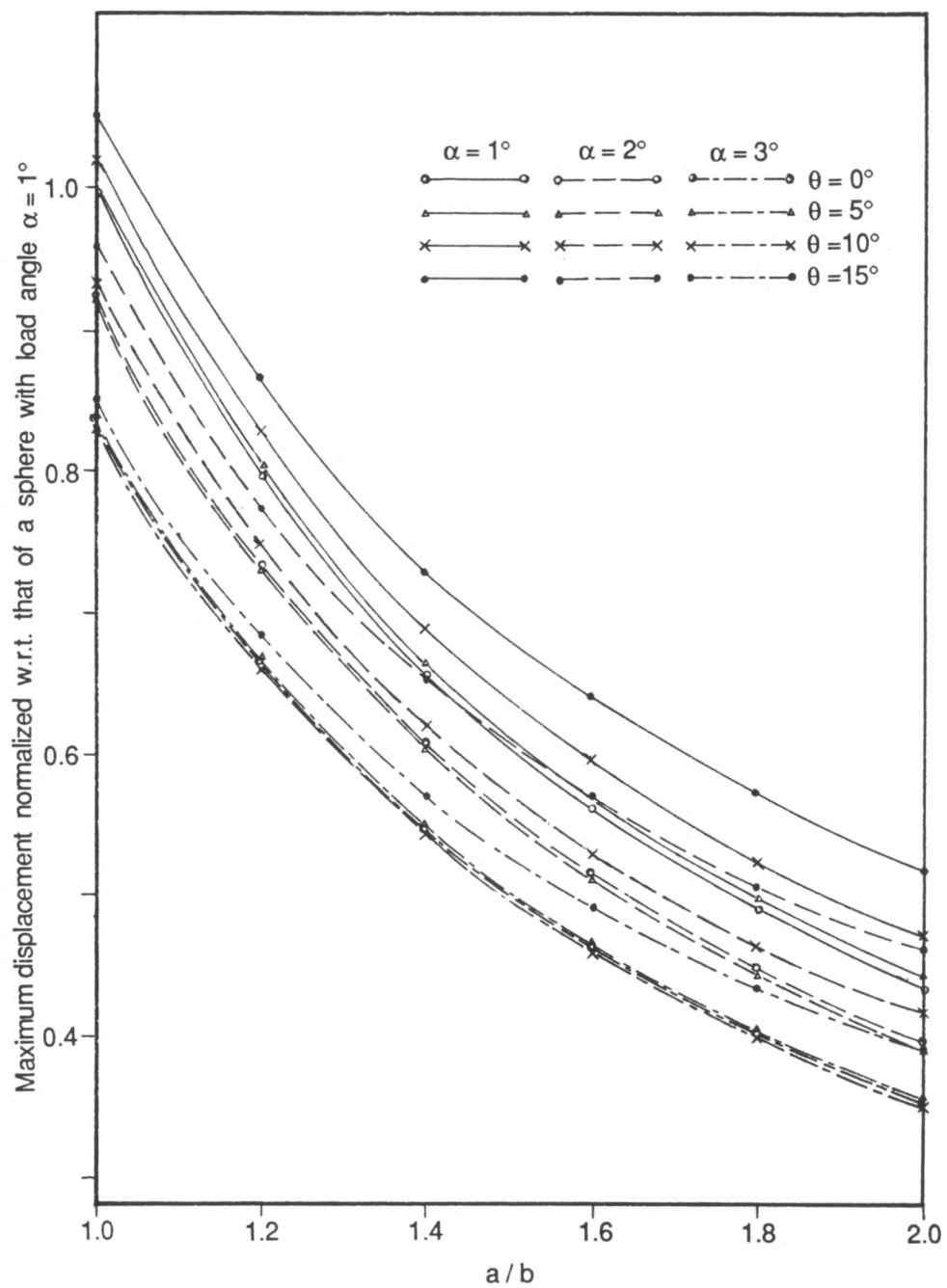
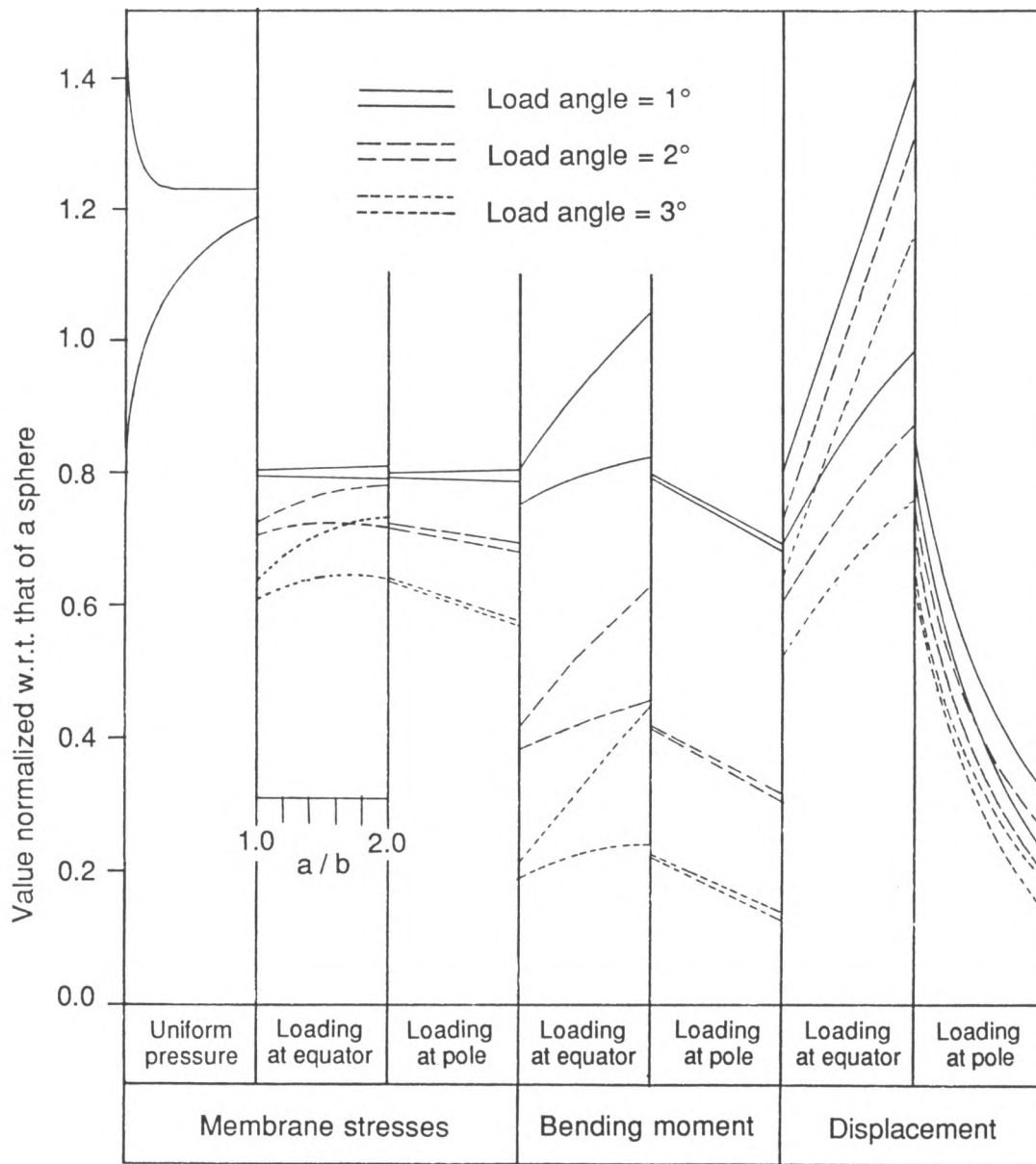Fig. 5.22 Maximum displacements of ovals with equal volumes and under flat plate loading at the pole

Fig. 5.23 Comparison of loading cases
(Values are normalized w.r.t. that of a sphere with 1° load angle)

Observations

The tendency of stress and displacement variation with respect to eggshape and loading condition is summarized in Fig.5.23. If one can measure the load angle accurately, the loading at the pole will give better prediction than the one at the equator. It seems to be better to specify the load condition by the load angle rather than the contact area because the former gives less dispersion.

The stresses due to uniform pressure vary significantly with the egg shape, while those due to flat plat loading depend more on the load area or load angle. This fact suggests that the load area be reflected in determining the eggshell strength by flat type loading. Egg shape is an easily predictable factor, while the load area is difficult to evaluate exactly. Therefore the strength predicted by the uniform pressure type loading is more reliable.

Deformation due to flat plate loading at the poles is also more dependent on the egg shape than the load area. Therefore, the non-destructive measurement of deformation can provide reliable information for a prediction of the eggshell strengh, if one can obtain a good correlation between the deformation and the strength as observed by several researchers (Voisey and Hunt, 1967).

5.1.4 Fracture of eggshell

The fracture analysis of an eggshell in this section has not been carried out to present specific analysis results. Rather it is intended to explore the possibility of fracture analysis using the finite element formulated in the present study.

There have been numerous studies on the eggshell failure under quasi-static, impact, cyclic, thermal and other loading conditions. Some researchers investigated experimentally the appearance of cracks due to various loading conditions. Others tried to predict the fracture by stress analysis or to relate the experimental observations with analysis results. Most of the previous studies are based on the simple notion that breakage occurs when the stress at some point in the shell exceeds the ultimate strength of the shell material at that point. However, the eggshell is known to be a brittle material (Voisey and Hunt, 1968; Manceau and Henderson, 1970a), and usually fails in the form of a fracture. There are often *microcracks* within a newly laid egg before its handling (Tyler and Moore, 1964). Those microcracks cause a fracture failure at stress level much less than the material strength. The measured apparent strength may have been influenced by this initial imperfection. Therefore, the failure of eggshell should also be examined from fracture mechanics view point.

Crack initiation

A material fails when a stress at a point exceeds its strength. A crack propagates when the *stress intensity factor* at the cracktip exceeds the *fracture toughness* of the material. Stress intensity factor and toughness are analogous, respectively, to stress and strength. In other words, the toughness is a material property while the stress intensity factor is a material response to external effects. The stress intensity factors should be determined by analysis, and the toughness is to be evaluated by experiment. Therefore, the major task of a fracture analysis is to find the stress intensity factors.

There are three modes of fracture: opening (mode I), sliding (mode II) and tearing (mode III), Fig.5.24. Different intensity factors are associated with each of these modes. The stresses and displacements in the immediate
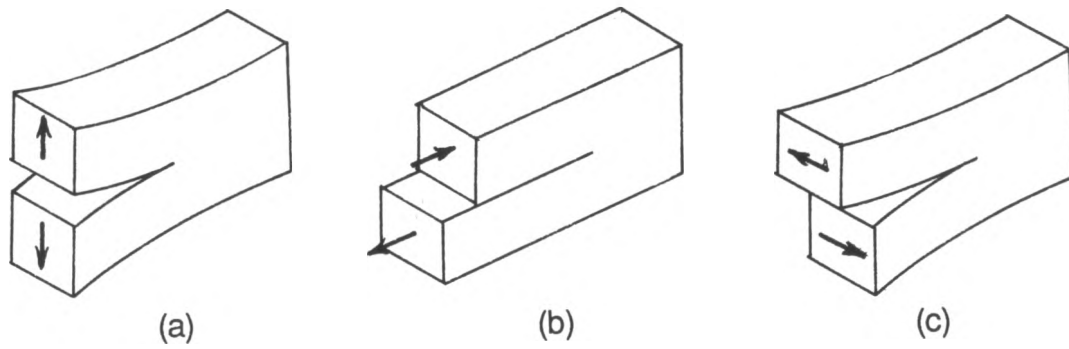
Fig. 5.24 Three modes of fracture
   (a) Mode I (opening)   (b) Mode II (sliding)
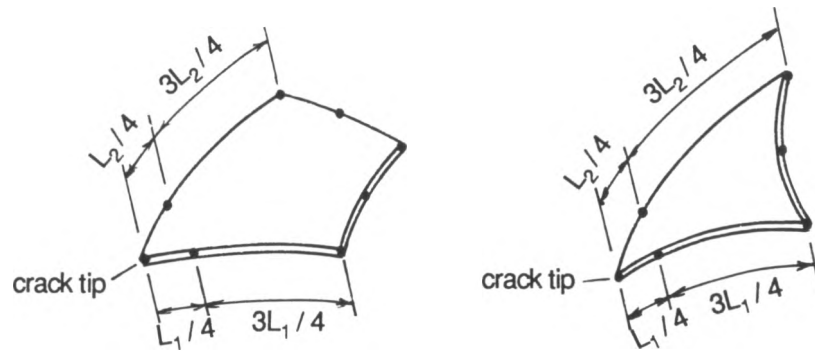   (c) Mode III (tearing)

Fig. 5.25 Quarter point singularity elements of shell

vicinity of the crack tip can be expressed in terms of these stress intensity factors as follows:

$$\sigma = \frac{1}{\sqrt{(r)}} \left(K_I \ g_I + K_{II} \ g_{II} + K_{III} \ g_{III} \right) \tag{5.1.4a}$$

$$\delta = \sqrt{(r)} \ \left(K_I \ h_I + K_{II} \ h_{II} + K_{III} \ h_{III} \right) \tag{5.1.4b}$$

in which

> σ = stresses in the vicinity of the crack tip
>
> δ = displacements in the vicinity of the crack tip
>
> $r = \sqrt{(x^2 + y^2)}$, the distance from the crack tip
>
> g_I, g_{II}, g_{III} = functions of θ with $\theta = \tan^{-1}(x / y)$
>
> h_I, h_{II}, h_{III} = functions of θ and material properties
>
> K_I, K_{II}, K_{III} = stress intensity factors for mode I, II and III respectively

The $1/\sqrt{(r)}$ singularity of stresses in Eqn. (5.1.4a), and $\sqrt{(r)}$ variation of displacements in Eqn. (5.1.4b) can be modelled using quadratic isoparametric finite elements. This is achieved simply by placing the side nodes adjacent to the crack tip at quarter points of their respective sides as shown in Fig. 5.25 (Barsoum,1974; Henshell and Shaw, 1975; Barsoum,1976a).

Stresses in shells also have a $1 / \sqrt{(r)}$ singularity (Folias,1967; Duncan--Fama and Sandar, 1972). Barsoum (1976b) proved that the degenerate shell elements can also be made to represent the required stress singularity by the quarter point elements described above. The stress singularity can be achieved by requiring the strain-displacement matrix, **B**, to be singular at the crack tip and the strains to vary in proportion to $1 / \sqrt{(r)}$. One can easily recognize that the strain-displacement matrices in the present formulation have, as multiplication factor, the Jacobian matrix **J** or transformation matrix **S***. If one uses a different coordinate transformation method discussed in Section 2.1, a matrix equivalent to **S*** is to be obtained by multiplying the Jacobian matrix with

coordinate transformation matices. Therefore, the singularity of the Jacobian matrix directly leads to the singularity of the strain-displacement matrices for the present formulation as well. It is already known that the Jacobian matrix is singular in quarter point elements. Thus, the singularity of **B** in quarter point elements is proved for the present formulation. The $1 / \sqrt{(r)}$ singularity of strains along the edge can be proved in the same manner as in other literature (Barsoum,1976), although its detailed proof is not within the scope of this study.

There are three techniques for computation of the stress intensity factors using the finite element method: the displacement correlation method, the global energy release method and the hybrid direct method. The displacement correlation method incorporated with the quarter point singularity element is believed to be the simplest and the most efficient one. According to the displacement correlation method, K_I, K_{II}, and K_{III} can be obtained by inserting the computed displacements into Eqn.(5.1.4b) and solving the equation. For example, in case of mixed mode I and mode II involving membrane actions only, the stress intensity factors can be expressed in terms of displacements at the nodes, facing the crack, of the quarter point elements (Ingraffea, 1977,1981).

$$K_I = \sqrt{(2\pi / L)} \, G \, \{ \, 4 \, (\, v_B{'} - v_D{'} \,) + v_E{'} - v_C{'} \, \} / (\, \kappa + 1) \qquad (5.1.5a)$$

$$K_{II} = \sqrt{(2\pi / L)} \, G \, \{ \, 4 \, (\, u_B{'} - u_D{'} \,) + u_E{'} - u_C{'} \, \} / (\, \kappa + 1) \qquad (5.1.5b)$$

in which u and v are displacements expressed in crack tip coordinates shown in Fig.5. . And G is the shear modulus, and $\kappa = (3 - v) / (1 + v)$ assuming locally plane stress state.

For linear fracture analysis of shell, the stress intensity factors can be evaluated by superposing the stress intensity factors for membrane actions and
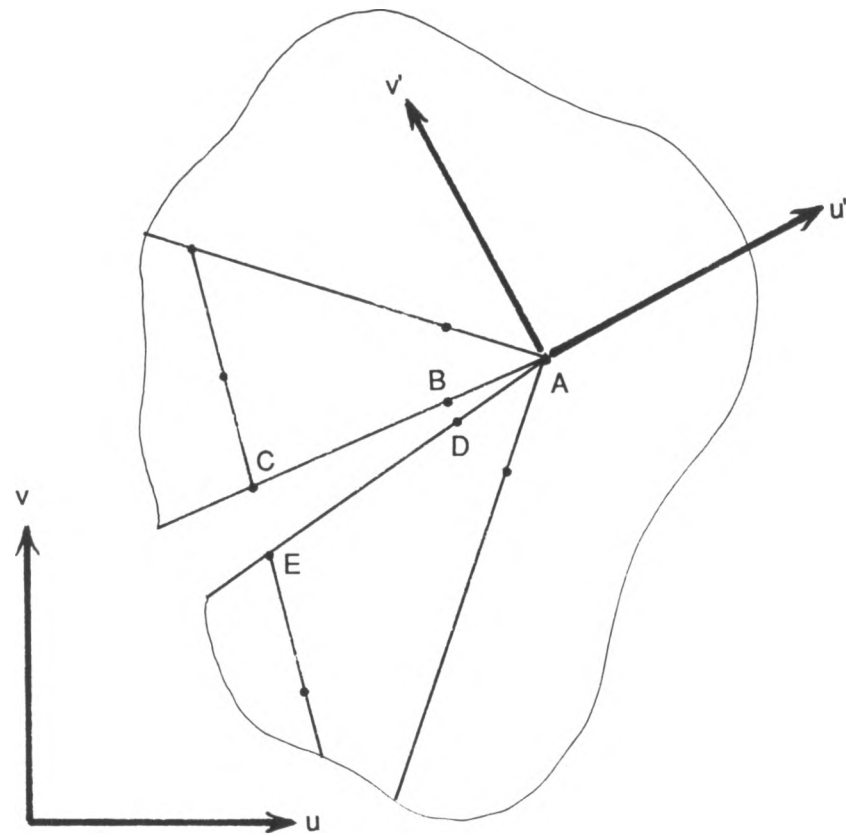
Fig. 5.26 Local coordinates relative to the crack tip

for bending actions (Lakshminarayana, 1982). Then, the total stress intensity factors, $K_I^{(tot)}$ and $K_{II}^{(tot)}$, are given by

$$K_I^{(tot)} = K_I^{(m)} + K_I^{(b)} \tag{5.1.6a}$$

$$K_{II}^{(tot)} = K_{II}^{(m)} + K_{II}^{(b)} \tag{5.1.6b}$$

in which $K_I^{(m)}$ and $K_I^{(b)}$ are mode I stress intensity factors due to the membrane and the bending actions, respectively.

The following is a simple example of fracture analysis for an eggshell under uniform internal pressure. It is assumed that there is a small through crack in the equatorial direction at the waist of the egg. The deformation and stresses are computed using quarter point triangular elements in the vicinity of the crack tip. Fig.5.28 shows the deformed shape. The stress in the equatorial direction is also shown in Figure 5.29. The stresses here, which were computed by linear extrapolation, are not expected to be accurate at the immediate vicinity of the crack tip. The actual stress distribution should be obtained by inserting the computed stress intensity factors into Eqn. (5.1.4a). For the present case with a small through crack, the stress intensity factors may be obtained from Eqn. (5.1.5), assuming that the thickness is small, the membrane action is dominant, and thus the transverse crack propagation is negligible. For uniform pressure p=10 KPa, the computed displacements are

$$u_b' = 2.71 \times 10^{-6} \text{ mm} \qquad v_b' = -7.24 \times 10^{-5} \text{ mm}$$

$$u_c' = -5.73 \times 10^{-6} \text{ mm} \qquad v_c' = 1.25 \times 10^{-4} \text{ mm}$$

$$u_d' = 2.14 \times 10^{-6} \text{ mm} \qquad v_d' = -8.10 \times 10^{-5} \text{ mm}$$

$$u_e' = -6.45 \times 10^{-6} \text{ mm} \qquad v_e' = 1.52 \times 10^{-4} \text{ mm}$$

Substituting the values into Eqn. (5.1.5), one obtains the following stress intensity factors:

$$K_I = 4.63 \ \text{Mpa}\sqrt{(\text{mm})}$$

$$K_{II} = 0.0412 \ \text{Mpa}\sqrt{(\text{mm})}$$

The force-deformation diagram in Fig.5.3 supports the notion that an eggshell is almost ideally brittle. For an ideally brittle material, the crack initiation leads to instantaneous fracture failure at constant load level. Therefore, overall failure of an eggshell is expected when the stress intensity factors reach the fracture toughness. The fracture toughness of eggshell is not available. But the physical properties of eggshell are known to be similar to that of limestone. The toughness of Indiana limestone, $K_{Ic} = 35 \ \text{Mpa}\sqrt{(\text{mm})}$, may be used as an approximate estimation of eggshell toughness.

There are a few theories of predicting the crack propagation in mixed mode fracture (Broek, 1974). In general, the condition for crack propagation is expressed by an interaction equation in the form of

$$F\left(\left(\frac{K_I}{K_{Ic}}\right)^2, \ \left(\frac{K_{II}}{K_{IIc}}\right)^2, \ \left(\frac{K_{III}}{K_{IIIc}}\right)^2\right) > 1 \tag{1.5.7}$$

in which K_{Ic}, K_{IIc} and K_{IIIc} are the toughnesses for modes I, II, and III, respectively. According to the energy release rate criterion, fracture occurs when the energy release rate is greater than the energy consumption rate. The criterion is given by

$$\left(\frac{K_I}{K_{Ic}}\right)^2 + \left(\frac{K_{II}}{K_{IIc}}\right)^2 + \left(\frac{K_{III}}{K_{IIIc}}\right)^2 > 1 \tag{1.5.8}$$

Assuming that $K_{Ic} = K_{IIc}^*$, and using Eqn.(5.1.8), one can predict that the fracture failure is expected at uniform pressure level, p=0.076 Mpa, which is approximately one third of the load level for the stress failure mentioned in Section 5.1.2.

---

*In reality, K_{IIc} and K_{Ic} are not necessarily the same. Their ratio is around unity and dependent on the Poisson's ratio.
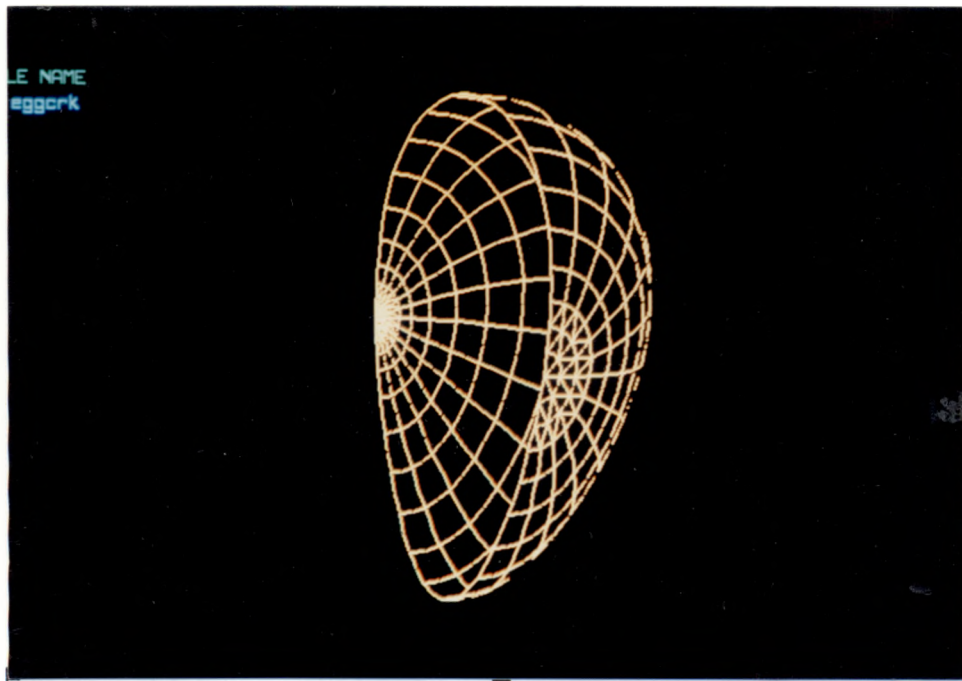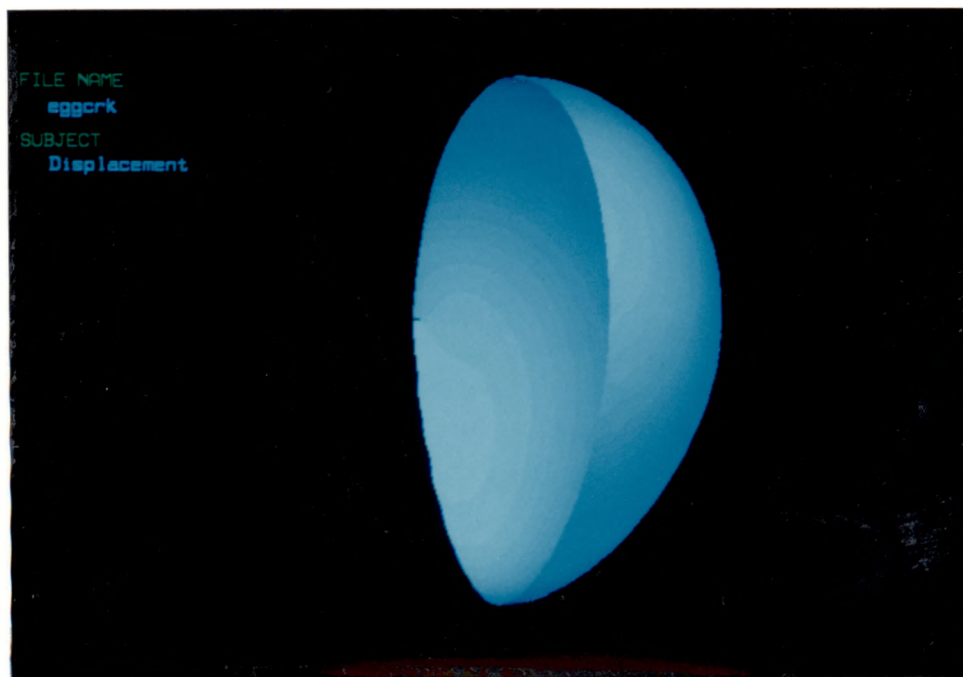
(a)
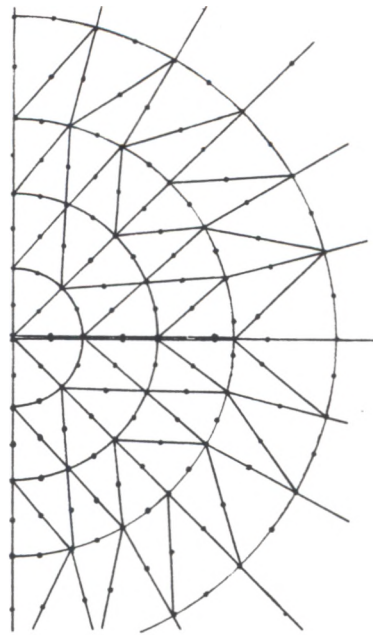
(b)

Fig. 5.27 Finite element mesh for an eggshell with a through crack
(a) Overall view
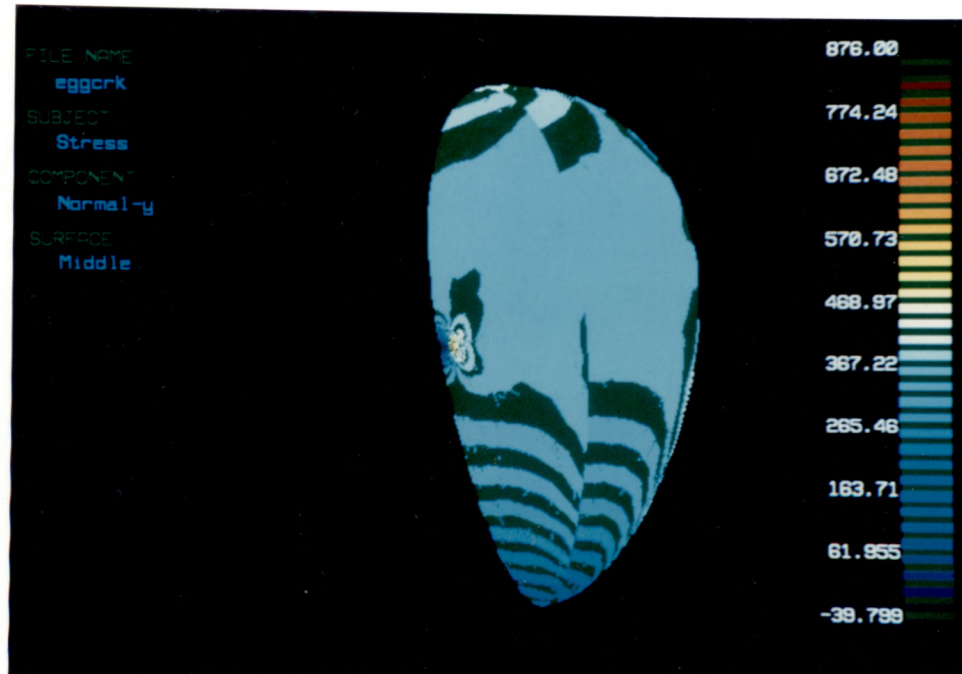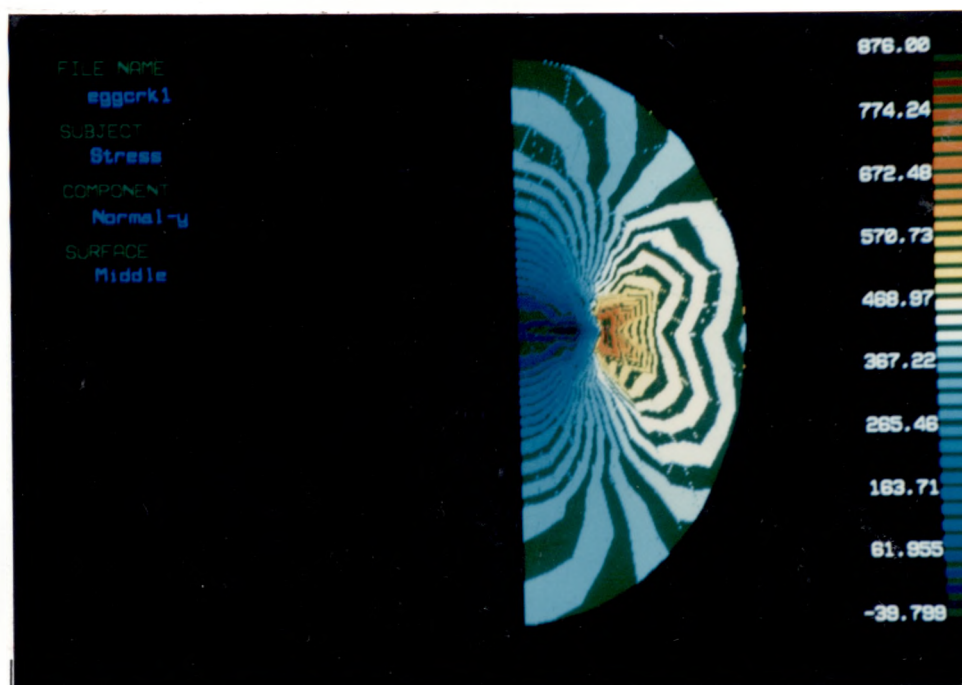(b) Close-up view in the vicinity of the crack tip

(a)

(b)

Fig. 5.28 Deformation of an eggshell with a through crack and under uniform
internal pressure
(a) Overall view
(b) Close up view in the vicinity of the crack tip

(a)

(b)

Fig. 5.29 Circumferential stresses of an eggshell with a through crack and
under uniform internal pressure
(a) Overall view
(b) Close up view in the vicinity of the crack tip

Crack trajectory

The criterion of Eqn.(1.5.8) is based on the assumption that the crack propagates in a self-similar manner. However, it is usually observed that *mixed mode crack* extension takes place under an angle with respect to the original crack. According to the maximum principal stress theory, a crack propagates in the direction perpendicular to the maximum principal stress. The angle between the original and extending direction, θ_m, can be obtained by the following relation:

$$K_I \sin \theta_m + K_{II} (3 \cos \theta_m - 1) = 0 \qquad (5.1.9)$$

And the fracture criterion is

$$K_{Ic} < K_I \cos^3 (\theta_m/2) - 3 K_{II} \cos^2 (\theta_m/2) \sin (\theta_m/2) \qquad (5.1.10)$$

Substitution of the computed K_I and K_{II} into Eqn.(5.1.9) gives $\theta_m = 0.5\ ^0$. Use of either Eqn. (5.1.8) or (5.1.10) does not make any significant difference for this case, because θ_m is small, and one can conclude the crack propagates in an essentially self-similar manner. In other words, crack propagates in the plane of the original crack.

There is another theory which states that crack growth takes place in the direction of minimum energy density. A detailed description of the criterion can be found in other literature (Sih, 1974).

5.2 Modeling of stomatal opening

Stomata are microscopic pores formed by guard cells, which are found in plant leaves. The opening and closure of these pores control 95 %, or more, of the photosynthesis and transpirations (Willmer, 1983). The mechanism of stomatal opening has long been of great interest for many researchers. It has

been frequently modelled by an analogy to a rubber tube or a balloon. Aylor *et al.* (1973) simulate the stomatal opening using a balloon and supplemented the experimental observation by an elastic analysis of tubular beam subject to pure bending. Shoemaker and Srivastava (1973) also used a beam analogy to relate the differential wall thickening of the guard cell to the opening mechanism. DeMichele and Sharpe (1973) idealized the guard cell as a rectangular composite beam to show that the opening is a result of opposing pressure of the guard cell and adjacent epidermal cells. These early primitive analyses, based on simplification and idealization of guard cell geometry, properties and external effects, led to many controversial conclusions. Cooke *et al.* (1976) were the first to analyze the stomatal mechanism using the finite element method. They modeled the guard cell as an elliptical torus with orthotropic material properties and variable thickness using triangular thin shell elements. Their modeling is considered to be far more realistic and complete than the previous ones. Cooke *et al.* (1977) went further with finite element analysis to include the geometric nonlinearity.

Analysis of the stomatal mechanism involves complex geometry, material properties, and external effects. This may be one of the typical problems which can exploit the powerful feature of the finite element method as a tool for biomechanics. The finite element method equipped with high speed computing and computer graphics has enabled not only realistic modeling but also lifelike visualization of the analysis results. Real time animation of stomatal movement is no loger a remote possibility.

The analysis of stomatal opening presented in this section is intended to validate the newly formulated finite element, rather than to derive specific conclusions. The computed results are compared with previous experimental or numerical analyses.

An elliptic stomate has been modelled as an elliptical torus with elliptic plates inside. The geometry of the middle surface of the doubly curved shell is defined by the following expressions (Cooke *et al.*, 1976).

$$x = \cos \theta \, [\, b + ac \, (1 + \sin \phi) \, \{ \, (a \cos \theta)^2 + (b \sin \theta)^2 \, \}^{-1/2} \,] \qquad (5.2.1a)$$

$$y = \sin \theta \, [\, a + bc \, (1 + \sin \phi) \, \{ \, (a \cos \theta)^2 + (b \sin \theta)^2 \, \}^{-1/2} \,] \qquad (5.2.1b)$$

$$z = d \cos \theta \qquad (5.2.1c)$$

with $0 \le \theta \le \pi/2$ and $-\pi/2 \le \phi \le \pi/2$. The parameters a, b, c, and d are defined in Fig. 5.30. The elliptical plate is perpendicular to and bounded by the curved shell at $\theta = \pi/2$. Uniform thickness and isotropic material property are assumed. A uniform internal pressure is applied perpendicular to the shell surface. Owing to its symmetry, only one octant of the torus need be analyzed. Boundary conditions are applied so as to take into account the symmetry. The type III triangular elements are used in these analyses. In this qualitative analysis, the geometry of the guard cell is defined by the nondimensionalized values, a = 7.3, b = 1.0, c = 5.35, d = 4.0 and thickness = 1.0. The material properties are assumed to be homogeneous throughout the guard cell and the elliptic plate with modulus of elasticity $E = 10^6$ units and Poisson's ratio = 0.0.

For better visualization, a quarter of the torus is graphically generated using symmetry. Fig. 5.31 shows the perspective view of the guard cell seen from two different angles. The deformed shapes are also shown in Fig. 5.32. The major principal stress in the middle surface is presented in Fig. 5.33.

Aylor *et al.* (1973, 1975) stressed that the stomatal opening requires the radially arranged cellulose microfibrils and the existence of constraints on the length of the stomatal system. Shoemaker and Srivastava (1973) argued that the non-uniform thickening of the guard cell walls is crucial for stomatal opening. None of these is required for the present analysis. However, the finite
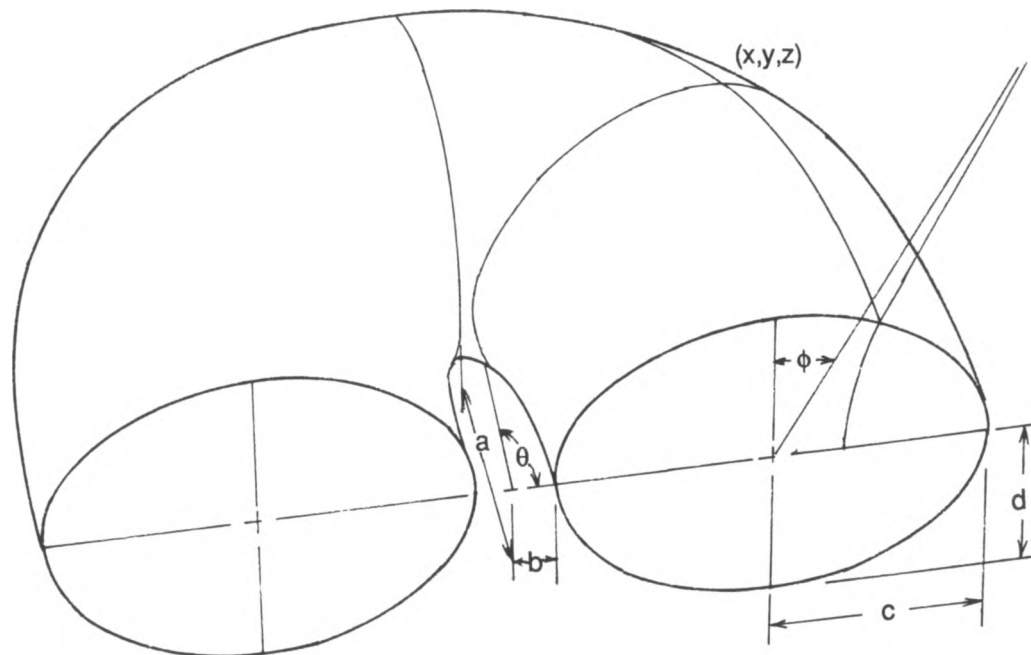
Fig. 5.30 Parameters defining the geometry of a guard cell middle surface
(Eqn.5.2.1, after Cooke *et al.*, 1976)

element model achieves proper opening of the guard cell as shown in Fig. 5.32. This fact has already been observed in the preceding finite element analyses (Cooke *et al.*, 1976; Cooke *et al.*, 1977), and is verified again by the present analysis.

To examine the effect of the stomatal geometry on its opening, guard cells with the following three different shapes, which are not possible in reality, are also analyzed.
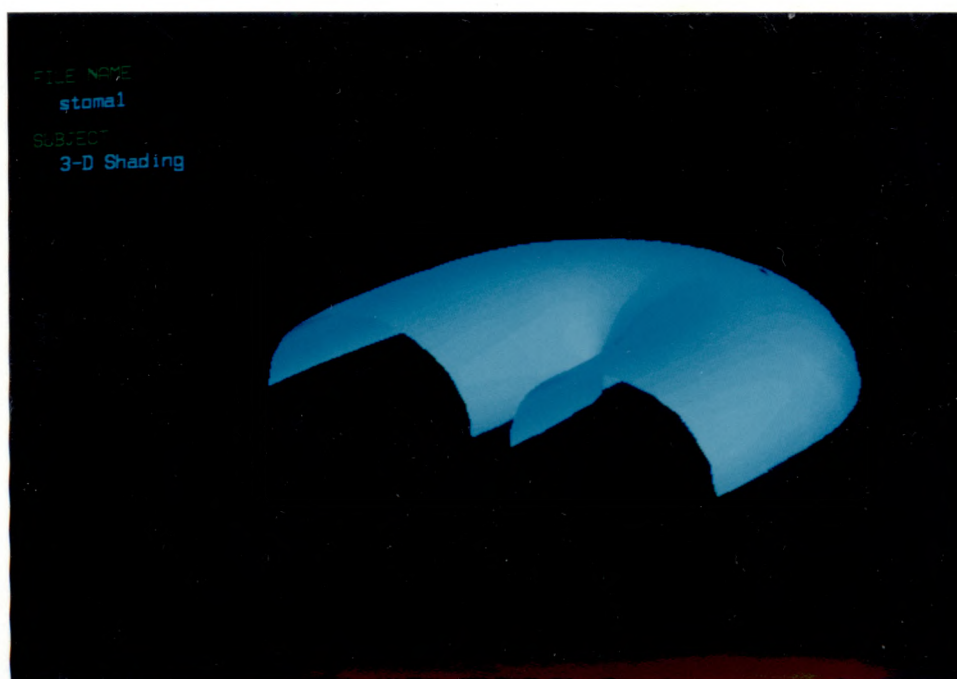
1) Elliptical torus with circular cross section: $a = 7.3$, $b = 1.0$, $c = d = 5.0$

2) Circular torus with circular cross section: $a = b = 2.5$, $c = d = 5.0$

3) Circular torus with elliptical cross section: $a = b = 2.5$, $c = 5.35$, $d = 4.0$

The deformed shapes overlaid with the undeformed finite element meshes are shown in in Figs.5.34 to 5.37. The graphically represented results clearly indicate that the elliptical cross section as well as the elliptical torus shape is an essential character for opening of the stomate.

An analytical solution (Cooke *et al.*, 1976) states that the pore of an isotropic circular torus decreases as the internal turgor pressure increases, unless $b/c > 1.77$ (Fig. 5.30). However, the present analysis shows that the pore increases slightly although $b/c < 1.77$. This discrepancy from the analytical observation may be partly due to the differences in Poisson's ratios and in the thickness-radius ratios. It should also be noted that membrane solution as well as the finite element solution by Cooke *et al.* (1976) is based on the assumption that the thickness is relatively small in comparison with other dimensions and thus the transverse shear strains are negligibe, while the present formulation takes into account the transverse shear strains. Furthermore, the bending actions are neglected in the membrane solution. Accordingly, the results of the present analysis for a thick shell may not match exactly with the analytical solution. The two give the bounded solutions for thin

and thick shells, respectively. This implies that the circular torus would not properly open for all thickness ranges. As shown in Figs. 5.34 and 5.36, tori with circular cross sections bulge out under uniform internal pressure. This corresponds to an intrusion of the guard cell into the neighboring epidermal cell region, which will cause mechanical disturbance to the rest of the leaf. From the results of the above analyses, it can be concluded that the elliptical shape of the torus (top view) seems to be a requirement for the opening of the guard cell and the elliptical cross section (elevation view) for the prevention of bulging into the neighboring region. The guard cell geometry plays an important role in stomatal opening.

A model without the elliptic plates is also analyzed in order to find whether the existence of the plates is essential to the opening. The deformed shape in Fig. 5.37 shows that the opening of the guard cell in the absence of the plates is similar to the case with elliptic plates (Fig. 5.32). Therefore, the opening of the guard cell seems not to be affected significantly by the existence of the elliptic plates. This agrees with an experimental observation (Sack, 1982).

(a)

(b)

Fig. 5.31 Computer-generated perspective views of a guard cell
(a) seen from outside   (b) seen from inside
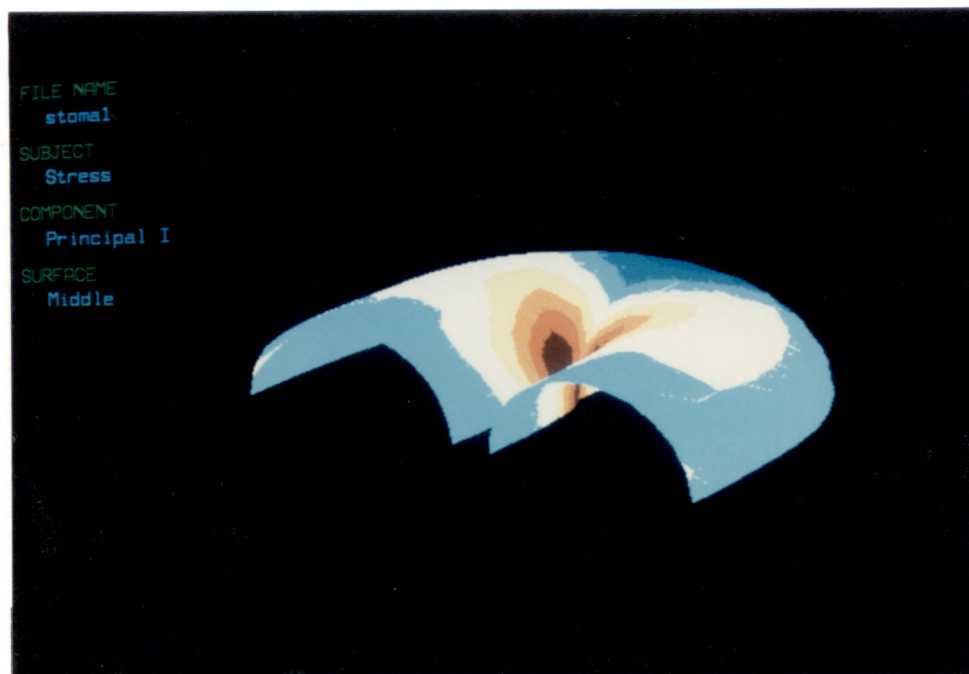
Fig. 5.32 Deformed shape (opening) of a guard cell

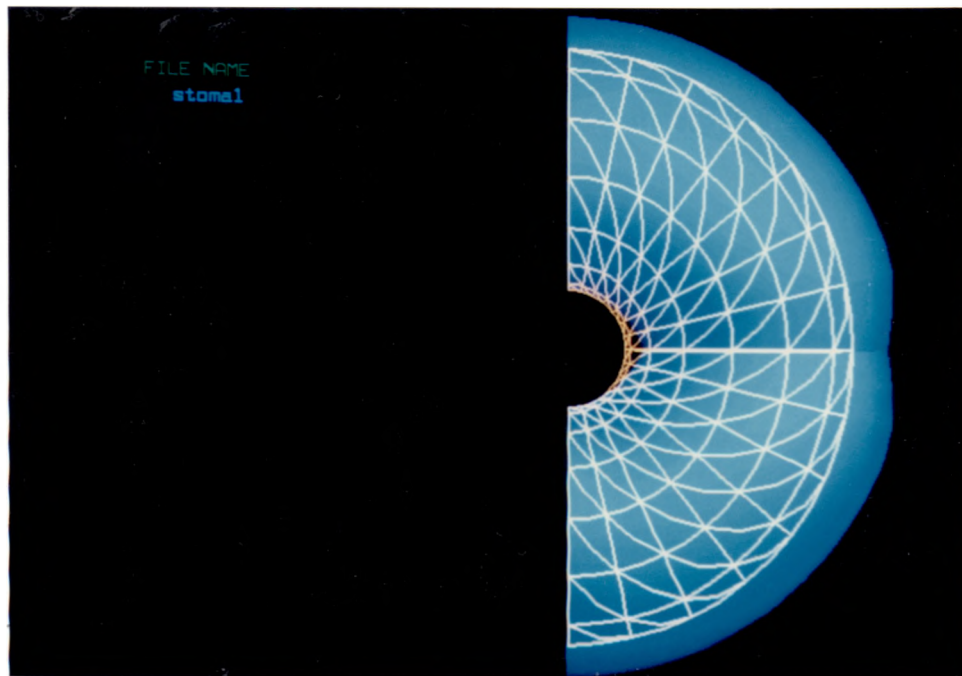Fig. 5.33 Major principal stresses in the middle surface

Fig. 5.34 Deformed shape of a circular torus with circular cross section and circular plates — overlaid with the undeformed mesh
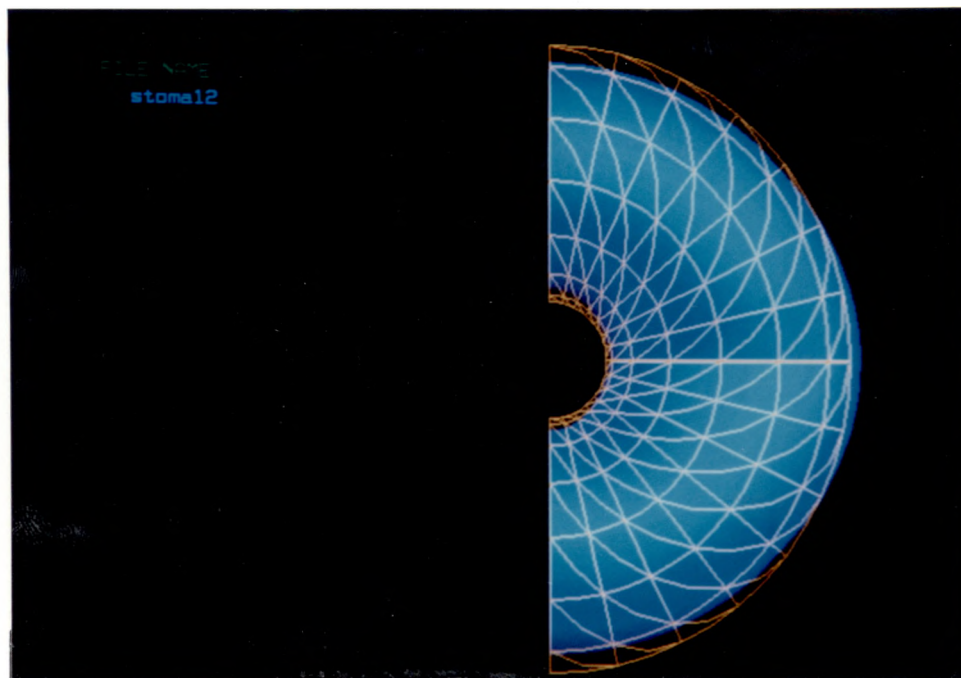

Fig. 5.35 Deformed shape of a circular torus with elliptical cross section — overlaid with the undeformed mesh
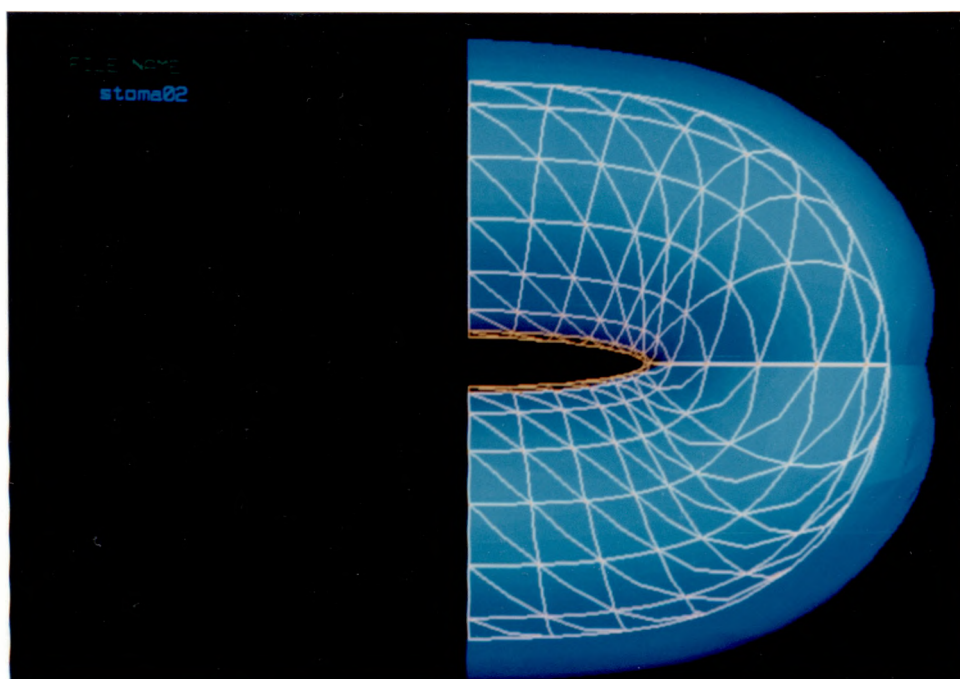
Fig. 5.36 Deformed shape of an elliptical torus with circular cross section
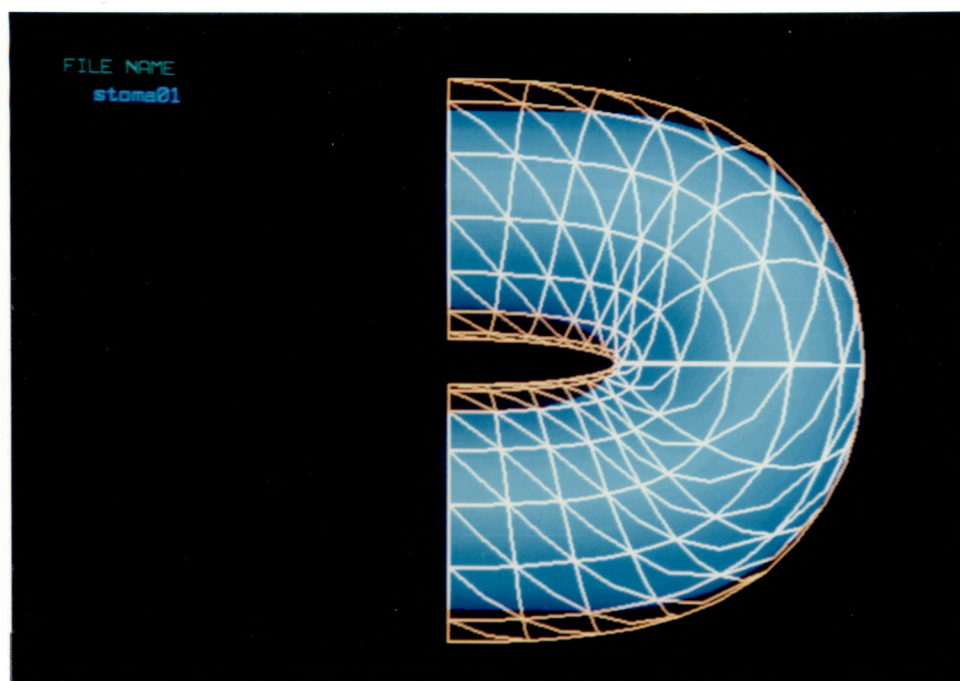– overlaid with the undeformed mesh

Fig. 5.37 Deformed shape of an elliptical torus with elliptical cross section
but without elliptic plate – overlaid with the undeformed mesh

Chapter 6

CONCLUSIONS

This study has integrated three different phases of finite element analysis, i.e., formulation, implementation, and application. The first part may be regarded as one of the numerous efforts to develop a reliable tool for thin and thick shell analysis. Not only the satisfactory performance achieved by the new formulation but also the methodology provided for a simple, systematic, and generalized formulation are the fruitful outcomes of this study. Another significance of the study can be found in its elaboration to bridge the analytical study and the practical application to biological problems.

6.1 Summary

Finite element analysis of shells

Many shell elements have been developed and are being used. Each element has its own advantages and disadvantages, but, none of them has appeared to become the uniquely best element. There have been ceaseless efforts to obtain an element applicable to both thin and thick shells. Ahmad's degenerate shell element is one of the most successful elements in this sense. The element, which was originally designed for thick shell applications, happened to become applicable to thin shells as well, using the reduced integration technique. Another advantage which was found later (Barsoum, 1976) is its capability of representing the stress singularity at a crack tip by use of quarter point nodes. Unfortunately, however, the element performs poorly when the shape of the element is triangular. As revealed by the numerical

188

study in Chapter 4, the element even with quadrilateral shape shows locking behavior for a certain type of problems.

To overcome these discouraging features of the degenerate shell element, a new finite element has been formulated as described in Chapter 2. A new method of element decomposition has been introduced as a basis of the formulation. A novel method of coordinate transformation has also been suggested. The formulation is based on five d.o.f. at each node, but the element shape or number of nodes per element may be varied in the formulation in order to achieve greater generality.

The displacement model is constructed by decomposing the actual element into translational and difference elements. The displacement field of each component element is expressed in a generalized format using a displacement function matrix. Differentiation of the displacement function matrix directly leads to the strain-displacement matrices. The element stiffness matrix is obtained by simple manipulation of these strain-displacement matrices.

There are many possible ways to decompose the elements. But only three different possibilities are discussed and put into practice in this study. As a result, three different elements, designated as type I, type II and type III elements, are obtained. Each of the three types has slight differences from the other in the derivation of the element stiffness matrix. However, the final forms of the displacement model, the strain-displacement relationship and the stiffness matrix are common to all three types of elements. The merit of the new formulation can be seen also from its simplicity and systematic methodology demonstrated in the derivation of the stiffness matrices.

Three different complementary devices, namely reduced integration, addition of internal d.o.f., and mixed formulation, are applied to the present

formulation in order to remove the locking phenomena encountered in sensitive problems. Four different combinations of the internal d.o.f. at the center of the element have been considered: three translations, IDOF(A); two rotations, IDOF(b); all the five d.o.f., IDOF(C); and two translations and two rotations, IDOF(D).

The mixed formulations based on Hellinger-Reissner principle and modified Hellinger-Reissner principle are also considered as a modification to the present formulation.

Combination of internal d.o.f. or mixed formulation with reduced integration can remove the locking phenomena successfully. However, an element with this combination of complementary devices may suffer from spurious zero energy mode. Two different methods of controlling the troublesome zero energy modes have been investigated in association of the present study: an α–control scheme and an e–control scheme.

The implementation of the finite element and other attendant computational procedures have been discussed in Chapter 3. Many operations involved in the element formulation are expressed so as to attain notational simplification as much as possible. Those operations can be economized by taking advantage of their characteristics. These practical aspects of implementation are not fully detailed in this chapter. However, they should be taken care of in an actual implementation.

Comprehensive numerical studies are also presented to validate the formulations and to examine their convergence behavior.

Application to biological objects

The new shell elements have been used in stress analysis of eggshell and for elastic modelling of stomatal opening. The stresses developed in an

eggshell under three different loading conditions are computed and graphically represented. The effects of egg shape and loading conditions on eggshell breakage are also examined on the basis of stress analysis. Consequently, the appropriateness of the widely used strength measuring techniques is evaluated.

Four different configurations of tori are analyzed to decide the effects of stomatal geomtry on its opening and closure mechanism. The effect of elliptic plate on the stomatal opening is also examined.

6.2   Conclusions

Finite element analysis of shells

The type I element gives slightly faster convergence than the other two, but converges to a value somewhat larger than the exact solution for certain types of problems. It may be due to the fact that the type I element does not satisfy the C^1 interelement continuity even though the element is based on the Kirchhoff assumptions for both the translation and the difference element. The type II and type III elements give almost equivalent convergence behavior. However, the type II element requires a more arduous derivation and computational procedure. Thus, the type III element is the best among the elements formulated in the present study. Especially the element of quadrilateral shape gives satisfactory convergence for both thick and thin shells. Numerical studies with various test problems reveals that the type III element performs better than the widely used degenerate shell element. Yet the element has all the advantageous features of the degenerate shell element.

However, the convergence of the type III triangular element is quite slow under the thin shell situations. This can be improved by complementary

devices together with zero energy control schemes. Not only the transverse locking but also the membrane locking are significant. Thus, the selective reduced integration cannot cure the locking phenomena completely. Furthermore, geometric isotropy is violated when the selective reduced integration is applied. On the other hand, the uniform reduced integration does violate the geometric isotropy, and improves drastically the convergence of the quadrilateral element. The performance of the quadrilateral element with reduced integration is satisfactory for all the test problems, but the reduced integration is not effective enough for triangular element. The convergence of the triangular element even with reduced integration is unacceptably slow for extremely thin shell cases with strong coupling of bending and membrane actions. The other two complementary devices are intended mainly for the triangular element.

Substantial improvement is achieved by adding the internal d.o.f. However, IDOF(B) cannot remove the locking phenomena sufficiently for certain problems. IDOF(C) produces fastest covergence. However, the solutions obtained with IDOF(C) and IDOF(D) converge to a value somewhat larger than the exact ones for some cases. Local oscillation is also observed in the computed displacements with IDOF(C). IDOF(D) gives almost identical convergence rate as that of IDOF(A). But this involves more rigorous computational procedure than IDOF(A), because two translational d.o.f. are expressed in local coordinates. IDOF(A) gives satisfactory convergence and accuracy for most of the test problems. Slight local oscillation of normal displacements appears for uniform pressure case. However, this vanishes as the mesh is refined. Therefore, IDOF(A) seems to be most favorable among the four schemes. But IDOF(A) suffers from spurious zero energy modes in the case of minimum boundary constraints such as the four-corner-supported plate.

This is not a case frequently encountered in practical problems; however, the trouble should be treated from the viewpoint of the generality of the element.

The two zero energy control schemes, considered in the present study, give almost equivalent effects. The difficulty with these schemes is that the scheme may induce the locking phenomenon when a large value of control index is applied. Therefore, an appropriate control index should be applied in order to avoid the locking as well as spurious modes. This is a subject which requires further studies.

In terms of convergence rate, there are no significant differences between the full order and the reduced order integrations for the mixed formulations. The combination of internal d.o.f. with the mixed formulation removes the locking phenomenon satisfactorily. The mixed formulation stabilizes the local oscillation of the normal displacement which is observed in the displacement formulation with IDOF(A) or IDOF(C).

Application to biological objects

The stresses under the flat plate loading depend much on the contact area; therefore, the strength measured by flat plate loading may be influenced by the contact area which is less predictable. The uniform pressure types of measurement may be more reliable if one can apply the uniform pressure accurately, because the stresses under uniform pressure can easily be predicted and do not depend on such an uncertain factor as the contact area in the flat plate loading case.

The opening of stomatal guard cell is largely influenced by its geomtry. An elliptical torus with elliptical cross section is an essential configuration for proper stomatal opening. The existence of the elliptic plate, the radial stiffening or the differential wall thickening is not required for opening of gaurd cell.

6.3   Suggestions for further study

The formulation of shell elements in this study is intended to provide a more generalized finite element applicable to both thick and thin shells. Although the newly formulated element provides satisfactory results in comparison with the currently available degenerate shell element, it is not yet ideal. There is room for improvement or extension of the present formulation. Especially the following subjects related to this study are suggested for further study.

Completion of the type I element

It has been observed in Chapter 4 that the type I element converges to a value a bit larger than the exact solution, although this gives somewhat faster convergence than the other type elements. It may be because the element does not satisfy C^1 interelement continuity in a strict sense, although the element is based on Kirchhoff assumptions. The C^1 continuity will be satisfied if the generalized coordinate, **a** in Eqn. (2.3.27) is expressed in terms of θ^{de}, in lieu of $\underline{\theta}^{de}$. That is

$$\mathbf{a} = \mathbf{G'}\,\theta^{de} \tag{6.2.1}$$

in which **G'** is equivalent to **G** in Eqn. (2.3.27). Evaluation of **G'** will require more complicated manipulation than that of **G**. However, by use of Eqn. (6.2.1), C^1 interelement continuity will be assured, and convergence to the correct solution is expected.

Control of spurious modes

Although various methods of controlling spurious modes have been mentioned in Chapter 2, only two schemes, i.e., $\alpha-$ and e-control; are discussed in detail and examined numerically in Chapter 4. It is discouraging

that both schemes depend on an artificial number, the control index. Other control methods, e.g., consistent spurious control method (Belytschko and Liu, 1984), may provide more thorough solutions. Therefore, it is suggested to investigate the possibilities of applying other control schemes to the present formulation.

Six d.o.f. per node element

The present formulation employs five d.o.f. per node. The in–plane rotation is not included as a nodal d.o.f. Shell elements missing this d.o.f. usually perform poorly for torsional effects. This may be the reason why the element formulated in this study shows relatively poor convergence behavior for the truncated half sphere case in Chapter 4. The in–plane rotation can be included in the formulation by a slight modification. This sixth d.o.f. can also be decomposed into the translational element and the difference element. For example, the in–plane rotation of translational element can be defined by the in–plane rigid body rotation.

$$\gamma^t = (u,_y - v,_x) \,/\, 2 \tag{6.2.2}$$

in which γ denotes the in–plane rotation. The stiffness is assigned directly to this in–plane rotation. Therefore, the meaning of this additional d.o.f. is different from that of the other six d.o.f. degenerate element (Kanok-Nukulchai, 1979) in which the three rotations are eventually transformed into two in local coordinates.

Investigation of stress singularity for fracture analysis

As already mentioned in Chapter 5, the type III element is expected to have the capability of representing stress singularity by placing the midside node at the quarter point, but this has not been proved either mathematically or

numerically. It is doubtful whether the element will have the same capability when complementary devices and zero energy control schemes are applied. This should be investigated for future fracture analysis using the element with or without complementary devices.

Application to biological objects

The eggshell breakage has been studied mainly on the basis of the stress and strength concept. It is suggested to study eggshell breakage from fracture mechanics view points as well. In the simplified fracture analysis, presented as an application example in this study, the bending behavior has been neglected. This type of analysis is not valid for the flat plate loading cases, because the bending action is the major driving force for crack propagation. Therefore, the contribution of the bending behavior should be included in the computation of the stress intensity factor. Evaluation of the stress intensity factor, using the finite element developed in the present formulation, is another subject for further study.

Appendix A

DERIVATION OF BENDING STRAIN-DISPLACEMENT MATRIX

In Chapter 2, the bending strain-displacement matrix $\mathbf{B}^b$ of Eqn. (2.4.19) is derived from Eqn. (2.4.18). The matrix $\mathbf{Q}$ in the right hand side of Eqn.(2.4.18) is constant. Thus, the differentiation of the last term in the equation can be done as follows:

$$\frac{\partial}{\partial x}(\mathbf{J}^{-1}\mathbf{N}) = (\frac{\partial \mathbf{J}^{-1}}{\partial x})\mathbf{N} + \mathbf{J}^{-1}\frac{\partial \mathbf{N}}{\partial x} \tag{A.1.1}$$

$$\frac{\partial}{\partial y}(\mathbf{J}^{-1}\mathbf{N}) = (\frac{\partial \mathbf{J}^{-1}}{\partial y})\mathbf{N} + \mathbf{J}^{-1}\frac{\partial \mathbf{N}}{\partial y} \tag{A.1.2}$$

The first terms in the right hand side of Eqns.(A.1.1) and (A.1.2) are

$$(\frac{\partial \mathbf{J}^{-1}}{\partial x})\mathbf{N} = \begin{bmatrix} \xi_{,xx} & \eta_{,xx} \\ \xi_{,xy} & \eta_{,xy} \end{bmatrix} \begin{bmatrix} N_1 & 0 & N_2 & 0 & \cdots & N_n & 0 \\ 0 & N_1 & 0 & N_2 & \cdots & 0 & N_n \end{bmatrix} \tag{A.1.3}$$

$$(\frac{\partial \mathbf{J}^{-1}}{\partial y})\mathbf{N} = \begin{bmatrix} \xi_{,xy} & \eta_{,xy} \\ \xi_{,yy} & \eta_{,yy} \end{bmatrix} \begin{bmatrix} N_1 & 0 & N_2 & 0 & \cdots & N_n & 0 \\ 0 & N_1 & 0 & N_2 & \cdots & 0 & N_n \end{bmatrix} \tag{A.1.4}$$

And the second terms are

$$\mathbf{J}^{-1}\frac{\partial \mathbf{N}}{\partial x} = \begin{bmatrix} \xi_{,x} & \eta_{,x} \\ \xi_{,y} & \eta_{,y} \end{bmatrix} \begin{bmatrix} N_{1,x} & 0 & N_{2,x} & 0 & \cdots & N_{n,x} & 0 \\ 0 & N_{1,x} & 0 & N_{2,x} & \cdots & 0 & N_{n,x} \end{bmatrix} \tag{A.1.5}$$

$$\mathbf{J}^{-1}\frac{\partial \mathbf{N}}{\partial y} = \begin{bmatrix} \xi_{,x} & \eta_{,x} \\ \xi_{,y} & \eta_{,y} \end{bmatrix} \begin{bmatrix} N_{1,y} & 0 & N_{2,y} & 0 & \cdots & N_{n,y} & 0 \\ 0 & N_{1,y} & 0 & N_{2,y} & \cdots & 0 & N_{n,y} \end{bmatrix} \tag{A.1.6}$$

Combining Eqns. (A.1.1) and (A.1.2), one obtains

$$
\begin{bmatrix} \dfrac{\partial}{\partial x}(\mathbf{J}^{-1}\mathbf{N}) \\[2mm] \dfrac{\partial}{\partial y}(\mathbf{J}^{-1}\mathbf{N}) \end{bmatrix}
=
\begin{bmatrix}
\xi_{,xx} & \eta_{,xx} & \xi_{,x} & \eta_{,x} & 0 & 0 \\
\xi_{,xy} & \eta_{,xy} & \xi_{,y} & \eta_{,y} & 0 & 0 \\
\xi_{,xy} & \eta_{,xy} & 0 & 0 & \xi_{,x} & \eta_{,x} \\
\xi_{,xy} & \eta_{,xy} & 0 & 0 & \xi_{,y} & \eta_{,y}
\end{bmatrix}
\begin{bmatrix}
N_1 & 0 & N_2 & 0 & \cdots & N_n & 0 \\
0 & N_1 & 0 & N_2 & \cdots & 0 & N_n \\
N_{1,x} & 0 & N_{2,x} & 0 & \cdots & N_{n,x} & 0 \\
0 & N_{1,x} & 0 & N_{2,x} & \cdots & 0 & N_{n,x} \\
N_{1,y} & 0 & N_{2,y} & 0 & \cdots & N_{n,y} & 0 \\
0 & N_{1,y} & 0 & N_{2,y} & \cdots & 0 & N_{n,y}
\end{bmatrix}
$$

$$\text{(A.1.7)}$$

Rearranging Eqn. (A.1.7), one arrives

$$
\begin{bmatrix}
\partial/\partial x & 0 \\
0 & \partial/\partial y \\
\partial/\partial y & \partial/\partial x
\end{bmatrix}
(\mathbf{J}^{-1}\mathbf{N})
\tag{A.1.8}
$$

$$
=
\begin{bmatrix}
\xi_{,xx} & \eta_{,xx} & \xi_{,x} & 0 & \eta_{,x} & 0 \\
\xi_{,yy} & \eta_{,yy} & 0 & \xi_{,y} & 0 & \eta_{,y} \\
2\xi_{,xy} & 2\eta_{,xy} & \xi_{,y} & \xi_{,x} & \eta_{,y} & \eta_{,x}
\end{bmatrix}
\begin{bmatrix}
N_1 & 0 & N_2 & 0 & \cdots & N_n & 0 \\
0 & N_1 & 0 & N_2 & \cdots & 0 & N_n \\
N_{1,x} & 0 & N_{2,x} & 0 & \cdots & N_{n,x} & 0 \\
N_{1,y} & 0 & N_{2,y} & 0 & \cdots & N_{n,y} & 0 \\
0 & N_{1,x} & 0 & N_{2,x} & \cdots & 0 & N_{n,x} \\
0 & N_{1,y} & 0 & N_{2,y} & \cdots & 0 & N_{n,y}
\end{bmatrix}
$$

Denote

$$
\mathbf{N}' =
\begin{bmatrix}
N_1 & 0 & N_2 & 0 & \cdots & N_n & 0 \\
0 & N_1 & 0 & N_2 & \cdots & 0 & N_n \\
N_{1,x} & 0 & N_{2,x} & 0 & \cdots & N_{n,x} & 0 \\
N_{1,y} & 0 & N_{2,y} & 0 & \cdots & N_{n,y} & 0 \\
0 & N_{1,x} & 0 & N_{2,x} & \cdots & 0 & N_{n,x} \\
0 & N_{1,y} & 0 & N_{2,y} & \cdots & 0 & N_{n,y}
\end{bmatrix}
\tag{A.1.9}
$$

and

$$\underline{\mathbf{N}}' = \begin{bmatrix} N_1 & 0 & N_2 & 0 & \cdots & N_n & 0 \\ 0 & N_1 & 0 & N_2 & \cdots & 0 & N_n \\ N_{1,\xi} & 0 & N_{2,\xi} & 0 & \cdots & N_{n,\xi} & 0 \\ N_{1,\eta} & 0 & N_{2,\eta} & 0 & \cdots & N_{n,\eta} & 0 \\ 0 & N_{1,\xi} & 0 & N_{2,\xi} & \cdots & 0 & N_{n,\xi} \\ 0 & N_{1,\eta} & 0 & N_{2,\eta} & \cdots & 0 & N_{n,\eta} \end{bmatrix} \qquad (A.1.10)$$

Then, $\underline{\mathbf{N}}'$ and $\mathbf{N}'$ have the following relation:

$$\underline{\mathbf{N}}' = \begin{bmatrix} 1 & 0 & 0 & 0 & 0 & 0 \\ 0 & 1 & 0 & 0 & 0 & 0 \\ 0 & 0 & \xi_{,x} & \eta_{,x} & 0 & 0 \\ 0 & 0 & \xi_{,y} & \eta_{,y} & 0 & 0 \\ 0 & 0 & 0 & 0 & \xi_{,x} & \eta_{,x} \\ 0 & 0 & 0 & 0 & \xi_{,y} & \eta_{,y} \end{bmatrix} \mathbf{N}' \qquad (A.1.11)$$

If one defines

$$\mathbf{N}^* = \begin{bmatrix} N_1 & 0 & N_2 & 0 & \cdots & N_n & 0 \\ 0 & N_1 & 0 & N_2 & \cdots & 0 & N_n \\ N_{1,\xi} & 0 & N_{2,\xi} & 0 & \cdots & N_{n,\xi} & 0 \\ 0 & N_{1,\eta} & 0 & N_{2,\eta} & \cdots & 0 & N_{n,\eta} \\ \tfrac{1}{2}N_{1,\eta} & \tfrac{1}{2}N_{1,\xi} & \tfrac{1}{2}N_{2,\eta} & \tfrac{1}{2}N_{2,\xi} & \cdots & \tfrac{1}{2}N_{n,\eta} & \tfrac{1}{2}N_{n,\xi} \end{bmatrix} \qquad (A.1.12)$$

then, Eqn. (A.1.8) can be simplified as

$$\begin{bmatrix} \partial/\partial x & 0 \\ 0 & \partial/\partial y \\ \partial/\partial y & \partial/\partial x \end{bmatrix} (\mathbf{J}^{-1}\mathbf{N}) = \begin{bmatrix} \xi_{,xx} & \eta_{,xx} & (\xi_{,x})^2 & (\eta_{,x})^2 & 2\xi_{,x}\eta_{,x} \\ \xi_{,yy} & \eta_{,yy} & (\xi_{,y})^2 & (\eta_{,y})^2 & 2\xi_{,y}\eta_{,y} \\ 2\xi_{,xy} & 2\eta_{,xy} & 2\xi_{,y}\xi_{,x} & 2\eta_{,y}\eta_{,x} & 2(\xi_{,y}\xi_{,x}+\eta_{,y}\eta_{,x}) \end{bmatrix} \mathbf{N}^* = \mathbf{S}^*\mathbf{N}^*$$

$$(A.1.13)$$

in which $\mathbf{S}^*$ is defined in Eqn. (2.1.14). The first term of Eqn. (2.4.18) is obtained using the relation in Eqn. (2.1.15) as follows:

$$\begin{bmatrix} \partial/\partial x & 0 \\ 0 & \partial/\partial y \\ \partial/\partial y & \partial/\partial x \end{bmatrix} \mathbf{L_3}' = \begin{bmatrix} \partial/\partial x & 0 \\ 0 & \partial/\partial y \\ \partial/\partial y & \partial/\partial x \end{bmatrix} \begin{Bmatrix} \partial/\partial x \\ \partial/\partial y \end{Bmatrix} \mathbf{L_3} = \nabla^*_x (\mathbf{L_3}) = \mathbf{S}^*\underline{\mathbf{L}}_3'' \quad \text{(A.1.14)}$$

in which $\mathbf{L_3}$, $\mathbf{L_3}'$ and $\underline{\mathbf{L}}_3''$ are defined in Eqns. (2.3.4), (2.3.6) and (2.4.14) respectively. Now, the bending-strain displacement matrix $\mathbf{B}^b$ can be obtained by combining Eqns (A.1.13) and (A.1.14).

$$\mathbf{B}^b = \begin{bmatrix} \partial/\partial x & 0 \\ 0 & \partial/\partial y \\ \partial/\partial y & \partial/\partial x \end{bmatrix} (\mathbf{L_3}' + \mathbf{J}^{-1}\mathbf{N}\,\mathbf{Q}) = \mathbf{S}^* (\underline{\mathbf{L}}_3'' + \mathbf{N}^*\mathbf{Q}) \quad \text{(A.1.15)}$$

Appendix B

RESULTS OF CONVERGENCE TESTS
AND OTHER NUMERICAL TESTS
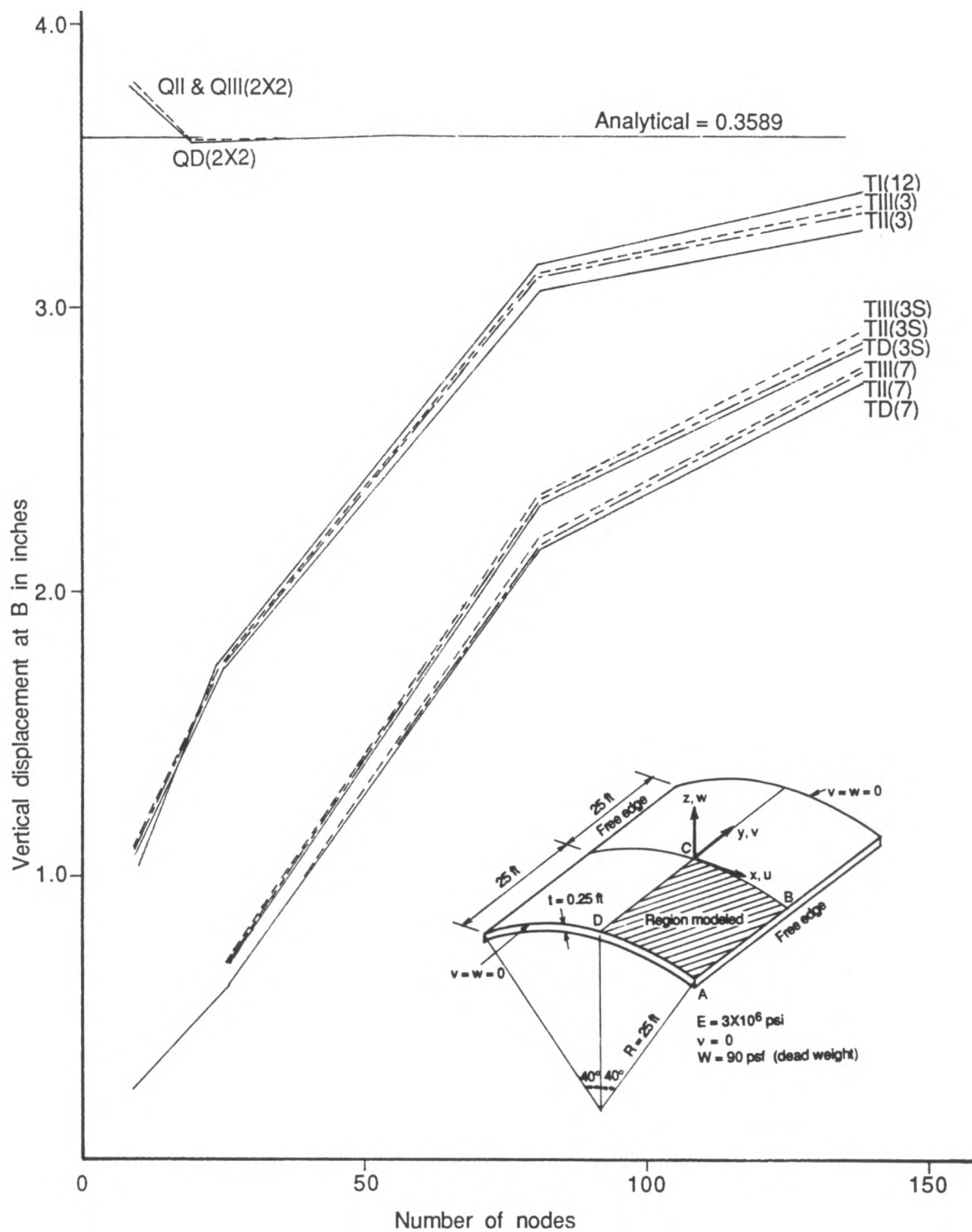
Fig. B.1   Comparison of the new formulation with the degenerate shell element
Cylindrical shell roof–vertical displacement at B
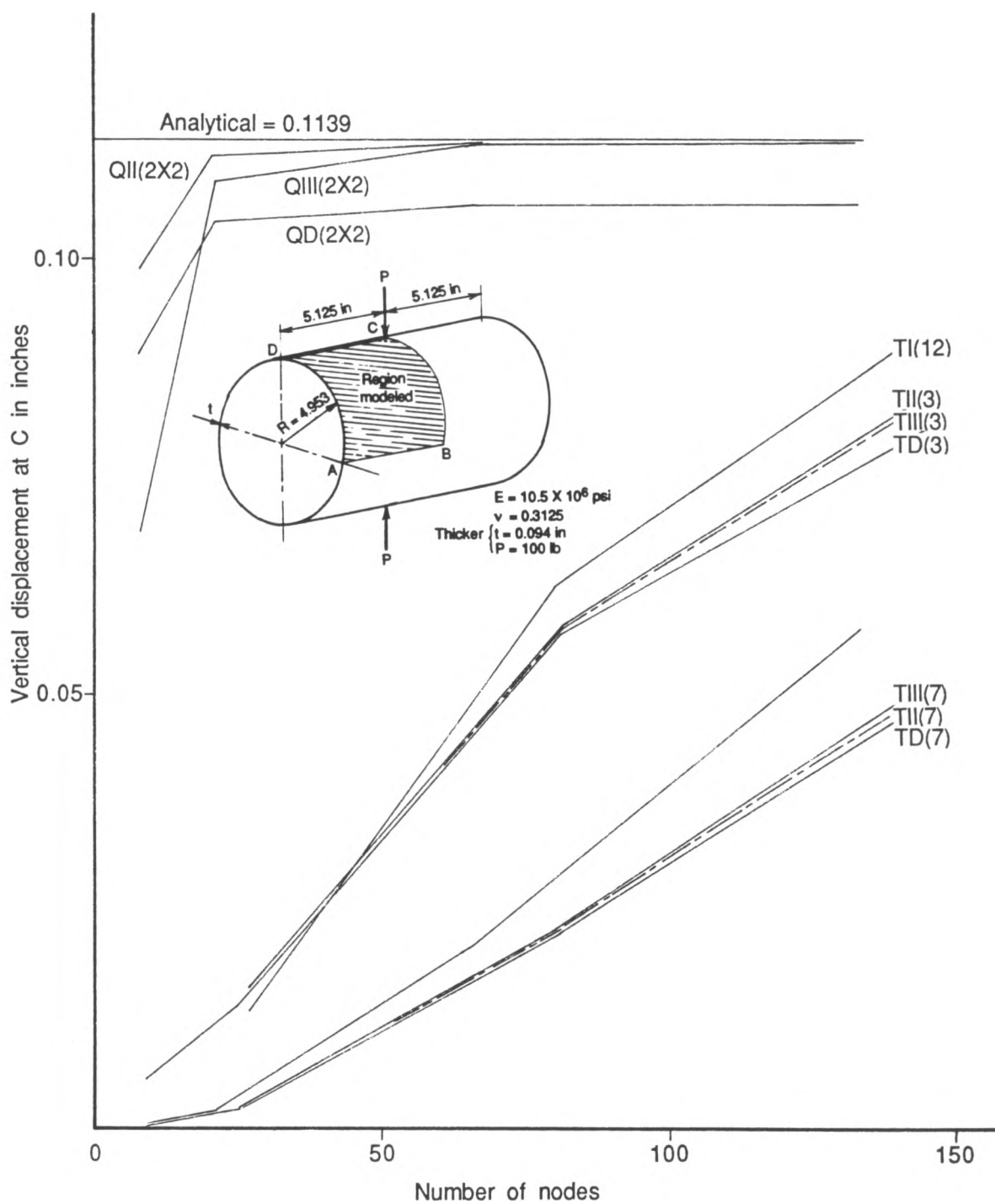
Fig. B.2   Comparison of the new formulation with the degenerate shell element
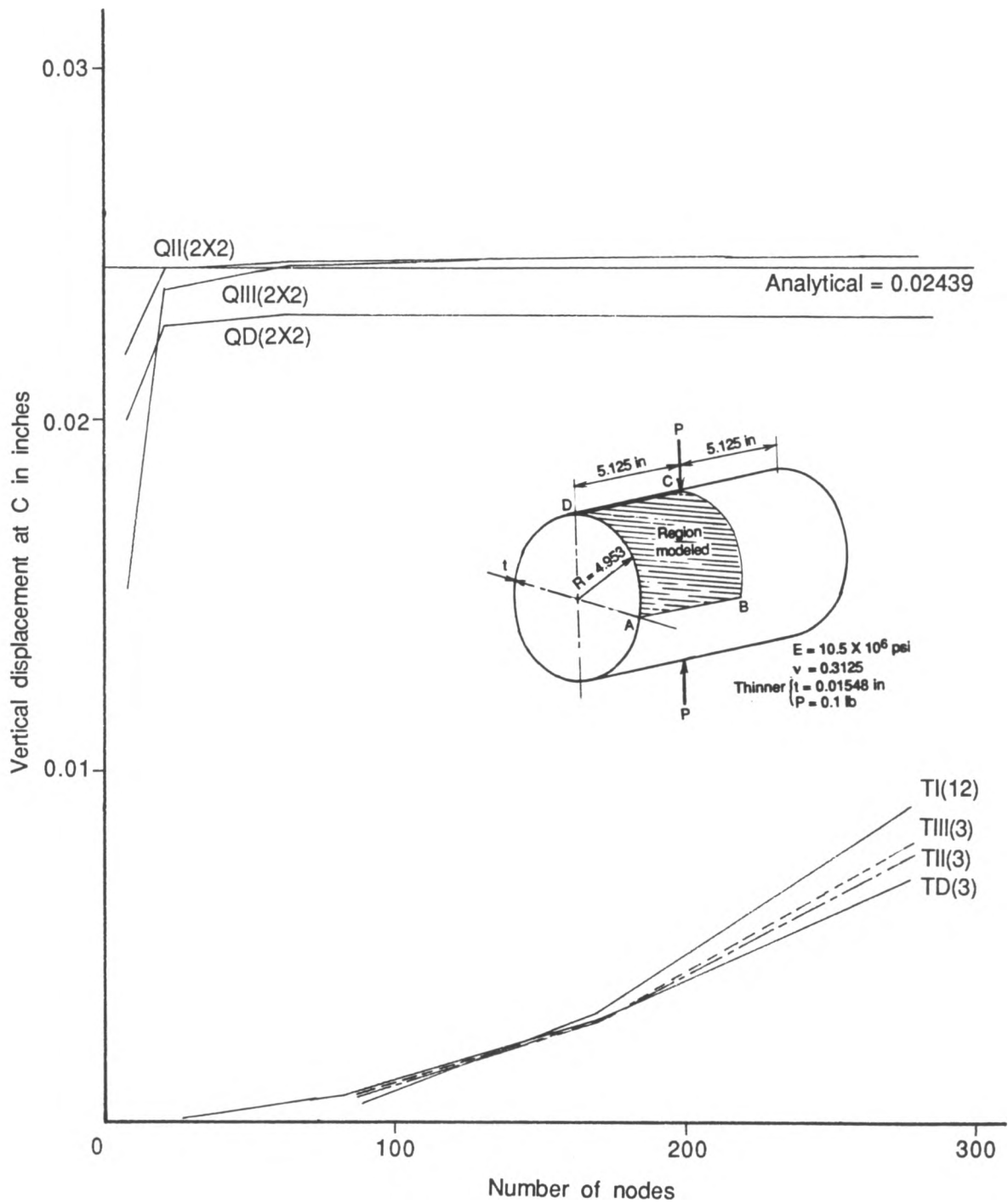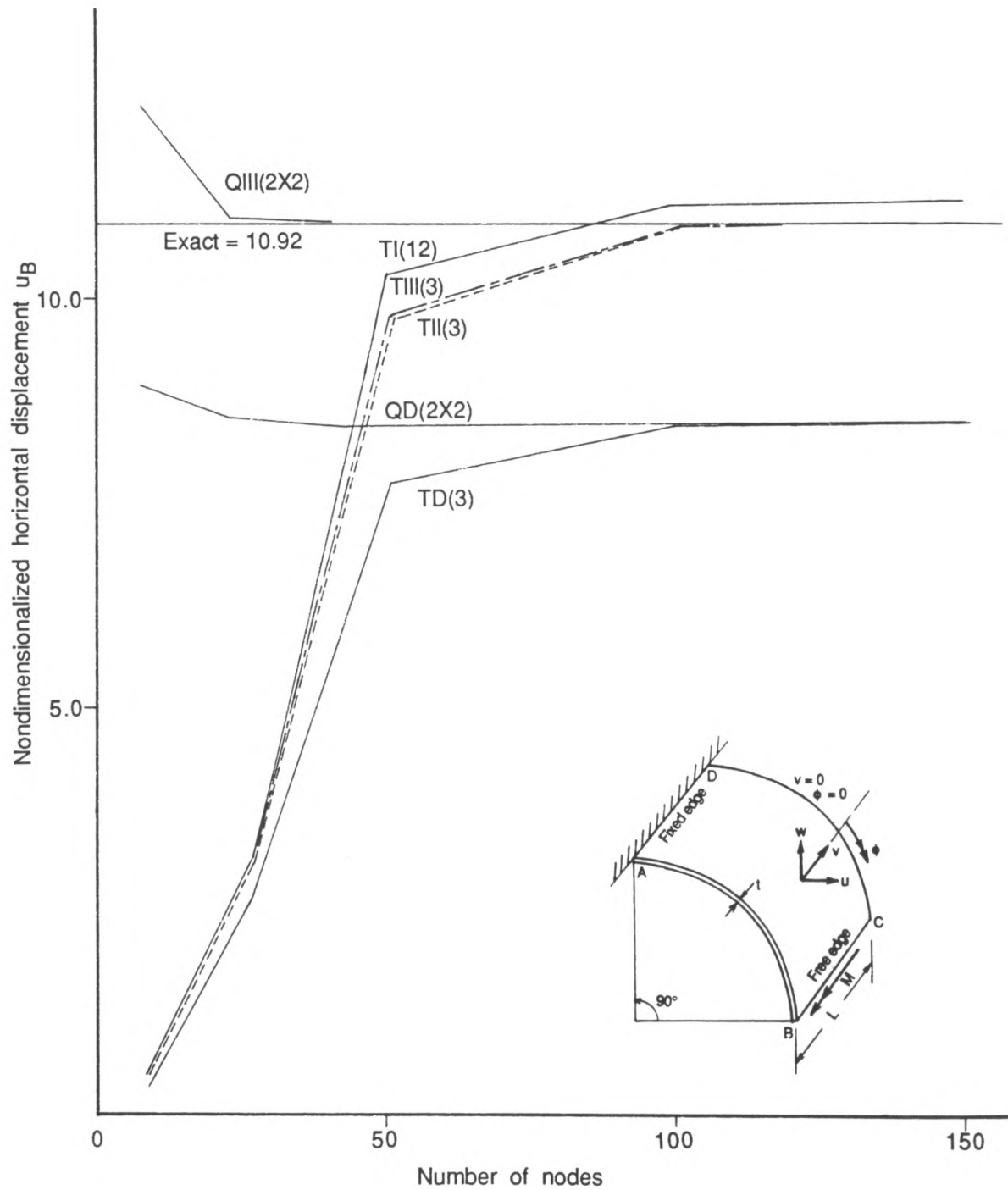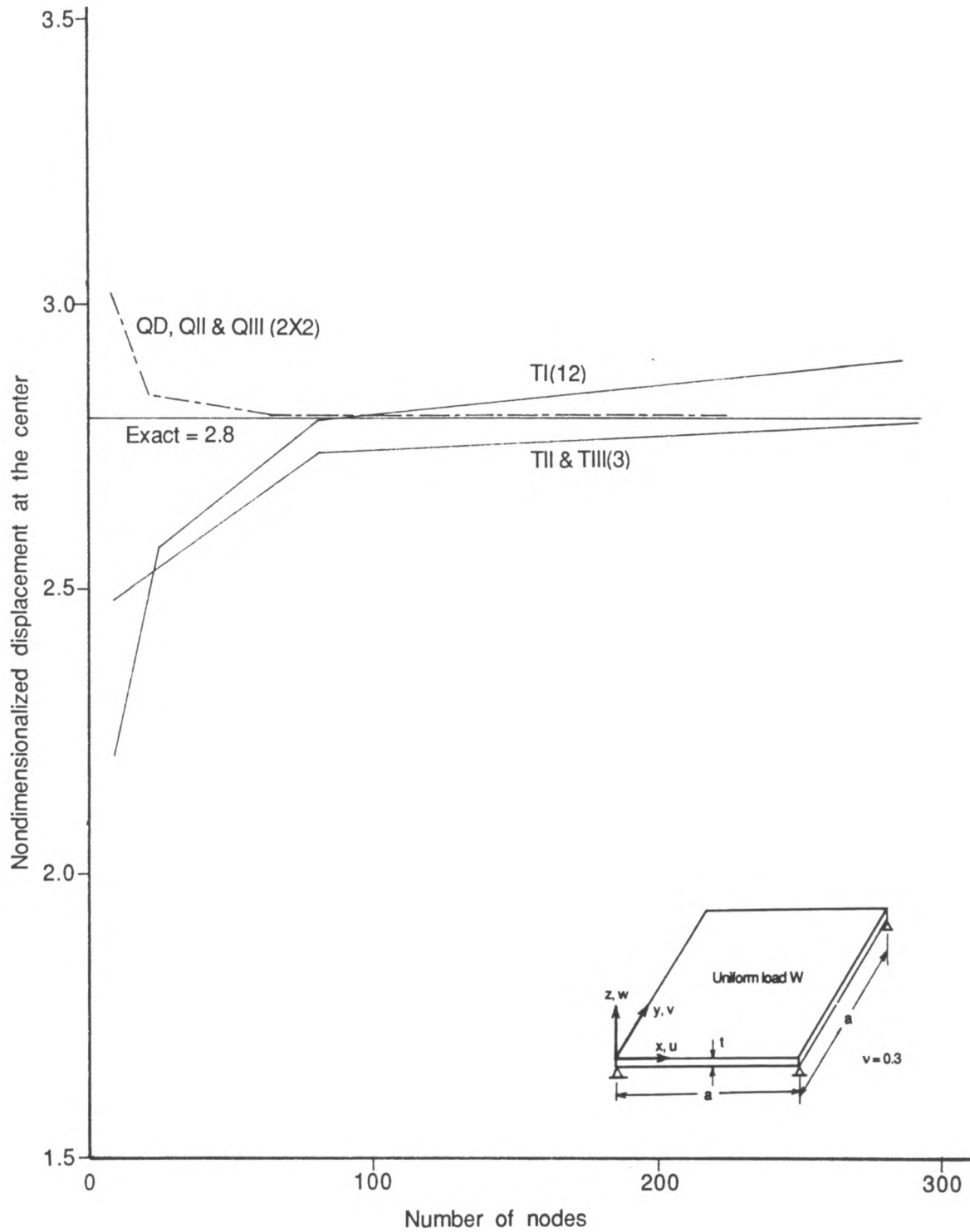Pinched cylinder (thick)–vertical displacement at C

Fig. B.3 Comparison of the new formulation with the degenerate shell element
Pinched cylinder (thin)–vertical displacement at C

Fig. B.4   Comparison of the new formulation with the degenerate shell element
Fixed-free quarter cylinder–horizontal displacement at C

Fig. B.5   Comparison of the new formulation with the degenerate shell element
Four-corner-supported plate—deflection at the center
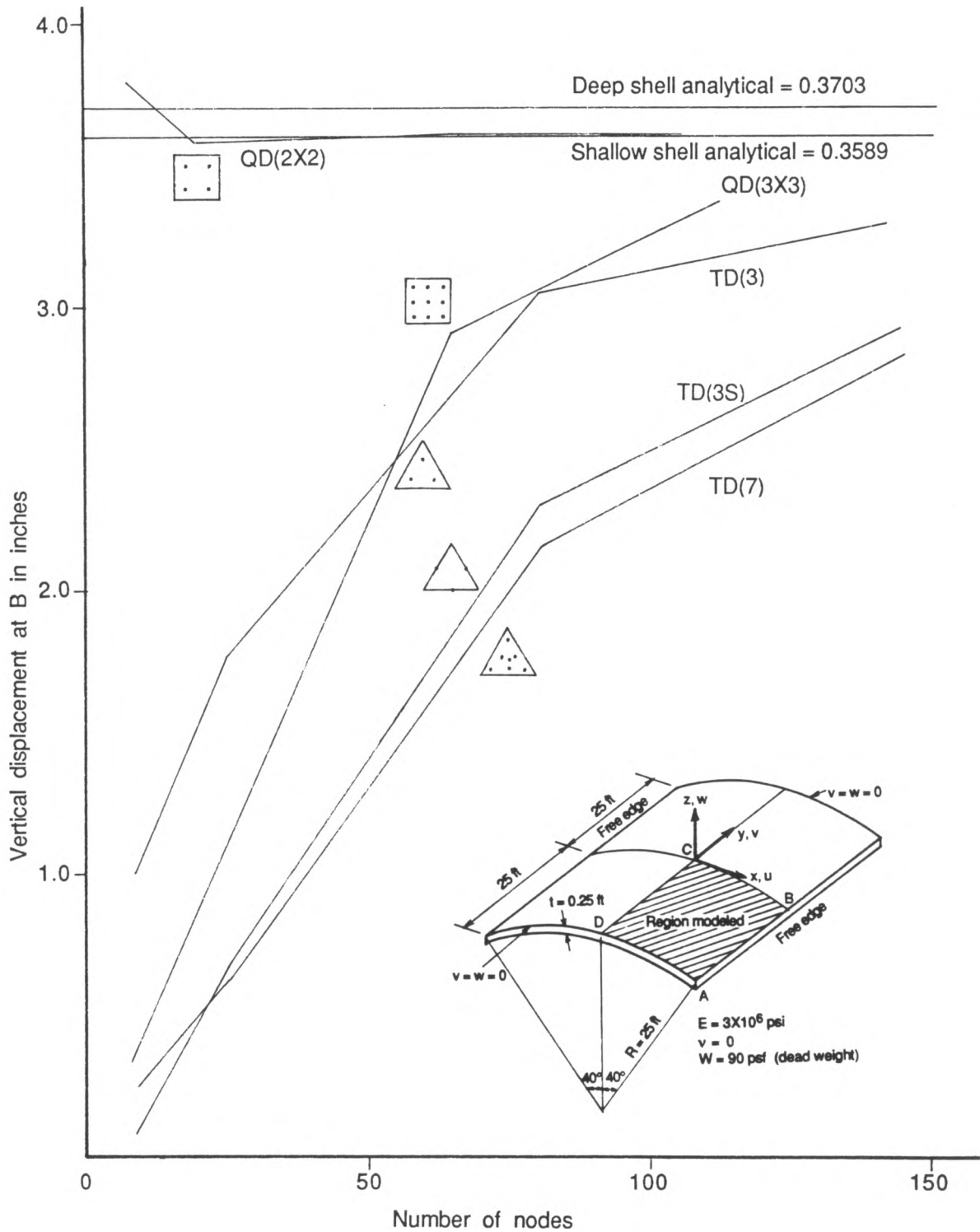
Fig. B.6   Convergence of the degenerate shell element
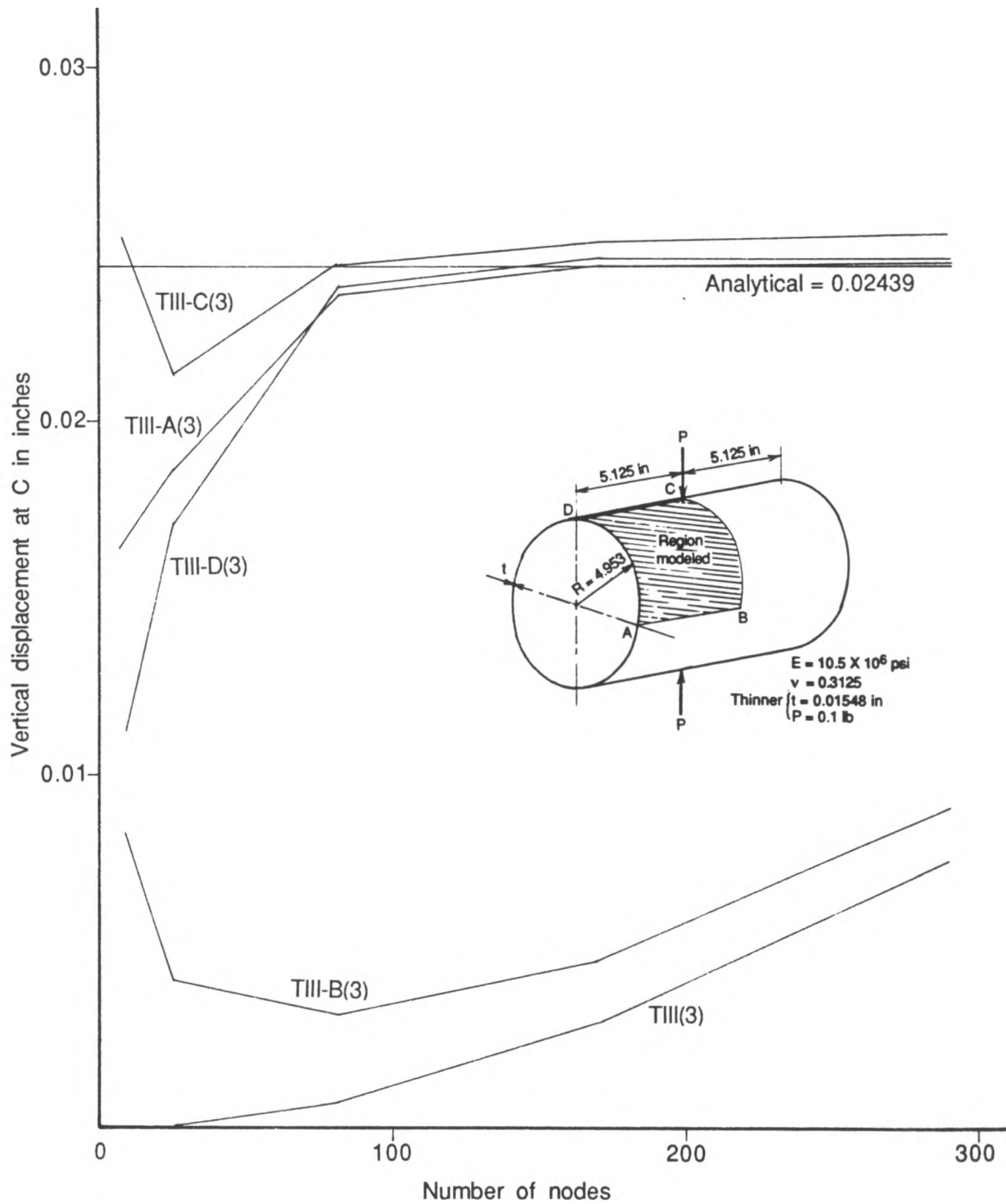Cylindrical shell roof–vertical displacement at B
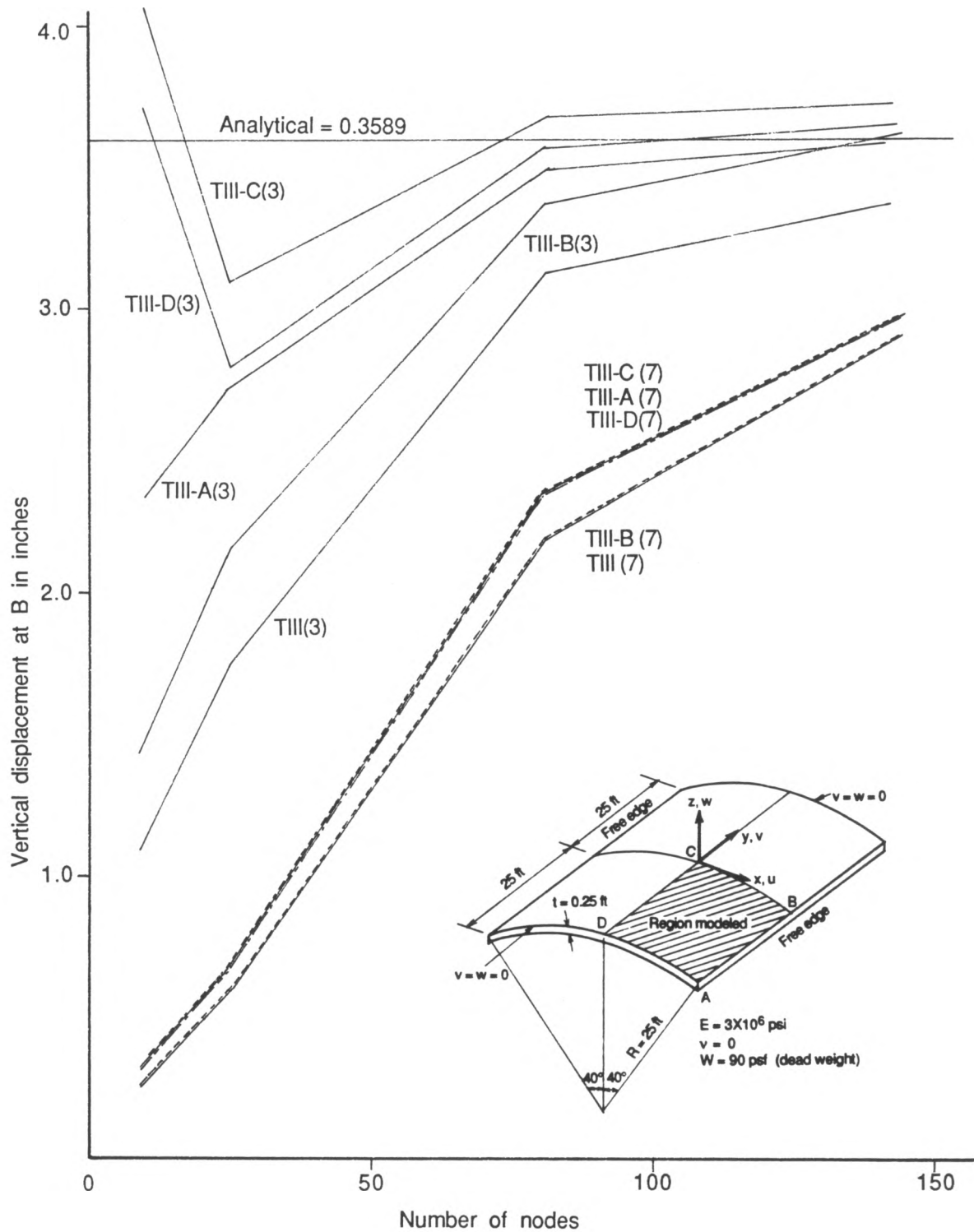
Fig. B.7 Convergence of the type III element
Triangular element with or without internal d.o.f.
Cylindrical shell roof–vertical displacement at B
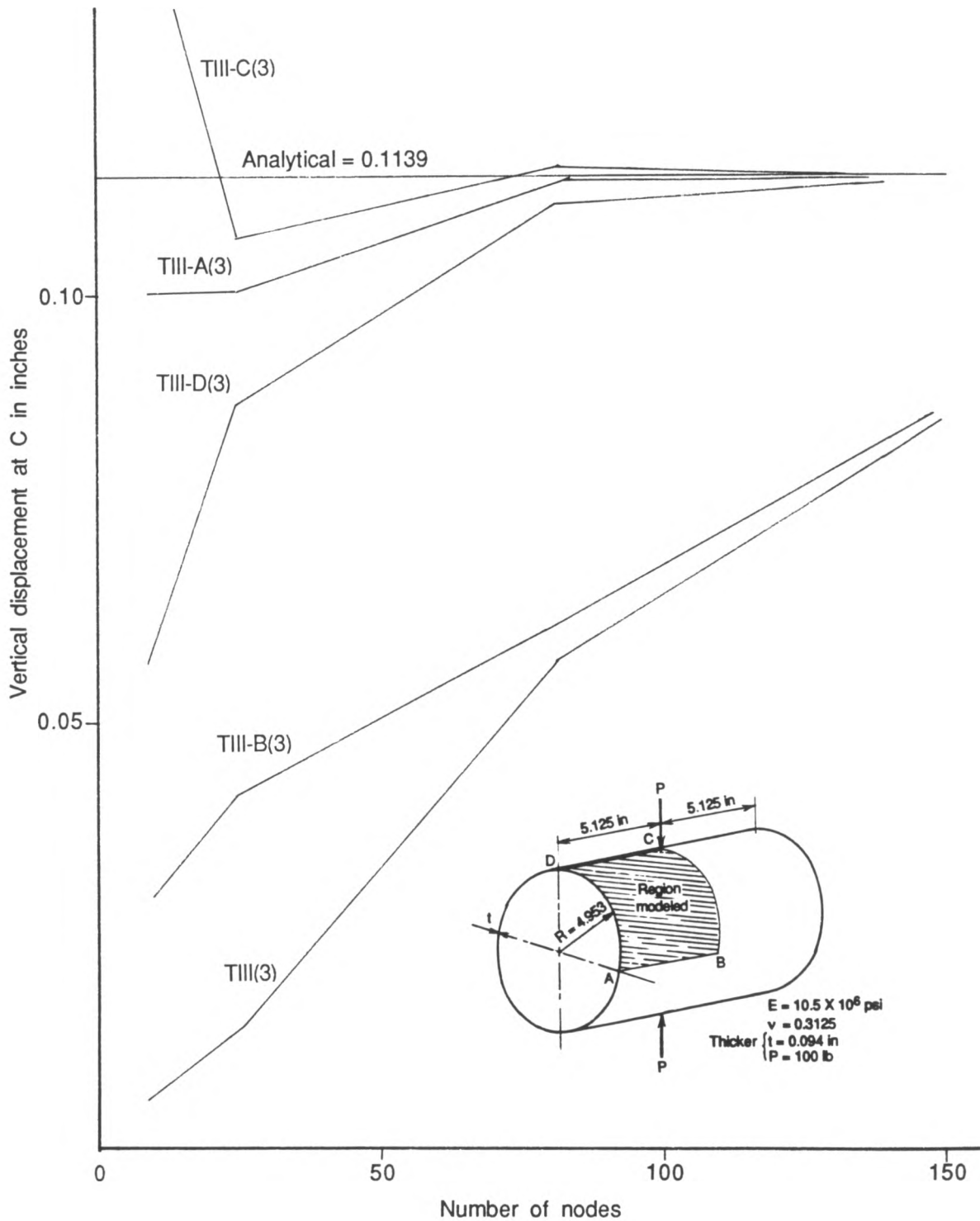
Fig. B.8   Convergence of the type III element
            Triangular element with or without internal d.o.f.
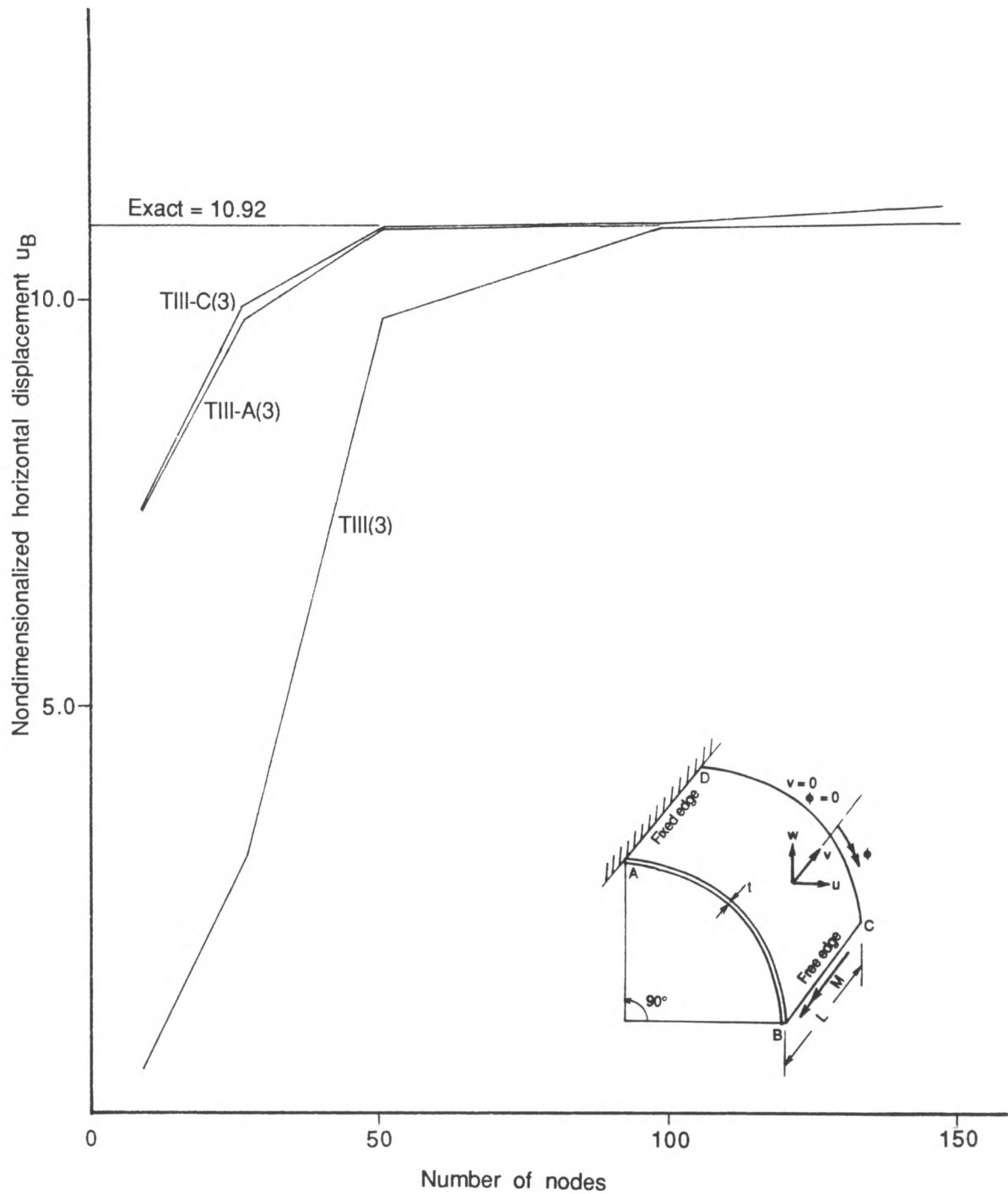   Pinched cylinder (thick)–vertical displacement at C

Fig. B.9   Convergence of the type III element
Triangular element with or without internal d.o.f.
Pinched cylinder (thin)–vertical displacement at C

211

Fig. B.10 Convergence of the type III element
Triangular element with or without internal d.o.f.
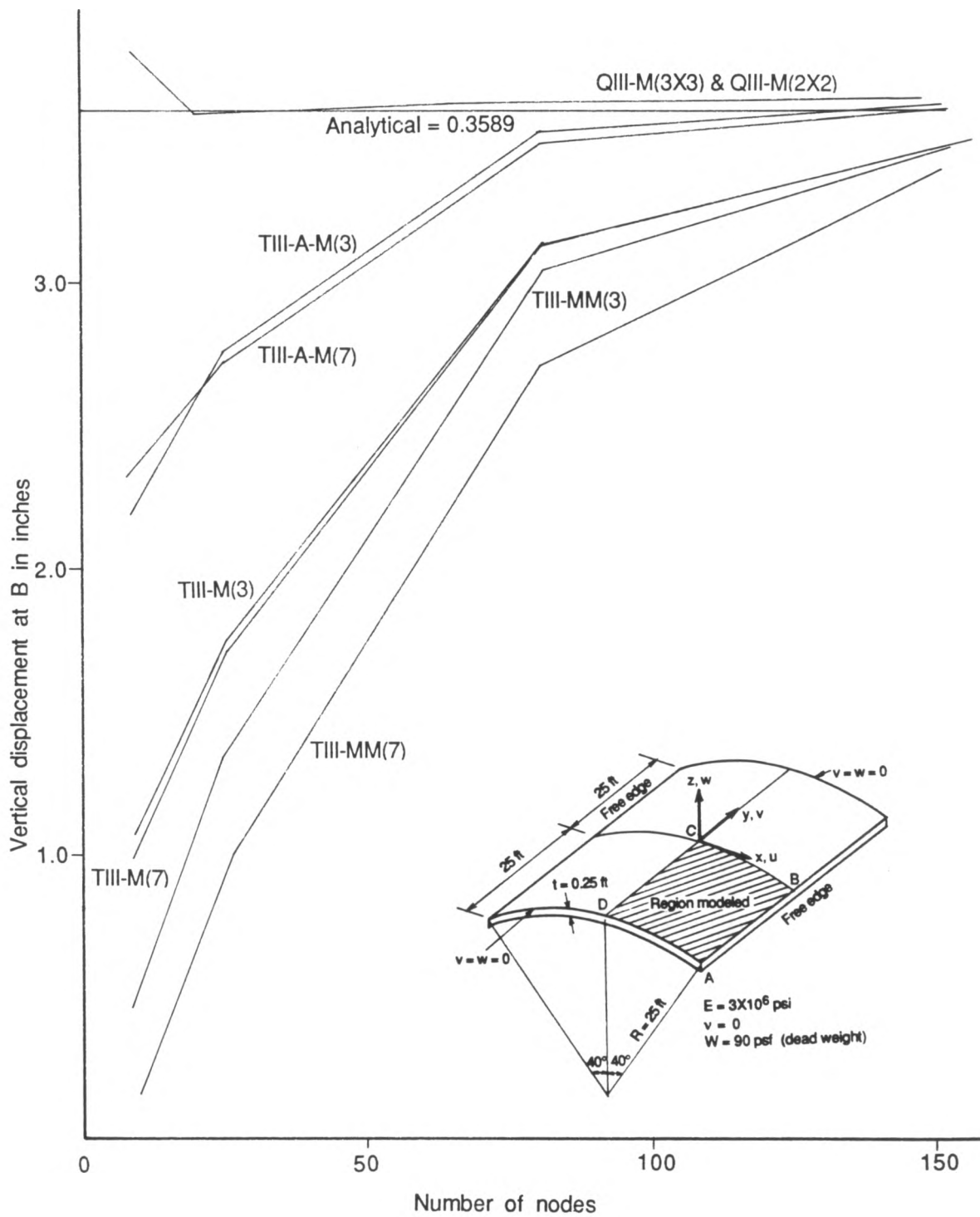Fixed-free quarter cylinder–horizontal displacement at C

Fig. B.11 Convergence of type III element by mixed formulation
Triangular and quadrilateral elements
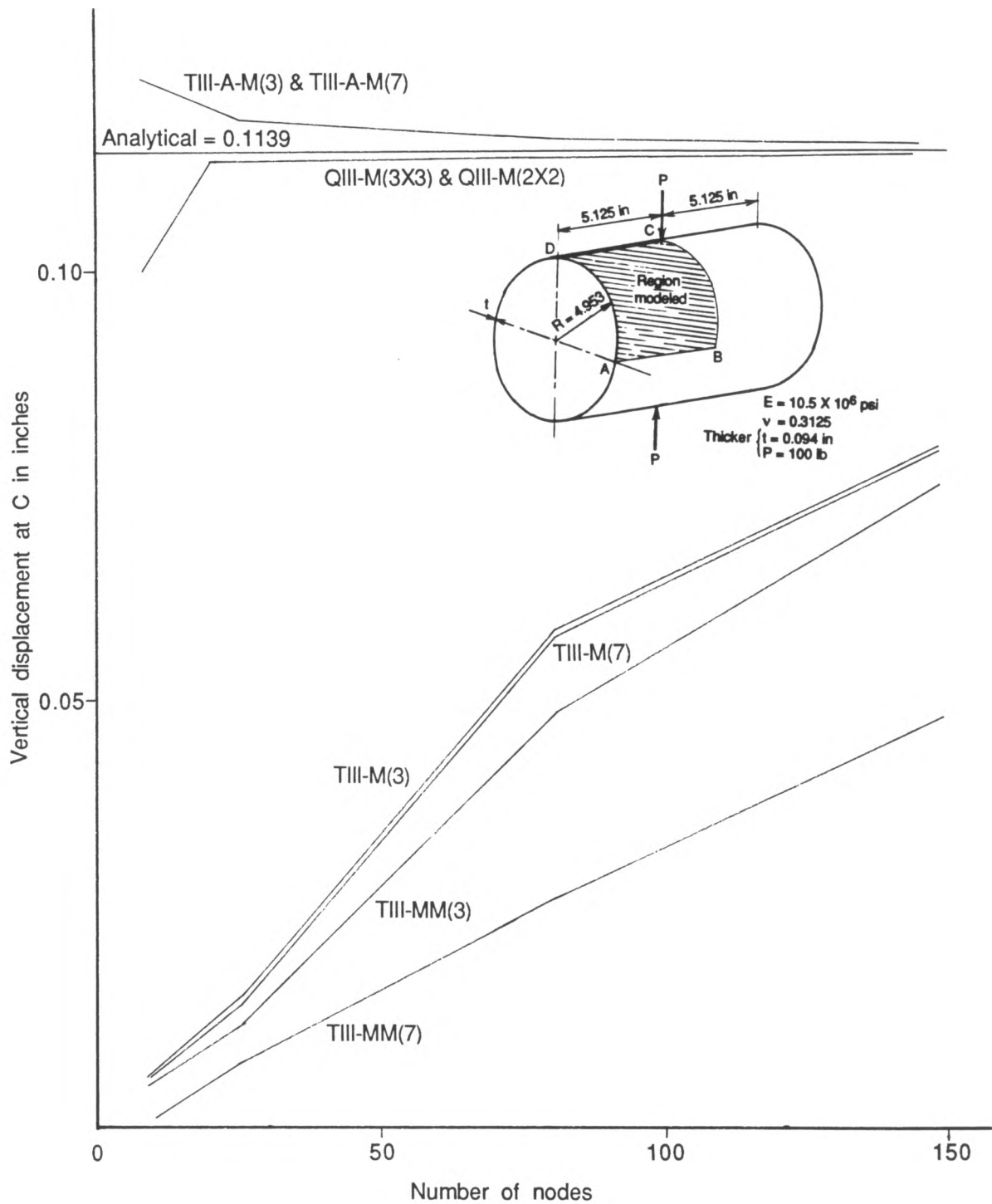Cylindrical shell roof–vertical displacement at B

Fig. B.12   Convergence of type III element by mixed formulation
Triangular and quadrilateral elements
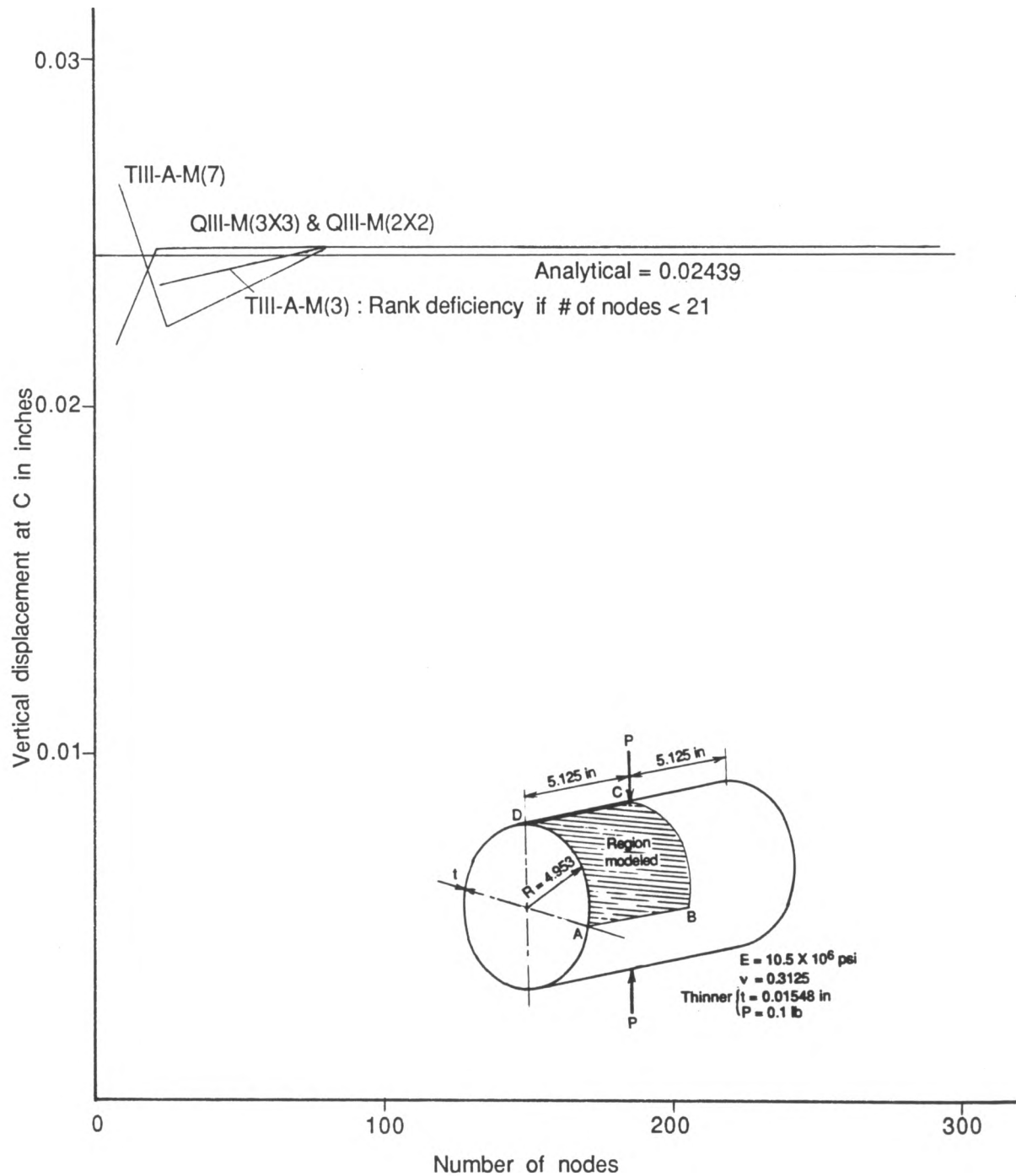Pinched cylinder (thick)–vertical displacement at C

Fig. B.13 Convergence of type III element by mixed formulation
Triangular and quadrilateral elements
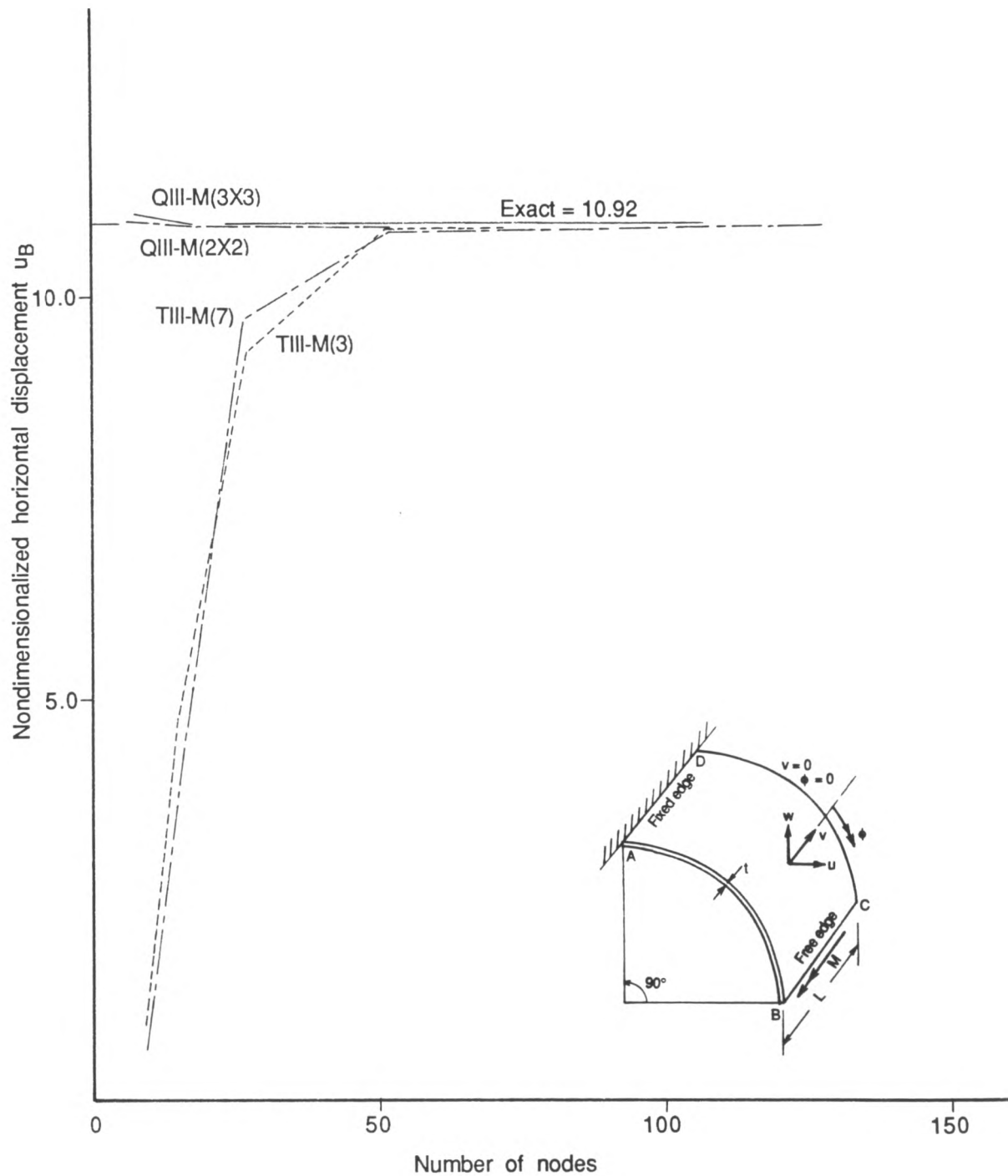Pinched cylinder (thin)–vertical displacement at C

Fig. B.14 Convergence of type III element by mixed formulation
Triangular and quadrilateral elements
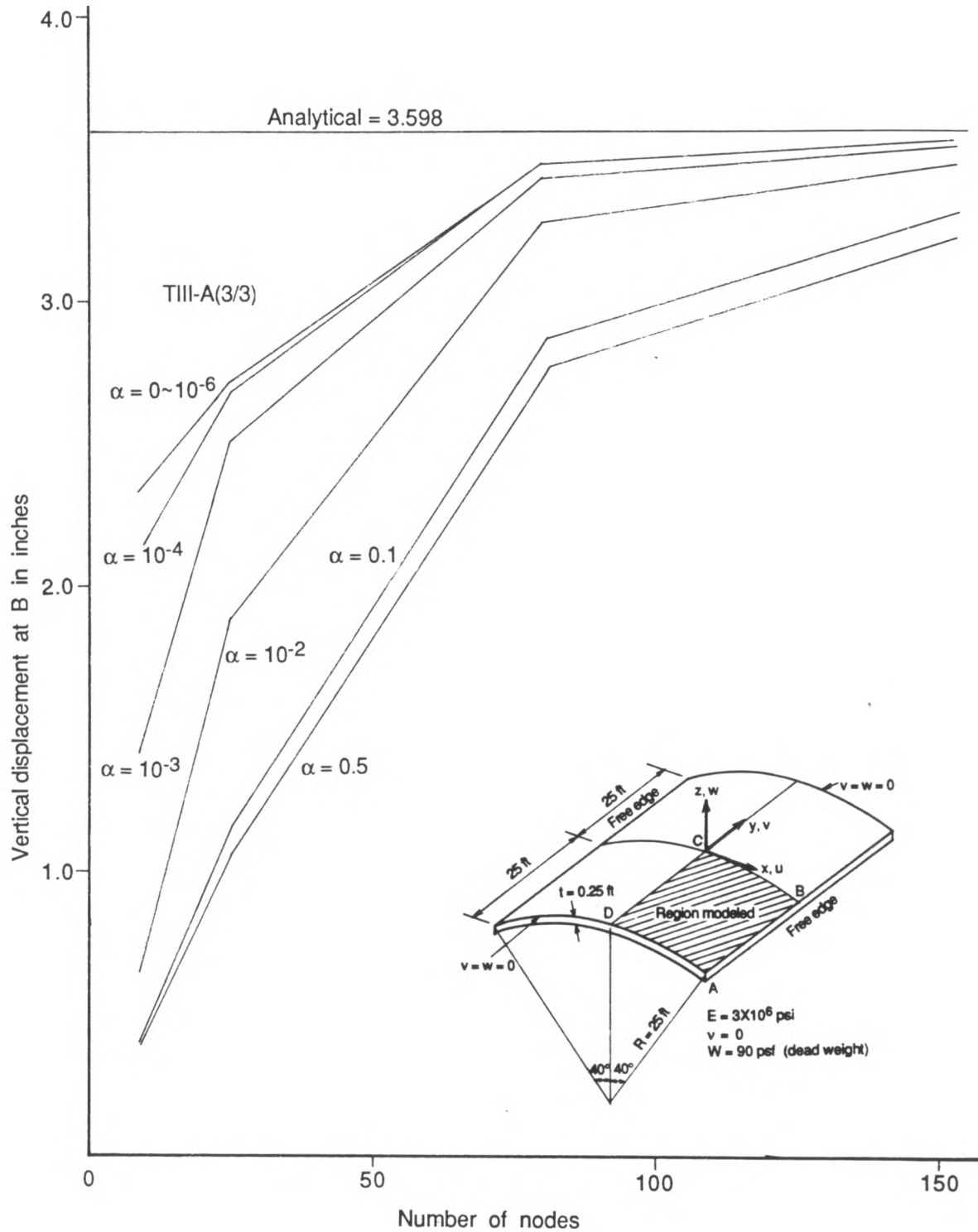Fixed-free quarter cylinder–horizontal displacement at C

Fig. B.15 Effect of zero energy control
α–scheme with 3/3 point integration for the type III element
with IDOF(A)
Cylindrical shell roof–vertical displacement at B

Fig. B.16   Effect of zero energy control
α–scheme with 3/3 point integration for the type III element
with IDOF(A)
Pinched cylinder (thin)–vertical displacement at C

Fig. B.17 Effect of zero energy control
α–scheme with 3/3 point integration for the type III element
with IDOF(A)
Four-corner-supported square plate–deflection at the center

Fig. B.18 Effect of zero energy control
α–scheme with 3/3 point integration for the type III element
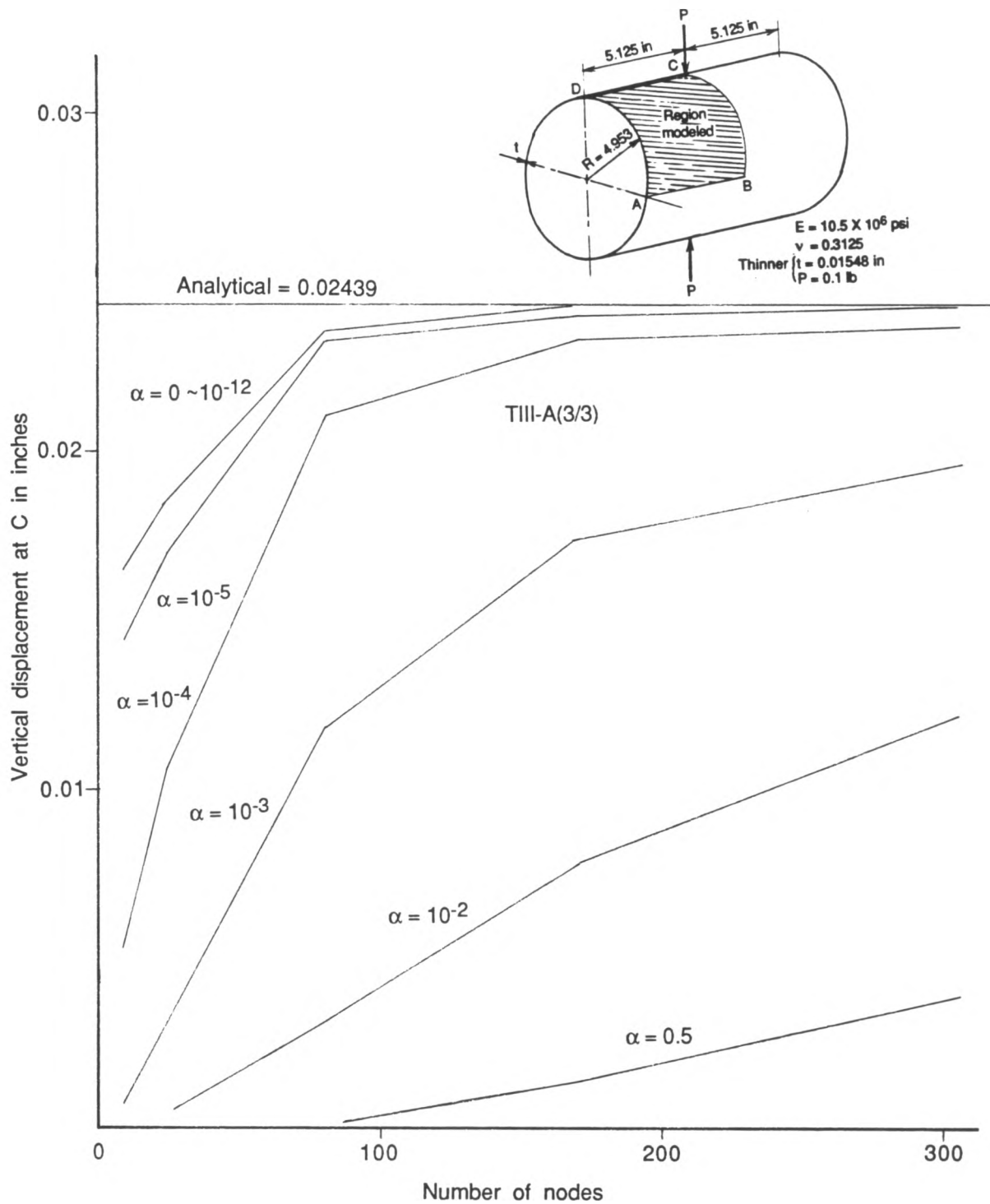with IDOF(D)
Cylindrical shell roof–vertical displacement at B

Fig. B.19 Effect of zero energy control
α–scheme with 3/3 point integration for the type III element
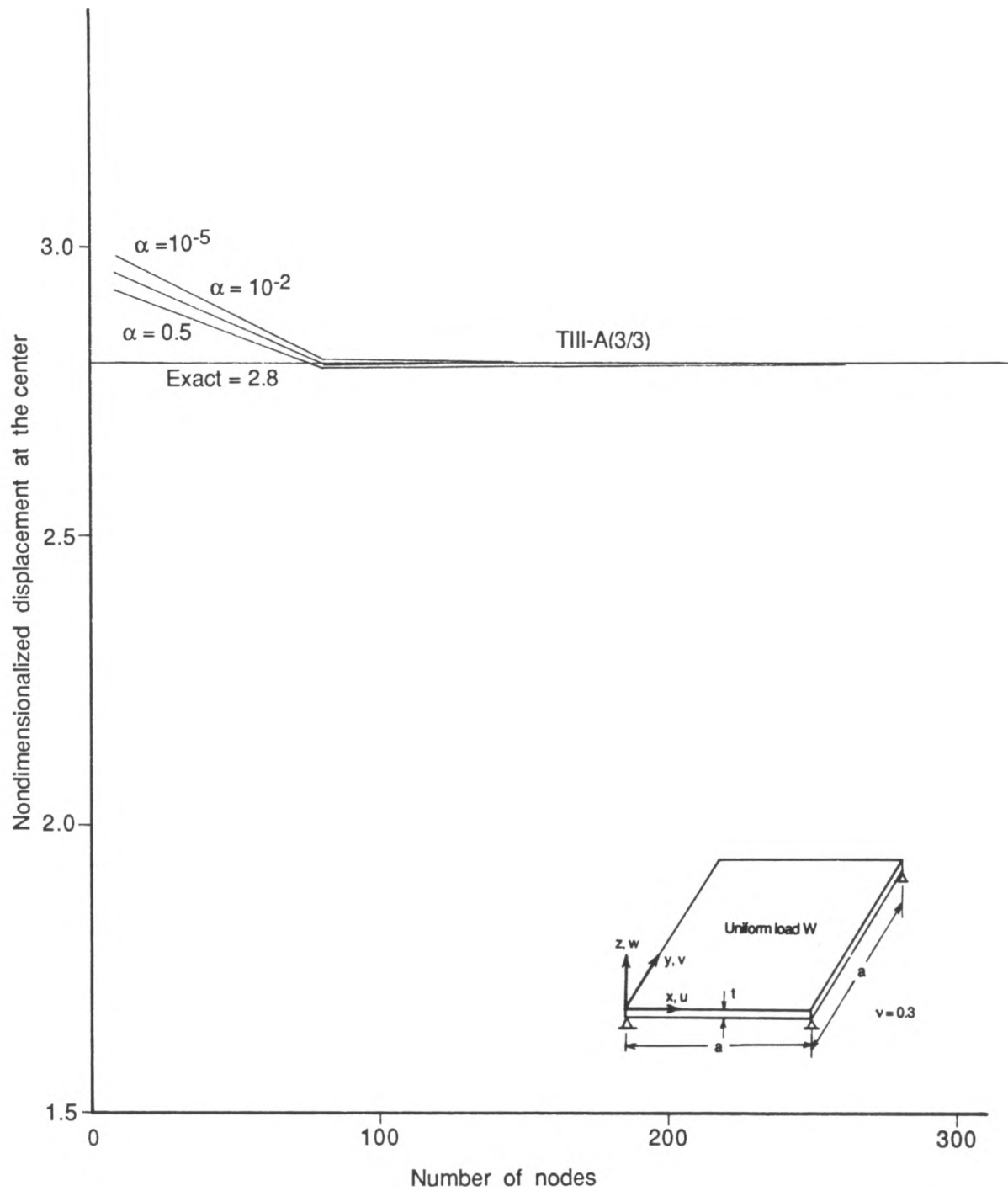with IDOF(D)
Pinched cylinder (thin)–vertical displacement at C

Fig. B.20 Effect of zero energy control
α–scheme with 3/3 point integration for the type III element
with IDOF(D)
Four-corner-supported square plate–deflection at the center

Fig. B.21   Effect of zero energy control
α–scheme with 3/7 point integration for the type III element
with IDOF(A)
Pinched cylinder (thin)–vertical displacement at C

Fig. B.22 Effect of zero energy control
α–scheme with 3/7 point integration for the type III element
with IDOF(A)
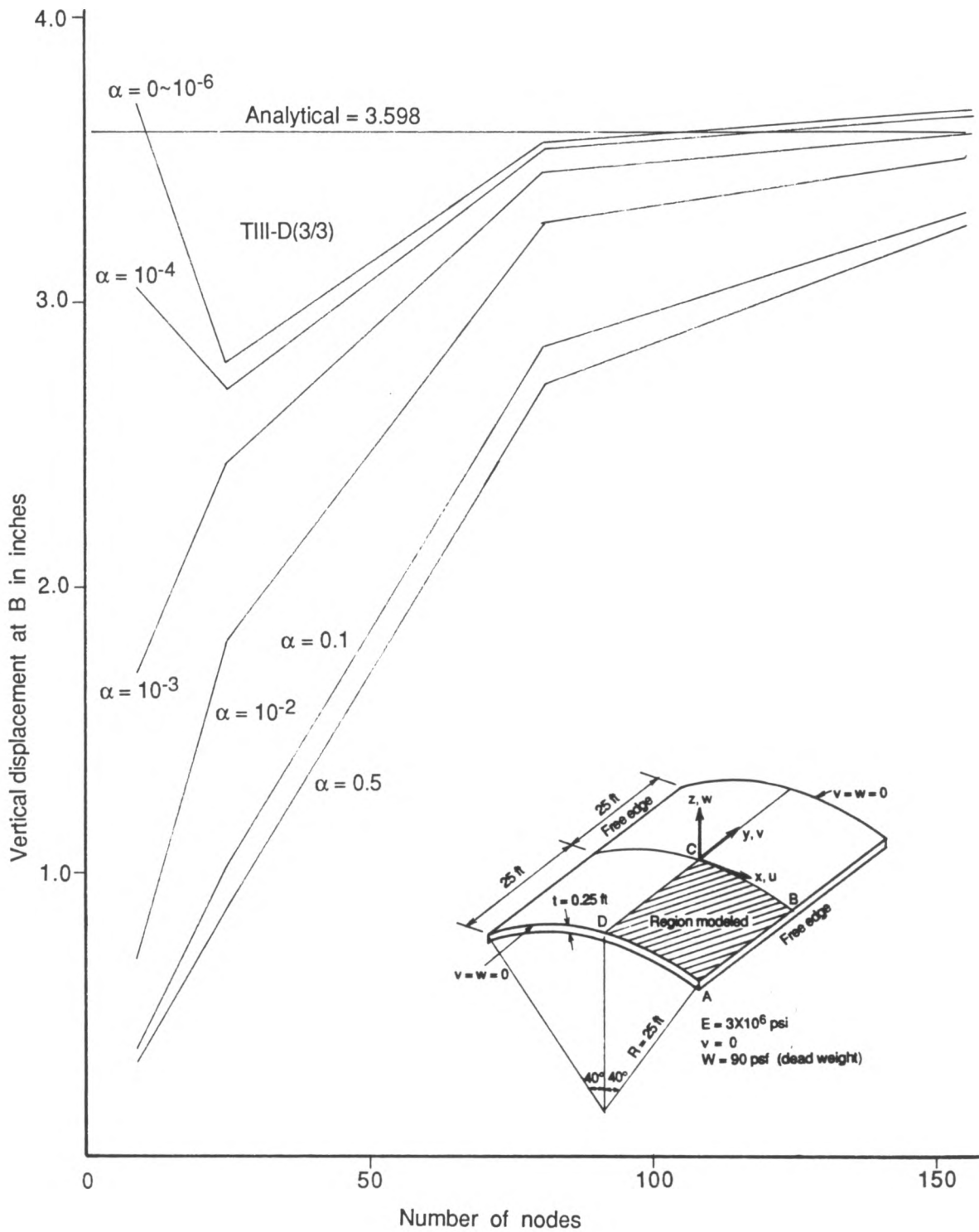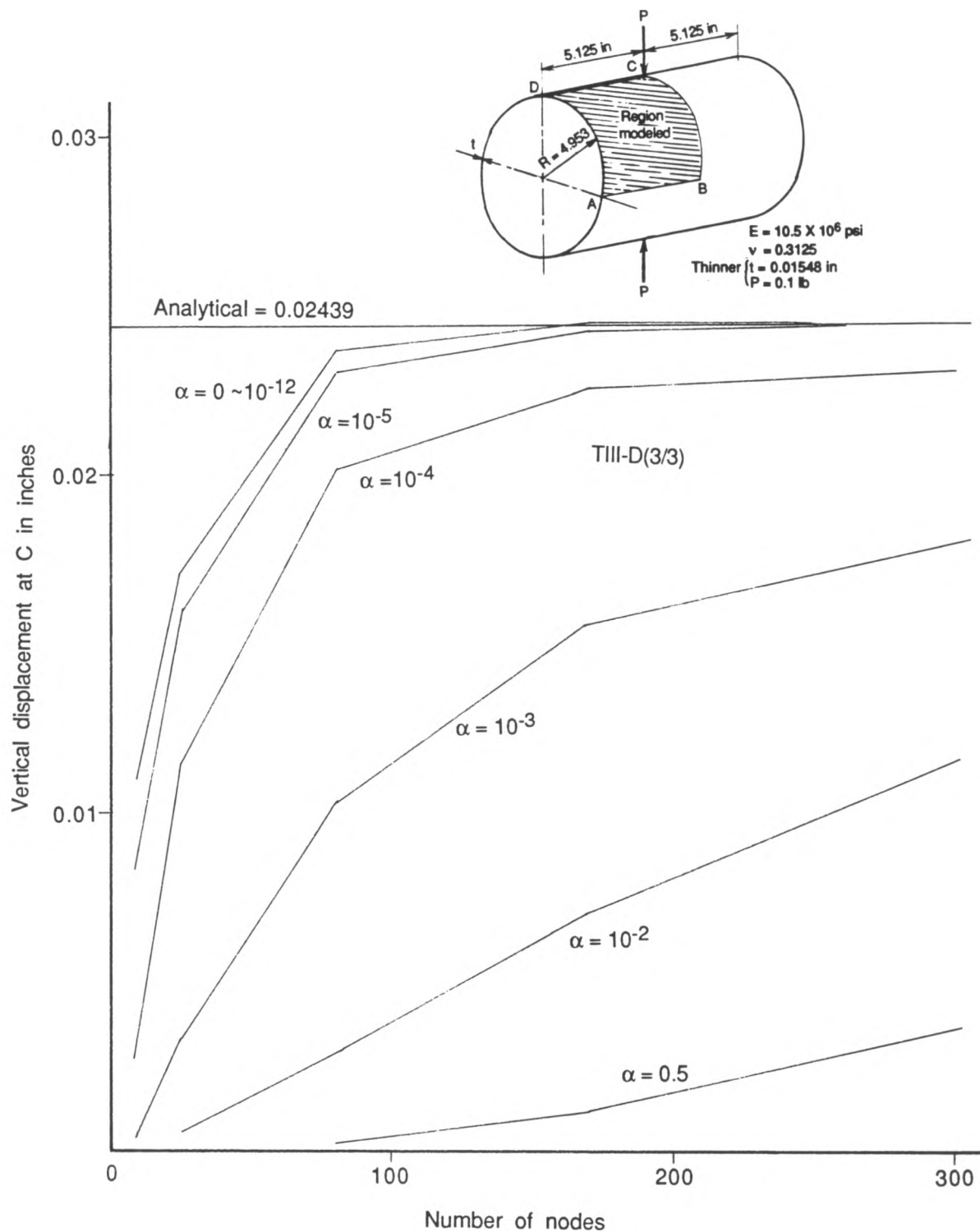Four-corner-supported square plate–deflection at the center

Fig. B.23   Effect of zero energy control
α–scheme with 3/7 point integration for the type III element
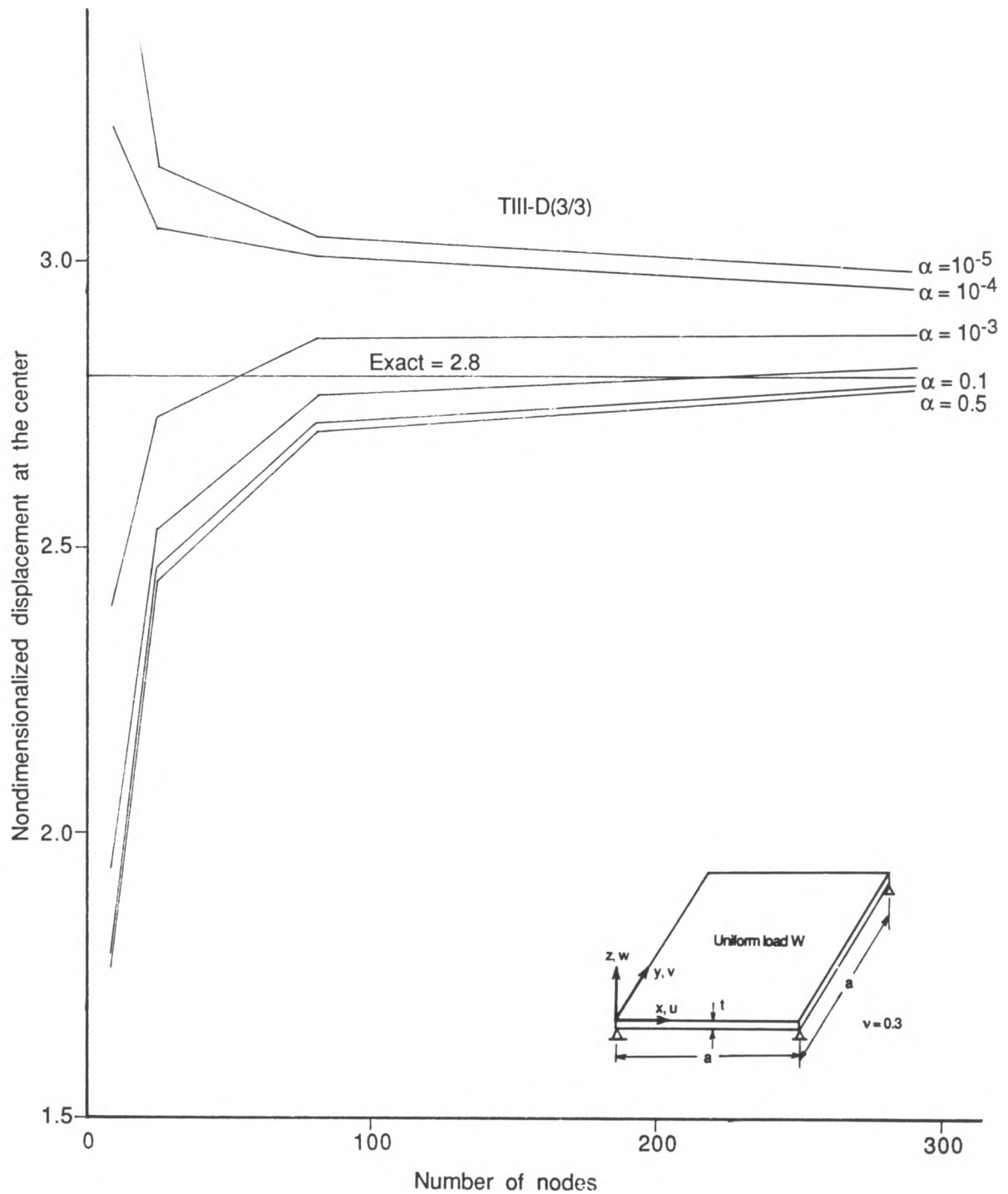with IDOF(D)
Pinched cylinder (thin)–vertical displacement at C
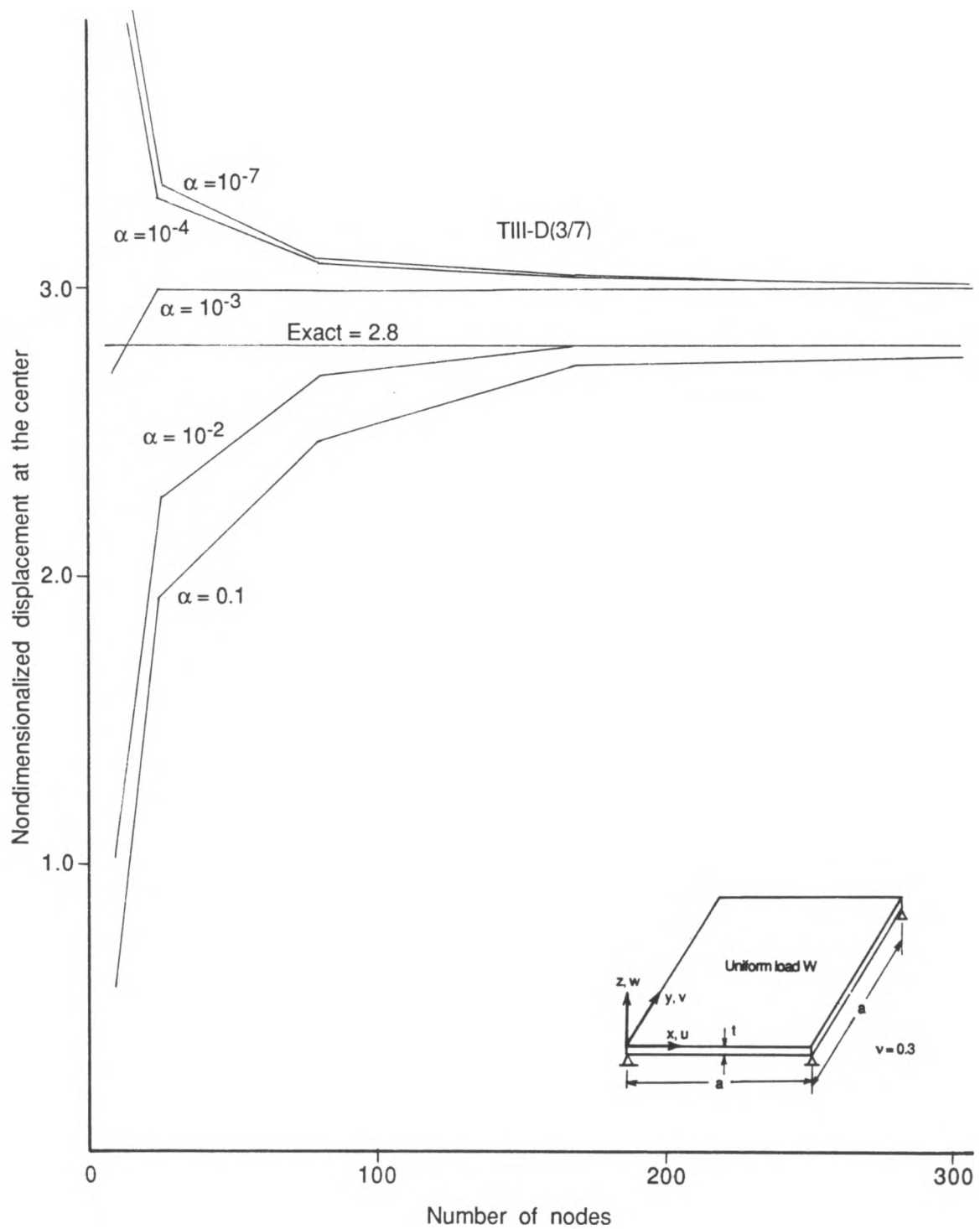
Fig. B.24 Effect of zero energy control
α–scheme with 3/7 point integration for the type III element
with IDOF(D)
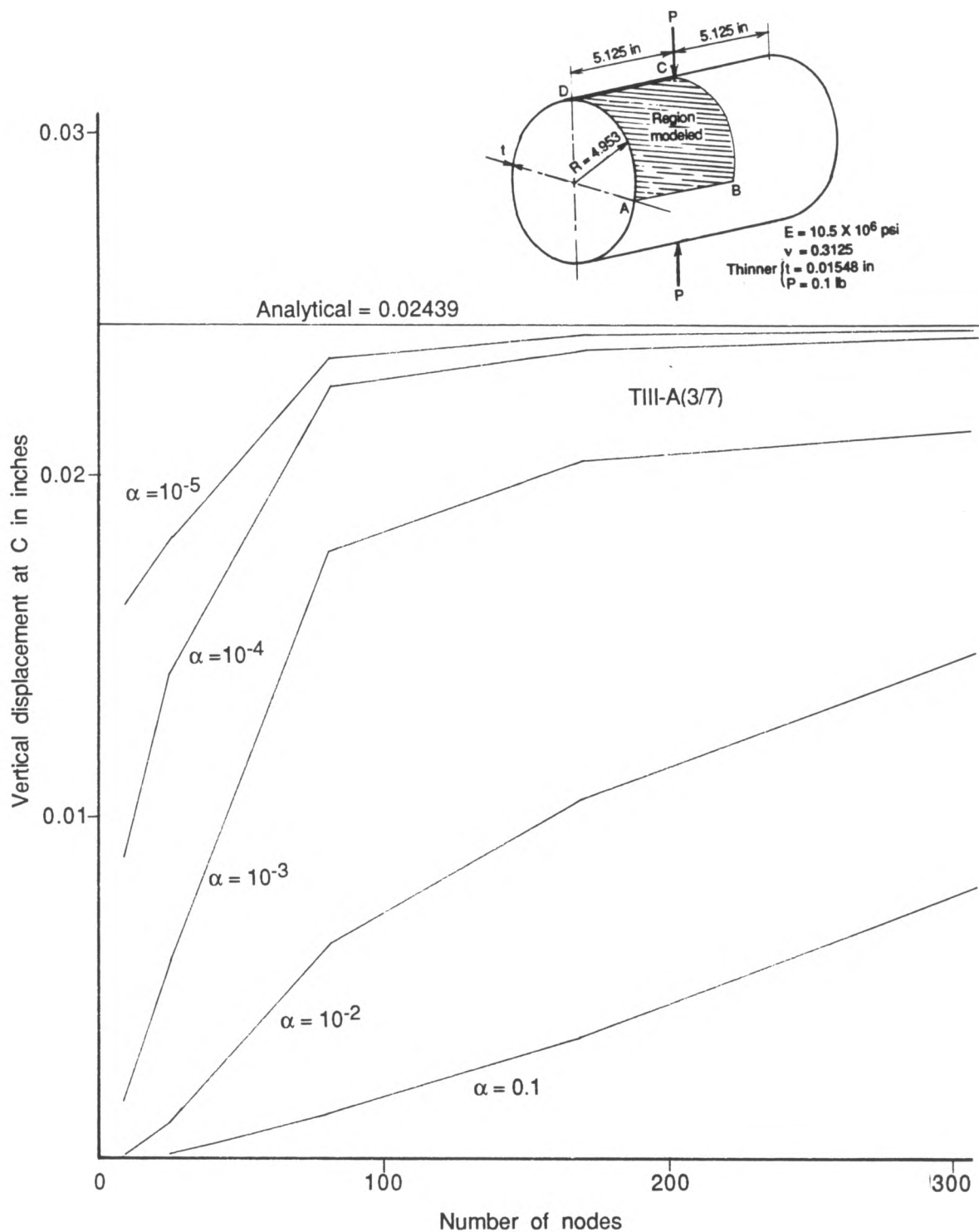Four-corner-supported square plate–deflection at the center
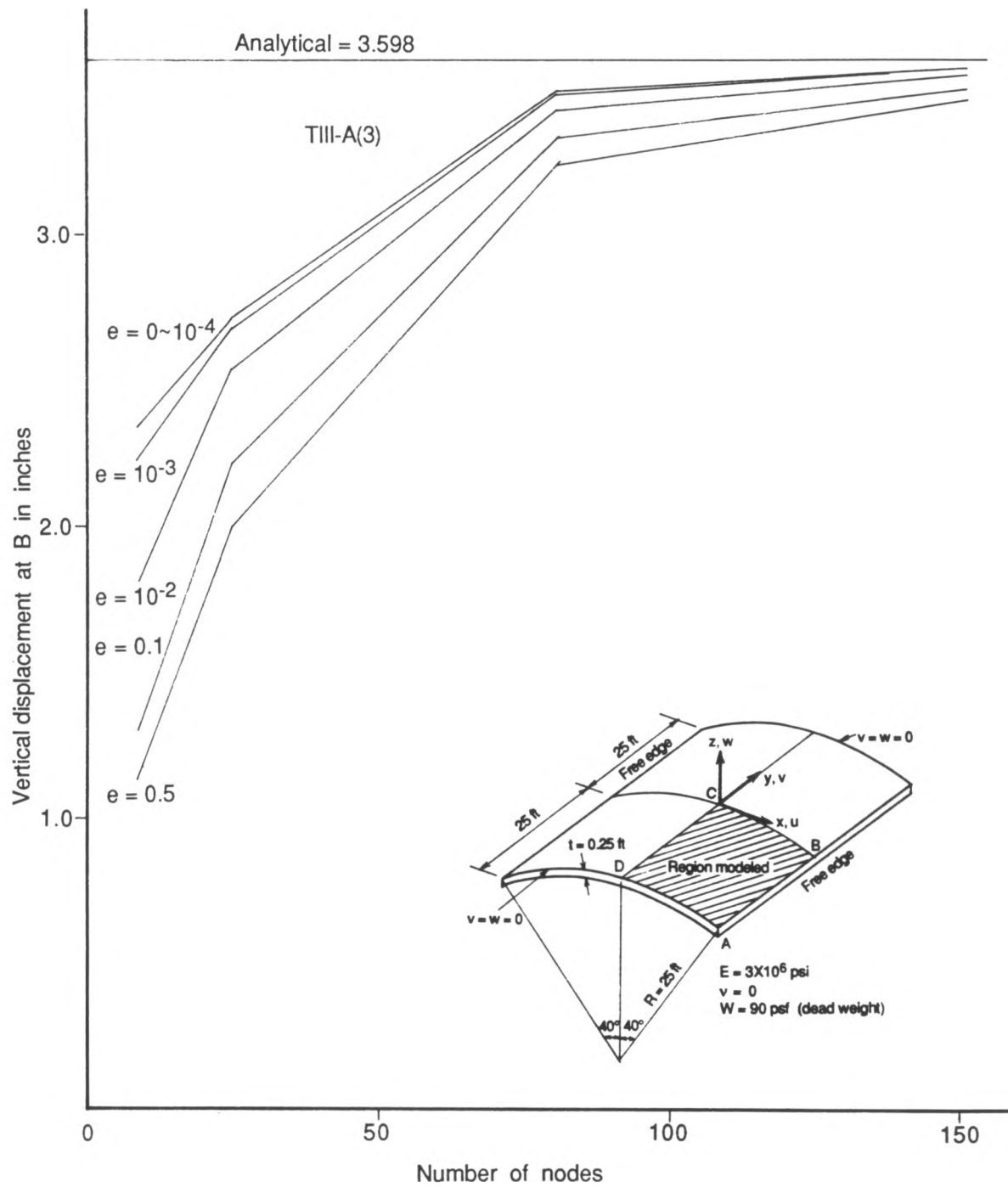
Fig. B.25   Effect of zero energy control
e–scheme for the type III element with IDOF(A)
Cylindrical shell roof–vertical displacement at B
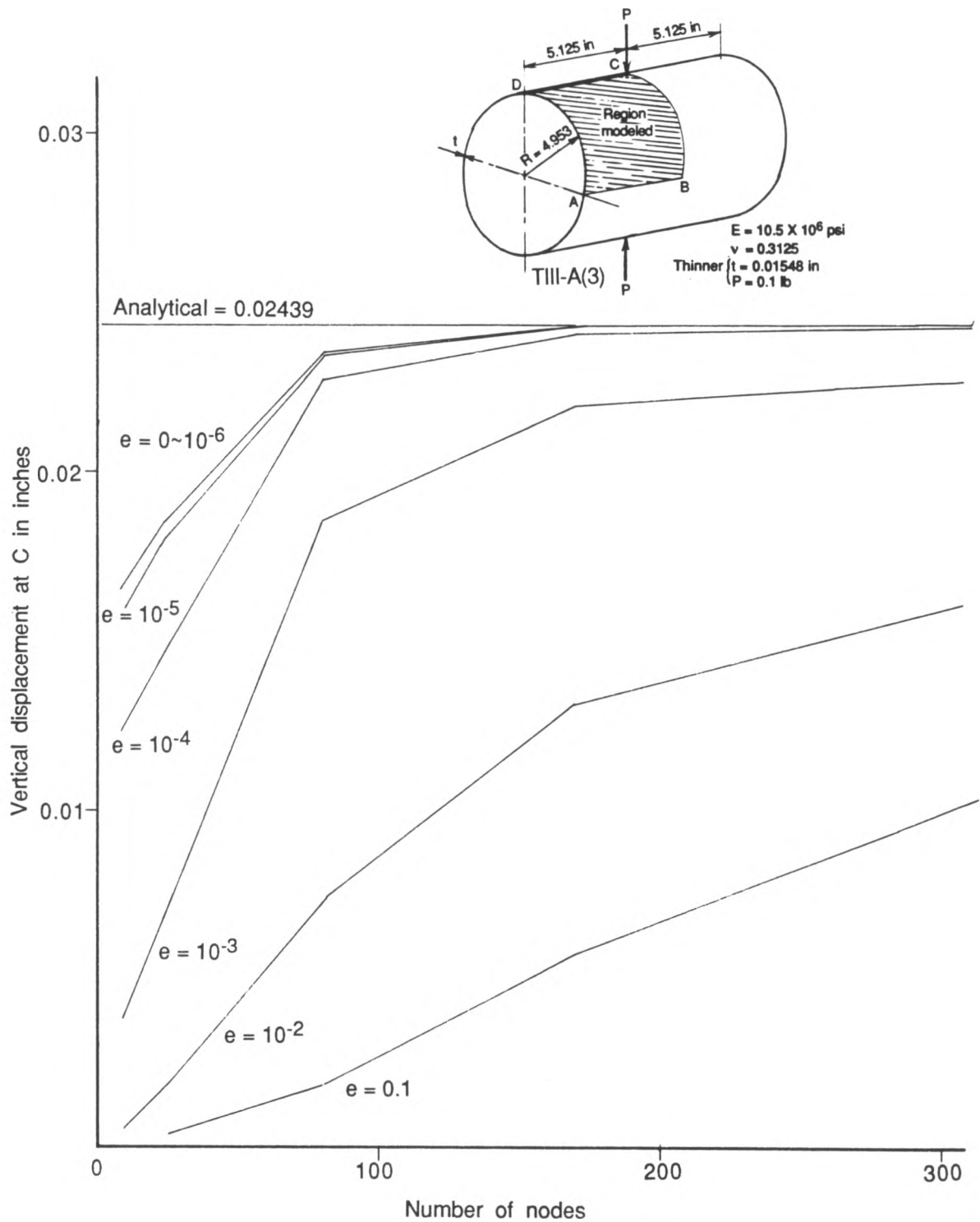
Fig. B.26 Effect of zero energy control
e–scheme for the type III element with IDOF(A)
Pinched cylinder (thin)–vertical displacement at C
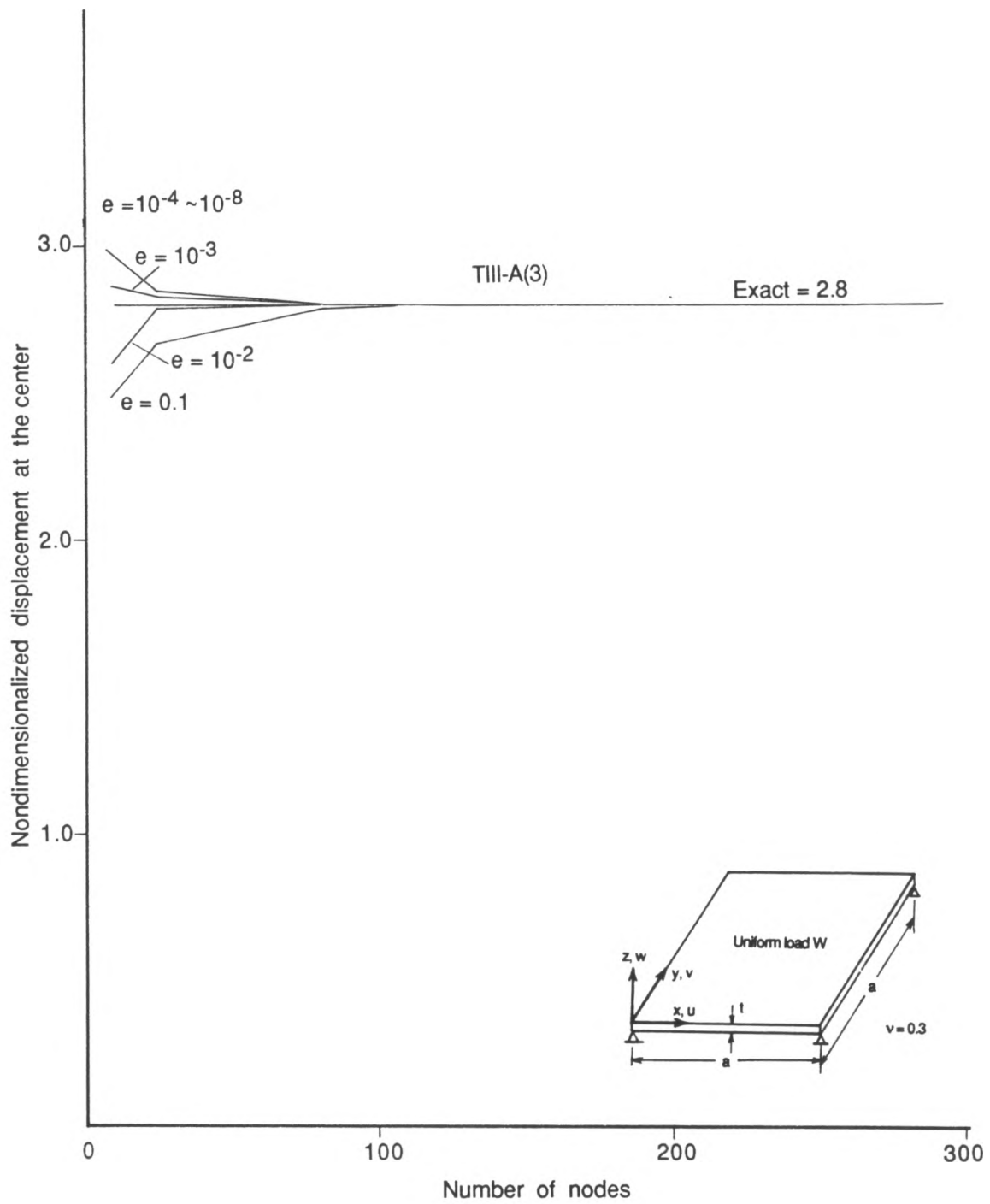
Fig. B.27 Effect of zero energy control
e–scheme for the type III element with IDOF(A)
Four-corner-supported square plate–deflection at the center
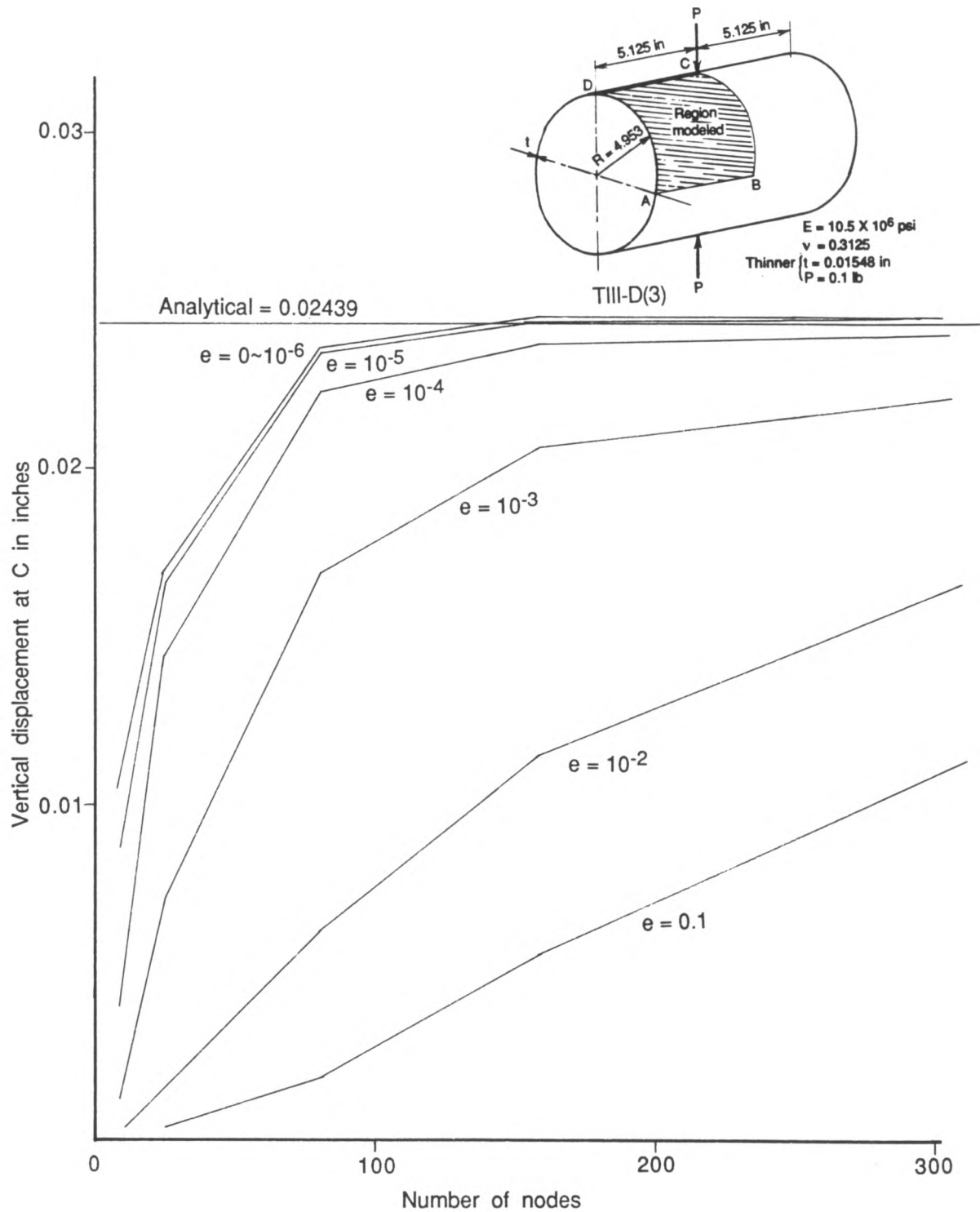
Fig. B.28 Effect of zero energy control
e–scheme for the type III element with IDOF(D)
Pinched cylinder (thin)–vertical displacement at C
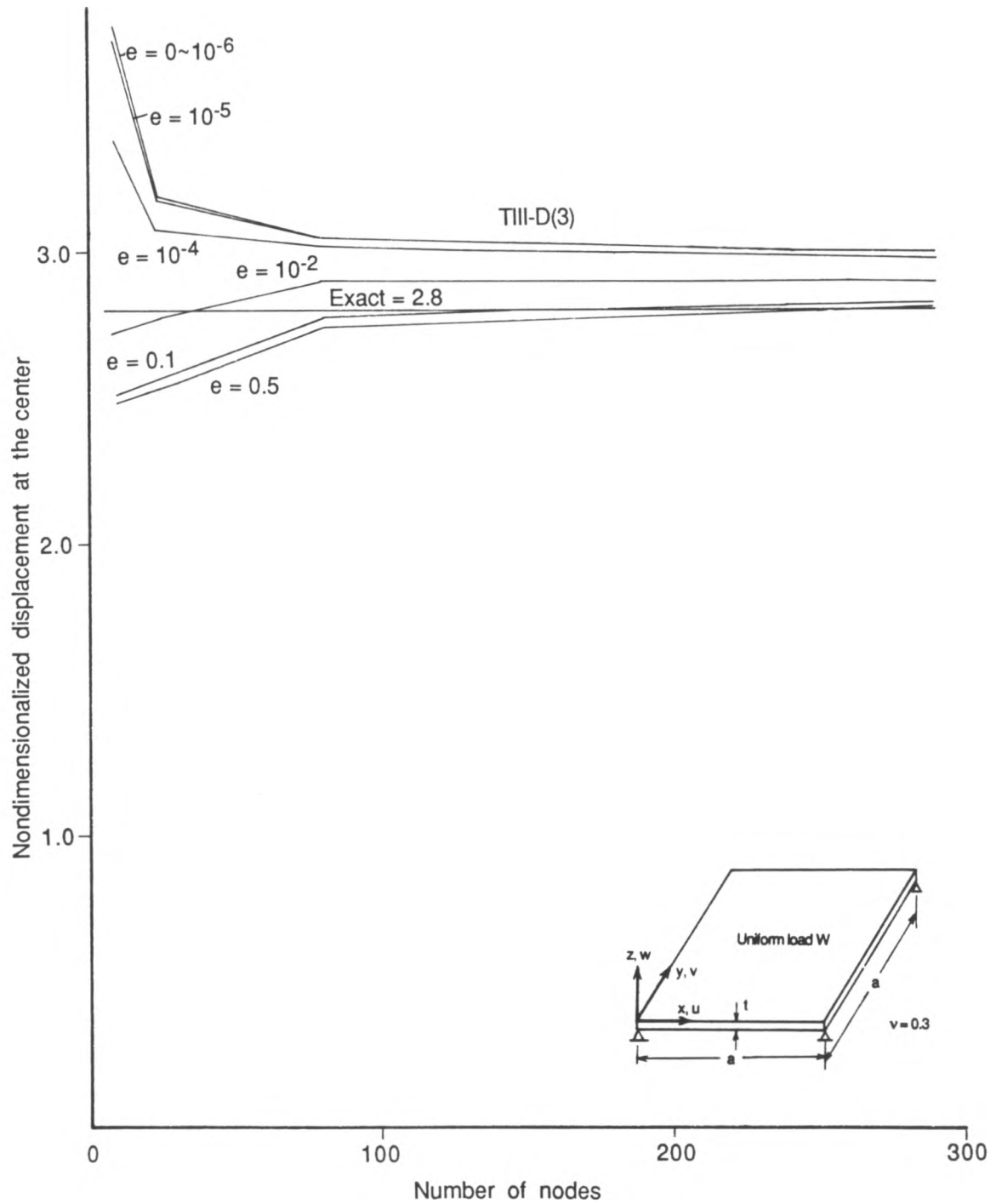
Fig. B.29 Effect of zero energy control
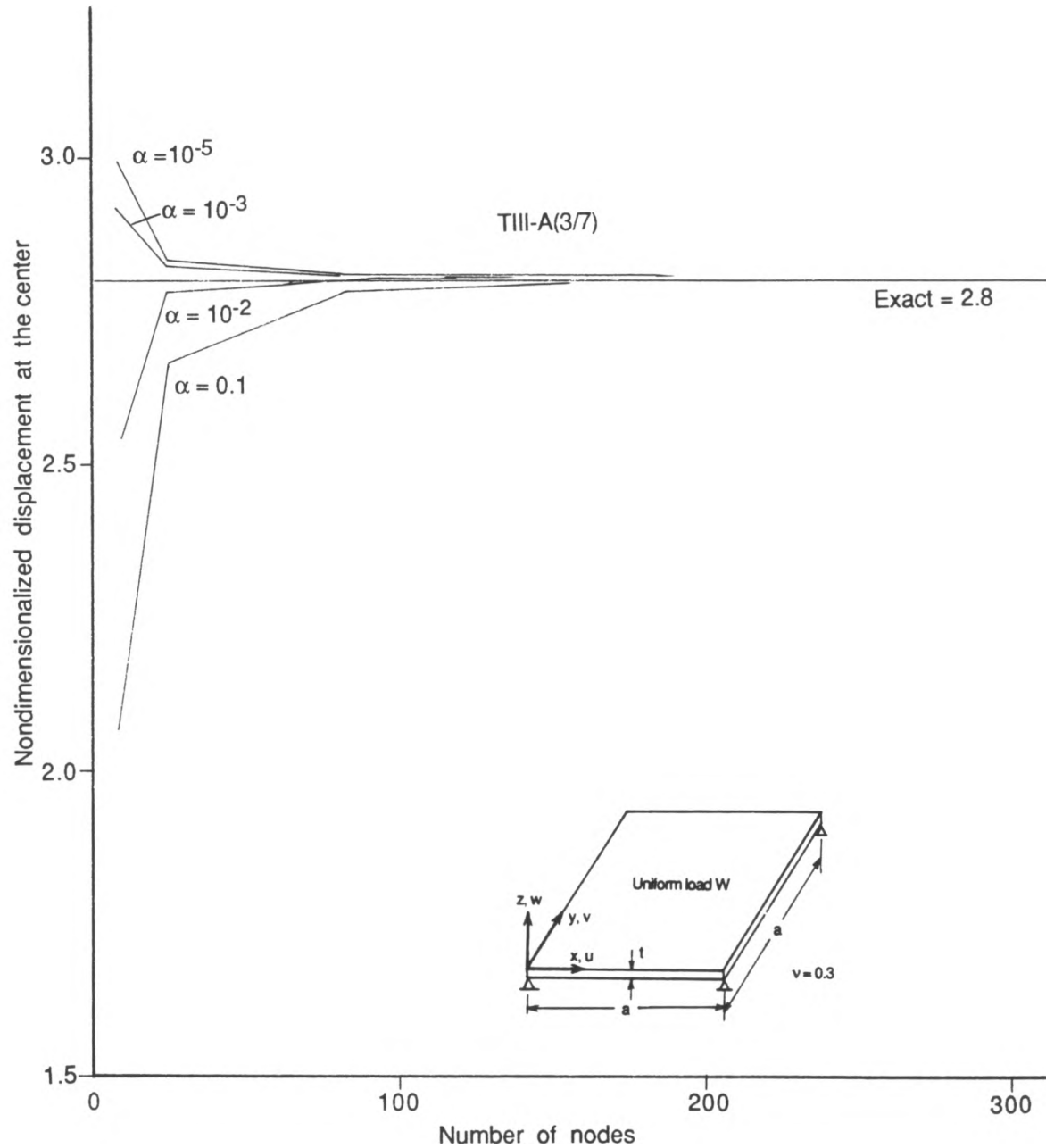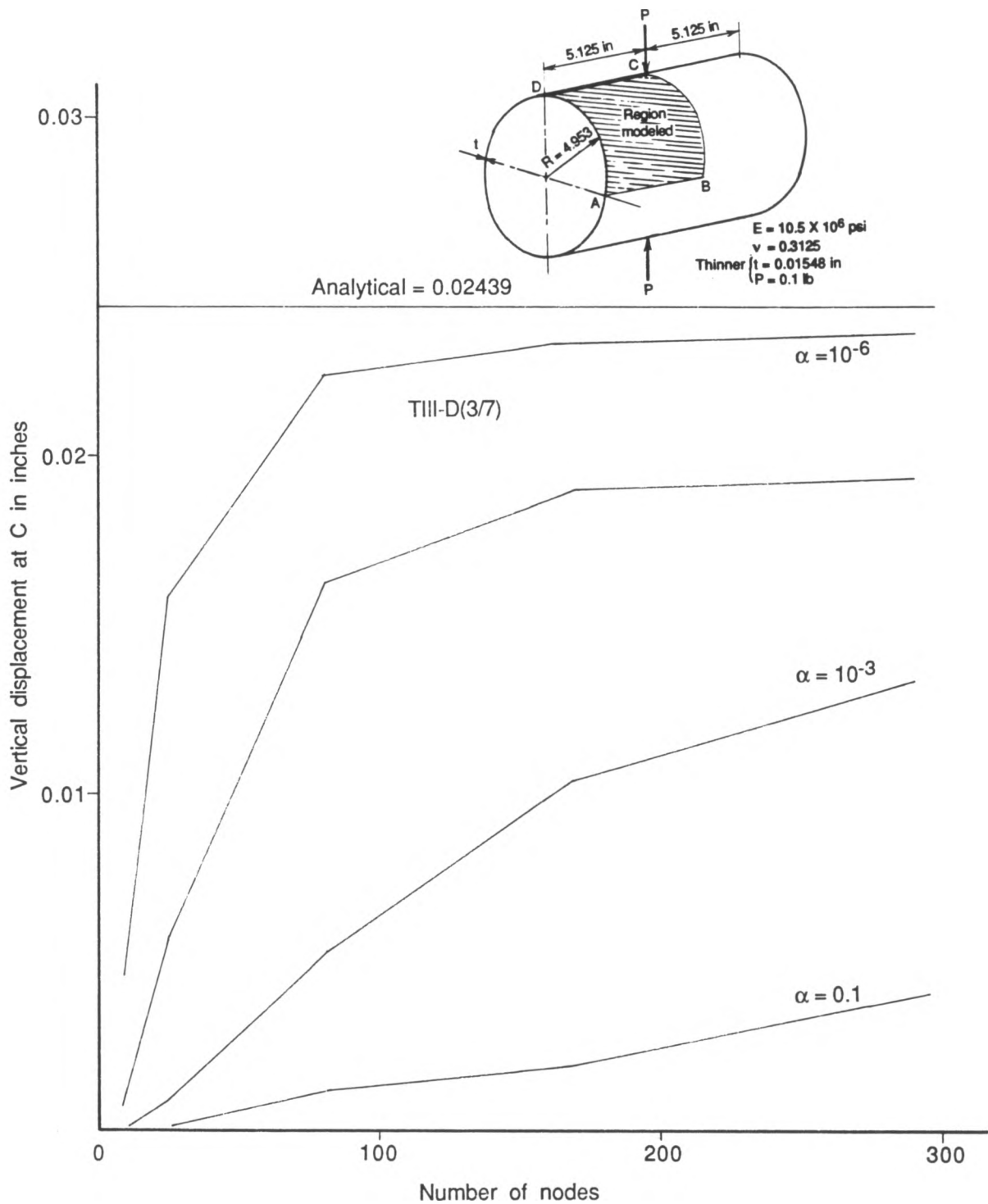e–scheme for the type III element with IDOF(D)
Four-corner-supported square plate–deflection at the center
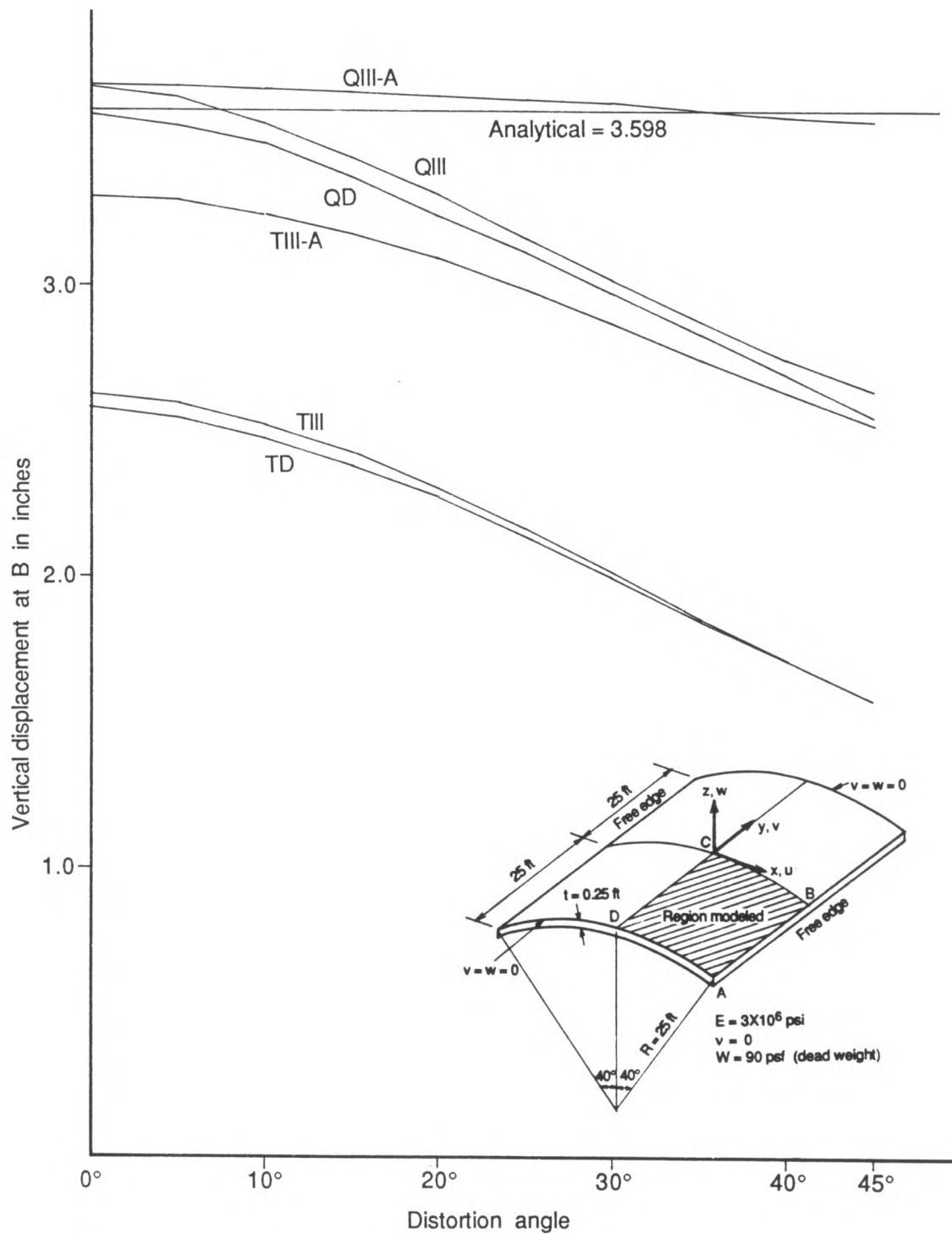
Fig. B.30 Effect of element distortion
Cylindrical shell roof–vertical displacement at B
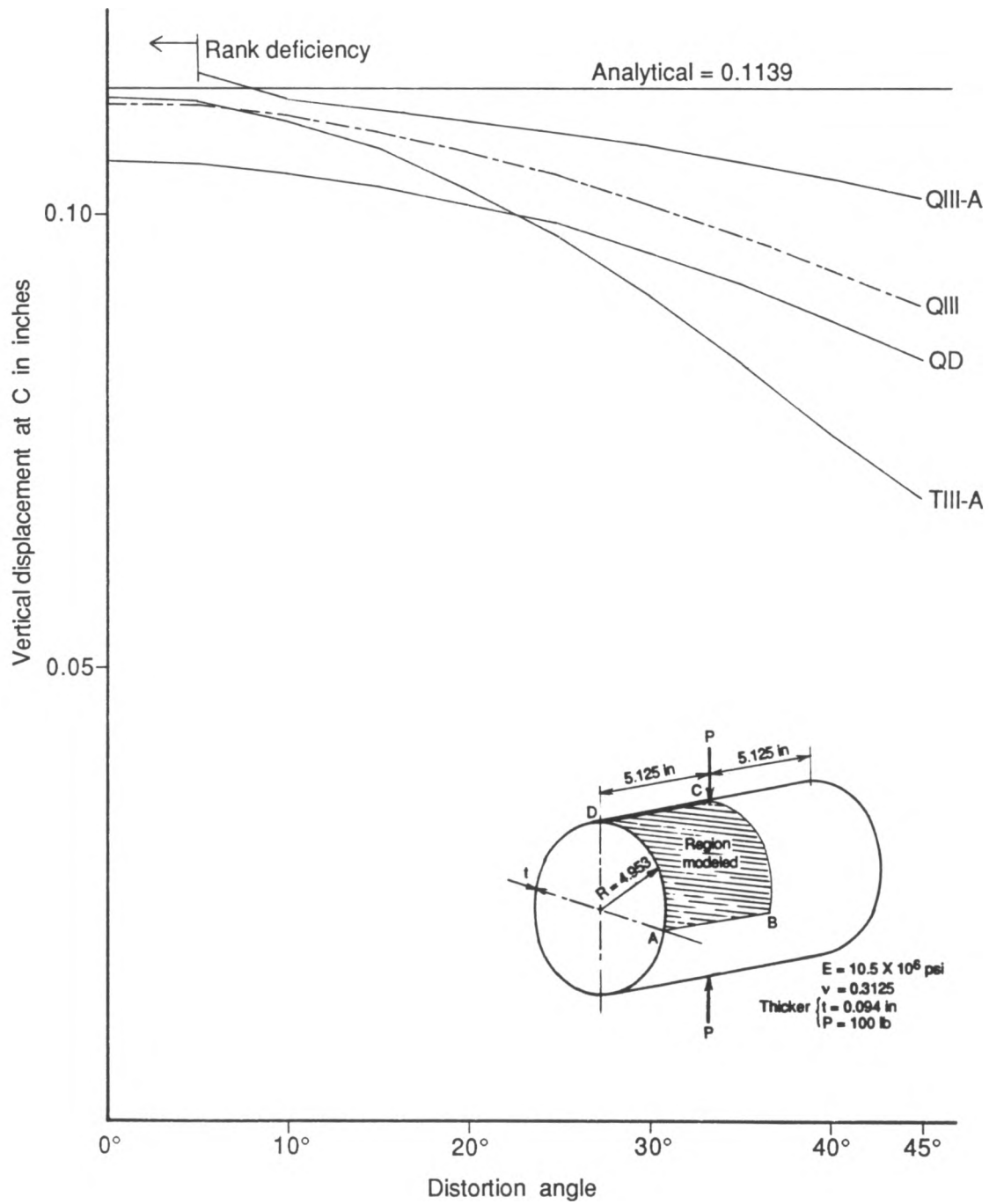
Fig. B.31 Effect of element distortion
          Pinched cylinder (thick)–vertical displacement at C
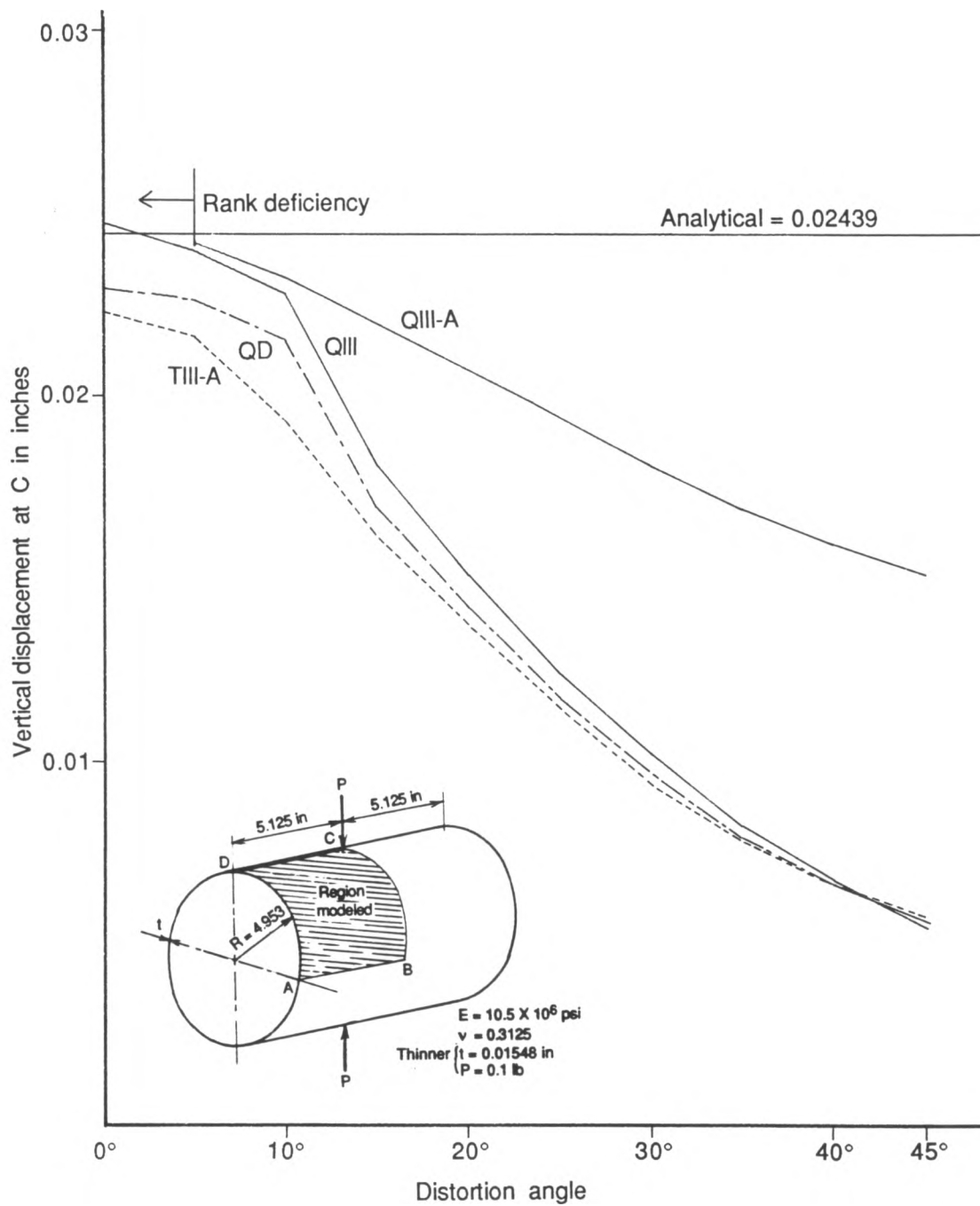
Fig. B.32 Effect of element distortion
          Pinched cylinder (thin)–vertical displacement at C
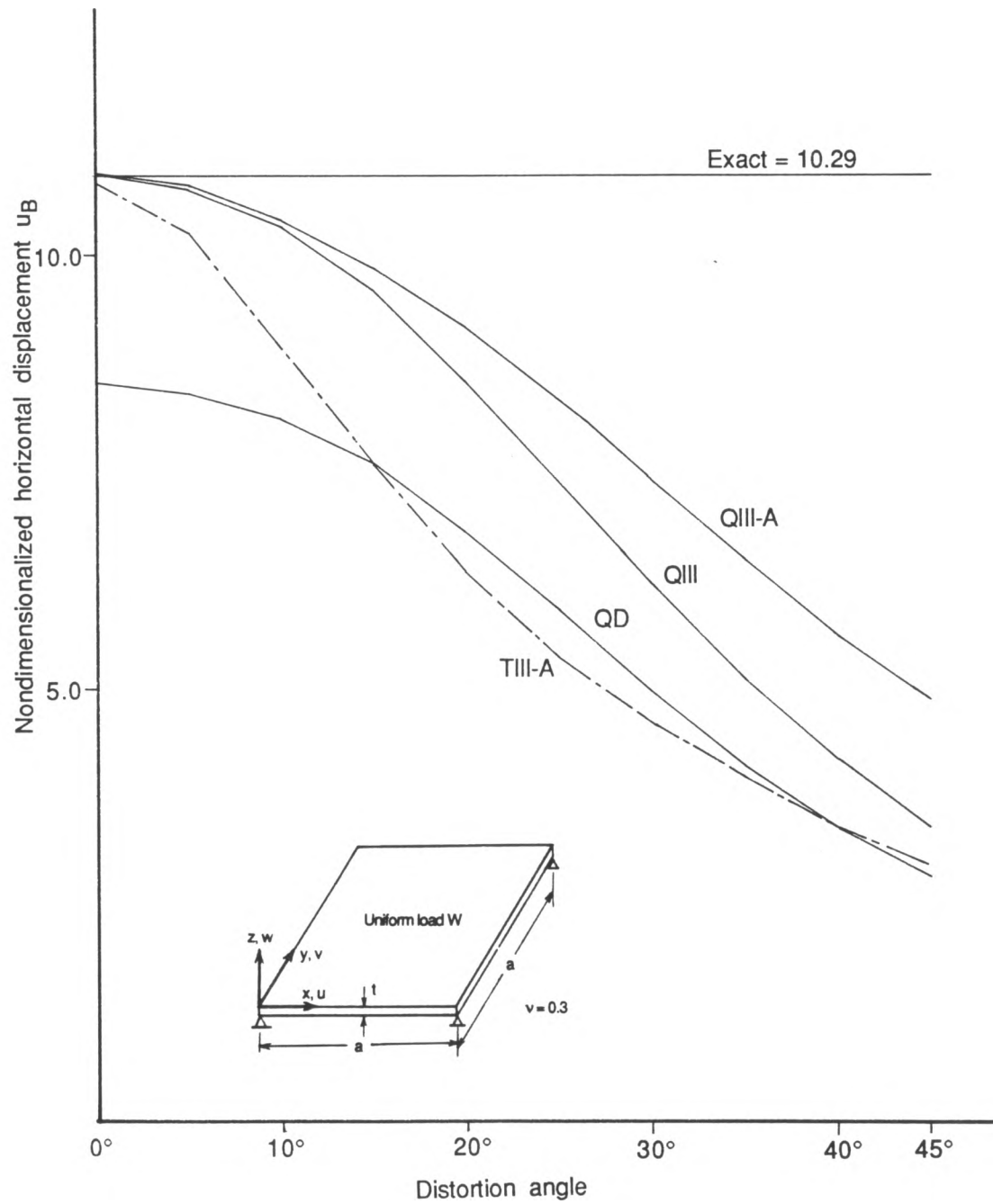
Fig. B.33   Effect of element distortion
            Four-corner-supported square plate—deflection at the center

REFERENCES

Abel,J.F., and C.S.Desai, 1972, Comparison of finite elements for plate bending, *J. Struct. Div.,* ASCE, ST9, pp2143-2148.

Ahmad,S., B.M.Irons, and O.C.Zienkiewicz, 1968, Curved thick shell and membrane elements with particular reference to axisymmetric problems,*Proc. 2nd Conf. Matrix Meth. Struct. Mech.*, Wright-Patterson Air Force Base, Ohio.

Ahmad,S., B.M.Irons,, and O.C.Zienkiewicz, 1970, Analysis of thick and thin shell structures by curved finite elements, *Int. J. Num. Meth. Engng.* , Vol.2., pp419-451.

Anderson,G.B., and T.C.Carter, 1976, The hen's egg: shell cracking at impact on a heavy, stiff body and factors that affect it, *Br.Poultry Sci.*, Vol.17, pp613-626.

Argyris,J.H., I.Fried, and D.W.Scharpf, 1968, The TUBA family of plate elements for the matrix displacement method, *Aeron. J.*, Vol.72, pp701-709.

Argyris,J.H., and D.W.Scharpf, 1968, The SHEBA family of shell elements for the matrix displacement method, *Aeron. J.*, Vol.72, pp873-883.

Argyris,J.H., and D.W.Scharpf, 1971, Finite element theory of plates, and shells including transverse shear strain effects, *High Speed Comp. Elastic Struct.*, Vol.61, pp253-292.

Argyris,J.H., and K.J.William,1974, Some consideration for the evaluation of finite element models, *Nuclear Engng. Design*, Vol.28, pp76-96.

Argyris,J.H., P.C.Dunne, G.A.Malejannakis, and E.Schelkle, 1977, A simple triangular facet element with applications to linear and non-linear equilibrium and elastic stability problems, *Comp. Meth. Appl. Mech. Engng.* Vol.10, pp371-403.

Ashwell,D.G., and Sabir,L.B., 1972, A new cylindrical shell finite element based on simple independent strain functions, *Int. J. Mech. Sci.,* Vol.14, pp171-183.

Aylor,D.E., J-Y.Parlange, and A.D.Krikorian, 1973, Stomatal mechanics, *Amer. J. Bot.* Vol.60, pp163-171.

Aylor,D.E., J-Y.Parlange, and A.D.Krikorian, 1975, Comment on some recent models of stomatal mechanics, *J. Theor. Biol.* Vol.54, pp395-397.

Barsoum,R.S., 1974, Application of quadratic isoparametric finite elements in linear fracture mechanics, *Int. J. Fracture*, Vol.10, pp603-605.

Barsoum,R.S., 1976a, On the use of isoparametric finite elements in linear fracture mechanics, *Int. J. Num. Meth. Engng*, Vol.10, pp25-37.

Barsoum,R.S., 1976b, A degenerate solid element for linear fracture analysis of plate bending and general shells,*Int. J. Num. Meth. Engng* , Vol.10, pp551-564

Bathe,K.J., 1982, *Finite Elment Procedures in Engineering Analysis*, Prentice-Hall, Inc., Englwood Cliffs.

Bathe,K.J., and E.L.Wilson, 1976, *Numerical methods in Finite Element Analysis*, Prentice-Hall, Inc., New Jersey.

Bathe,K.J., and E.L.Wilson, 1974, Thick shells, *Structural Mechanics Computer Programs-Survey, Assessment and Availability*, University Press of VIrginia, Charlottesville, pp123-141.

Bathe,K.J. E.N.Dvorkin, and L.W.Ho, 1983, Our discrete-Kirchhoff and isoparametric shell elements for nonlinear analysis - an assessmment, *Comp. Struct.*, Vol.16, pp89-98.

Bathe,K.J., and E.N.Dvorkin, 1985, A formulation of general shell elements - the use of mixed interpolation of tensorial components, *Proc. of the NUMETA'85 Conf.*, Swansea, U.K., pp551-563.

Bathe,K.J., and E.N.Dvorkin, 1985, A four node plate bending element based on Mindlin/Reissner plate theory and a mixed interpolation, *Int. J. Num. Meth. Engng.*, Vol.21, pp367-393.

Batos,J-L., K.J.Bathe, and L.W.Ho, 1980, A study of three-node triangular plate bending elements, *Int.. J. Num. Meth. Engng.*, Vol.15, pp1771-1812.

Bazeley,G.P., Y.K.Cheung, B.M.Irons, and O.C.Zienkiewicz, 1965, Triangular elements in plate bending - conforming and non-conforming solution, *Proc. Conf. Matrix Meth. Struct. Mech.*, Wright-Patterson Air Force Base. Ohio.

Belyavin,C.G., and K.N.Boorman, 1981, Physical characteristics of intact and cracked eggs, *Br. Poultry Sci.*, Vol. 22, pp9-12

Belytschko,T., C.S.Tsay, and W.K.Liu, 1981, A stabilization matrix for the bilinear mindlin plate element, *Comp. Meth. Appl. Mech. Engng.*, Vol.29, pp313-327.

Belytschko,T., and W.K.Liu, 1984, Nine node Largrange shell elements with spurious mode control, *A Collection of Technical Paper*, AIAA 25th Structures, Structural Dynamics and Materials Conference, Palm Springs.

Belytschko,T., H.Stolarski, and N.Carpenter, 1984, A C^0 triangular plate bending element with one-point quadrature, *Int. J. Num. Meth. Engng.*, Vol.20, pp787-802.

Bhashyam,G.R., and R.H.Gallagher, 1984, An approach to the inclusion of transverse shear deformation in finite element plate bending analysis, *Comp. Struct.*, Vol.19, No.1-2.

Bonnes,G., G.Dhatt, Y.M.Giroux, and P.A..Robichaud, 1968, Curved triangular elements for the analysis of shells, *Proc. 2nd Conf. Matrix Meth. Struct. Mech.*, Wright-Patterson Air Force Base. Ohio.

Brebbia,C.A., 1985, *Finite Element System*, 3rd rev. ed., Springer-Verlag, Berlin Heidelberg New York Tokyo.

Brooks ,J., and H.P.Hale, 1955, Strength of the shell of the hen's egg, *Nature*, Vol.175, pp848-849.

Cantin,G., 1976, Rigid body motions and equilibrium in finite elements, *Finite Elements for Thin Shells and Curved Members*, John Wiley & Sons, London, pp55-61.

Cantin,G., and R.W.Clough, 1968, A curved, cylindrical-shell, finite element, *AIAA J.*, Vol.6, pp1057-1062.

Caramanlian,C., K.A.Selby, and G.T.Will, 1978, A quintic conforming plate bending triangle, *Int. J. Num. Meth. Engng.*, Vol.12, pp1109-1130.

Carter,T.C., 1976, The hens egg: shell forces at impact, and quasi-static compression, *Br. Paultry. Sci.*, Vol.17, pp199-214.

Cataloglu,A., P.L.Gould, and R.E.Clark, 1977, Stress analysis of aortic valve leaflets with smoothed geometrical data, *J. Biomechanics*, Vol.10, pp153-158.

Cataloglu,A., R.E.Clark, and P.L.Gould, 1977, Refined stress analysis of human heart valves, *J. Engng. Mech. Div.*, ASCE, Vol.103, pp135-150.

Chatterjee,A., and A.V.Setlur, 1972, A mixed finite element formulation for plate problems, *Int. J. Num. Meth. Engng.*, Vol.4, pp67-84.

Chuong,C.J., and Y.C.Fung, 1983, Three-dimensional stress distribution in arteries, *J. Biomech. Engng.*, ASME, Vol.105, pp268-274.

Clough,R.W., and J.L.Tocher, 1965, Finite element stiffness matrices for analysis of plate bending, *Proc. Conf. Matrix Meth. Struct. Mech.*, Wright-Patterson Air Force Base, Ohio.

Clough,R.W., and C.P.Johnson, 1968, A finite element approximation for the analysis of thin shells, *Int. J. Solids Struct.*, Vol.4, pp43-60.

Connor,J.J., and C.Brebbia, 1967, Stiffness of shallow rectangular element, *J. Engng. Mech. Div.*, ASCE, Vol. 93, EM5, pp43-65.

Cook,W.A., 1982, The effect of geometric shape on two-dimensional finite elements, *Nuclear Engng. Design*, Vol.70, pp13-26.

Cook,R.D., 1972, More on reduced integration and isoparametric elements, *Int. J. Num. Meth. Engng.*, Vol.3.

Cook,R.D., 1981, *Concepts and Applications of Finite Element Analysis*, 2nd edn., John Wiley & Sons, New York.

Cooke,J.R., J.G.DeBaerdemaeker, R.H.Rand, and H.A.Mang, 1976, A finite element shell analysis of guard cell deformations, ASAE paper no. 76-5526.

Cooke,J.R., R.H.Rand, H.A.Mang, and J.G.DeBaerdemaeker, 1977, A nonlinear finite element analysis of stomatal guard cells, ASAE paper no. 77-5511.

Cowper,G.R., 1970, G.M.Lindberg, and M.D.Olson, A shallow shell finite element of triangular shape, *Int. J. Solids Struct.*, Vol.6, pp1133-1156.

Cowper,G.R., G.M.Lindberg, and M.D.Olson, 1971, Comparison of two high-precision triangular finite elements for arbitrary deep shells, *Proc. 3rd Conf. Matric Meth. Struct. Mech.*, Wright-Patterson Air Force Base, Ohio.

Crisfield,M.A., 1985, Some recent research on numerical techniques for structural analysis, *Proc. of the NUMETA'85 Conf.* , Swansea, U.K., pp565-575.

Crisfield,M.A., 1983, A four-noded thin plate bending elements using shear constraints-a modified version of Lyons' element, *Comp. Meth. Appl. Mech. Engng.*, Vol.38, pp93-120.

Danielson,D.A., 1971, Stability of the thin elastic shell model of the red blood cell, *J. Biomechanics*, Vol.4, pp611-617.

Dawe,D.G., 1972, Rigid body motions and strain-displacement equations of curved shell finite elements, *Int. J. Mech. Sci.*, Vol.14, pp569-578.

Dawe,D.G.,1975, Higher order triangular finite element, *Int. J. Solids Struct.*, Vol.11, pp1097-1110.

Dawe,D.G., 1976, Some higher order elements for arches and shells, *Finite Elements for Thin Shells and Curved Members*, John Wiley & Sons, London, p131-153.

DeMichele,D.W., and P.J.H.Sharpe, 1973, An analysis of the mechanics of Guard cell motion, *J.Theor. Biol.*, Vol.41, pp77-06.

Desai,C.S., and J.F.Abel, 1972, *Introduction to the Finite Element Method,* Van Nostrand Reinhold Company, New York.

Doherty,W.P., E.L.Wilson, and R.L.Taylor, 1969, *Stress Analysis of Axisymmetric Solids Using Higher Order Quadrilateral Finite Elements, Structural Engineering Laboratory Report* No. SESM 69-3, Univ. of California, Berkeley.

Dovey,H.H., 1974, *Extension of Three Dimensional Analysis to Shell Structures Using the Finite Element Idealization, Structural Engineering Laboratory Report* No. SESM 72-2, Univ. of California, Berkeley.

Duncan-Fama,M.E., and J.L.Sandar, 1972, A circumferential crack in a cylindrical shell under tortion, *Int. J. Fracture Mech.* Vol.8, pp15-20.

Dupuis,G., and J.J.Goel, 1970, A curved element for thin elastic shells, *Int. J. Solids Struct.* Vol.6, pp1413-1428.

Essary,E.O., B.W.Sheldon, and S.L.Crews, 1977, Relationship between shell and shell membrane strength and other egg shell characteristics, *Poultry Sci.*, Vol.56, pp1882-1886.

Fezans,G., and G.Verchery, 1982, Some results on the behavior of degenerate shell elements, *Nuclear Engng. Design*, Vol.70, pp27-35.

Flanagan,D., and T.Belyschko, 1981, A uniform strain hexahedron and quadrilateral with orthogonal hourglass control, *Int. J. Num. Meth. Engng.*, Vol.17, pp679-706.

Flügge,W., 1960, *Stresses in Shells*, Springer-Verlag, Berlin.

Folias,E.S., 1967, A circumferential crack in a pressurized cylindrical shell, *Int. J. Fracture Mech.*, Vol.3, pp1-12.

Fricker,A.J.,1985, An improved three-node triangular element for plate bending, *Int. J. Num. Meth. Engng.*, Vol.21, pp105-114.

Fried,I., 1974, Residual energy balancing technique in the generation of plate bending finite elements, *Comp. Struct.*, Vol.4, pp771-778.

Fung,Y.C., Biomechanics, *Proc.* 14th IUTAM Congress, Delft, Netherlands, pp7-31.

Gallagher,R.H., 1975, *Finite Element Analysis: Fundamentals*, Prentice Hall, Englewood Cliffs.

Gallagher,R.H., 1975, Shell elements, *Proc. World Cong. F.E.M. in Struct. Mech.*, Baurnemouth, Dorset, England, ppE1-35.

Gallagher,R.H., 1976, Problems and progress in thin shell finite element analysis, *Finite Elements for Thin Shells and Curved Members*, pp1-13, John Wiley & Sons, London.

Gate,R.S., J.R.Cooke, and S.K.Upadhyaya, 1984, Eggshell stresses from flat plate and thermal load, ASAE technical paper No.84-5519, ASAE.

Ghista,D.N., 1972, A.S.Kobayashi, N.Davis, and G.Ray, Finite element analysis in biomechanics, *Proc. Int. Conf. Variational Methods in Engng.,*, Univ. of Southampthon.

Gould,p., D.N.Ghista, L.Brombolich, and I.Mirsky, 1972, *In vivo* stresses in the human left ventricular wall: analysis accounting for the irreegular three-dimensional geometry and comparison with idealized geometry analyses, *J. Biomechanics*, Vol.5, pp521-539.

Gould,P.L., A.Cataloglu, G.Dhatt, A.Chattopadhyay, and R.E.Clark, 1973, Stress analysis of the human aortic valve, *Comp. and Struct.*, Vol.3, pp377-384.

Green,B.E., 1961, D.R.Strome, and R.C.Weikel, Application of the stiffness method to the analysis of shell structures, *Proc. Aviation Conf.*, ASME, Los Angeles.

Hamid,M.S., H.N.Sabbah, and P.D.Stein, 1985, Comparison of finite element stress analysis of aortic valve leaflet using eiher membrane elements or solid elements, *Comp. and Struct.*, Vol.20, pp955-961.

Hammerle,J.R., and N.N.Mohsenin, 1967, Determination and analysis of failure stresses in egg shells, *J. Agric. Engng. Res.*, Vol.12, pp13-21.

Hatze,H., 1974, The meaning of the term 'biomechanics', *J. Biomechanics*, Vol.7, pp189-190.

Herrmann,L.R., 1965, A bending analysis for plates, *Proc. Conf. Matric Meth. Struct. Mech.*, Wright-Patterson Air Force Base, Ohio.

Herrmann,L.R., 1967, Finite element analysis for plates, *J. Engng. Mech. Div.*, ASCE,Vol.93, pp13-26, Oct..

Herrmann,L.R., 1965, Elasticity equations for incompressible and nearly incompressible materials by a variational theorem, *AIAA J.*, Vol.3, pp10.

Herrmann,L.R., and D.M.Campbell, 1968, A finite element analysis for thin shells, *AIAA J.*, Vol.6, pp1842-1847.

Henshell,R.D. and K.G.Shaw, Crack tip finite elements are unnecessary, *Int. J. Num. Meth. Engng.*, Vol.9, pp495-507.

Hinton,E., and J.S.Campbell, 1974, Local and global smoothing of discontinuous finite element functions using a least squares method, *Int. J. Num. Meth. Engng.*, Vol.8, pp641-480.

Hinton,E., F.C.Scott, and R.E.Ricketts, 1975, Local least squares stress smoothing for parabolic iaoparametric element, *Int. J. Num. Meth. Engng.*, Vol.9, pp235-256.

Hinton,E., and D.R.J.Owen, 1977, *Finite Element Programming*, Academic Press, Lodon.

Hrabok,M.M., and T.M.Hrudey, 1984, A review and catalogue of plate bending finite elements, *Comp. Struct.*, Vol.19, pp479-495.

Hughes,T.J.R., 1977, Equivalence of finite elements for nearly incompressible elasticity, *J. Appl. Mech.*, ASME, Vol.44, pp181-183.

Hughes,T.J.R., R.L.Taylor, and W.Kanoknukulchai, 1977, A simple and efficient finite element for plate bending, *Int. J. Num. Meth. Engng.*, Vol.11, pp1529-1543.

Hughes,TJ.R., and M.Cohen, 1978, The Heterosis finite element for plate bending, *Comp. Struct.*, Vol.9, pp445-450.

Hughes,T.J.R., M.Cohen, and M.Haroun, 1978, Reduced and selective integration techniques in the finite element analysis of plates, *Nuclear Engng. Design*, Vol.46, pp203-222.

Hung,T-K., Skalak,R., G.Bugliarello, Y.K.Liu, D.J.Patel, and Albin,M.S., 1978, Perspectives in biomechanics research and education for next decade, *J. Engng. Mech. Div.*, ASCE, Vol.104, p3-9.

Hunt,J.R., and P.W.Voisey, 1966, Physical properties of egg shells, 1. relationship of resistance to compression, and force at failure of egg shells, *Poultry Sci.*, Vol.45, p1398-1404.

Ingraffea,A.R., 1977, Fracture propagation in rock: laboratory tests and finite element analysis, Ph.D. dessertation, U. of Colorado.

Ingraffea,A.R., 1983, Numerical modelling of fracture propagation, *Rock Fracture Mechanics*, Inernational Center for Mechanical Sciences, Udine, Italy.

Irons,B.M., and K.J.Draper, 1965, Inadequacy of nodal connections in a stiffness solution for plate bending, *AIAA J.*, Vol.3, pp961.

Irons,B.M., 1969, A conforming quartic triangular elements for plate bending, *Int. J. Num. Meth. Engng.*, Vol.1, pp29-45.

Irons,B.M., 1970, A frontal solution program for finite element analysis, *Int. J. Num. Meth. Engng.*, Vol.2, pp5-32.

Irons,B.M., 1973, A technique for degenerating brick-type isoparametric elements using hierarchical midside nodes, *Int. J. Num. Meth. Engng.*, Vol.15, pp558-589.

Irons,B.M., and A. Razzaque, 1973, Further modification to Ahmad's shell element, *Int. J. Num. Meth. Engng.*, Vol. 5, pp558-589.

Irons,B.M., and A. Razzaque, 1972, Shape function formulation for elements other than displacement models, *Proc. Int. Conf. Variational Methods in Engng.*, Univ. of Southampton.

Irons,B.M., The SemiLoof shell element, 1976, *Finite Elements for Thin Shells and Curved Members*, pp197-222, John Wiley & Sons, London.

Irons,B.M., and Ahmad,S., 1980, *Techniques of Finite Elements*, Ellis Horwood Ltd., Chichester.

Jeyachandrabose,C., J.Kirkhope, and C.R.Babu, 1985, An alternative explicit formulation for the DKT plate-bending element, *Int. J. Num. Meth. Engng.*, Vol.21, pp1289-1293.

Jones,R.E., and D.R.Strome, 1965, A survey of analysis of shells by the displacement method, *Proc. Conf. Matric Meth. Struct. Mech.*, Wright-Patterson Air Force Base, Ohio.

Kanok-Nukulchai,W., 1979, A simple and efficient finite element for general shell analysis, *Int. J. Num. Meth. Engng.*, Vol.14, pp179-200.

Karamanlidis,D., and S.N.Atluri, 1984, Mixed finite element models for plate bending analysis: theory , *Comp. Struct.*, Vol.19, pp431-445.

Karamanlidis,D., H.L.The and S.N.Atluri, 1984, Mixed finite element models for plate bending analysis: a new element and its applications, *Comp. Struct.*, Vol.19, pp565-581.

Kavanagh,K.T., and S.W.Key, 1972, A note on selective and reduced integration techniques in the finite element method, *Int. J. Num. Meth. Engng.*, Vol.4, pp148-150.

Key,S.W., and Z.E.Beisinger, 1970, The analysis of thin shells by the finite element method, *Symp. High Speed Computing for Elastic Struct .*, IUTAM Liege Univ. Press, Vol.1, pp209-256.

Kiciman,O.K., and E.P.Popov, 1978, A general finite element model for shells of arbitrary geometry, *Comp.. Meth. Appl. Mech. Engng.*, Vol.13, pp45-48.

King,A.I., 1984, A review of biomechanical models, *J. Biomech. Engng.*, ASME, Vol.106, pp97-104.

Knowles,N.C., A.Razzaque, and J.B.Spooner, 1976, Experience of finite element analysis fo shell structures, *Finite Elements for Thin Shells and Curved Members*, p245-262, John Wiley & Sons, London.

Koiter,W.T., 1963, A spherical shell under point load, *Progress in Appied Mechanics: The Prager Anniversary Volume*, Macmillan, New York.

Laursen,M.E., and M.Gellert, 1978, Some criteria for numerically integrated matrices and quadrature formulas for triangles, *Int. J. Num. Meth. Engng.*, Vol.12, pp67-76.

Lakshminarayana,H.V., M.V.V.Murthy, and L.S.Srinath, 1982, On an analytical-numerical precedure for the analysis of cylindrical shells with arbitrarily oriented cracks, *Int. J. Fracture*, Vol.19, pp257-275.

Lee,S.W., and T.H.H.Pian, 1978, Improvement of plate and shell finite elements by mixed formulations, *AIAA J.*, Vol.16, pp29-34.

Lee,S.W., and S.C.Wong, 1982, Mixed formulation finite elements for Mindlin theory plate bending, *Int. J. Num. Meth. Engng.*, Vol.18, pp1297-1311.

Lee,S.W., S.C.Wong, and L.F.Ruberl, 1984, Experience with finite element modeling of thin plate bending, *Comp. Struct.* Vol.19, pp747-755.

Lee,S.W., and J.C.Zhang, 1985, A six-node finite element for plate bending, *Int. J. Num. Meth. Engng.*, Vol.21, pp131-143.

Macneal,R.H., 1982, Derivation of element stiffness matrices by assumed strain distributions, *Nuclear Engng. Design*, Vol.70, pp3-12.

MacNeal,R.H., and R.Harder, 1984, A proposed standard set of problems to test finite element accuracy, *Proc. AIAA conf., Structures and Structuc. Dynamics*, Parlm Spring, Ca.

Malkus,D.S., and T.J.R.Hughes, 1978, Mixed finite element methods-reduced and selective integration technique: a unification of concepts, *Comp. Meth.Appl.Mech.Engng.*, Vol.15, pp63-81.

Maltzahn,W.W., D.Besdo, and W.Wiemer, 1981, Elastic property of arteries: a nonlinear two-layer cylindrical model, *J. Biomechanics*, Vol.6, pp389-397.

Manceau,J.R., and J.M. Henderson, 1970a, Physical properties of egg shells, *Transaction*, ASAE, Vol.13, pp436-439.

Manceau,J.R., and J.M. Henderson, 1970a, Stress analysis of egg shells, *Transaction*, ASAE, Vol.13, pp440-443.

McRae,D.C., and J.W.Duff, 1969, The measurement of compression stress in eggshells, *J. Agric. Engng Res.*, Vol.14, pp1-10.

Melosh,R.J., 1965, A flat triangular shell element stiffness matrix, *Proc. Conf. Matrix Meth. Struct. Mech.*, Wright-Patterson Air Force Base, Ohio.

Mohr,G.A., 1980, Numerically integrated triangular element for doubly curved thin shells, *Comp. Struc.*, Vol.11, pp565-571.

Morley,L.S.D., 1983, Approximation to bending trial functions for shell triangular finite elements in quadratic parametric representation, *Comp. Struct.*, Vol.16, pp657-668.

Morley,L.S.D., 1984, An assumed stress hybrid curvilinear triangular finite element for plate bending, *Int. J. Num. Meth. Engng.*, Vol.20, pp529-548.

Morris,A.J., 1973, A deficiency in current finite elements for thin shell applications, *Int. J. Solids Struct.*, Vol.9, pp331-346.

Morris,A.J., 1976, A summary of appropriate governing equations and functionals in finite element analysis of thin shell, *Finite Elements for Thin Shells and Curved Members*, p1-15, John Wiley & Sons, London.

Nelson,L.H., and J.M.Henderson, 1975, A study of the mechanical properties of egg shell, *Br. Poultry Sci.*, Vol. 16, pp225-293.

Olson,M.D., 1972, Analysis of arbitrary shells using shallow shell finite elements, *Thin Shell*, Prentice Hall, New York.

Olson,M.D., and T.W.Bearden, 1979, A simple flat triangular shell element revisited, *Int. J. Num. Meth. Engng.*, Vol.14, pp51-68.

Orr,H.L., G.W.Friars, B.S.Reinhart, and I.Y.Pevzener, 1976, Classification of shell damage resulting from egg handling practices, *Poultry Sci.*, Vol.56, pp611-614.

Owen,J., and G.Q.Liu, 1985, Elasto-viscoplastic analysis of anisotripic laminated plates and shells, *Proc. of the NUMETA'85 Conf.*, Swansea, U.K., pp557-591.

Pao,Y.C., L.L.Ritman, and E.H.Woods, 1974, Finite element analysis of left ventricular myocardial stresses, *J. Biomechanics*, Vol.7, pp469-474.

Pao,Y.C., 1982, Finite elements in stress analysis and estimation of mechanical properties of the working heart, *Finite elements in Biomechanics*, John Wiley & Sons, New York, pp127-157.

Pawsey,S.F., and R.W.Clough, 1971, Improved numerical integration of thick shell finite elements,' *Int. J. Num. Meth. Engng.*, Vol.3., pp575-586.

Pawsey,S.F., 1972, Discussion of papers by O.C.Zienkiewicz, R.L.Taylor and J.M.Too and S.F.Pawsey and R.W.Clough, *Int. J. Num. Meth. Engng*, Vol.4, pp449-450.

Pherson,G.K, and T.J.Kriewall, 1980, Fetal head modelling,: an investigation utilizing a finite element of model of the fetal parietal bone, *J. Biomechanics*, Vol.13, pp17-26.

Pian,T.H.H., 1964, Derivation of element stiffness matrices by assumed stress distributions, *AIAA J.*, Vol.2, pp1333-1335.

Pian,T.H.H., 1971, Hybrid models, *Numerical and Computer methods in Applied Mechanics*, Academic Press, pp59-78.

Pian,T.H.H., 1983, Reflections and remarks on hybrid and mixed finite element methods, *Hybrid and Mixed Finite Element Methods*, John Wiley & Sons, Ltd. pp565-570.

Pian,T.H.H., and P.Tong, 1969, Basis of finite element methods for solid continua, *Int. J. Num. Meth. Engng.*, Vol.1, pp3-28.

Pitt,R.E. adn D.C.Davis, 1984, Finite element analysis of fluid-filled cell response to external loading, *Transactions,* ASAE, Vol.27, pp1976-1983.

Prathap,G., 1985, A simple plate/shell triangle, *Int. J. Num. Meth. Engng.*, Vol.21, pp1149-1156.

Prato,C.A., 1969, Shell finite element method via Reissner's Principle, *Int. J. Solids Struc.*, Vol.5, pp1119-1133.

Pugh,E.D.L., E.Hinton, and O.C.Zienkiewicz, 1978, A study of quadrilateral plate bending elements with 'reduced' integration, *Int. J. Num. Meth. Engng.*, Vol.12, pp1059-1079.

Razzaque,A., 1973, Program for triangular bending elements with derivative smoothing, *Int. J. Num. Meth. Engng.*, Vol.6, pp333-343.

Rehkugler,G.E., 1963, Modulus of elasticity and ultimate strength of the hen's egg shell, *Agric. Engng. Res.*, Vol.8, pp352-354.

Rehkugler,G.E.,1973, Thermally induced stresses in eggshells, *J. Agric. Engng. Res.*, Vol.18, pp275-279.

Reissner,E., 1947, Stresses and small displacements of shallow spherical shells., *J. Mathematics and Physics*, Vol.25, pp80-85, 279-300.

Reissner,E., 1950, On a variational theorem in elasticity, *J. Mathematics and Physics*, Vol.29, pp90-95.

Robinson,J., 1972, Automatic extraction of rigid body modes from stress and strain elements, *Proc. Int. Conf. Variational Mehtods in Engng.*, Univ. of Southampton.

Romanoff,A.L., and A.J.Romanoff, 1949, *The Avian Egg*, John Wiley & Sons Inc. NY,pp60-173.

Rossow,M.P., and K.C.Chen, 1977, Computational efficiency of plate elements, *J. Struct. Div.*, ASCE, ST2, pp447-451.

Rubinstein,R., E.F.Punch, and S.N.Atluri, 1983, An analysis of, and remedies for, kinematic models in hybrid-stress finite elements: selection of stable, invariant stress field, *Comp. Meth. Appl. Mech. Engng.*, Vol.38, pp63-69.

Sack,F.D., 1982, *The Development and Ultrastructure of the Stomata of Funaria Hygrometrica, HEDW.*, Ph.D. Thesis, Cornell Univ., Ithaca, New York.

Schmid-Schonbein,G.W., and Skalak,R., 1984, Mechanics of single cell, *J. Biomech. Engng.*, ASME, Vol.106, pp1.

Schoorl ,P., and Boersma,H.Y. , 1962, Research on the quality of the egg shell. A new method of determination, *12th World's Poultry Congr.*, Sydney, pp432-435.

Scordelis,A.C., and K.S.Lo, 1964, Computer analysis of cylindrical shells, *ACI J.*, Vol. 61, pp539-561.

Shih,C.F., H.G.DeLorezi, and M.D.German, 1967, Crack extension modeling with singular quadratic isoparametric elements, *Int. J. Fracture*, Vol.12, pp647-650.

Sih,G.C., 1974, Strain energy density factor applied to mixed mode crack problems, *Int. J. Fracture*, Vol. 10, pp305-321.

Shimodaira,H., 1985, Equivalence between mixed models and displacement models using reduced integration, *Int. J. Num. Meth. Engng .*, Vol.21, pp89-104.

Shoemaker,E.M., and L.M.Srivastava, 1973, The mechanics of stomatal opening in corn leaves, *J. Theor. Boil.*, Vol.42, pp219-225.

Sluka,S.J., E.L.Besch, and A.H.Smith, 1965, A hydrostatic test for eggshell strength, *Poultry Sci.*,Vol.44, pp1494-1500.

Smart,H.M., 1967, The curve of the avian egg, *J.Anatomy*, Vol.101, pp634-635.

Spilker,R.L., A simplified hybrid-stress finite element model of the intervertebral disc, *Finite elements in Biomechanics*, John Wiley & Sons, New York, pp295-312.

Stewart,G.F., 1936, Shell characteristics and their relationships to the breaking strength, *Poultry Sci.*, Vol.15, pp119-124.

Stolarski,H., and T.Belytschko, 1982, Membrane locking and reduced integration for curved elements, *J. of Appl. Mech.,* ASME, Vol.49, pp172-176.

Stolarski,H., and T.Belytschko, 1983, Shear and membrane locking in curved C^o elements, *Comp. Meth. Appl. Mech. Engng.,* Vol.41, pp279-296.

Stolarski,H., T.Belytschko, and N.Carpenter, 1984, A simple triangular curved shell element, *Engng. Comput.,* Vol.1, pp210-218.

Stolarski,H., N.Carpenter and T.Belytschko, 1985, A Kirchhoff-mode method for C^o bilinear, and serendipity plate elements, *Computer Methods in Applied Mechanics amd Engineering,* Vol.50, pp121-145.

Strickland,E.S., and W.A.Loden, 1968, Doubly curved triangular element, *Proc. 2nd Conf. Matrix Meth. Struct. Meth.,* Wright-Patterson Air Force Base, Ohio.

Surana,K.S., 1980, Transition finite elements for three-dimensional stress analysis, *Int. J. Num. Meth. Engng,* Vol.15, pp991-1020.

Takemoto,H., and R.D.Cook, 1973, Some modifications of an isoparametric shell element, *Int. J. Num. Meth. Engng.,* Vol.7, pp401-405.

Tessler,A., and T.J.R.Hughes, 1983, An improved treatment of transverse shear in the Mindlin-type four-node quadrilateral elements, *Comp. Meth. Appl. Mech. Engng.,* Vol.39, pp311-335.

Timoshenko,S., and S. Woinowsky-Krieger, 1959, *Theory of Plates and Shells,* 2nd ed., McGraw-Hill Book Co., New York.

Torenzen,A., 1983, Static analysis of the left ventricle,*J. Biomech. Engng.,* ASME, Vol.105, pp39-46.

Tsach,U., 1981, Locking of thin plate/shell elements, *Int. J. Num. Meth. Engng.,* Vol.17, pp633-644.

Tung,M.A., L.M.Staley, and J.F.Richards, 1969, Studies on eggshell strength, shell stiffness, shell quantity, egg size and shape, *Br. Poultry Sci.,* Vol.9, pp221-229.

Tung,M.A., L.M.Staley, and J.F.Richards, 1969, Estimation of Young's modulus and failure stresses in the hen's egg shell, *Can. Agric. Engng.,* Vol.11, pp3-5.

Tyler,C., 1961, Shell strength: its measurement and its relationship to other factors. *Br. Poultry Sci.,* Vol.5, pp19.

Tyler,C., and D.Moor, 1964, Type of damage caused by various cracking and crushing methods used for measuring eggshell strength,*Br. Poultry Sci.*, Vol.6, pp175-182.

Upadhyaya,S.K., J.R.Cooke, R.S.Gates, and R.H.Rand, 1984, A finite element analysis of the mechanical and thermal strength of avian eggs, summitted for publication.

Upadhyaya,S.K., J.R.Cooke, and R.H.Rand, 1985, A fluid-filled spherical shellmodel of the thermo-elastic behavior of avian eggs, J. Agric. Engng. Res., Vol.32, pp95-109.

Utku,S., Stiffness matrices for thin triangular element of nonzero Gaussian curvature, *AIAA J.*, Vol.5, pp1659-1657.

Utku,S., and J.L.Melosh, 1968, Behavior of triangular shell-element stiffness matrices associated with polyhedral deflection distributions, *AIAA J.*, Vol.6, pp374-376.

Voisey,P.W., and J.R.Hunt, 1967, Relationship between applied force, deformation of eggshells and fracture force, *J. Agric. Engng. Res.* Vol. 12, pp1-4.

Voisey,P.W., and J.R.Hunt, 1968, Physical property of egg shell, *Br. Poultry Sci* ., Vol.8, pp263-271.

Voisey,P.W., and J.R.Hunt, 1974, Measurement of eggshell strength, *J.Texture Studies,* Vol.5., pp135-182.

Voisey,P.W., and R.M.G.Hamilton, 1977 The effect of deformation rate and other factors on the force required to fracture egg shells in measuring shell strength, *Poultry Sci*, 1977, Vol.56, pp1994-2002.

Washburn,K.W., 1982, Incidence, cause, and prevention of egg shell breakage in commercial production, *Poultry Sci.* Vol.61, pp2005-2012.

Wells,R.G., Eggshell strength, 1967, I: The relationship between egg breakage in the field and certain laboratory assessments of shell strength, *Br. Poulry Sci.*, Vol.8, pp131-139.

Wempner,G.A., J.T.Oden, and D.A.Kross, 1968, Finite elements analysis of thin shells, *J. Engng. Mech. Div.*, ASCE, EM6, pp1273-1293.

Willmer,C.M., 1983, *Stomata*, Longman Inc., New York

Wilson,E.L., R.L.Taylor, W.P.Doherty, and J.Ghaboussi, 1971, Incompatible displacement models, *Numerical and Computer Methods in Applied Mechanics*, Academic Press, pp43-57.

Wu,S.G., G.C.Lee, and N,T.Tseng, 1984, Nonlinear elastic analysis of blood vessels, *J. Biomech. Engng.*, ASME, Vol.106, pp376-383.

Wunderlich,W., 1983, Mixed models for plates and shells: principle-elements-examples, *Hybrid and Mixed Finite Element Methods*, John Wiley & Sons,Ltd., pp215-241.

Yang,T.Y., 1973, High order rectangular shallow shell finite element, *J. Engng. Mech. Div.*, ASCE, Vol.99, EM1, pp157-181.

Yettram,A.L., C.A.Vinson, and D.G.Gibson, 1982, Computer modeling of the human left ventricle, *J. Biomech. Engng.*, ASME, Vol.104, pp148-152.

Zarda,P.R., S.Chien, and R.Skalak, 1976, Elastic deformation of red blood cells, *J. Biomechanics*, Vol.10, pp211-221.

Zienkiewicz,O.C., and E.Hinton, 1976, Reduced integration, function smoothing and non-conformity in finite element analysis(with special reference to thick plates), *J. Franklin Inst.*, Vol.302, pp443-461.

Zienkiewicz,O.C., R.L.Taylor, and J.M.Too, 1971, Reduced integration technique in general analysis of plates and shells, *Int. J. Num. Meth. Engng.*, Vol.3, pp275-290.

Zienkiewicz,O.C., Reply by O.C.Zienkiewicz, 1972, *Int. J. Num. Meth. Engng.*, Vol.4, pp450.

Zienkiewicz,O.C., and S.Nakazawa, 1984, On variational formulation and its modifications for numerical solution, *Comp. Struct.*, Vol.19, pp303-313.

Zienkiewicz,O.C., 1977, *The Finite Element Method*, 3rd Edn., McGraw-Hill, New York.

The Committee on Masonry and Reinforced Concrete of Structural Division,1952, *Design of Cylindrical Concrete Shell Roofs*, ASCE-Manual of Engineering Practice-No.31, ASCE, New York.